

**DESIGN OF A PATTERN RECONFIGURABLE MASSIVE  
MIMO ANTENNA FOR 5G TECHNOLOGY**

BY

**Saeed Ahmad Saeed Haydhah**

A Thesis Presented to the  
DEANSHIP OF GRADUATE STUDIES

**KING FAHD UNIVERSITY OF PETROLEUM & MINERALS**

DHAHRAN, SAUDI ARABIA

In Partial Fulfillment of the  
Requirements for the Degree of

**MASTER OF SCIENCE**

In

**ELECTRICAL ENGINEERING**

**DECEMBER 2019**

KING FAHD UNIVERSITY OF PETROLEUM & MINERALS  
DHAHRAN- 31261, SAUDI ARABIA  
DEANSHIP OF GRADUATE STUDIES

This thesis, written by **Saeed Ahmad Saeed Haydhah** under the direction of his thesis advisor and approved by his thesis committee, has been presented and accepted by the Dean of Graduate Studies, in partial fulfillment of the requirements for the degree of **MASTER OF SCIENCE IN ELECTRICAL ENGINEERING**.



Dr. Abdallah Said Al-Ahmari  
Department Chairman

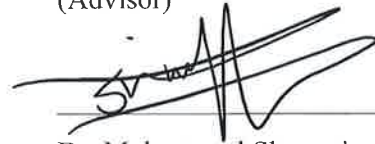


Dr. Salam A. Zummo  
Dean of Graduate Studies

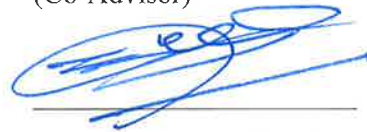
25/12/19  
Date



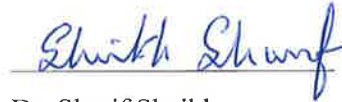
Dr. Azzedine Zerguine  
(Advisor)



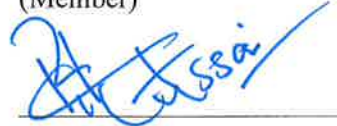
Dr. Mohammad Sharawi  
(Co-Advisor)



Dr. Abdelmalek Zidouri  
(Member)



Dr. Sharif Sheikh  
(Member)



Dr. Rifaqat Hussain  
(Member)





© Saeed Ahmad Saeed Haydhah

2019

*To my parents, brothers and sisters, and to my great professors and friends.*

# ACKNOWLEDGMENTS

It is the time to thank all people who supported me in this great journey. With huge respect, many thanks to my family who accepted being absent for long times and who supported me a lot in this journey.

With huge respect, I would really like to thank Prof. Mohammad Sharawi for his always support and guidance. It is always a huge pleasure for me to work with Prof. Mohammad Sharawi. In addition, it is time to thank the great professor Prof. Azzedine Zerguine for his support and guidance. Many thanks also to Prof. Fabien Ferrero and Prof. Leonardo Lizzi since they give me the opportunity to use the LAB in University of Côte d'Azur and I really thank them for their great support and guidance. In addition, I really thank Prof. Ali Muqaibel for his support and guidance, it was really a huge honor to work with Prof. Ali Muqaibel, so many thanks to Prof. Muqaibel.

I would like to thank my committee members: Prof. Abdelmalek Zidouri, Prof. Sharif Sheikh and Dr. Rifaqat Hussain for their useful response, advice, guidance and the time they spent reviewing this thesis.

I would like also to thank my friends who supported me a lot in this great journey.

# Contents

<b>ACKNOWLEDGMENTS</b> .....	v
<b>LIST OF TABLES</b> .....	ix
<b>LIST OF FIGURES</b> .....	x
<b>LIST OF ABBREVIATIONS</b> .....	xvii
<b>ABSTRACT</b> .....	xix
ملخص الرسالة.....	xxi
<b>CHAPTER 1 INTRODUCTION</b> .....	1
1.1 Wireless Communication Evolution.....	3
1.2 5G Technology .....	7
1.3 MIMO Antennas.....	19
1.4 Array Processing.....	21
1.5 DOA Estimation .....	21
1.6 Work Motivation .....	22
1.7 Thesis Objectives.....	23
<b>CHAPTER 2 THEORETICAL BACKGROUND</b> .....	24
2.1 Reconfigurability .....	24
2.2 5G Technology .....	31
2.3 MIMO Systems.....	43
2.4 Massive MIMO.....	50
2.5 Direction of Arrival (DOA) Estimation.....	73
2.6 FPGA .....	76
2.7 Summary.....	77
<b>CHAPTER 3 LITERATURE REVIEW</b> .....	78
3.1 Literature Review Trees .....	78
3.2 Pattern Reconfigurable Antennas .....	85



3.3	Frequency Reconfigurable Antennas.....	85
3.4	Pattern and Frequency Reconfigurable Antennas .....	86
3.5	Pattern Reconfigurable Slot Antennas.....	86
3.6	Frequency Reconfigurable Antennas.....	87
3.7	Pattern and Frequency Reconfigurable Antennas .....	87
3.8	MIMO Systems.....	87
3.9	Massive MIMO Systems .....	89
3.10	DOA Estimation for Massive MIMO Systems.....	94

**CHAPTER 4 DESIGNS OF PATTERN RECONFIGURABLE ANTENNAS AND A MASSIVE MIMO ANTENNA..... 96**

<b>4.1</b>	<b>Dual-Band Pattern and Frequency Reconfigurable Slot-Based Antenna</b>	<b>97</b>
4.1.1	Antenna Design.....	98
4.1.2	Simulation Results .....	102
4.1.3	Experimental Results .....	115
4.1.4	Comparison Tables and Discussions .....	116
4.1.5	Summary of the first pattern reconfigurable slot-based antenna .....	118
<b>4.2</b>	<b>A Slot Based Pattern Reconfigurable Antenna</b> .....	<b>119</b>
4.2.1	Antenna Design.....	120
4.2.2	Theory of Operation.....	121
4.2.3	Simulation Results .....	128
4.2.4	Experimental Results .....	130
4.2.5	Comparison Table and Discussions .....	133
4.2.6	Summary of the second slot-based pattern reconfigurable antenna.....	134
<b>4.3</b>	<b>A Compact Pattern Reconfigurable Antenna for UHF Internet of Things Applications</b> .....	<b>136</b>
4.3.1	Antenna Geometry .....	136
4.3.2	Simulation Results .....	142
4.3.3	Experimental Results .....	146
4.3.4	Summary of the IoT antenna.....	149
<b>4.4</b>	<b>A New Pattern Reconfigurable Slot Antenna for 5G Technology</b> .....	<b>150</b>

4.4.1	Design Geometry .....	150
4.4.2	Simulation Results .....	153
4.4.3	Table of Comparison and Discussions.....	158
4.4.4	Summary of the third slot-based pattern reconfigurable antenna .....	160
<b>4.5</b>	<b>A New Pattern Reconfigurable Massive MIMO Antenna for 5G Technology .....</b>	<b>161</b>
4.5.1	Design Description.....	161
4.5.2	Simulated Results.....	163
4.5.3	Comparison Table and discussions .....	177
4.5.4	Summary about the pattern reconfigurable mMIMO Antenna.....	179
<b>4.6</b>	<b>Summary of Contributions .....</b>	<b>180</b>
 <b>CHAPTER 5 CONCLUSIONS AND FUTURE WORK.....</b>		<b>181</b>
5.1	Conclusions .....	181
5.2	Future Work.....	182
<b>REFERENCES.....</b>		<b>183</b>
<b>VITAE.....</b>		<b>194</b>
<b>LIST OF PUBLICATIONS .....</b>		<b>195</b>

# LIST OF TABLES

Table 1.1. Comparison between the different generations as shown in [2].	5
Table 2.1. Comparison between different switches in [4].	27
Table 3.1. Comparison table# 1 for many mMIMO systems in literature.	90
Table 3.2. Comparison table# 2 for many mMIMO systems in literature.	91
Table 3.3. Comparison table# 3 for many mMIMO systems in literature.	92
Table 4.1. The parameter of the proposed antenna.	99
Table 4.2. Results for configurations when more than 1 diodes are on at 5 GHz	106
Table 4.3. Varactors' capacitances values at different resonant	112
Table 4.4. Comparison the simulated results of the antenna under investigation and the results of the proposed antenna in [121].	116
Table 4.5. Comparison between the proposed antenna and available antennas in literature.	117
Table 4.6. The possible phases feeding the used slots.	124
Table 4.7. The attained configurations by switching the diodes bridging the slots.	125
Table 4.8. Comparison table between the proposed slot-based pattern reconfigurable antenna and other slot-based pattern reconfigurable antennas in literature..	133
Table 4.9. The summary of the pattern configurations of the proposed pattern reconfigurable L-slot antenna.	134
Table 4.10. Dimensions of the proposed antenna	140
Table 4.11. Correlation coefficients between the patterns of the antenna at 870 MHz	145
Table 4.12. The maximum ECC between the 8 patterns of the antenna in the band from 3.5 GHz to 3.8 GHz.	158
Table 4.13. A comparison table between the third slot-based pattern reconfigurable antenna and other slot-based pattern reconfigurable antennas in literature	159
Table 4.14. A comparison table between the proposed mMIMO antenna and other mMIMO antennas in the literature.	178

# LIST OF FIGURES

Fig. 1.1. Global mobile data traffic from 2017 to 2022.....	1
Fig. 1.2. Global mobile traffic by connection type.....	2
Fig. 1.3. The access network and the core network.....	4
Fig. 1.4. The estimated performance levels of 5G.....	8
Fig. 1.5. A schematic diagram of next generation 5G wireless networks.....	9
Fig. 1.6. Device-centric architecture example, [2].....	12
Fig. 1.7. D2D communication scenarios, [3].....	12
Fig. 1.8. MmWave spectrum availability in 3 – 300 GHz.....	13
Fig. 1.9. Massive MIMO and beamforming.....	14
Fig. 1.10. The massive and dense deployment for LOS environment.....	15
Fig. 1.11. Multipath and NLOS communication.....	16
Fig. 1.12. The block diagram of a MIMO system.....	19
Fig. 1.13. The model of the MIMO system used to model the channel mathematically.....	20
Fig. 2.1. The model of cognitive radio system.....	29
Fig. 2.2. A network with mmWave technology and phantom cells.....	37
Fig. 2.3. Downlink operation for massive MIMO link.....	52
Fig. 2.4. Uplink operation of a massive MIMO link.....	53
Fig. 2.5. Point-to-point MIMO link.....	54
Fig. 2.6. Multi-user MIMO TDD protocol.....	58
Fig. 2.7. Matched filter decoding for uplink massive MIMO.....	60
Fig. 2.8. Downlink massive MIMO with Conjugate beamforming.....	61
Fig. 2.9. Slot structure for TDD massive MIMO.....	63
Fig. 2.10. Slot structure for FDD massive MIMO.....	63
Fig. 2.11. Time-shifted pilot scheme.....	69
Fig. 2.12. Spatial power spectrum when isotropic antenna array is used.....	75
Fig. 2.13. The pattern of the directional element.....	75
Fig. 2.14. Spatial power spectrum when directional antenna array is used.....	76
Fig. 2.15. FPGA digital electronic circuit.....	76

Fig. 3.1. Tree of Literature review about reconfigurable antennas when antennas are reconfigured electronically. ....	79
Fig. 3.2. Tree of Literature review about reconfigurable antennas when antennas are slot based antennas.....	80
Fig. 3.3. Tree of Literature review about reconfigurable antennas when antennas are reconfigured by changing excited modes of antennas. ....	81
Fig. 3.4. Tree of Literature review about reconfigurable antennas when antennas are reconfigured mechanically.....	81
Fig. 3.5. Tree of Literature review about reconfigurable antennas when feeding networks are reconfigured.....	82
Fig. 3.6. Tree of Literature review about other types of reconfigurable antennas, and about some other useful topics.....	83
Fig. 3.7. Tree of Literature review about some useful antennas for this research work..	84
Fig. 3.8. The proposed 8*8 MIMO antenna in [143].....	88
Fig. 3.9. The geometry of the 24 ports massive MIMO system proposed in [144]. ....	89
Fig. 3.10. The model of the massive MIMO system used in [161]. ....	95
Fig. 4.1. The geometry of the proposed reconfigurable antenna. (a) Top view. (b) Side view.....	99
Fig. 4.2. (a) The transmission line details. (b) Biasing network details. ....	99
Fig. 4.3. (a) The single U-slot antenna. (b) Reconfigurable feeding network. (c) The simulated feeding point in HFSS. ....	100
Fig. 4.4. The dominant electric current around the radiating U-slot.....	102
Fig. 4.5. The simulated $S_{21}$ results of the reconfigurable feeding network in Fig. 4.3(b).....	103
Fig. 4.6. The simulated $S_{11}$ of the first four pattern configurations of the proposed antenna. ....	103
Fig. 4.7. The simulated radiation patterns of the first four pattern-configurations (when one diode is ON) of the proposed antenna at 3.6 GHz. (a) – (d) The 3-D radiation patterns. (e) – (h) The xy-plane (2-D) patterns.....	104
Fig. 4.8. The simulated $S_{11}$ results when two diodes or more are ON. ....	105

Fig. 4.9. The simulated radiation patterns at 5 GHz when two diodes are ON. (g) Solid line (D1, D2 are ON), Dashed line (D1, D3 are ON), Dashed line with a cross (D1, D4 are ON). (h) Dotted line with a star (D2, D3 are ON), Dotted line (D2, D4 are ON), Dashed line with dots (D3, D4 are ON).....	107
Fig. 4.10. The simulated radiation patterns at 3.6 GHz when two diodes are ON. (g) Solid line (D1, D2 are ON), Dashed line (D1, D3 are ON), Dashed line with a cross (D1, D4 are ON). (h) Dotted line with a star (D2, D3 are ON), Dotted line (D2, D4 are ON), Dashed line with dots (D3, D4 are ON).....	108
Fig. 4.11. The simulated radiation patterns at 5 GHz when more than two diodes are ON. (f) Solid line (D1, D2, D3 are ON), Dashed line (D2, D3, D4 are ON), Dashed line with a cross (D1, D3, D4 are ON). (g) Dotted line with a star (D1, D2, D4 are ON), Dotted line (D1, D2, D3, D4 are ON). .....	108
Fig. 4.12. The simulated radiation patterns at 3.6 GHz when more than two diodes are ON. (f) Solid line (D1, D2 D3 are ON), Dashed line (D2, D3 and D4 are ON), Dashed line with a cross (D1, D3 D4 are ON). (g) Dotted line with a star (D1, D2 D4 are ON), Dotted line (D1, D2, D3 D4 are ON). .....	109
Fig. 4.13. The simulated $S_{11}$ showing the frequency reconfigurability at the lower and higher bands. ....	110
Fig. 4.14. The simulated radiation patterns at 3.7 GHz. ....	111
Fig. 4.15. The simulated radiation patterns at 3.4 GHz. Fig. 4.16. The simulated radiation patterns at 3.1 GHz. ....	111
Fig. 4.17. The Effects on simulated $S_{11}$ of the Parameters: (a) $LSL$ , (b) $Ws$ .....	113
Fig. 4.18. The Effects on simulated $S_{11}$ of the Parameters: (a) $TL$ and $TW$ , .....	114
Fig. 4.19. The fabricated design of the first reconfigurable antenna. ....	115
Fig. 4.20. Measured $S_{11}$ results of the fabricated antenna when tapes are used.....	115
Fig. 4.21. The measured $S_{11}$ of the antenna when the PIN diodes are used.....	116
Fig. 4.22. The antenna design (a) Top view. (b) Side view.....	120
Fig. 4.23. The Geometry of the proposed pattern reconfigurable antenna. ....	122
Fig. 4.24. The antenna geometry showing the distances between the L-slots. ....	123
Fig. 4.25. The antenna geometry showing the used phase shifters.....	123
Fig. 4.26. The number of slots in the antenna.....	124

Fig. 4.27. The diodes used to bridge the slots for more configurations.....	126
Fig. 4.28. The biasing circuits for the diodes.....	127
Fig. 4.29. Simulated $S_{11}$ results at the lower band of the proposed antenna. The used diodes and phase shifters are mentioned.....	128
Fig. 4.30. Simulated $S_{11}$ results at the higher band of the proposed antenna. The used diodes and phase shifters are mentioned.....	128
Fig. 4.31. 3-D radiation patterns at 2.3 GHz, scales might change. ....	129
Fig. 4.32. 3-D radiation patterns at 3.7 GHz.....	130
Fig. 4.33. The fabricated design of the proposed pattern reconfigurable L-slot antenna. ....	131
Fig. 4.34. The measured $S_{11}$ results of the antenna when no phase shifter is used. ....	131
Fig. 4.35. The measured $S_{11}$ results of the antenna when the right 90 degrees phase shifter is used. ....	132
Fig. 4.36. The measured $S_{11}$ results of the antenna when the right 90 degrees phase shifter is used. ....	132
Fig. 4.37. The measured $S_{11}$ results of the antenna when the right 90 degrees phase shifter is used. ....	132
Fig. 4.38. The antenna prototypes in designing the proposed antenna. ....	137
Fig. 4.39. The electric field distribution around the slots at 868 MHz for Slot 1 and Slot 2 configurations. ....	138
Fig. 4.40. The geometry of the proposed antenna.....	139
Fig. 4.41. The proposed antenna with important dimensions. ....	140
Fig. 4.42. The simulated S-parameters to different ports in the antenna. ....	141
Fig. 4.43. The simulated $S_{11}$ results (in dB) of the proposed reconfigurable antenna. ....	143
Fig. 4.44. The simulated Peak Gain Results (in dB) of the proposed reconfigurable antenna. ....	143
Fig. 4.45. The simulated Efficiency results (in linear scale) of the proposed reconfigurable antenna.....	143
Fig. 4.46. The simulated 2D-patterns (in dB) of the proposed reconfigurable antenna for three configurations. Scales are different to show details. ....	145
Fig. 4.47. The fabricated pattern reconfigurable IoT antenna. ....	147

Fig. 4.48. Radiation pattern of Slot 1 Configuration. ....	147
Fig. 4.49. Radiation pattern of Slot 2 Configuration. ....	148
Fig. 4.50. Radiation pattern of Monopole Configuration. ....	148
Fig. 4.51. Radiation patterns of the antenna for different important cases. ....	149
Fig. 4.52. The resulted pattern reconfigurable antenna with the four U-slots. ....	151
Fig. 4.53. The proposed antenna with the reflector behind it. ....	151
Fig. 4.54. The resulted antenna with four pin diodes and four slits to reduce coupling currents. ....	152
Fig. 4.55. The proposed pattern reconfigurable U-slot antenna with the biasing circuits. ....	152
Fig. 4.56. The simulated $S_{11}$ results of the antenna when one slot is activated. ....	154
Fig. 4.57. The simulated Peak Gains of the antenna when one slot is activated. ....	154
Fig. 4.58. The simulated radiation efficiency of the antenna when one slot is activated. ....	155
Fig. 4.59. The radiation patterns of the antenna when one slot is activated. ....	155
Fig. 4.60. The simulated $S_{11}$ when two slots are activated. ....	156
Fig. 4.61. The simulated Peak Gains when two slots are activated. ....	156
Fig. 4.62. The simulated radiation efficiencies when two slots are activated. ....	157
Fig. 4.63. The radiation patterns of the antenna when 2 slots are activated. ....	157
Fig. 4.64. The pattern reconfigurable 4x4 massive MIMO for 5G technology. ....	162
Fig. 4.65. The simulated $S_{11}$ of the mMIMO when elements 3, 6, 7 and 8 are activated. ....	163
Fig. 4.66. The simulated $S_{21}$ of the mMIMO when elements 3, 6, 7 and 8 are activated. ....	164
Fig. 4.67. The patterns at 3.63 GHz when elements 3, 6, 7 and 8 are activated and $B_x=0$ degrees and $B_y=0$ degrees. ....	164
Fig. 4.68. The patterns at 3.63 GHz when elements 3, 6, 7 and 8 are activated and $B_x= - 50$ degrees and $B_y= - 100$ degrees. ....	165
Fig. 4.69. The patterns at 3.63 GHz when elements 3, 6, 7 and 8 are activated and $B_x= +50$ degrees and $B_y= + 100$ degrees. ....	166



Fig. 4.70. The simulated $S_{11}$ of the mMIMO when elements 2, 12, 13 and 14 are activated. ....	167
Fig. 4.71. The simulated $S_{21}$ of the mMIMO when elements 2, 12, 13 and 14 are activated. ....	167
Fig. 4.72. The patterns at 3.63 GHz when elements 2, 12, 13 and 14 are activated and $B_x = + 50$ degrees and $B_y = + 100$ degrees. ....	168
Fig. 4.73. The patterns at 3.63 GHz when elements 2, 12, 13 and 14 are activated and $B_x = - 250$ degrees and $B_y = + 100$ degrees. ....	168
Fig. 4.74. The simulated $S_{11}$ of the mMIMO when elements 1, 2, 3, 4, 5, 6, 14, 15 and 16 are activated. ....	169
Fig. 4.75. The simulated $S_{21}$ of the mMIMO when elements 1, 2, 3, 4, 5, 6, 14, 15 and 16 are activated. ....	170
Fig. 4.76. The patterns at 3.63 GHz when elements 1, 2, 3, 4, 5, 6, 14, 15 and 16 are activated and $B_x = + 50$ degrees and $B_y = + 100$ degrees. ....	170
Fig. 4.77. The patterns at 3.63 GHz when elements 1, 2, 3, 4, 5, 6, 14, 15 and 16 are activated and $B_x = + 100$ degrees and $B_y = + 0$ degrees. ....	171
Fig. 4.78. The patterns at 3.63 GHz when elements 1, 2, 3, 4, 5, 6, 14, 15 and 16 are activated and $B_x = + 100$ degrees and $B_y = - 100$ degrees. ....	171
Fig. 4.79. The simulated $S_{11}$ of the mMIMO when elements 1, 2, 3, 4, 5, 6, 7, 8, 9, 10, 11 and 12 are activated. ....	172
Fig. 4.80. The simulated $S_{21}$ of the mMIMO when elements 1, 2, 3, 4, 5, 6, 7, 8, 9, 10, 11 and 12 are activated. ....	173
Fig. 4.81. The patterns at 3.63 GHz when elements 1, 2, 3, 4, 5, 6, 7, 8, 9, 10, 11 and 12 are activated and $B_x = - 50$ degrees and $B_y = + 100$ degrees. ....	173
Fig. 4.82. The patterns at 3.63 GHz when elements 1, 2, 3, 4, 5, 6, 7, 8, 9, 10, 11 and 12 are activated and $B_x = - 100$ degrees and $B_y = + 0$ degrees. ....	174
Fig. 4.83. The patterns at 3.63 GHz when elements 1, 2, 3, 4, 5, 6, 7, 8, 9, 10, 11 and 12 are activated and $B_x = - 100$ degrees and $B_y = - 100$ degrees. ....	174
Fig. 4.84. The simulated $S_{11}$ of the mMIMO when all elements are activated. ....	175
Fig. 4.85. The simulated $S_{21}$ of the mMIMO when all elements are activated. ....	175

Fig. 4.86. The patterns at 3.63 GHz when all elements are activated and  $B_x = -50$  degrees and  $B_y = +100$  degrees. .... 176

Fig. 4.87. The patterns at 3.63 GHz when all elements are activated and  $B_x = 0$  degrees and  $B_y = +100$  degrees. .... 176

Fig. 4.88. The patterns at 3.63 GHz when all elements are activated and  $B_x = 100$  degrees and  $B_y = +100$  degrees. .... 177

## LIST OF ABBREVIATIONS

<b>MIMO</b>	:	Multiple-Input Multiple-Output
<b>mMIMO</b>	:	massive Multiple-Input Multiple-Output
<b>ECC</b>	:	Envelope Correlation Coefficient
<b>RF</b>	:	Radio Frequency
<b>GBpS</b>	:	Giga Bits per Second
<b>Ipv6</b>	:	Internet protocol version 6
<b>TARC</b>	:	Total Active Reflection Coefficient
<b>MEG</b>	:	Mean Effective Gain
<b>DG</b>	:	Diversity Gain
<b>C</b>	:	System or channel Capacity
<b>TDD</b>	:	Time Division Duplex
<b>FDD</b>	:	Frequency Division Duplex
<b>OFDM</b>	:	Orthogonal Frequency Division Multiplexing
<b>BS</b>	:	Base Station
<b>N<sub>t</sub></b>	:	Number of transmitting antennas

<b>Nr</b>	:	Number of receiving antennas
<b>CSI</b>	:	Channel State Information
<b>ZF</b>	:	Zero-Forcing Filter
<b>SISO</b>	:	Single-Input Single-Output
<b>DOA</b>	:	Direction of Arrival
<b>MUSIC</b>	:	MUltiple SIgnal Classification
<b>BW</b>	:	Bandwidth
<b>SLL</b>	:	Side Lobe Level
<b>FTBR</b>	:	Front To Back Ratio
<b>HPBW</b>	:	Half-Power Beam-Width
<b>BER</b>	:	Bit Error Rate
<b>MSE</b>	:	Mean Square Error

## ABSTRACT

Full Name : Saeed Ahmad Saeed Haydhah  
Thesis Title : Design of A Pattern Reconfigurable Massive MIMO for 5G  
Technology  
Major Field : Electrical Engineering  
Date of Degree : December 2019

The amounts of data rates is increasing sharply with time. In addition, the number of connected devices to the network is increasing sharply with time. 5G networks with the use of advanced technologies such as the use of massive MIMO systems, and with the use of developed wireless standards will be able to serve this huge number of data rates and connected devices to the network. Hence, contributions to 5G technology is very important for the future communication networks. Therefore, one pattern reconfigurable 4X4 massive MIMO slot-based antenna at 3.6 GHz with a size of 21 X 21 X 2  $cm^3$  and with an enhanced performance compared to previous mMIMO designs was proposed and presented in the work of this thesis. The used single element in the mMIMO is a compact and low-profile pattern reconfigurable slot-based antenna with 8 different directional patterns at 3.6 GHz.

In addition, and in the direction of supporting 5G technology, a new compact and low-profile pattern reconfigurable antenna for IoT applications was proposed and presented. The size of this antenna is like the size of a credit card, such that it is suitable to be used for some specific applications where it is required to put the antenna in the pocket of a worker in a factory for example. The resonant frequency of the antenna is 868 MHz with three different patterns and with an overlapped bandwidth of 10 MHz; which is enough for IoT applications. The ECC between the three patterns are well below 0.5. The antenna is composed of two slots and one monopole, and it was concluded that the slot radiating elements are less sensitive to hand and plastic casing effects compared to monopole radiating elements.

In addition, one compact and low-profile pattern reconfigurable slot-based antenna with 8 different patterns at 2.3 GHz, and 8 different patterns at 3.7 GHz was proposed and presented. This antenna can be used to localize the locations of oil wells in a large area.

Finally, a new, compact and low-profile pattern reconfigurable slot-based antenna was proposed for future drones. The antenna has 4 different patterns at 3.7 GHz and 4 different patterns at 5.2 GHz.

All the antennas designed in this work supports future 5G technology bands and applications, and all of them are controlled electrically. The used substrate for all antennas is FR-4 substrate.

## ملخص الرسالة

الاسم الكامل: سعيد أحمد سعيد هيضه

عنوان الرسالة: تصميم نظام مايمو ضخم مع أنمطة إشعاعات مختلفة لتقنية الجيل الخامس.

التخصص: هندسة كهربائية

تاريخ الدرجة العلمية: ديسمبر 2019

كميات معدلات البيانات في زيادة حادة مع مرور الوقت. وعدد الأجهزة المتصلة بالشبكة يزداد أيضا زيادة حادة مع مرور الوقت. ستنمك شبكات الجيل الخامس، التي تستخدم التقنيات المتقدمة مثل استخدام أنظمة MIMO الضخمة، ومع استخدام المعايير اللاسلكية المتقدمة، من خدمة هذا العدد الهائل من معدلات البيانات والأجهزة المتصلة بالشبكة. و بالتالي، تعد المساهمات في تقنية الجيل الخامس مهمة جدا لشبكات الاتصال المستقبلية. لذلك، تم اقتراح نظام MIMO ضخم مع أنمطة إشعاعات مختلفة عند 3.6 جيجا هيرتز ومع أداء محسن مقارنة بتصميمات MIMO سابقة، تم تقديمه وعرضه في هذه الأطروحة. إن العنصر الفردي في هذا النظام MIMO الضخم هو عبارة عن هوائي مكون من فتحات تم حذفها من أساس الهوائي المصنوع من النحاس، وهذا الهوائي له ثمانية أنمط إشعاعية تتجه إلى اتجاهات مختلفة عند التردد 3.6 جيجا هيرتز. هذا الهوائي تم تصميمه مع حجم صغير وارتفاع منخفض.

بالإضافة إلى ذلك، وفي اتجاه دعم تقنية الجيل الخامس، تم اقتراح وتقديم هوائي جديد بحجم مناسب مع القدرة على إعادة تشكيل الأنمط الإشعاعية وقد صمم ليعمل في تطبيقات إنترنت الأشياء. حجم هذا الهوائي هو مثل حجم بطاقة الائتمان بحيث يكون مناسباً لاستخدامه في بعض التطبيقات التي يحتاج فيها عامل في مصنع مثلا أن يضع هذا الحساس في جيب القميص. التردد لهذا الهوائي هو 868 ميجا هيرتز مع ثلاثة أنمط إشعاعية مختلفة ومع عرض نطاق ترددي متداخل لهذه الأنمط الثلاثة قدره 10 ميجا هيرتز، وهذا كافي لتطبيقات إنترنت الأشياء. التشابه بين الأنمط الإشعاعية هو أقل بكثير من 0.5. يتكون الهوائي من فتحتين تم قطعها من أساس الهوائي النحاسي ومن هوائي أحادي القطب. وقد استنتجنا أن إشعاعات الفتحات هي أقل تأثراً بقرب اليد وبالغلاف البلاستيكي حول الهوائي إذا ما قورنت بالهوائي أحادي القطب.

بالإضافة إلى ذلك، تم اقتراح وتقديم هوائي جديد بحجم صغير ومظهر منخفض وهو يحتوي على 4 فتحات مقطوعة من أساس الهوائي النحاسي. هذا الهوائي قادر على إشعاع 8 أنمط مختلفة عند التردد 2.3 جيجا هيرتز و 8 أنمط مختلفة عند التردد 3.7 جيجا هيرتز. يمكن استخدام هذا الهوائي لمعرفة أماكن تواجد النفط في مناطق واسعة.

وأخيرا، تم اقتراح هوائي جديد ومناسب الحجم يحتوي على أربع فتحات في الأساس النحاسي ويمكن استخدامه في تطبيقات الدرونز المستقبلية. هذا الهوائي قادر على إشعاع 4 أنمط مختلفة عند التردد 3.7 جيجا هيرتز و 4 أنمط مختلفة عند التردد 5.2 جيجا هيرتز.

تدعم جميع الهوائيات التي صممت وعرضت في هذه الأطروحة نطاقات وتطبيقات الجيل الخامس المستقبلية، ويتم التحكم بها جميعا كهربائيا. كما أن المادة البلاستيكية المستخدمة في جميع الهوائيات المصممة في هذه الأطروحة هي مادة بلاستيكية لها سعر منخفض لتخفيض تكلفة تصنيع هذه الهوائيات.





# CHAPTER 1

## INTRODUCTION

As presented in [1], it is expected that the global mobile data traffic by 2022 reaches 77 Exabytes per month. Also, the number of mobile connected devices will increase to 11.6 billion devices, and Machine-to-Machine (M2M) devices will increase to 7.8 billion devices by 2022. Fig. 1.1 shows the global mobile data traffic in the time period from 2017 to 2022.

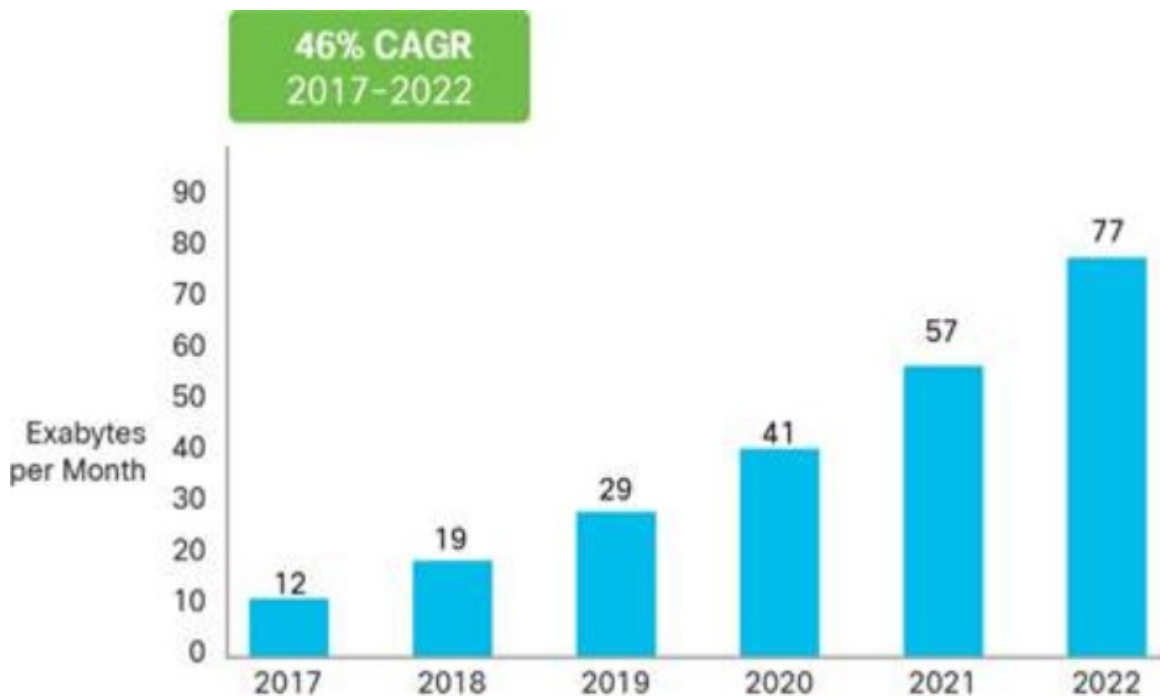


Fig. 1.1. Global mobile data traffic from 2017 to 2022.

The average global mobile connection speed is expected to exceed 20 Mbps by 2021 [1]. It is expected also that 71% of total mobile connections will be 4G connections and three-fourths of total mobile traffic will be for 4G technology by 2022. On the other hand, 5G technology will occupy 0.2% of connections and 12% of total traffic by 2022. Fig. 1.2 shows the global mobile traffic by connection type in the time period from 2017 to 2022.



Fig. 1.2. Global mobile traffic by connection type.

In addition, it is expected that 73% of whole global mobile devices will have the capability to be connected to IPv6 mobile network. Also, 50% of all IP traffic will be WiFi, 30% will be wired, and 20% will be mobile.

Many factors contribute to this growth of mobile data traffic. For example, the requirement of having smarter mobile devices will cause the mobile data traffic to increase. In addition, the network is becoming smarter as it is evolving from 2G to 5G; 5G networks provides much higher bandwidth (more than 1 Gbps), faster connectivity on the move, broader coverage, ultra-low latency and higher security. Also, the adoption of Machine-to-Machine (M2M) communications, Internet of Things (IoT), the coming wearable devices, and supporting many other applications in 5G will contribute to the increase in mobile data traffic. Furthermore, the expanding role and coverage of WiFi offload will contribute to the growth of mobile data traffic. Also, new mobile applications and requirements will be identified and will require more data traffic; for example, Virtual Reality and Augmented Reality require huge amount of data rates to be supported. In addition, the speeds of mobile networks are improving, and they contribute to the growth of mobile data traffic. Also, commercial forces will contribute to the growth of mobile networks such that more commercial benefits will be achieved.

5G technology will provide the capability of communications with huge amounts of data rates. So, it is important to work in research to enhance this technology. Massive Multiple-Input Multiple-Output (mMIMO) systems help a lot in achieving the goals of 5G technology. Beamforming is

required in 5G technology since radiated patterns from base stations to users will be directed and dedicated to users, and these patterns are required to follow the moving users. Therefore, assessing the Direction of Arrival capabilities of the massive MIMO is important and this will contribute to achieve the goals of 5G technology also. This chapter presents some introductions about the wireless communication evolution, 5G technology, MIMO antennas, massive MIMO antennas, and direction of arrival estimation.

## **1.1 Wireless Communication Evolution**

The first-generation mobile technology (1G) was introduced in 1981. The latest technology used for 1G was the Nordic Mobile Telephone. At that time, scientists worked a lot on improving telecommunication systems such that user reliability will be enhanced, wastage of precious time will be reduced, and users will be able to communicate and transport data with high encryption. In 1991 and in Finland, the second generation (2G) technology was initiated by Global System for Mobile Communications (GSM). It is good to mention that the most important improvements of 2G were the introductions of Short Message Service (SMS), the multimedia messaging service, and picture messages. 2G is digital, while 1G was analog. After that, 2.5G and 2.75G were introduced. 2G technology is available and used in many countries because of its commercial importance. However, the spectral efficiency of the new access technologies in GSM is higher than that available for 2G technology. This is due to many new functionalities introduced in GSM such as Dynamic Frequency and Channel Allocation (DFCA) and Orthogonal Sub-channel (OSC) functionalities.

General Packet Radio Service (GPRS) technology was used in 2.5G technology; GPRS is implemented in the circuit switching domain and in the packet switching domain. The most important factor of making the third-generation networks to be arisen for GSM is the introduction of GPRS. The introduction of 8PSK in 2.75G made the Enhanced Data rates for GSM Evolution (EDGE) technology to be arisen also in 2003 in United States. Data rates were improving dramatically by the introduction of this mobile phone technology which is a digital technology. Wireless communication data rates can reach to 2 Mbps in 3G. So, in order to be able to serve this high data rate, the access network and the core network have to be improved and developed. The access network and the core network are shown in Fig. 1.3. 3G mobile telecommunications is a generation of standards for mobile telecommunication services and mobile phones that agrees with

the International Mobile Telecommunications-2000 (IMT-2000) disclaimers by the International Telecommunication Union. Application services including video calls, wide-area wireless voice telephone, mobile TV, and mobile Internet access can be used in this mobile environment.

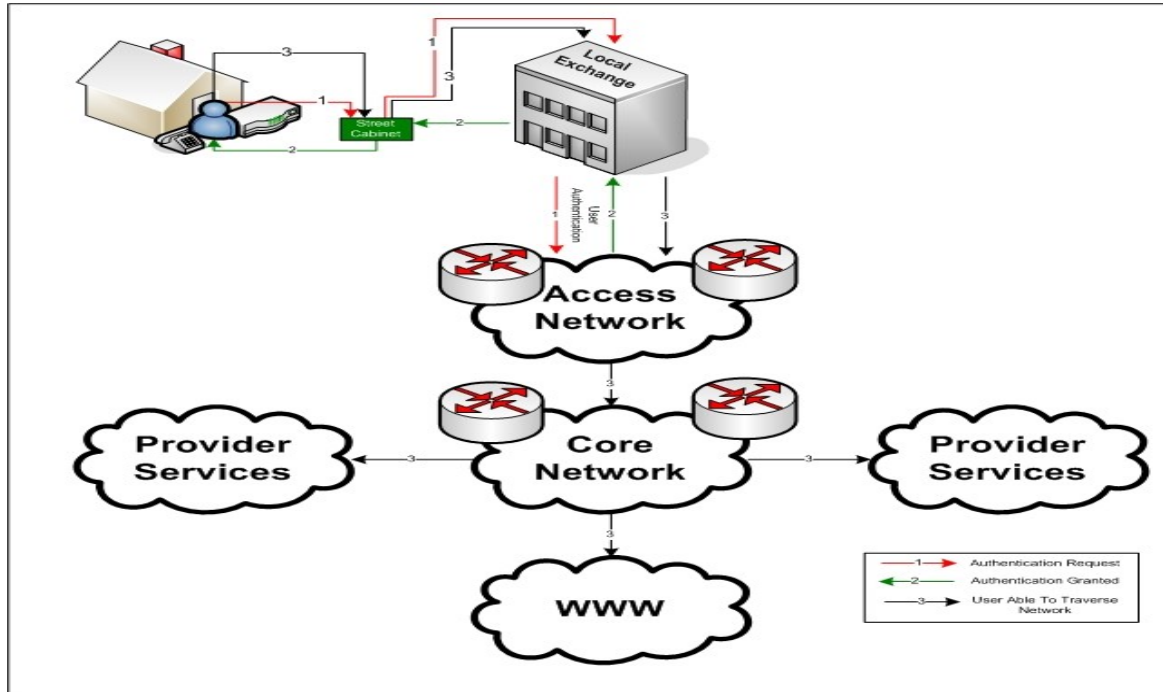


Fig. 1.3. The access network and the core network.

4G was the wireless cellular standards in 2009. This technology is supported by the International Telecommunication Advanced (IMT-Advanced) technology at a maximum speed (for 4G technology) of 1 Gbps for low-mobility communications and of 100 Mbps for high-mobility communications. The first Long-Term Evolution (LTE) service in the world was achieved on December 14, 2009 in Oslo (a Huawei system) and Stockholm (Nokia, Ericsson, and Siemens network systems).

Fifth-generation (5G) mobile networks is the name of the next generation of mobile telecommunication standards after the 4G/IMT-advanced standards and this area is under study since 2011. 5G technology will be deployed in 2020s as per many expectations. In 5G technology, users will be provided with larger data rates by 100 times and larger bandwidths by 1000 times. Therefore, the large amounts of applications of the coming mobile networks will be supported by this technology. Many new technologies will be there for 5G networks to support the users' requirements; for example terahertz band can be used for mobile communications. The 5G wireless mobile Internet networks will be supported by Orthogonal Frequency-Division Multiplexing (OFDM), Large Area Synchronized Code Division Multiple Access (LAS-CDMA), UltraWide

Band (UWB), Network-Local Multipoint Distribution Service (LMDS), Multicarrier Code-Division Multiple Access (MC-CDMA), and Internet Protocol version 6 (IPv6). 4G and 5G technologies use the same IPv6. A comparison table between the different generations is shown in table 1.1.

Large Area Synchronized Code Division Multiple Access (LAS-CDMA) is a technology which will improve the spectral efficiency and allowable moving speed used for superior mobile application support, and it will enhance the channel throughput, and reduce the delay. Multicarrier Code-Division Multiple Access (MC-CDMA) is a multiple access scheme in which the system is allowed to support multiple users instantaneously by using OFDM telecommunications.

**Table 1.1 Comparison between the different generations as shown in [2].**

Generation	Definition	Throughput/speed	Technology	Time period	Features
1G	Analog	14.4 Kbps (peak)	TACS, AMPS, NMT	1981 to 1990	Voice only is used by wireless phones.
2G	Digital narrowband circuit data	9.6/14.4 Kbps	CDMA, TDMA	1991 to 2000	Multiplexing can be used to accommodate many users in a single channel. Data with voice can be used by cellular phones.
2.5G	Packet data	171.2 Kbps (peak) 20-40 Kbps	GPRS	2001 to 2004	Internet was used by many people. Streaming and multimedia services begin to grow. Web browsing becomes supported by phones.
3G	Digital broadband packet data	3.1 Mbps (Peak) 500 – 700 Kbps	CDMA 2000 (1* RTT, EVDO)	2004 to 2005	Streaming and multimedia services were supported.

			UMTS, EDGE		Portability and universal access were supported.
3.5G	Packet data	14.4 Mbps (peak) 1-3 Mbps	HSPA	2006 to 2010	Higher data rates were supported by providing higher speeds and throughputs.
4G	Digital broadband packet, all IP, very high throughput	100 – 300 Mbps (peak) 3 – 5 Mbps 100 Mbps (Wi-Fi)	Wi-Fi, WiMAX, LTE	Now, (transitioning to 5G)	Roaming is used in whole world. More portability. HD capabilities provided to new phones. Higher speeds and high definition streaming were provided.
5G	Not yet	Gigabits	LAS- CDMA, UWB, OFDM, MC- CDMA, Network- LMDS	Soon (probably 2020)	No 5G technology deployed now. Very high speeds and better utilization of bandwidths.

Network-Local Multipoint Distribution Service (LMDS) is a wideband wireless access technology operated for digital television transmission originally, and it was used for fixed wireless systems, it is operating across 26 – 29 GHz. The throughput capacity and the reliable distance of the link for this technology depends on the used method of modulation and on the common radio link constraints. Distance for this technology is around 2.4 Kms due to attenuation constraints.

In order to define the Internet protocol version 6 (IPv6), it is required to explain first the communications protocols. A communication protocol is a group of rules which allow two or more entities of a communication system to transmit information through any kind of variation of a physical quantity. The rules, syntax, possible error recovery methods, semantics and

synchronization of communication are defined by the protocol. Communication systems use well-defined formats for exchanging different messages. Communication protocols are agreed on by the involved parties. In other words, protocols are to communication systems like the programming languages are to computers. These protocols provide also the identification and the location for computers and devices connected to networks and traffic ways across the Internet. Now, IPv6 is the most recent version of the Internet protocols and it will be used as Internet standards in 2017. Each device connected to the Internet has a specific IP address such that its identification and its location are known. With the fast growth of the Internet, the number of required addresses has increased dramatically in a way that the addresses provided by IPv4 are not able to cover the demand of new addresses. IPv6 provides  $3.4 * 10^{38}$  addresses which are much much more than those provided by IPv4.

## **1.2 5G Technology**

5G is a very important technology because of the coming very high traffic rates of voice, video streaming and data. Also, the available 3G and 4G technologies will no longer be able to handle the requirements of the Internet data traffic. Now, the background of the cellular system has transformed into a global set of interconnected networks because of the generation changes happened by mobile technologies. By 2020, 5G will be used and above 9 billion users will be supported by video and voice streaming in addition to many advanced communication services. Also, billions of devices will be connected to each other. In 5G, radical network design will be used in installing machine-type communication (MTC). Variable operational parameters and advanced support applications will be used in 5G networks such that greater elasticity will be provided for the installed services. 5G is composed of many developed network technologies and it will provide the capability to exchange data every time, everywhere, by everyone and everything, and hence individuals, businesses, society and the technological environment will be benefited from this technology since the used bandwidth will be of unlimited access for carrying information. Many activities have started in 2016 such that machinery and equipment of 5G will be commercially available in 2020, and a lot of work is required to develop equipment, machinery and devices used for this new technology. In addition, this technology will be built on the previous developed telecommunication systems. The complementary technologies; a combination of cloud and core technologies, used in the available radio access will be employed also in 5G. In addition, different

types of equipment with different operational requirements will be employed as well in order to be able to handle the very high data traffics in this technology. In order to understand the previous sentence very well, let's introduce the radio access network which is related to a mobile telecommunication system, and uses the radio access technology. This radio access network is available between a device such as a computer, a mobile phone or any other remotely controlled machine and the devices in the core network. On the other hand, we have the cloud radio access network which will be used for future wireless technologies, and it utilizes the advantages of the found advances in optical, wireless and IT communication systems. It uses the recent standards of CPRI, Dense Wavelength Division Multiplexing technology or low cost Coarse, and mmWave technology to provide transmission of baseband signal across long distances, and hence the deployment of large scale centralized base station can be attained. Also, it uses latest Data Centre Network Technology in order to provide a high reliable and a low-cost interconnected networks with large bandwidths and low latency. Also, it utilizes open platforms such that it can be reprogrammed, and real-time virtualization technology used in cloud computing to obtain dynamic shared resource allocation and have multi-vendor, and multi-technology environments. CPRI is a good industry cooperation which defines the public specifications for the key internal interface of radio base stations between the Radio Equipment and the Radio Equipment Control. Real-time virtualization technology is like allowing many operational systems to work on the same computer.

The required performance levels for 5G technology to meet what is expected from it are shown in Fig. 1.4. Fig. 1.5 shows a schematic diagram of next generation 5G wireless network.

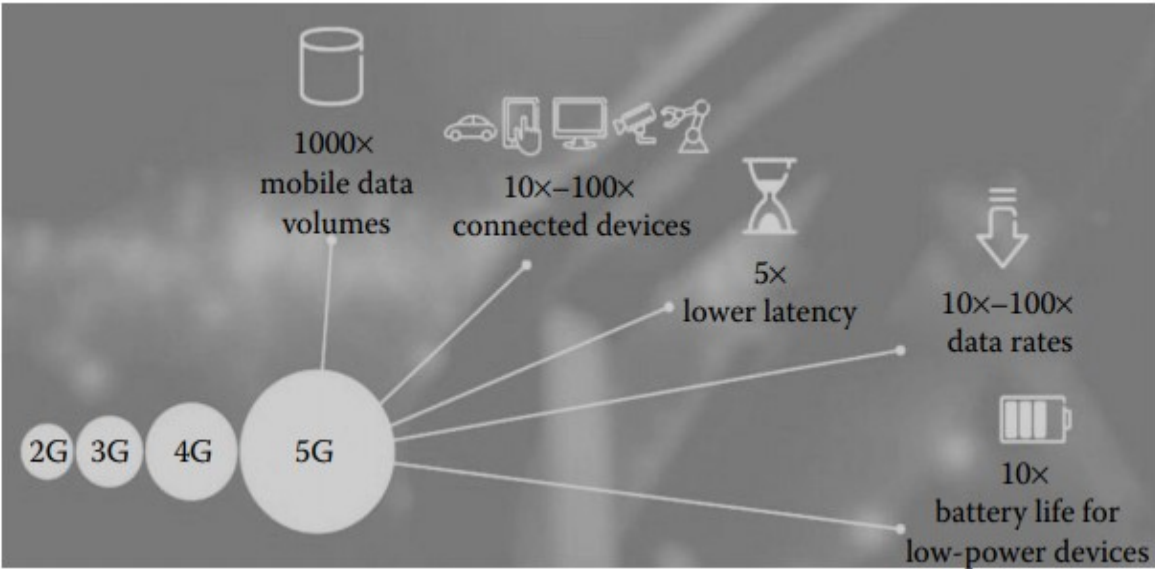


Fig. 1.4. The estimated performance levels of 5G.



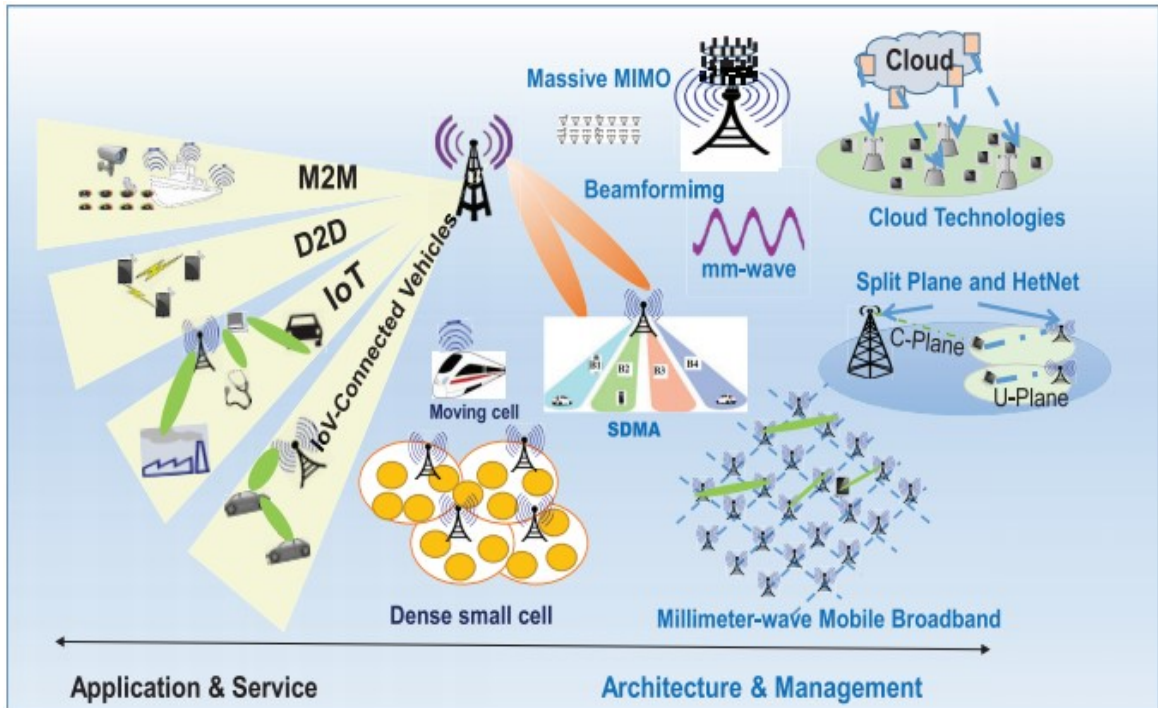


Fig. 1.5. A schematic diagram of next generation 5G wireless networks.

As can be shown from Fig. 1.4, the required performance levels of 5G technology are:

1. Typical user data rate will increase by 10 – 100 times.
2. Battery life will be longer for low-power devices by 10 times.
3. Number of connected devices will increase by 10 – 100 times.
4. End-to-end latency will be reduced Five times.
5. Mobile data volume per area will increase 1000 times.

This technology will not be in isolation from other technologies, and this 5G technology will be required to allow huge amounts of connectivity. This coming technology will require the study of many important points such as the long-term sustainability, security and cost. Now, the comprehensive conditions for 5G are not set yet, but even though, it is obvious that this technology can be implemented because of the flexibility in accommodating thousands of applications. 5G technology will be developed on many parameters such as:

1. Data integrity which is the assurance of the accuracy and consistency, and the maintenance of data over its entire life-cycle.
2. Latency.
3. Smart communication.
4. Traffic capacity; the amount of links in the channel.

5. Data throughput.
6. Energy consumption.
7. Technology convergence; which is the tendency towards performing the tasks of the developed systems as the technology changes, and as different technological systems evolve.

5G technology is more advanced than 4G technology because of developments in technologies as well as developments in wireless standards. The five potential advances which can change component design and the architectural design for 5G technology are:

1. Device-centric architecture.
2. Millimeter wave (mmWave).
3. Massive multiple-input multiple-output (MIMO) antennas.
4. Smarter devices.
5. Machine-to-machine (M2M) communication.

### **1.2.1 Device-Centric Architecture**

In 5G technology, different BS architectures for cellular systems may be used. The concepts of data and control channels, and the concepts of uplink and downlink need to be reconsidered in order to have better information about the traffic routes inside the network which have different purposes and preferences to go to different sets of nodes. Inside the radio access system, the hardware parts of cells are very important factors for the cellular designs in general. A device can be served by having a downlink connection, and then an uplink connection will carry data and control traffic signals to the BS which commands the cell. Recently, it was mentioned that the cell-centric structure will be changed by different trends:

- a. The BS density is increasing quickly, and this increase is determined by the rise of heterogeneous systems. Real changes may take place in 5G technology because of the use of system densification. For example, the organization of BSs with too many different transmitted powers and coverage areas requires a decoupling of uplink and downlink in a way which allows the signaling data to be communicated between different set of nodes.
- b. There will be different propagation attributes in the same framework because new frequency bands will be used in order to increase the used spectrum. In this case, phantom cell idea was proposed in which the control and information planes will be different; in

other words, the control data will be transmitted from nodes with high power and at microwave frequencies, while the information data will be transmitted from low power nodes and at mmWave frequencies.

- c. The idea called incorporated baseband was proposed to be used in the cloud-based wireless access systems. In this work, the network topology will be virtualized, in other words, an actual equipment can be connected to a virtualized network node which is in a different physical location from the equipment in the network. For instance, the equipment parts will be in a specific area, and it can be connected to different nodes depending on some measurements specified by the system administrator.
- d. The radio access system can be affected by the use of smarter devices. Especially, smart caching calls and device-to-device (D2D) communications because it will be required to redefine some designs since the center of gravity will not be at the center of the system while it will move to the outskirts regions.

Furthermore, the cell-centric architecture will be developed into a device-centric one. A given device should be capable to communicate many data signals using some heterogeneous nodes. These nodes are integrated with the given device. The objectives of these nodes should be custom-made for the used device in a specific communication session. Hence, the ideas of downlink/uplink and an information/control channel will be studied again, these ideas are shown in Fig. 1.6 for 5G technology. It is clear that a big change in the architectural design is required.

In other words and as an example, the devices which are close to each other will be enabled to communicate to each other without the use of the BS, and Fig. 1.7 shows some D2D communication scenarios. This type of communications will be required to have lower latency, better energy efficiency, better interference management and better scalability in order to be used in 5G technology, and these are the challenges facing the 5G technology [3].

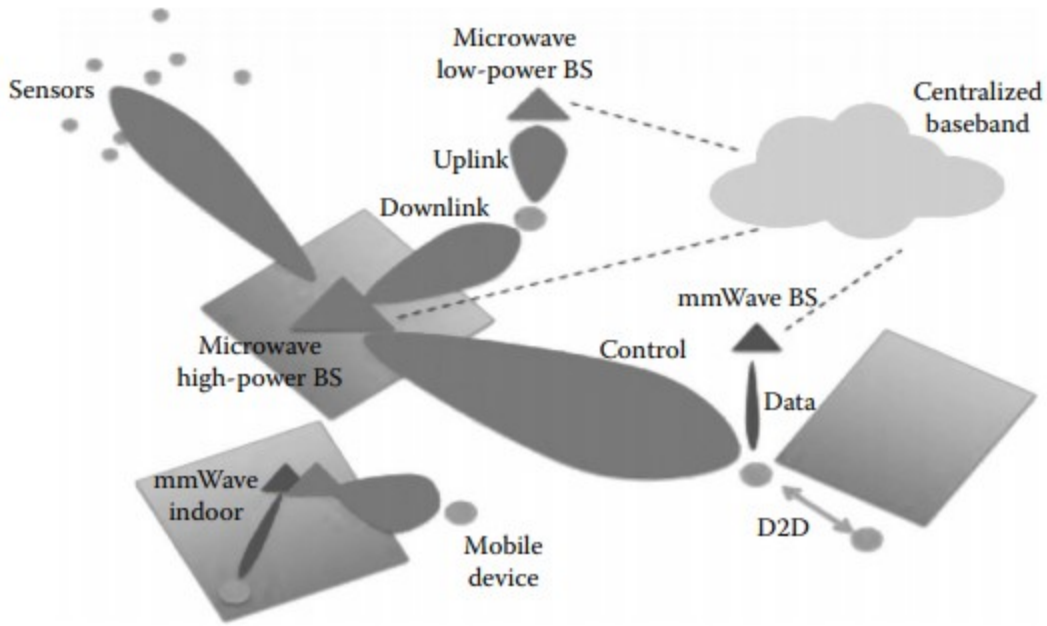


Fig. 1.6. Device-centric architecture example, [2].

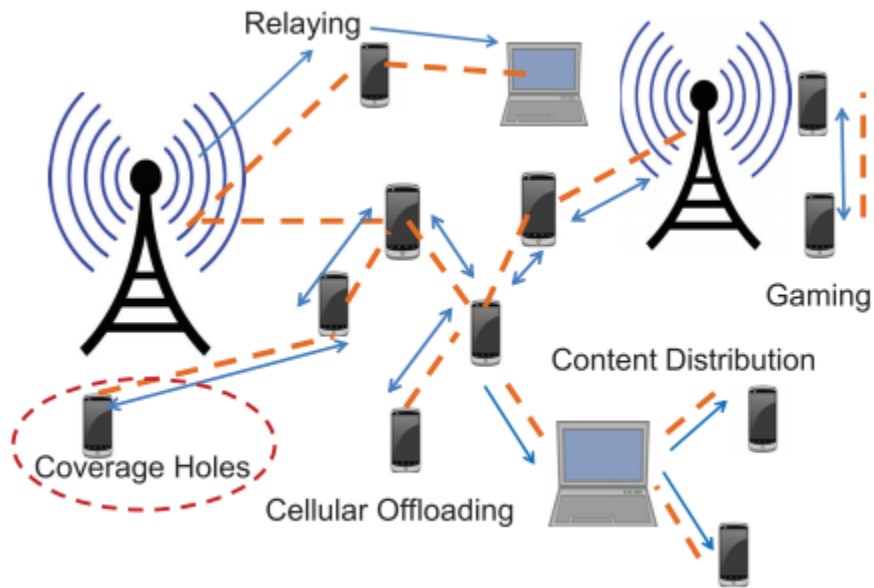


Fig. 1.7. D2D communication scenarios, [3].

## 1.2.2 Millimeter Wave (mmWave)

The fast increase in the number of smartphones and in mobile data growth with the shortage in bandwidths presents a big challenge for future communication networks. Nowadays, the 600 MHz microwave spectrum available for cellular applications is used by all operators. It can be seen that there is a need for a wider microwave spectrum for modern communications. Hence, two ways can be used to increase the microwave spectrum for cellular communications:

- By refarming the spectrum. 80 MHz with high cost can be added by this method. It was used when the TV spectrum was used for rural broadband access applications.
- To utilize the spectrum as much as possible using different techniques, like using cognitive radio techniques. The problem with this method is that the occupant who is not very well ready to share the used channel will stop the spectrum efficiency for more users.

So, the best approach is to double the current cellular bandwidth at the microwave frequencies. The mmWave spectrum available for cellular communication is from 3 to 300 GHz (as shown in Fig. 1.8) and it can be used also to enhance the bandwidth. The major difference between the mmWave and microwave frequencies is the blockage sensitivity; the path loss exponent for line-of-sight propagation is 2, and for the non-line-of-sight propagation is 4 in addition to more power losses. It is required for mmWave research to study the effects of blockages, and to come up with more precise channel models. It is required also to study the effect of enablers such as high-density infrastructure and relays.

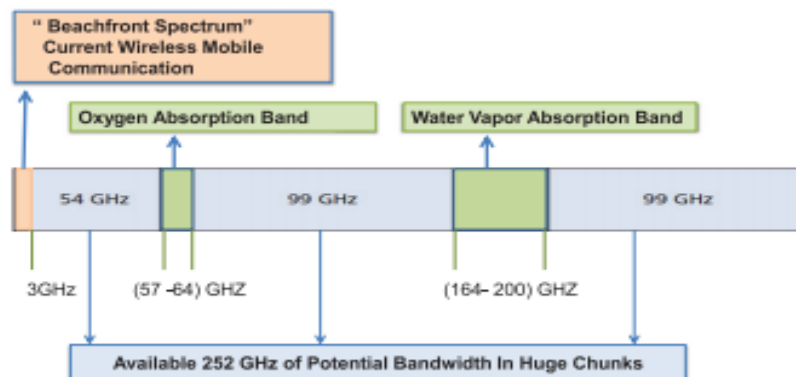


Fig. 1.8. MmWave spectrum availability in 3 – 300 GHz.

The antenna arrays are very important to be used in the mmWave systems. The effect of interference is reduced using adaptive arrays with narrow beams. Important communications will be performed by acceptable array gains which will require new random-access protocols. These protocols consider that the antenna arrays emit powers to specific directions and receivers will receive powers from specific directions as shown in Fig. 1.9. It is required that when antenna beams were blocked by objects, people or by the user's body, adaptive array-processing algorithms can respond quickly. Hardware used for mmWave systems will also need some modifications.

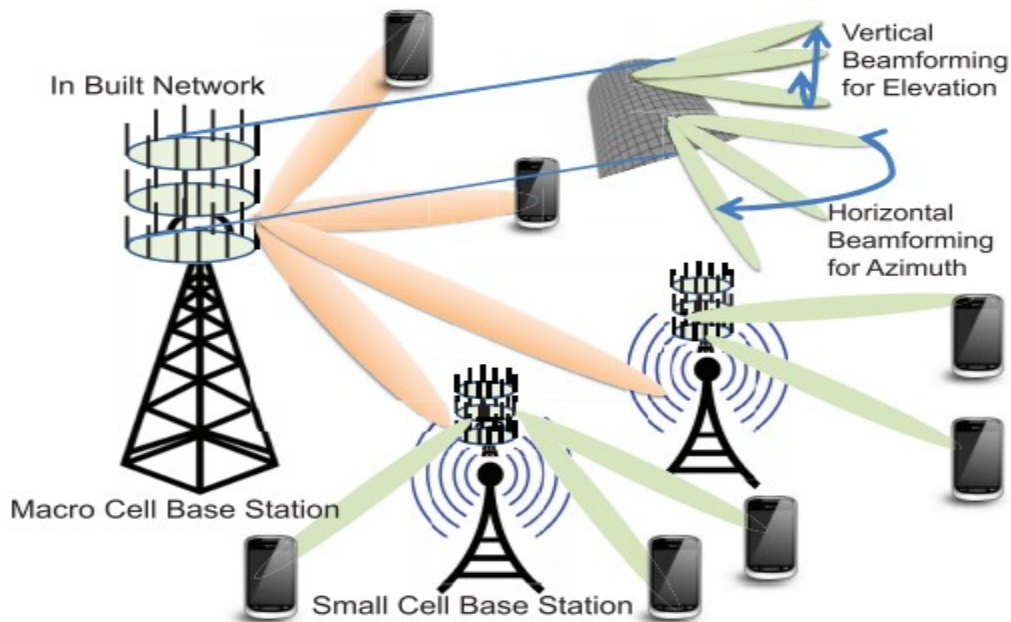


Fig. 1.9. Massive MIMO and beamforming.

It is noted that mmWave is a very important technology for the implementation of 5G network because it could provide very high data rates with much different user experience. Therefore, many changes are going to take place in the system for the implementation of mmWave.

It is important to be able to have a model for the channel for mmWave applications. If the channel model is known, then new architectural techniques, different multiple access and novel methods of air interface will rise up. It was shown in [3] that the channel can be characterized by the following:

a. Propagation loss:

It is shown by the loss equation, shown in [3], that the propagation loss increases sharply for higher frequencies. However, increasing the frequency will make the wavelength to be decreased and hence we can have more and more antennas in a communication system; in the BS for example,

which will enhance the spatial diversity in the communication system and hence more data rates can be transmitted. Also, the beams for higher frequencies is narrower than those at lower frequencies, and hence the spatial diversity will increase in this case also. The attenuation happening by this propagation loss can be good if microcells are to be used because the interference between cells will be reduced.

b. Penetration and LOS (Line-of-Sight) communication:

It is required to study the impact of the environment on the mmWave signals. The behavior of the signals through and around common structures, foliage and human beings should be known. Diffraction, scattering, penetration and reflection of mm-waves in different possible environments should be studied and these studies lay the foundation for 5G network deployment. The indoor and outdoor environments should be studied. It was shown in [3] that there is a good isolation between the mm-waves in indoor and outdoor environments because little energy goes through glass and open doors, and this means that the energy will be confined in the required areas, and this is a good point. In addition, human body causes large attenuation for mm-waves, and moving bodies cause shadowing for these mm-waves, and the solution is to transmit beams with wider beamwidths. Small cells are used now with around 200 meters such that we make use of large attenuation drawback of mm-waves. Fig. 1.10 shows the massive and dense deployment for LOS communication.

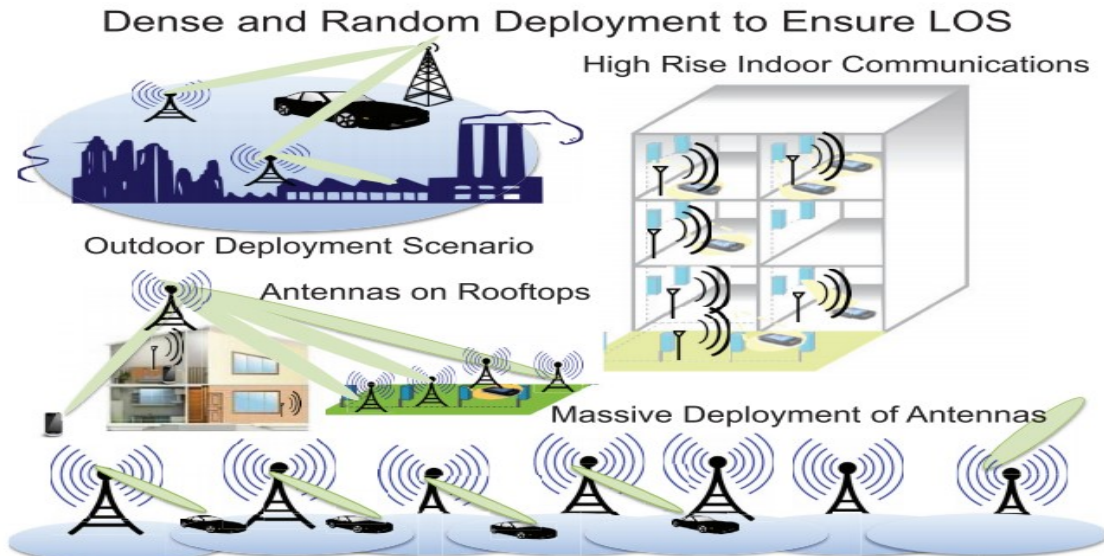


Fig. 1.10. The massive and dense deployment for LOS environment.

c. Multipath and NLOS:

Multipath is the effect of signal reception in antenna by more than one path. It is very important to mitigate NLOS problem, and this can be done by understanding multipath well. In other words, it is important to know what will happen if the links were partially LOS or NLOS. For example, more multipath components are detected during rain compared to clear, dry weather conditions. Building corners, edges and human activities cause shadowing. It was found also that wider-beamwidth antennas provide accurate estimation of received signals, and on the other hand, smaller beamwidth antennas provide more spatial diversity. In order to mitigate NLOS problem, equalizers will be required to be used, and hence high latency, increased power consumption and low data rates will be there as challenges for 5G technology. Fig. 1.11 shows the multipath and NLOS communication.

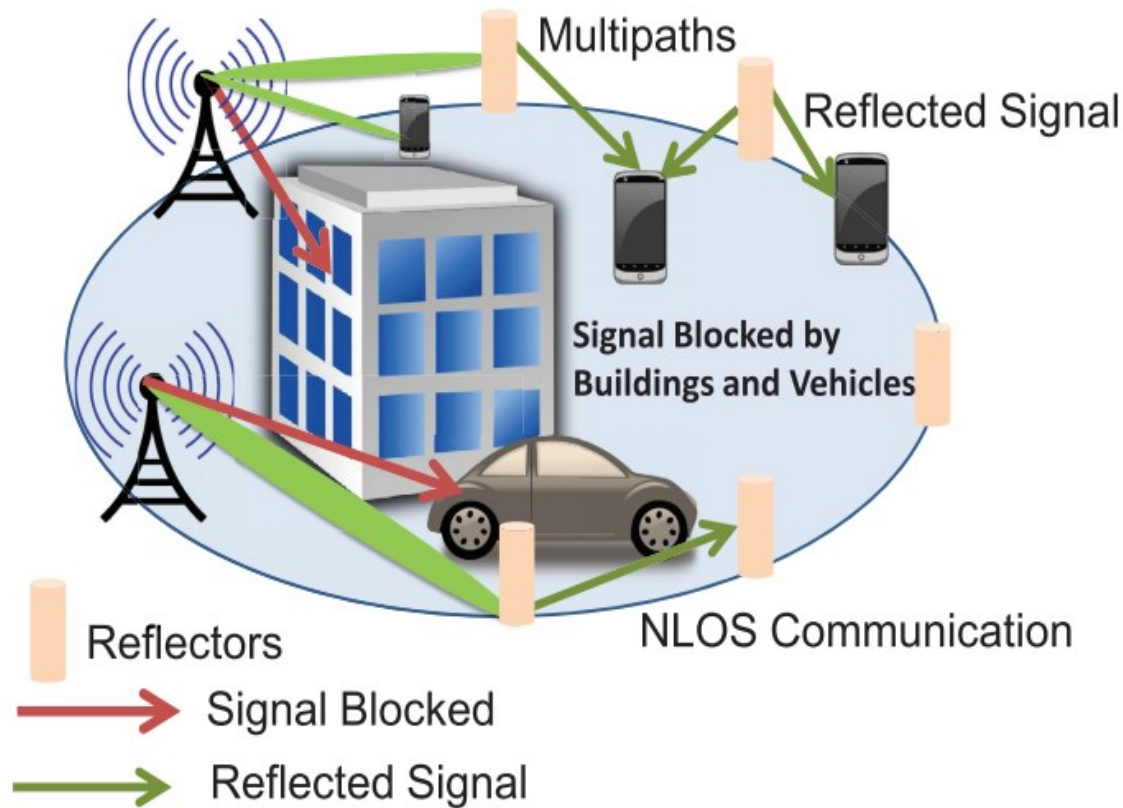


Fig. 1.11. Multipath and NLOS communication.

d. Doppler:

Doppler impact is characterized by the carrier frequency and mobility. The received incoming waves have different shift values, and as a result of that, a Doppler spread took place. The included



Doppler time-selective fading can be alleviated by packet sizing and suitable coding over coherence time of the channel. Also, Doppler spread can be reduced by reducing the angular spread of the narrow beam, it can be seen that Doppler effect is not a big challenge for 5G technology.

### **1.2.3 Massive Multiple-Input Multiple-Output Antennas (mMIMO)**

This MIMO refers to the large scale MIMO systems in which the number of BS (Base Station) antennas are much larger than that of connected devices per signaling resource. With this large number of antennas in BS, channels can be provided to different devices. Massive MIMO is a large opportunity for 5G because:

- a. It can be scaled up at any node. These MIMO systems used in 5G technology are different than those used in 4G technology which cannot be scaled. The cells cannot be sectorized more for 4G technology because of the following :
  - i. The space for heavy azimuth directional antennas is limited.
  - ii. The number of antennas in the MIMO system of the user is limited to the size of the users' cell phones. As a result of that, the angle spread of propagation is limited.

On the other hand, the number of antennas in massive MIMO systems available on BSs is nearly with no restrictions, given that the time-division duplexing is chosen to be used such that the channel estimation by uplink pilots will be empowered.

- b. New deployments and architectures will be used. For example, arrays of antennas with low-gains will replace the macro BSs, in addition to more deployments in rural areas which can be used. In addition, the same massive MIMO standards, which are used for assembled antenna arrays, can be applied to many distributed deployments in a city or a campus; these distributed antennas will serve huge number of users.

However, massive MIMO systems face many research challenges. For example, the number of orthogonal training sequences is limited due to user movement and critical channel estimation. This limit in the number of training sequences is available because training time will be required and this time is a part of the time slot reserved for a user. Massive MIMO can be designed with low-cost hardware, low power, and each antenna can work semi independently. The cost-effectiveness of massive MIMO is under investigation also.

The massive MIMO in BSs is shown in Fig. 1.9. The massive MIMO has a huge number of antennas, and hence spectral and energy spectral will be enhanced. The wavefronts of the massive MIMO will add up constructively to one direction, and destructively to the not-required direction, and hence narrow beams can be directed to the required direction. Therefore, spatial multiplexing took place and hence the capacity will increase by several magnitudes. Time division duplexing is preferred to be used with massive MIMO in order to avoid the complexity associated with channel estimation and channel sharing in frequency division duplexing [3].

#### **1.2.4 Smarter Devices**

5G will help in having smarter devices. The concentration here is on three different technologies which are: advanced interference rejection, D2D, and local caching.

- a. The local communications can be taken care of by the use of D2D. Other technologies like Bluetooth or WiFi technologies can be used to obtain local high data rates. The use of D2D can be justified by showing the need of applications where a combination of local and nonlocal data, or a combination of high data rate and low latency are required. Applications with low latency can be implemented using D2D technology, especially when future systems requiring radio virtualizations and baseband centralization will be used. D2D is under study using the Third Generation Partnership Project (3GPP) as a 4G technology, and this test is available in limited areas for the public safety.
- b. Caching huge amounts of data at the end of wire-line system before the wireless node is applied to delay-tolerant traffic, but it is not applied for the voice centric systems. Caching could be used in future for data-centric systems. Cell phones can be implemented with no huge amount of memory because of this technology. Local caching is a good choice to be used at the radio access system edge and cell phones, especially when mmWave and D2D are going to be used.
- c. The D2D capabilities will be large. Future cell phones might have varying form factors. Also, devices will include many antennas and hence they will be able to reject interference actively using spatial multiplexing and beamforming.

### 1.2.5 Important Support for M2M Communications

M2M communication is very important technology in 5G and it will require fulfilling three different important factors which are related to different types of low data rate services: supporting huge number of low rate devices, low latency transfer of data, and sustaining a negligible data rate in all conditions. To achieve these requirements in 5G, new techniques and ideas at the component and architectural levels are required to be added.

Wireless communication is a good commercial opportunity and to utilize this opportunity very well, the huge amounts of services should be provided with the following prerequisites:

- a. A huge number of devices should be possible to be connected to networks.
- b. Providing very high reliable links.
- c. The ability to operate in real-time and having the feature of low latency.

### 1.3 MIMO Antennas

The huge increase in the data rates in wireless communications requires the evolution of MIMO systems, and to increase the data rates more, massive MIMO systems can be used. MIMO stands for multiple input multiple output, and they are the most important reasons for the 3G and 4G wireless systems to be available. Massive MIMO are used for the coming 5G systems. By the use of MIMO systems, data rates increase, and the block diagram for a MIMO system is shown in Fig. 1.12.

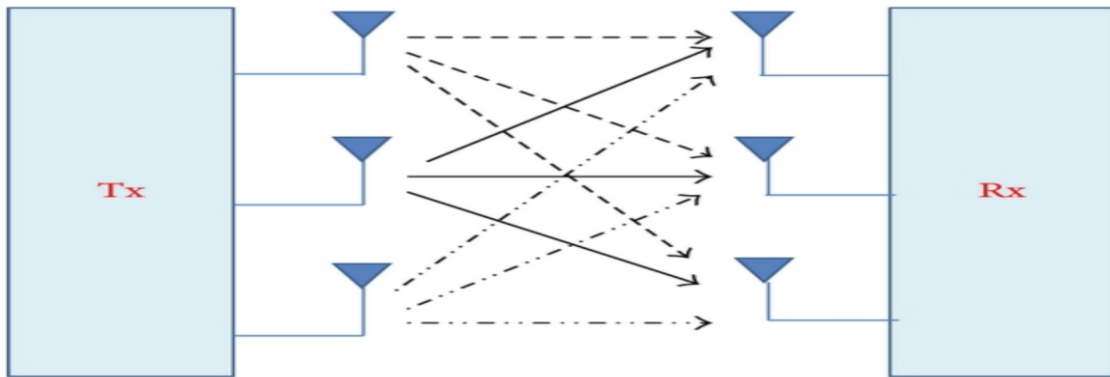


Fig. 1.12. The block diagram of a MIMO system.

As it can be seen from Fig. 1.12, because of the high number of paths for each transmitted signal, we have many fading coefficients for the channel and hence spatial multiplexing took place and data rates increase. Therefore, because of the increase in spatial diversity done by the use of MIMO systems, data rates can be increased. In addition, this big increase in data rates took place because many information streams can be sent in a parallel manner simultaneously from each antenna in the MIMO system, and the whole frequency bandwidth can be used for transmission.

In order to have a model for a MIMO system, assume that the number of transmitting antennas is  $t$ , and the number of receiving antennas is  $r$ . Then, the  $t$  dimensional vector or the transmitting vector can be written as shown in Eq. (1.1), and the  $r$  dimensional vector or the receiving vector can be written as seen in Eq. (1.2).

$$\tilde{x} = \begin{bmatrix} x1 \\ x2 \\ \vdots \\ xt \end{bmatrix}, x \text{ is the transmitted symbol} \quad (1.1)$$

$$\tilde{y} = \begin{bmatrix} y1 \\ y2 \\ \vdots \\ yr \end{bmatrix}, y \text{ is the transmitted symbol} \quad (1.2)$$

Therefore, it is possible to model the system as shown in Fig. 1.13. A mathematical equation can represent a MIMO system and it can be written as shown in Eq. (1.3).



Fig. 1.13. The model of the MIMO system used to model the channel mathematically.

$$\tilde{y} = \mathbf{H}\tilde{x} + \tilde{W} \quad (1.3)$$

H should be therefore a matrix with a size of  $r \times t$  and it is the channel matrix, and W is the noise.

## 1.4 Array Processing

Array processing is very important subject in communication. The signals coming to an array of antennas will come from certain directions, and it is required that the antenna array will have its maximum gain directed to the direction of arrival; the direction from where the required signals are coming. And because of that, the performance of the communication system will be enhanced. It should be mentioned in the beginning that the used antennas in the array are usually assumed to be isotropic antennas which means that the antenna radiates to all directions with equal gain and phases. This is not the case in real applications where antennas usually have large gain towards some directions and very low gains to other directions. Arrays are used in many applications, such as in radar, in radio astronomy, in Sonar, in communications, in applications of direction of arrival, in Seismology, and in medical diagnosis and treatment. Therefore, it is very important to be able to process these arrays used in different areas.

In addition, beamforming is very important such that the direction of the antenna's beam goes to the direction of the received signal which is of interest. Also, beamforming is important in order to direct a null for example to the direction of incoming interference signals or jamming signals. Therefore, beamforming is very important for antenna arrays in order to enhance the antenna array performance. However, before going to beamforming operation, it is important to know from which direction the signal of interest is coming; this is done by estimating the Direction of Arrival (DOA) of the coming signals to the antenna array.

## 1.5 DOA Estimation

One well known algorithm used in estimating the DOA is called MUSIC Algorithm. This method is based on subspace Eigen-structure of covariance matrix. In this method, the covariance matrix is decomposed into eigenvectors of signal and noise subspaces. By steering the vectors which are orthogonal to the noise subspace, the peak of the spatial power spectrum will be found

and hence the direction of sources is found. The performance of this method provides good resolution and consistency.

By using MUSIC algorithm for example, the direction of arrival of incoming signals can be known. After that, beamforming is required in order to receive the required incoming signals and filtered out the unrequired interference signals. It should be mentioned that many other advanced algorithms are available in the literature. This part here is just to give briefly an idea on how the DOA is done.

## 1.6 Work Motivation

Building a massive MIMO antenna at 3.6 GHz with pattern reconfigurability is an important contribution to 5G technology. Research work is going on these days on massive MIMO systems, and implementing massive MIMO for 5G technology is a serious challenge and it will enhance communication networks in future [3]. So, more research on theoretical studies, simulation and experimental works on massive MIMO is extremely important. The used antenna elements in the massive MIMO will be pattern reconfigurable antennas which can direct the pattern to many directions to enhance the spatial diversity of the massive MIMO. Frequency reconfigurability can be added also to the antenna element such that the massive MIMO will be capable to work at many operational frequencies; from 3 – 3.7 GHz for example.

The pattern reconfigurable antennas, which this research work will concentrate on, is reconfigurable antennas with slot radiating elements. Having a pattern reconfigurable antenna with slot radiating elements is another challenge and it is not common in literature. In the literature review of this research work, the references [108] – [123] discuss single band pattern reconfigurable antennas with slot radiating elements. The problem with slot antennas is that their patterns are bi-directional, and having slot-radiating elements which are uni-directional is not an easy job. Therefore, usually antenna designers use metallic reflectors with a separation distance of quarter-wavelength, or they use frequency selective surfaces in order to solve the problem of bi-directional patterns for slot antennas. Also, having a pattern reconfigurable slot-based antenna is another challenge. Frequency reconfigurable antennas based on slot radiating elements is not actually a challenge in general, since it is just required to reconfigure the length of the slot to achieve frequency reconfigurability. However, reconfiguring patterns of slot antennas is a challenge and it

can be done by changing the current path around the slot, by having two slots radiating electric fields with same magnitude and 180 degrees phase shift between their radiated fields, by changing the slot orientation, or by using the ground plane as a reflector.

After designing the pattern reconfigurable massive MIMO, it is a good opportunity to assess the DOA capabilities of the proposed massive MIMO antenna. It is desired to achieve more accurate with less root-mean-square error DOA estimation when pattern reconfigurable antennas are used in the estimation. This expected enhanced DOA estimation is because of the many different patterns directed to different directions. These patterns will collect different received data, and by feeding these data back to the DOA estimation algorithm and using other beams to other directions and feeding them back to the algorithm, DOA estimation can be enhanced.

## **1.7 Thesis Objectives**

1. Design of two new pattern reconfigurable slot-based antennas at 3.6 GHz. These two antennas should compete the other pattern reconfigurable slot-base antennas available in literature.
2. Design of a 4X4 pattern reconfigurable massive MIMO antenna operating at 3.6 GHz for 5G technology. This pattern reconfigurable mMIMO should also compete the other mMIMO antennas available in the literature and operating in the Sub-6 GHz bands.

## CHAPTER 2

# THEORETICAL BACKGROUND

### 2.1 Reconfigurability

Reconfigurability in antennas can be attained if currents, electromagnetic fields or excited modes of antennas' effective aperture were redistributed intentionally. As a result, changes in antenna's input impedance and/or radiation properties will take place. Therefore, it is possible to get pattern, frequency or polarization reconfigurable antennas.

#### 2.1.1 Types of Reconfigurable Antennas

1. Pattern reconfigurable antennas.
2. Polarization reconfigurable antennas. (For example, polarization may be vertical, horizontal,  $\pm 45$  degrees slant and linear, left hand circular polarization (LHCP) or Right hand circular polarization (RHCP)).
3. Frequency reconfigurable antennas.
4. Polarization and frequency reconfigurable antennas.
5. Pattern and frequency reconfigurable antennas.
6. Polarization and pattern reconfigurable antennas.
7. Polarization, pattern and frequency reconfigurable antennas.



## **2.1.2 Basic Principles Used to Achieve Different Reconfigurable Antennas**

The distribution of the surface current on the antenna or on the antenna structure needs to be changed to have frequency reconfigurable antennas. Slots, radiating edges, current distribution or feeding network need to be changed in order to have pattern reconfigurable antenna. The antenna's surface structure, current distribution or feeding network need to be changed to have polarization reconfigurable antennas. Combinations of principles of different types of reconfigurabilities may result in many reconfigurable capabilities in one antenna. It is good to mention here that changing the current distribution will change the distribution of the electromagnetic fields in the antenna's aperture. Other parameters in the antenna may be affected and changed if one parameter in the antenna characteristics was changed.

## **2.1.3 Advantages of Reconfigurable Antennas**

1. More than one wireless standard can be supported in one antenna. The acquired benefits gained by having this advantage are:
  - a. The cost will be reduced; the cost in radio technology depends on the complexity of the hardware and on the incompatible communication systems.
  - b. Volume requirement will decrease.
  - c. Integration will be simplified.
  - d. Good isolation between different wireless standards will be attained.
2. Front-end processing requirements will be lower. The acquired benefits from this point are:
  - a. Front-end filtering will not be required.
  - b. Out-of-band rejection will be very good.
3. Very good to be used for software-defined radio:
  - a. These antennas can be adapted and they can learn.
  - b. They can be automated and controlled using an FPGA or a microcontroller.
4. Multifunctional capabilities:
  - a. It can work as an array or as a single element.
  - b. It can provide narrowband or wideband operation.
  - c. Functionality can be altered if the mission was changed.

5. Enhances the performance of mMIMO systems and enhances the reliability of IoT systems.

## 2.1.4 Reconfiguration Techniques

- **Electrical Switches**

This method is used most of the times. Switches can be used to bridge a slot, to connect different elements, to obtain specific radiation characteristics like having circular polarization for example, or to increase the length of an antenna element. Slots are bridged sometimes to redirect the surface current distributions.

This technique is attractive because it is easy to integrate switches in the antenna. These switches are usually used to redirect the surface current. This technique can be done by one of the subsequent switches:

- a. Using RF-MEMs:

RF-MEMs use mechanical forces to obtain an open circuit or a short circuit in the path of a surface current of an antenna structure. These forces are achieved using electrostatics, magnetostatics, piezoelectric where voltage will be applied and movement will be attained, or thermal forces.

- b. Using PIN-diodes:

PIN diodes have two modes. Pin diode is either ON or OFF depending on the applied voltage across the pin diode's terminals.

- c. Using Varactors:

A varactor contains a p-n junction diode and a reverse voltage will be applied across the p-n junction such that a capacitance will be acquired. As the reverse voltage applied across the p-n junction varies, the capacitance of the varactor will change also. Typical values of the varactors' capacitance are tens to hundreds of Pico-Farads.

- **The Drawbacks of Using Electrical Switches**

1. Complexity will be added to antenna structure because biasing networks will be used for activation or deactivation of switching elements.

2. The power consumption and cost will increase because active components are incorporated in these antennas.
3. Harmonics and intermodulation products can be generated.
4. Fast tuning for the radiation characteristics of antennas is required such that correct functioning of the system is guaranteed.

- **Optical Techniques**

This technique can be done by using photoconductive materials. For a photoconductive material, when it is illuminated by light with appropriate wavelength, electrons move from valance band to conduction band, and the material will conduct current and hence switch will move from OFF to ON state. A laser might be integrated in the antenna, or light can be derived to antenna by using an optical fiber in the design.

The good thing about optical switches is that they do not produce harmonics and intermodulation distortion since their behavior is linear. In addition, they do not require complex biasing lines, and hence unwanted losses, radiation pattern distortion and interference are eliminated. However, optical techniques are lossy and require complex activation mechanisms.

- **Comparison Between Different Switches**

Table 2.1 shows a comparison between different switches. It can be seen that the PIN diodes are a very good option for antenna designers.

**Table 2.1 Comparison between different switches in [4].**

Electrical property	PIN diode	RF MEMs	Optical Switch
Voltage [V]	3 – 5	20 – 100	1.8 – 1.9
Current [A]	3 – 20	0	0 – 87
Power Consumption [mW]	5 – 100	0.05 – 0.1	0 – 50
Switching Speed	1 – 100 nsec	1 – 200 usec	3 – 9 usec
Isolation [1 – 10 GHz]	High	Very high	High
Loss [1 – 10 GHz] [dB]	0.3 – 1.2	0.05 – 0.2	0.5 – 1.5

- **Physical or Mechanical Techniques**

This technique can be done by changing the structure of the antenna, and because of that, current will be redistributed and radiation properties can be changed. The advantages of this technique are that biasing lines, lasers or switching will not be required. However, their response is slow, their cost is high, their sizes are large, their power consumption is high, and it is complex to integrate them with an antenna. Also, the use of this method will be constrained to device limitations which might prevent the capability to alter the antenna mechanically.

- **Material Change Technique or by the Use of Smart Material**

It can be done by using Ferrites or Liquid crystals for example. Liquid crystal has nonlinear behavior and its dielectric constant changes by changing applied voltage. Ferrite's permittivity or permeability depends on the applied static electric field or magnetic field. The main advantage for this technique is the small sizes of smart materials, but the disadvantage is their low efficiencies especially for ferrites.

- **By Using Different Biasing Networks; Biasing Different Elements**

- **By Using Antenna Arrays**

- **By Using Reconfigurable Feeding Network**

### **2.1.5 Best Technique to be Used**

It depends on the application of interest. However, most of the times, FR-4 material with a dielectric constant of 4.4, a thickness of 0.72 mm and a loss tangent of 0.02 is used. Also, PIN diodes and varactors are mostly used in antenna designs.

### **2.1.6 Important Points to be Considered Before Starting the Design of an Antenna**

1. Which application is targeted for this antenna?
2. Which reconfigurable property is required to be modified? (Frequency, Pattern or Polarization)?

3. What are the antenna characteristics which are required to be reconfigured to achieve this reconfigurable antenna?
4. What are the techniques which will reduce negative impacts on the impedance characteristics and on the antenna radiation?

### 2.1.7 Applications of Reconfigurable Antennas

1. Modern, agile, RF systems used for satellite and wireless communications.
2. Imaging.
3. Sensing.
4. Agile, cognitive and smart RF devices: They can monitor the surrounding RF environment and allow communications in any congested environment.
5. Military applications.
6. MIMO and mMIMO communication systems.
7. Cellular and personal communication systems.
8. GSM, WLAN, PCS, UMTS, Bluetooth.

- **Cognitive Radio System**

It needs a frequency reconfigurable antenna which performs data transfer, and it uses another ultra-wideband antenna for monitoring the finite frequency spectrum. When gaps (white spaces) are available in the spectrum, then the transmit/receive characteristics will work at these free frequency bands. Therefore, interference is minimized, and throughput will be maximized. The model of Cognitive radio is shown in Fig. 2.1.

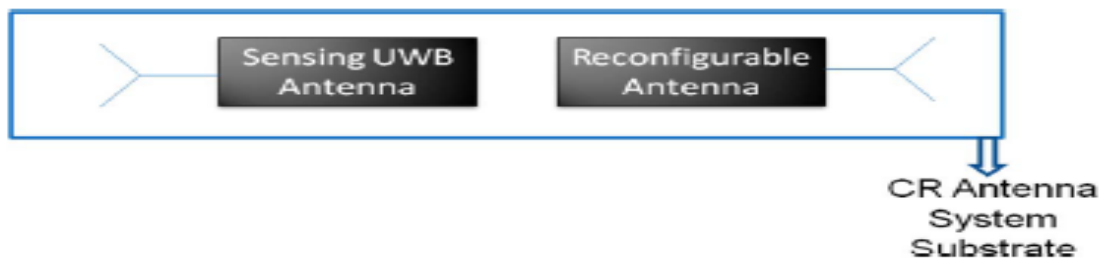


Fig. 2.1. The model of cognitive radio system.

- Four important key parameters are required for this application:
  1. The isolation between the sensing antenna port and the port of the reconfigurable antenna should be very high.
  2. Dimensions should accommodate both antennas.
  3. The two antennas should be capable to receive signals from all directions.
  4. The two antennas should be capable to produce nulls towards the directions of incoming interference or jamming signals.

- **MIMO Systems**

In such systems, there are multiple antennas in transmitter and multiple of them in receiver. Different signals can be sent simultaneously. The feature of such systems is that the communication spectral efficiency in a multipath environment will increase. These systems acquire the use of pattern reconfigurable antennas, and by doing so, the performance of MIMO system will be enhanced since pattern reconfigurable antennas maintain good communication links for MIMO systems. Adding polarization reconfigurability to the MIMO system will enhance the spatial diversity and hence the channel capacity will be enhanced.

- **Satellite Applications**

They need pattern reconfigurable antennas to cover different zones, reduce fading in rainy regions, and to assure having high data rates at all available frequency bands for this application. They also need frequency reconfigurable antennas.

### **2.1.8 Future Uses of Reconfigurable Antennas**

1. The reconfigurable antennas should be smart, completely multifunctional and software controlled with machine learning capabilities, such that they can monitor changes in the surrounding RF environment and then they react correctly.
2. Implementation of cognitive radio will depend on a new generation of antenna systems and communication protocols.
3. More efficient use of frequencies.
4. Pattern reconfigurable antennas and polarization reconfigurable antennas will be used to transmit over busy frequencies.

5. In MIMO channels, reconfigurable antennas will enhance the channels efficiencies and reduce their costs, in addition to improving channel capacity.
6. New opportunities for the design of antennas used for space communications will take place because of the coming reconfigurable antennas.

## 2.2 5G Technology

In [5], many developments in 5G technology are summarized and overviewed. Wireless networks will face a big increase (increase by a factor of 100) in the amount of IP data. They will jump from 3 Exabytes in 2010 to more than 190 Exabytes in 2018, and they might be more than 500 Exabytes in 2020. Also, the number of devices and the amounts of data rates will grow exponentially in the coming years. Therefore, it is very important to utilize 5G technology in order to be able to let these large data rates communicating between different devices.

### 2.2.1 Interesting Factors in 5G Technology

5G technology is very interesting because of some factors, like:

1. The big move into millimeter wave spectrum.
2. The new ways of allocating and reallocating bandwidth.
3. Major virtualization in the core network.
4. The coming of “Internet of things” containing billion of devices.
5. High data rates and low latency will be provided because the past and current cellular and WiFi standards will be improved and integrated with each others.

After that the author in [5] presented the three big 5G technologies which are: mmWave, ultra-densification, and massive multiple –input-multiple-output (MIMO).

### 2.2.2 Some Engineering Requirements for 5G Technology

The author in [5] presented some engineering requirements for the 5G technologies, such as:

1. **Data rate:** 5G is required to be available because the very large mobile data traffic should be supported. Data rates are measured by many metrics:

- a. *Area capacity or aggregate data rate*: It measures the amount of data which the network can support, and it is measured in bits/s per unit area. This rate should increase in 5G by around 1000 times than those used in 4G.
  - b. *5% rate or edge rate*: It is the minimum expected data rate received by a user who is in the network. The aim for this metric is to move from 100 Mbps to 1 Gbps in 5G technology.
  - c. *Peak rate*: It is the maximum hoped rate of data received by a user who is connected to the network. The aim of this metric is to be in the range of tens of Gbps in 5G technology.
2. **Latency**: The latency in current 4G technologies is around 15 ms. It should be 1 ms in 5G.
  3. **Energy and cost**: In the movement from 4G to 5G, energy consumptions and costs decrease ideally. The cost per bit and the joules per bit will decrease by 100 times, because the data rates per link will increase by about 100 times. However, the major cost for 5G will be contributed by the change of the backhaul from the network edges to the core.

In addition to what was mentioned previously, 5G should support much higher number of devices and more diverse set of devices.

### 2.2.3 Major Techniques Used for 5G Technology

In [5], the three big 5G technologies were presented and they are: mmWaves technology, ultra-densification techniques, and massive multiple input multiple output antennas (mMIMO). These three major techniques are used to achieve the required 1000 times more in the amounts of data rates. The mentioned three techniques are based on having more Hz, more nodes per unit area and Hz, and more bits/s/Hz per node. The three points which were mentioned are:

- **Extreme Densification and Offloading**

The spectral efficiency in a specific area will be enhanced by the use of this method, since more operating nodes will be installed per unit area and Hz. The cells are becoming smaller, and this is a very good method which will increase the network capacity. In 1980s, the cells had areas of the order of hundreds of square Kms. Nowadays, the cell sizes in urban areas are fractions of a square Km. In Japan, the cell sizes are less than a tenth of a square Km. The new coming cells are like femtocells (WiFi-like range) and picocells (range under 100 meters). Reducing the cell sizes more has many advantages such as:

- a. The spectrum across a geographic area can be reused.



- b. The number of users who compete for the resources of a BS will be less.

The signal to interference ratio will be preserved as the network densifies more if the power-law pathloss models are satisfied. Also, the cells can be shrunk almost indefinitely without a dangerous loss in SIR. However, as the densification increases too much, many challenges will take place.

- Challenges of More Densification

- a. *Base station densification gains*: Each BS will become more lightly loaded, and hence preserving the expected cell-splitting gains is a challenge.

The increase in data rates will be relative to the increase in the density of the network, this happens because of the applied BS densification. The SINR (Signal to Interference and Noise Ratio) increases as the density increases. The best densification gain is when it is equal to around 1. The densification gain can be 1 for macrocells, and can be much more than 1 for mmwave frequencies.

- b. *Multi-RAT Association*: Methods used to achieve appropriate associations between BSs and users across multiple Radio Access Technologies (RAT) are challenges facing densification techniques.

Networks will be more heterogeneous as we move to 5G. Hence, determining the standards and spectrum which will be utilized, and determining which BSs or users to associate with each others are complex tasks. The optimization problem used to determine the best user association is complex problem and it depends on many factors like:

1. The received SINR by every BS from every user.
2. The choices of other users in the network.
3. The instantaneous load available at each BS.
4. Other constraints like utilizing the BS and standards in uplink and downlink.

Hence, simplified procedures must be available. The association approach which depends on blanking about half of the macrocells transmissions, and on aggressive and static biasing to small cells, is simple, highly suboptimal and it increased the edge rate by around 500%.

- c. *Mobility support*: The challenge is how to support mobility in such highly heterogeneous network.

The increase in heterogeneity and the continuing densification for the network have made supporting the mobility to be a challenge. The most important feature of cellular networks is that they are supporting always-on connectivity and mobility. Hence, it is very important for networks to support mobility.

- d. *Cost*: The challenge is to afford the increasing costs due to installation, maintenance and backhaul.

Having smaller cells will require lower power consumption and cheaper BSs. However, the high cost will come from many factors, like:

1. Getting permits.
2. Making sure that the backhaul connections are reliable and fast.
3. Site rental fees are required to be paid; these fees are large and they are paid monthly.

In addition, these previous factors are facing and trying to stop the growth of picocells, small cell deployments, and distributed antennas. The backhaul also will be the major technical challenge.

- **Millimeter Waves**

The bandwidth will be increased in this method. The terrestrial wireless systems used the small range of microwave frequencies largely. The microwave signals have frequencies starting from many hundreds of MHz to few GHz, and these frequencies correspond to wavelengths going from about a meter to few centimeters. Nowadays, this spectral band is nearly fully used especially at peak markets and peak times. Therefore, much more bandwidth is required. Even though this microwave bandwidth will be used more efficiently if allocation procedures and modernizing regulatory were used, it is required to use higher frequencies and to go up in frequency such that large bandwidths will be gained from the new used spectrum. There is a large relatively free spectrum available in the mmWave frequency range starting from 30 GHz to 300 GHz, with wavelengths ranging from 10 mm to 1 mm. In addition, there are many GHz which can be used for cellular applications in the range from 20 – 30 GHz range.

- Reasons Behind Idle mmWave Spectrum

It was assumed that the mmWave spectrum is not suitable for cellular applications because of its not good propagation qualities which includes the subsequent points:

1. Pathloss is strong.
2. Rain and atmospheric absorption is high.
3. Diffraction around obstacle is low.
4. Penetration through objects is low and weak.
5. Strong phase noise.
6. Very costly equipment.

However, the good points are that costs and power consumption by semiconductors are decreasing, and semiconductors nowadays are maturing.

- Challenges and Solutions for Using mmWave Spectrum

Some problems facing the movement towards mmWave and how to solve them are viewed in the subsequent points.

1. **Pathloss:**

The antenna will be shrunk if the required electrical size is fixed and the frequency of operation increases. Therefore, the free-space pathloss between the transmitting and receiving antennas in this case will increase. For example, if the frequency was increased from 3 to 30 GHz (one order of magnitude) as an example, then 20 dB power loss will be added regardless of the distance between the receiving and transmitting antennas. It should be mentioned also that when the frequency of operation increases, then the effective aperture of an antenna scales with the factor  $\frac{\lambda^2}{4\pi}$ . Therefore, if the aperture of an antenna at one side of the link was kept constant, the free space pathloss will remain constant. On the other hand, if the apertures of both transmitting and receiving antennas were kept constant, the free space pathloss will decrease sharply as the frequency of operation increases. By the use of arrays, the aperture of an antenna can be held constant, because the apertures of many antennas are added up. The main challenge now is to find the ways which will make these antennas co-phase such that these antennas will be capable to steer and/or receive energy properly. Rapid channel changes by mobility or by quick variations of the devices' physical orientations will make this challenge to be more complex.

## 2. **Blocking:**

The diffraction for mmWave signals is less and their specular propagation is more compared with microwave signals, and therefore, they are much more susceptible to blockages. As a result of that, the channel will be a bimodal channel which depends on either the line of sight is present or absent. The available link can face rapid transitions from usable to unusable link and vice versa because of this sensitivity to blockages. Also, standard small-scale diversity countermeasures will not be able to solve large-scale obstructions. Therefore, it is required to have new channel models having solutions to previous problems.

## 3. **Rain and atmospheric absorption:**

Rain and air absorption is high, for example, 15 dB/Km absorption loss due to oxygen molecules is available within the 60 GHz band. However, this large absorption will not affect the urban cellular deployments much since BS areas has a diameter of around 200 m. Actually, this absorption is useful such that it will attenuate the interference signals coming from other close BSs, and hence the isolation between cells will increase. Two more points can be added in this metric, large antenna arrays are required to direct the beam energy and to collect the signal coherently. The other point is that narrow beam communication is facing some difficulties which are required to be solved.

## 4. **Large arrays and narrow beams:**

Designing a wireless system which uses focused and narrow beams is not an easy job. mmWave beams are highly directional, and this property will completely change the sensitivity to miss-aligned beams and the interference behavior.

## 5. **Link acquisition:**

If narrow beams are to be used, then it is a difficult challenge to associate BSs with corresponding users for initial access and for handoff. For the BS to find the user, the BS will try to find a narrow beam by scanning many angular positions until the narrow beam is found. Otherwise, a multistage acquisition can be done in which very large coding/spreading gains will be deployed in a wider beam, and this wide beam will be successively narrowed until the required user is found. However, finding solutions to this problem is a very important work.

## 6. Leveraging the Legacy 4G network:

Phantom cells are an interesting proposal where mmWave frequencies are used for information transmission and they are transmitted from micro cell BSs. On the other hand, the control signals will be sent at microwave frequencies from macro BSs. The mmWave network is shown in Fig. 2.2. This will ensure reliable and stable control connections. The interruptions of the mmWave links will not be a big problem because the control links are always available and lost data could be retrieved through retransmission.

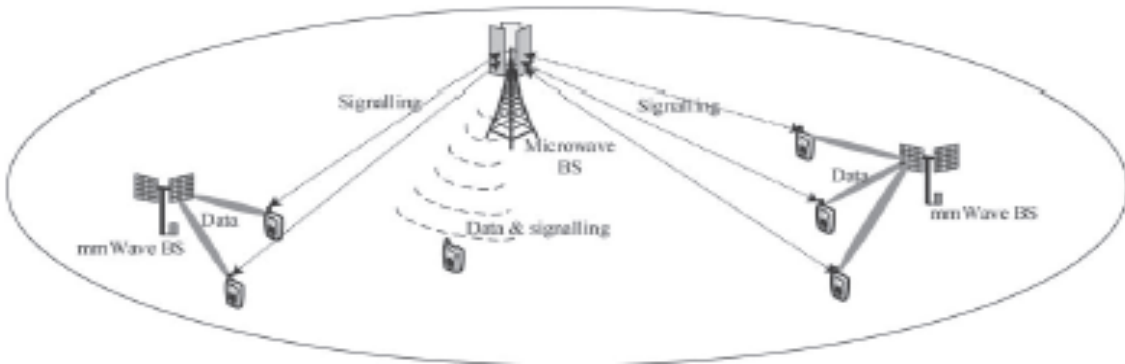


Fig. 2.2. A network with mmWave technology and phantom cells.

## 7. Novel transceiver architectures are needed:

Hardware is very important and nontrivial issue for communication systems which will be designed for 5G technology. The challenge in this part is the large power consumption taken place by the digital to analog and analog to digital converters which operate on large bandwidths. Therefore, although it is required to use large antenna arrays with high receiving sensitivities such that pathloss will be alleviated, using digital beamformers per an antenna in the array is very difficult to be done. However, analog phase shifters can be used, or a group of antennas can use one D/A and A/D system; such systems are called hybrid structures.

- **Massive MIMO**

The spectral efficiency by using massive MIMO systems will increase. In other words, more bits/s/Hz per node will be supported. MIMO communications were used in WiFi systems in 2006, and then they were used in 3G cellular systems. When multiple of antennas are used in mobile devices and BSs, then the spatial dimensions of communication systems increase. Better multiple spatial dimensions will be there for signaling if the channel matrix elements have good statistical independence, and as a result of that, the spectral efficiency will be enhanced also. The signaling dimensions, for single user MIMO systems, are limited by the number of antennas in the user's device. If many users are communicating with one BS, then the multi-user MIMO will make antennas to give connections for those users to the BS. The smallest number of antennas at the users' devices or at BSs determine the available signaling dimensions.

Accurate channel estimation for few tens of users per resource can be achieved if the number of antennas in a BS is much more than the number of active users per time-frequency signaling resource and under reasonable time-frequency selectivities. Therefore, the number of antennas in a BS should be in hundreds in order to achieve the previous condition. This is why massive MIMO systems were required to be introduced. The benefits provided by massive MIMO are:

- a. Big enhancements in spectral efficiency without increasing BS densification.
- b. The channel responses are smoothed out because of the large spatial diversity.
- c. Simple transmitting/receiving structures can be attained because the channels of mMIMO systems between the active users who joined the same signaling resource and the BS are quasi-orthogonal. This orthogonality will be enhanced if the number of antennas in BSs is more for a provided number of active users.

Because of these benefits and the large data capacity provided by the use of massive MIMO, they are very important to be used in 5G technology.

- Challenges and Solutions for Massive MIMO

There are some challenges which need to be solved, and they are viewed in the next points:

a. **Pilot interference and overhead reduction:**

The pilot training sequences are orthogonal to each others for the users of a specific cell such that better estimates for the channels will take place. However, it is required to reuse these pilots in other surrounding cells. If the pilots were not reused for other cells, then it will be required to consume all available resources by training pilots. Therefore, interference between pilots of different cells takes place and hence the quality of the channel estimates will be limited. This phenomenon is called pilot contamination, and this interference will not be eliminated if the number of BSs was increased.

Pilot contamination can be reduced or even eliminated using some techniques which some of them will be mentioned in more details later in this report. For example, this interference can be reduced by using low intensity BS coordination. In addition, spatial correlations can be exploited such that pilot symbols will be shared by antennas. In addition, pilot contamination can be reduced if the pilots were divided into classes and each class of pilots will be transmitted in a necessary rate.

b. **Architectural challenges:**

Each antenna in an array will be integrated with its own amplifier. These amplifiers are low power amplifiers. This way will reduce power consumption. Using some high-power amplifiers to feed a sector of antennas will consume more power.

Antenna correlations, mutual couplings and costs are important factors which must be considered also.

c. **Full-dimension MIMO and beamforming in elevation plane:**

The number of antennas which can be accommodated in linear horizontal arrays (available in tower structures) is limited. Hence, only azimuth angle dimension is exploited. If a planar 2D arrays were used then the elevation angle can be exploited also, and this structure is known as full-dimension MIMO where many more antennas can be accommodated compared to linear arrays. The ability of beamforming in elevation plane reduces interference to users available in close to cells and enhances the signal powers reaching them.

d. **Channel models:**

Antenna couplings and channel correlations for massive MIMO systems with important topologies must be studied, and a correct modeling of their effects should be found. In addition,

how much the channels are orthogonal with the available nonideal conditions should be studied and verified.

e. **Coexistence with small cells:**

BSs with massive MIMOs should coexist with many small cells. These small cells have small form factor and hence installing massive MIMO arrays in these cells is difficult. This challenge should be solved.

f. **Coexistence with mmWave:**

There will be a need for many antennas in order to have beam steering for mmWave communication. The antennas at mmWave frequencies are very small and hence very large number of antennas can be fit in portable devices, and hence beam steering can be achieved.

## 2.2.4 Research Areas in 5G Technology

After that the authors in [5] mentioned important design issues for 5G. It was mentioned that the use of 5G will increase the data rates by 1000 times, decrease power consumption, decrease latency, decrease costs, and support many connections with low data rates. The subsequent points discuss some important research areas:

- **The Waveform; Signaling and Multiple Access**

Signaling and multiple access formats will be different in 5G technology.

a. *OFDM and OFDMA:*

For high speed wireless communications, OFDM is the dominant signaling format. OFDM is used in LTE and in all current WiFi standards. Its features are:

- It is much easier to be used if frequency selectivity is required.
- It can be implemented efficiently with easy frequency-domain equalizers and with FFT/IFFT blocks.
- It is good for pairing in MIMO systems.



b. *Drawbacks of OFDM:*

The envelope samples in this signaling format are almost Gaussian, and hence the peak to average power ratio for this format is more than that in other formats. OFDM's spectral efficiency can be improved if the cyclic prefixes are smaller and the strict orthogonality is relaxed.

c. *Potential alternatives to OFDM:*

1. Time-frequency packing: it can provide solutions to limitations of strict orthogonality and cyclic prefixes.
2. Nonorthogonal signals.
3. Filterbank Multicarrier.
4. Generalized frequency division multiplexing.
5. Single carrier.
6. Tunable OFDM.

- **Cloud-Based Networking**

The data can be moved to the cloud and then it is possible to access these data from anywhere and through different platforms. Two technologies will be very important and used in future: software defined networking (SDN) and network function virtualization (NFV).

a. Network function virtualization:

In this technology, the cloud will be the place where the network functions will run. Hence, infrastructure will be computed in a data center. These network functions are traditionally done with the use of hardware appliances. However, these functions are done in the cloud with this technology.

b. Software-defined network:

By the use of this technology, intelligent programmable networks will be created. This technology is an architectural framework.

- **Energy Efficiency**

In communications, the energy efficiency is measured in bits/joule or joules/bit. This efficiency should increase by the same amount of increase in data rate such that the power consumption will be maintained at fixed and reasonable amounts. Hence, increasing the energy

efficiency by many orders of magnitudes is a big challenge. The largest part consuming energy is the access network, and research is focusing on the subsequent topics:

a. **Resource allocation:**

The design of resource allocation is optimized such that the system energy efficiency increases. Large energy can be saved if a reasonable reduction in data rates took place.

b. **Network planning:**

The energy efficiency can increase using some techniques like having a smaller number of BSs in a specific area. In addition, if adaptive BSs were designed with sleep/wake algorithms, the energy efficiency will increase. Also, BSs can be off during very low traffic durations or when there are no active users.

c. **Renewable energy:**

Some works showed that if the traffic loads for some BSs were reasonable, then these BSs can be equipped with energy harvesting systems such that they will be served by the renewable energy sources. Also, resource allocation can be done using both traditional and renewable energy sources.

d. **Solutions achieved by the use of Hardware:**

Most of energy is consumed by hardware and there are many works trying to provide antenna muting property, antennas with low loss, and adaptive sectorization directing beams to directions of more traffic loads.

To sum up, energy efficiency is a very important research theme for 5G Technology. The following points are some research factors related to energy efficiency:

1. Increase in energy efficiency can be provided if True cloud-RAN was used.
2. The tradeoff between having fewer macrocells and many small cells with their power consumptions is a very important topic.
3. The consumed energy by the circuits used for massive MIMO should be studied in details and this is another important topic which will help in enhancing the energy efficiency.
4. The bandwidths of mmWave technology are very wide, and hence energy efficiency will be very crucial for this technology.

## 2.3 MIMO Systems

In [6], the performance metrics which characterize the behavior of MIMO systems is presented. It is noticed that the data rates increase as the number of antennas in the transmitter or in the receiver increases even though the bandwidth and power levels are kept with no change. Ideally, the capacity of the channel is directly proportional to the number of antennas in the receiver and in the transmitter, and Eq. (2.1) shows this relation.

$$C = B * \log_2(1 + M * N * SNR) \quad (2.1)$$

B is the bandwidth of operation, C is the channel capacity, N and M are the number of antennas in the receiver and in the transmitter, respectively, and SNR is the absolute value of the signal to noise ratio. The device size is a limiting factor if it is required to have multiple antennas in the terminal. The antennas should cover multiple bands of operation. Therefore, designing MIMO antennas with reasonable sizes and good performance is very important for the designers of wireless-terminals.

The performance of antennas is affected because of antenna miniaturization; especially its bandwidth and its efficiency. The coupling between the radiated fields from antennas and between the MIMO ports through the shared ground will increase as the distance between the antennas in MIMO decreases, and this decrease is required if the number of antennas is required to increase. This coupling between the ports affects the diversity performance of the MIMO antenna system; if coupling increases, diversity will be degraded. As the antenna size is reduced, the other performance metrics will be affected and optimized system with competing results is required.

In [6], the author presented some important metrics which can assess the performance of the MIMO antenna systems, and these metrics are shown in the subsequent paragraphs. In order to fully characterize a MIMO antenna system, then the typical antenna-performance metrics should be evaluated, in addition to other parameters which should be evaluated as well. Typical antenna-performance metrics and parameters which will be used to evaluate the MIMO performance are like frequency bandwidth of operation, resonant frequency, efficiency, radiation patterns, and the gain.

### 2.3.1 The Correlation Coefficient ( $\rho$ )

This metric assesses the correlation or the isolation between the communications channels; higher values for this metric mean high correlation between the channels and this is not desired for MIMO systems. This metric measures how much the channels are correlated or isolated from each others. This metric considers the radiation patterns and how they affect each other when they are radiated at the same time. The square of the correlation coefficient provides the envelop correlation coefficient. Eq. (2.2) shows the envelope correlation coefficient.

$$\rho_e = \frac{\left| \iint_{4\pi} \vec{F}_1(\theta, \varphi) * \vec{F}_2(\theta, \varphi) d\Omega \right|^2}{\iint_{4\pi} |\vec{F}_1(\theta, \varphi)|^2 d\Omega * \iint_{4\pi} |\vec{F}_2(\theta, \varphi)|^2 d\Omega} \quad (2.2)$$

Where  $\rho_e$  is the envelop correlation coefficient,  $\vec{F}_i(\theta, \varphi)$  is the 3-D radiation pattern of ith antenna used in the MIMO system,  $\Omega$  is the solid angle. This equation is very complicated to be used for calculations since it might require numerical integration for the 3-D radiation patterns. In addition, this equation is valid in an isotropic environment. However, it has been shown that the S-parameters can be used to calculate the correlation coefficient when single mode and lossless antenna are assumed. The expression is shown in Eq. (2.3).

$$|\rho_{ij}|^2 = \rho_{eij} = \left| \frac{|S_{ii}^* S_{ij} + S_{ji}^* S_{jj}|}{\sqrt{(1 - |S_{ii}|^2 - |S_{ji}|^2)(1 - |S_{jj}|^2 - |S_{ij}|^2)} \eta_{radi} \eta_{radj}} \right|^2 \quad (2.3)$$

Where  $\rho_{ij}$  is the correlation coefficient between ports j and i,  $S_{ij}$  is the S-parameter between ith element and jth element, and  $\eta_{radi}$  is the radiation coefficient for the ith element. If the correlation coefficient value was less than 0.3 then this is acceptable.

Low coupling results in high isolation. Isolation can be found using (isolation =  $-20 \log(|S_{ij}|)$ ). However, isolation is different than the correlation coefficient, even though the higher the isolation the lower the correlation coefficient, but the correlation coefficient considers the radiated fields while the isolation does not. The isolation gives a measure of the coupling between the ports. Also, it cannot be concluded that the correlation

coefficient is low if isolation between ports was high, and vice versa. If the diversity performance of a MIMO system was good, then it is required to have low correlation coefficients and high isolation between the MIMO ports.

In order to achieve a low correlation coefficient, then each wave coming from a specific and different path should be weighted by a weight which is different than that for the other wave coming from another path or direction. Hence, this weight is given to the incoming wave based on its direction of arrival. This can be done by optimizing the antenna locations (spatial diversity), angle diversity (through the patterns) or polarization diversity.

### 2.3.2 Total Active Reflection Coefficient (TARC)

The S-parameters only are not enough in characterizing the bandwidth and efficiency of MIMO system, and TARC is another performance metric which provides better characterization for the performance of the MIMO systems. In a multi-port antenna system, the ratio of the square root of the sum of all reflected powers to the square root of the sum of all incident powers is the definition of TARC. The TARC is given in Eq. (2.4) for N-element antenna.

$$\Gamma_a^t = \frac{\sqrt{\sum_{i=1}^N |b_i|^2}}{\sqrt{\sum_{i=1}^N |a_i|^2}} \quad (2.4)$$

Where  $a_i$  and  $b_i$  are the incident and reflected voltages, respectively, ( $b=S \times a$ ) where S is the S-parameter. The TARC metric accounts for random signal combinations between ports and it accounts for coupling. The value of TARC is between zero and one, where a TARC value of one indicates that all incident powers were not transmitted from the antenna because of impedance mismatch for example, and zero TARC shows that all incident powers are radiated from the antenna. The effects of the fed phases to the ports of the antenna are included in TARC also. For a specific phase excitation between the ports, a curve of TARC provides information about the resonant frequency of the whole antenna system and the bandwidth of the whole system as well. Eq. (2.5) can provide the TARC value for two port MIMO antenna system.

$$\Gamma_a^t = \frac{\sqrt{(|S_{11} + S_{12}e^{j\theta}|^2) + (|S_{21} + S_{22}e^{j\theta}|^2)}}{\sqrt{2}} \quad (2.5)$$

$\theta$  is the phase of the input feeding. The effect of variations of input phase on resonant frequency and on bandwidth can be determined now using Eq. (2.5) for this specific system with 2 ports.

### 2.3.3 Mean Effective Gain (MEG)

The typical methods of measuring the gain of antennas are not enough for measuring the gain of MIMO antennas because the environment effects are not included in typical gain equations. However, another method can be used to have a better measure for the gain of an antenna system, and this method includes the environment effects also. In this method, after fabricating the new antenna, it will be operated under some specific conditions. Another standard antenna with known characteristics will be operated under the same specific conditions, and then it is possible to get the performance of the new fabricated antenna after it is compared with the standard antenna's performance. If the performance was not as expected, then another new prototype can be designed and its performance will be measured again until expected performance is acquired. This procedure takes lots of time.

Another method which can measure the gain of antennas is called the mean effective gain where the three-dimensional radiation patterns and a model of the environment or the channel will be used to calculate it. Eq. (2.6) can be used to calculate the MEG, and it can be noticed that the simulated or measured radiation pattern are used in Eq. (2.6).

$$MEG = \int_0^{2\pi} \int_0^\pi \left[ \frac{XPD}{1 + XPD} G_\theta(\theta, \varphi) P_\theta(\theta, \varphi) + \frac{1}{1 + XPD} G_\varphi(\theta, \varphi) P_\varphi(\theta, \varphi) \right] \sin\theta d\theta d\varphi \quad (2.6)$$

$$\int_0^{2\pi} \int_0^\pi [G_\theta(\theta, \varphi) + G_\varphi(\theta, \varphi)] \sin\theta d\theta d\varphi = 4\pi \quad (2.7)$$

$$\int_0^{2\pi} \int_0^\pi [P_\theta(\theta, \varphi)] \sin\theta d\theta d\varphi = \int_0^{2\pi} \int_0^\pi [P_\varphi(\theta, \varphi)] \sin\theta d\theta d\varphi = 1 \quad (2.8)$$

$$XPD = \frac{P_V}{P_H} \quad (2.9)$$

Where XPD is the ratio of cross-polarization power representing how the incoming power is distributed.  $P_H$  is the horizontal mean incident power,  $P_V$  is the vertical mean incident power.  $G_\theta(\theta, \varphi)$  and  $G_\varphi(\theta, \varphi)$  are the gain components of the antenna,  $P_\theta(\theta, \varphi)$  and  $P_\varphi(\theta, \varphi)$  are the environmental statistical distributions of the incoming waves, when waves are assumed to be uncorrelated. Eq. (2.7) and Eq. (2.8) are the conditions which need to be satisfied in order for Eq. (2.6) to be applied. The complexity of the MEG is reduced if the received waves are assumed to be available in the horizontal plane only.

### 2.3.4 Diversity Gain (DG)

When the transmitted stream of data is received by the antenna from different channel paths, then diversity is achieved. If the received signals are uncorrelated, then SNR will be higher, and reception of signals will be better. The impact of diversity on the communication system is measured by this diversity gain metric. Diversity gain shows the difference between the SNR (SNRs are time averaged) of all received signals within the diversity system and the SNR of received signals by a system including one antenna with one diversity channel only under the condition that the received SNR is above a certain level. Eq. (2.10) shows equation used to calculate the diversity gain of a MIMO system.

$$Diversity\ Gain = \left[ \frac{\gamma_c}{SNR_c} - \frac{\gamma_1}{SNR_1} \right]_{P(\gamma_c < \gamma_s/SNR)} \quad (2.10)$$

Where  $SNR_c$  and  $\gamma_c$  are the mean and instantaneous SNR for the diversity system, respectively.  $SNR_1$  and  $\gamma_1$  are the mean and instantaneous SNR for the single branch of maximum values in the diversity system, respectively.  $\gamma_s/SNR$  is the specific level of the reference. If it was assumed that the signals are uncorrelated and with Rayleigh distribution, then the probability that instantaneous mean SNR of the diversity system is less than the reference level  $P[\gamma_c < \gamma_s/SNR]$  can be found using Eq. (2.11).

$$P\left(\gamma_c < \frac{\gamma_s}{SNR}\right) = \left[1 - e^{-\left(\frac{\gamma_s}{SNR}\right)}\right]^M \quad (2.11)$$

M is the number of antennas. In a diversity system (MIMO system), the received combined power will increase if the number of antennas increases. In addition, as the number of antennas increases, the obtained gain will be larger until the number of antennas is six or higher. Also, it should be mentioned that lower correlation coefficient yield higher diversity gain.

### 2.3.5 Branch Power Ratio

Power levels between MIMO branches should be very close to each others. In order to represent the differences in power levels, Eq. (2.12) can be used, where k is the two branch power level ratio.

$$k = \frac{P_{min}}{P_{max}} \quad (2.12)$$

$P_{min}$  is the minimum received power by an antenna, while  $P_{max}$  is the maximum received power by an antenna in the same MIMO system. The overall diversity gain will be affected by the power level ratio; the overall diversity gain will be divided by k such that the actual diversity gain can be found. In addition, Eq. (2.11) will change into Eq. (2.13).

$$P\left(\gamma_c < \frac{\gamma_s}{SNR}\right) \cong \frac{1}{k} * \left[1 - e^{-\left(\frac{\gamma_s}{SNR}\right)}\right]^M \quad (2.13)$$

The power level ratio can be found also from MEG as shown in Eq. (2.14).

$$k = \min\left(\frac{MEG_2}{MEG_1}, \frac{MEG_1}{MEG_2}\right) \quad (2.14)$$

Where  $MEG_1$  and  $MEG_2$  represent the MEGs of antennas 1 and 2, respectively.



### 2.3.6 System Capacity

Since the most important advantage of MIMO antenna systems is the provided increase in data rates in a multi-path environment, and the upper bound for the system capacity is an important performance metric as well. Channel matrix and the radiation characteristics of the MIMO antenna elements have large impact on the channel capacity of a MIMO system. The channel matrix includes the environmental effects of the communication channel. If the channel conditions are not known for the transmitter, equal power will be fed to all elements in a MIMO system.

The channel capacity can be given as shown in Eq. (2.15) in bits/sec/Hz.

$$C = \log_2 \left[ \det \left( I_N + \frac{\rho}{N} HH^T \right) \right] \quad (2.15)$$

$\rho$  is the average SNR,  $I_N$  is an  $N \times N$  identity matrix,  $H$  is the normalized channel covariance matrix, and  $N$  is the number of antenna elements at the transmitter and at the receiver.

$HH^T$  will become an identity matrix when the following points occur:

- a. Transmitting or incoming waves are uncorrelated.
- b. MIMO elements have zero correlation coefficients at the two sides of a MIMO system (transmitter and receiver sides), when powers going to antennas are similar, and mean effective gain values are normalized.

As a result of that, Eq. (2.15) becomes as shown in Eq. (2.16) and channel capacity will increase in a linear manner compared with the channel capacity of a SISO (single-input-single-output) system.

$$C = N * \log_2 \left( 1 + \frac{\rho}{N} \right) \quad (2.16)$$

Eq. (2.16) shows the ideal channel capacity limit for a MIMO system. This ideality can be reached because of the zero correlation between the radiated patterns from the antennas, and it is impossible to have a correlation coefficient of zero for a MIMO system. Higher coupling between antenna elements and higher correlations between patterns of elements yield more degradation in the channel capacity and hence in the MIMO system's performance. In a line-of-sight environment,

the MIMO system's performance is like the performance of a SISO system because channels are completely correlated but the effective aperture of the MIMO antenna is larger because of the used multiple antennas. However, environments in practical wireless mobile communication applications are multipath environments and the MIMO systems are designed to be operated in such environments. In these environments, the  $H$  matrix will contain information about the correlation between distinct channels due to propagation environment, and due to used antennas. Therefore, it is important to calculate the channel coefficient matrix  $H$  of a MIMO antenna system, and the knowledge of this channel matrix will be used in calculating the channel capacity.

## 2.4 Massive MIMO

In [7], the importance, the limiting factors, and the research problems of massive MIMO are shown. This paper focuses on developments happened for massive MIMO systems in the three years before the publish date of the paper. Improving the coming wideband networks require the use of Massive MIMO antennas. These future networks will be energy efficient, robust, secure, and spectrum efficient by the use of massive MIMO antennas. Spatial multiplexing is used for massive MIMO antennas. The massive MIMO antennas depend on spatial multiplexing. Time division duplexing is used as the operation mode for the massive MIMO systems under the condition that the uplink and downlink channels are reciprocals. Frequency division duplexing can be used in certain cases.

In [8], an introduction for massive MIMO is presented. There are two facts which should be mentioned; first, the demand for more data is always there, and second, the electromagnetic spectrum will not increase. The fundamental problem in wireless communications is how to provide reliable communications for the very high data rates in a specific area. The available solutions for this fundamental problem can be divided into three categories:

1. The use of the un-utilized spectrum (mmWaves is an example).
2. The installation of more access points to support smaller areas (example: small cells).
3. Many antennas will be used at the access point and in the terminals (examples are point-to-point MIMO and massive MIMO systems).

In [9], a detailed overview for massive MIMO systems was shown. In addition, if the used channel state information CSI was perfect, then the transmitted power from a single antenna in a massive MIMO antenna can be reduced by a factor equal to the number of antennas in the BS compared to the transmitted power used by an SISO system. On the other hand, if the used channel state information was not perfect, then the transmitted power from a single antenna will be reduced by a factor equals the square root of the number of antennas in the BS. Therefore, the use of massive MIMO enhances the energy efficiency.

The idea of massive MIMO can be applied at different regions other than cellular applications like applying the idea to distributed deployments.

In [10], many opportunities and challenges are shown for very large arrays. LTE standards allow 8 antennas at BS and this is the maximum allowed number of antennas. But, having more antennas in the receiver and in the transmitter enhances the link reliability and data rates in a communication system. Also, the achieved data rate can be equal to  $\min(n_t, n_r) * \log(1 + SNR)$  if the channel changes quickly as a function of time and frequency and if coding across channel coherence intervals is possible.

However, the drawbacks of using MIMO is the more complex hardware, and the complex and power consumed by signal processing at both ends. Also, difficulty in achieving optimal signal detection increases exponentially as a function of transmitter antennas.

The number of served users is limited because it is not possible to get channel-state information for infinite number of users. However, by the use of very large MIMO systems with TDD and FDD and via orthogonal frequency division multiplexing (OFDM), then it is possible to serve large number of users. In addition, the power consumed from antennas in very large MIMO systems is in milli-watts.

It should be mentioned here that there are some coding schemes which reduces error rates to very small values under the condition that the transmission rate is less than the channel capacity; this is correct as per the theorem of noisy-channel coding.

## 2.4.1 Downlink and Uplink Operations for Massive MIMO Systems

Fig. 2.3 shows the downlink operation for massive MIMO antennas used in BSs, where an array of antennas is used to serve many users. The terminals or users may have one antenna for each one of them. The main task is to let the stream of data to reach to the required user with least possible interference from other data streams. This task can be achieved using frequency division multiplexing or time division multiplexing. Spatial division multiplexing is used in massive MIMO systems; the data streams go to the required users simultaneously and using the same frequency bands. It is required to have many independently controlled antennas in order to do this job. In addition, in a line of sight environment the data streams will go to the users in focused beams directed towards the required users. On the other hand, in non-line of sight scenarios, the data streams will go to the required users through different ways and they combine constructively at the required user, and destructively at the other non-required users. The frequency responses of the channel between each user and each MIMO element should be known in order for the spatial multiplexing to be done. These frequency responses of the channel will be entered in a matrix and this matrix is called channel state information (CSI) and it will be entered to the precoding block shown in Fig. 2.3, and after some signal processing in the precoding block, the required antennas in the MIMO system will send the intended signals to the corresponding users. As the number of antennas in the MIMO increases, Beams can be more focused to users. Fig. 2.3 shows the downlink operation where signals are going from the transmitters to the corresponding receiving users or terminals.

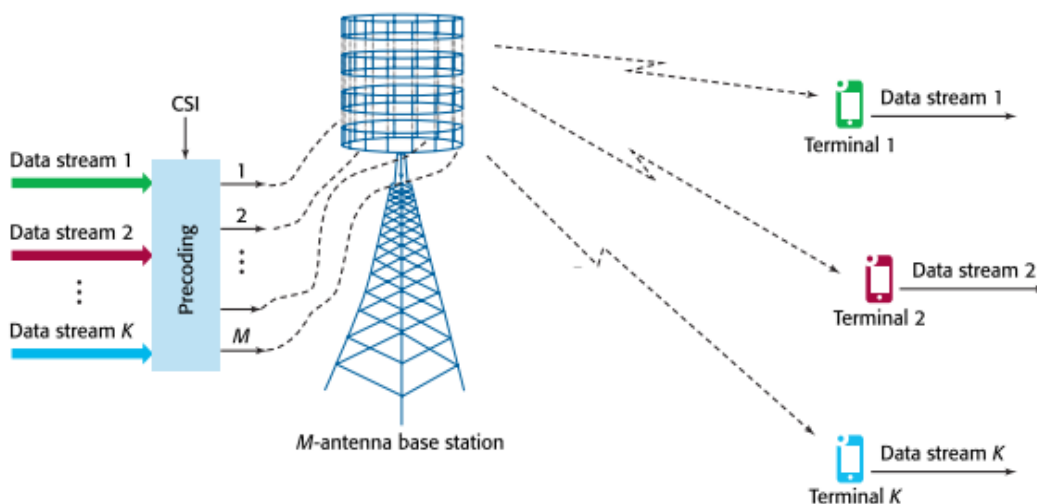


Fig. 2.3. Downlink operation for massive MIMO link.

Fig. 2.4 shows the uplink operation where the data streams are going from the users to the base stations (BSs) simultaneously and using same frequency bands. The antenna arrays receive the data signals modified by the channel properties and these data signals or streams go to the decoding block where the signals will be separated, and individual data streams will be produced. The spatial multiplexing and demultiplexing are achieved by using the measured (and not assumed) channel characteristics. The communication system performance will be enhanced as the number of antennas increases if the channel responses were perfect and even if some noise was added to these measured responses. Increasing the number of serving antennas compared to active users' number has many benefits including the following:

1. More selectivity in transmitting and receiving data streams, and hence more data rates and less radiated power will be achieved.
2. Simpler signal processing units will be acquired.
3. Effective power control can be achieved which results in uniform and good service in the cell.

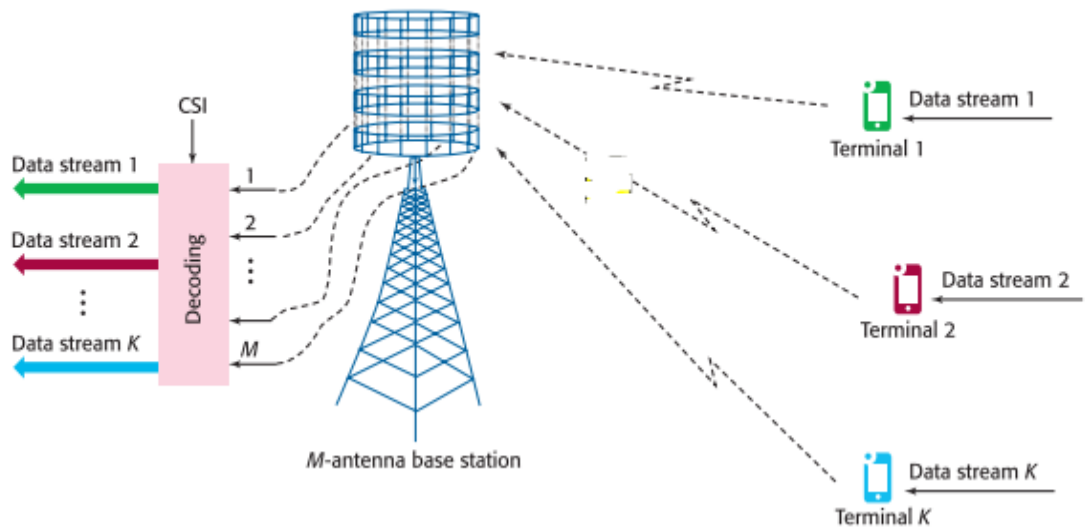


Fig. 2.4. Uplink operation of a massive MIMO link.

## 2.4.2 MIMO Types

- **Point to Point MIMO**

Fig. 2.5 shows a point-to-point MIMO where an array of  $M$  antennas at the BS transmit data streams to a receiving terminal with an array of  $K$  antennas. Many data streams are sent to the many users at disjoint time blocks or disjoint frequency blocks, and hence time division multiplexing or frequency division multiplexing are used. When the channel is used, a signal vector will be transmitted, and the received signal vector will include linear combinations of transmitted signals; modified transmitted signals by the channel. The combining coefficients can be known by knowing the channel propagation coefficients between ends of the link.

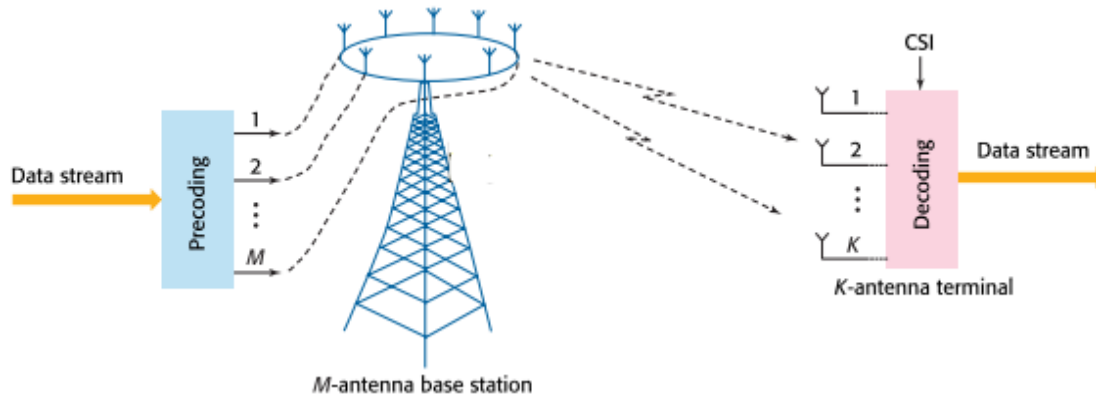


Fig. 2.5. Point-to-point MIMO link.

The spectral efficiency of the link with the unit bits/second/Hz under sufficiently high signal to noise ratios will be approximated using the expression in Eq. (2.17):

$$C \propto \min(M, K) \log_2(\rho_d), \quad \rho_d \gg 1, \quad (2.17)$$

$\rho_d$  is the expected signal to noise ratio at any receiver if one of the transmitting antennas was fed by full power. Therefore, the throughput can be increased by having a greater number of antennas at both ends of the link, this increase can be achieved without increasing radiated power or spectral bandwidth.

The system capacity in bits/s/Hz can be found by the use of Shannon theory which is stated in Eq. (2.18).

$$C = \log_2 \det \left( \mathbf{I}_K + \frac{\rho_d}{M} \mathbf{G}_d^H \mathbf{G}_d \right) = \log_2 \det \left( \mathbf{I}_K + \frac{\rho_d}{M} \mathbf{G}_d \mathbf{G}_d^H \right) \quad (2.18)$$

Where the matrix  $\mathbf{G}_d$  is the  $M \times K$  channel frequency responses; this channel is available between the antennas in the BS and the terminal antennas.  $\mathbf{I}_K$  is the  $K \times K$  identity matrix, and “H” represents “conjugate transpose”. In order for equation (2.18) to be valid, then two conditions must be satisfied:

1. The receiver additive noise is complex Gaussian.
2. The knowledge of the matrix of the downlink channel at the receiver.

The channel is not required to be known by the transmitter, although more simplified and improved operation will be attained if both ends of link know the channel.

Eq. (2.17) can be resulted for sufficiently high SNR by the asymptotic random matrix theory if the elements of  $\mathbf{G}_d$  satisfy the subsequent conditions:

1. Elements are Independent to each others.
2. They have Identical distribution.
3. The mean of the complex Gaussian is equal to zero.
4. Their variance random variable is equal to one (i.i.d. Rayleigh fading).

Eq. (2.18) can be applied for downlink and uplink operations. The downlink channels are not the same as the uplink channels in FDD systems. On the other hand, channels are the same for uplink and downlink channels in TDD systems; FDD is frequency division demultiplexing, TDD is time division demultiplexing.

The important idea in point-to-point MIMO is that a vector valued signal is transmitted from the BS and modified by the channel matrix such that the received signals vector will be obtained. The different transmitted signals can be recovered reliably by the receiver. If the channel matrix was well-conditioned, then the received vector will contain linear combinations of the transmitted signals, and hence the receiver can also recover the transmitted signal easily.

The transmitter sends known training sequences through the channel such that the channel matrix will be known by the receiver. These training sequences are called pilots. The optimum training signals are mutually orthogonal. As a result of that, the number of transmitting antennas will be equal to the least possible sample duration for the pilot sequences if downlink operation is taking place. For uplink operation, the period of uplink pilots should be at least equal to the number of antennas in the array of the user or terminal. Therefore, the required time for training for a complete communication operation equal to the period of time required for downlink pilots plus the time required for uplink pilots, and this amount of time is the same for TDD or FDD operations.

Point-to-point MIMO was not scaled by more than 8\*8 and this is for many reasons:

1. The propagation environment does not support more than 8 data streams.
2. Line of sight condition limits the scalability.
3. The training time will increase as the number of antennas increases.
4. SINR are low at the edge of the cell and the multiplexing gains fall.
5. The equipment for a user will be complex. Also, the required electronics chains for each antenna should be independent of each others.
6. Complex signal processing at BS and user sides.

For a point-to-point MIMO, the instantaneous channel capacity in bits/s/Hz can be found as in Eq. (2.19), given that the transmitted signals are independent and identically distributed (i.i.d.) Gaussians.

$$C = \log_2 \left[ \det \left( I_N + \frac{\rho}{N_t} H H^H \right) \right] \quad (1.19)$$

Where  $N_t$  is number of transmitting antennas. If the channel matrix  $H$  includes normalized propagation coefficient such that  $Tr(H H^H) \approx N_t * N_r$ , then the upper and lower bound for the channel capacity can be found as shown in Eq. (2.20).

$$\log_2 \left[ \left( 1 + \frac{\rho}{N_t} \right) \right] \leq C \leq \min(N_t, N_r) \log_2 \left[ \left( 1 + \frac{\rho * \max(N_t, N_r)}{N_t} \right) \right] \quad (2.20)$$



It should be mentioned here also that for a point-to-point MIMO system consisting of  $N_t$  transmitting antennas, and  $N_r$  receiving antennas, and having a channel between the transmitting and receiving antennas, then each receiving antenna will receive a combined action of all transmitting antennas.

- **Multi-User MIMO:**

The advantages of Multi-user MIMO systems over the point-to-point MIMO systems are:

1. They are less sensitive to the environment of propagation.
2. Terminals with a single antenna will be required.

For multi-user MIMO systems, the Shannon-theoretic version not scalable because:

1. The dirty paper coding and decoding are becoming complex in an exponential manner.
2. The time occupied for CSI acquisition will increase.

Multi-user MIMO achieves the feature of the massive MIMO systems of multiplexing gains, and it can eliminate the problems coming from having unfavorable propagation environments. The channel capacity on uplink is shown in Eq. (2.21) for multi-user MIMO systems.

$$C = \sum_{k=1}^K \log_2[(1 + N\rho_u d_k)] \quad (2.21)$$

$d$  is the complex small and large scale fading.  $N$  is the number of BS's antennas, and  $K$  is the number of terminal's antennas. Using matched filtering processing method, the capacity in Eq. (2.21) can be achieved.

For downlink operation, the used operation scheme is the TDD (time-division duplexing) mode for most of the times. It is important to mention that the downlink channel can be found by taking the transpose of the uplink channel. Now, the channel capacity for downlink and with power allocation can be found by the use of Eq. (2.22).

$$C \approx \max_{\mathbf{P}} \log_2[\det(I_K + \rho_d \mathbf{NPD})] \quad (2.22)$$

$\mathbf{P}$  is the positive diagonal matrix with its diameter includes the power allocations, and the total sum of these diagonal elements is 1.  $\mathbf{D}$  is the matrix of small and large scale fading.

If TDD is used, then CSI is required to be known by the BS such that multi-user precoding will be done in downlink operations and detection will be done in uplink operations. The number

of transmitting antennas will affect the time or frequency resources used for channel estimation, while number of receiving antennas will have no effect on these resources.

If FDD is used, which means that different frequency bands are used for uplink and downlink operations, the CSI in downlink is different than that in uplink. For channel estimation in uplink, all users send their different pilots to BS, and the number of BS's antennas does not affect the time required for uplink pilot transmission at all. On the other hand, to get CSI for downlink operation, the BS sends pilots to all users, after that, the users feed the BS back with the estimated CSI of the channels. Here, the number of BS's antennas has a direct impact on the time required for downlink pilots. If the number of BS's antennas is large, then downlink channel estimation will be infeasible because the whole slot time will be consumed for downlink pilots.

Therefore, TDD systems are used and estimating the channel there is feasible even if the number of BS's antennas is large. In this case, the channel is reciprocal, and hence CSI should be estimated for uplink only. Fig. 2.6 shows a TDD protocol which was proposed. It can be seen from Fig. 2.6 that the users send data to BS in the beginning, and then they send their different pilots, then the CSI is estimated in the BS and the transmitted data from users can be detected, and beamforming can be achieved and generated and hence downlink data transmission to the correct user can be done. The pilots are orthogonal in the same cell, but they are reused at other cells because of the limited channel coherence time, and hence pilot contaminations arise.

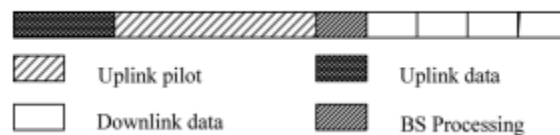


Fig. 2.6. Multi-user MIMO TDD protocol.

Channel estimation based on linear MMSE is used commonly. A time-frequency training sequences has been proposed such that the spectral efficiency of the communication system will be enhanced.

- **Scaled Multi-User MIMO, Massive MIMO Systems**

In massive MIMO, there are no attempts to reach full Shannon limit, and the size of the system will increase. Massive MIMO system provides channel capacity which is closer to Shannon-theoretical in practice by three ways:

1. Only the BS is required to know the downlink channel. In addition, the number of BS's antennas has no impact on the time required to obtain CSI in a TDD system.
2. The number of users is less than the number of BS's antennas by many times.
3. In downlink operation, easy linear precoding multiplexing will be used, and it is coupled with linear decoding demultiplexing used for uplink operation.

It should be mentioned that the linear precoding and decoding performance can approach Shannon limit if the number of BS's antennas increases.

The Shannon sum-capacity for uplink massive MIMO is shown in Eq. (2.23), and in this case only the BS is required to know the channel matrix.

$$C_{sum\_up} = \log_2 \det \left( \mathbf{I}_K + \frac{\rho_u}{K} \mathbf{G}_u^H \mathbf{G}_u \right) \quad (2.23)$$

The Shannon sum-capacity for downlink massive MIMO is expressed in Eq. (2.24), and in this case the whole downlink channel should be known by the transmitter, and each user will be required to know the corresponding downlink channel.

$$C_{sum\_down} = \sup_{\mathbf{a}} \{ \log_2 \det(\mathbf{I}_M + \rho_d \mathbf{G}_d \mathbf{D}_a \mathbf{G}_d^H) \}, \quad \mathbf{a} \geq 0, \quad \mathbf{1}^T \mathbf{a} = 1 \quad (2.24)$$

Where  $\mathbf{D}_a$  is a diagonal matrix where diagonal elements are  $M \times 1$  vectors,  $\mathbf{a}$ .  $\mathbf{1}$  indicates the  $M \times 1$  vector which includes ones.

It can be seen from Eq. (2.24) that the downlink massive MIMO can provide higher capacity compared to that provided by point-to-point MIMO, and this is because of the additional channel state information assumed in massive MIMO systems. In order to attain near-capacity performance, dirty paper coding or decoding should be used. Acquiring very accurate estimates for the channel will make the dirty paper coding more successful.

Uplink CSI will be acquired for the BS by the use of uplink pilots, and if TDD is used then the downlink CSI can be acquired for the BS because it is equal to that of uplink operation because of channel reciprocity; downlink and uplink channels are mathematically equal for TDD operations. The downlink CSI is acquired for users from orthogonal downlink pilots, and this downlink CSI is important to be acquired for the dirty paper decoding. Therefore, the complete acquisition for CSI require the time of uplink and downlink pilots for FDD operations.

### 2.4.3 Linear Precoding and Decoding for Massive MIMO

Nonlinear and linear precoding techniques can be used for typical MIMO systems. Nonlinear methods, like vector perturbation, lattice-aided methods, and dirty-paper-coding have better performance and more complex implementations compared with linear precoding methods. If the number of antennas in BS increases, then linear precoders like MF and ZF are nearly optimum. Also, using simpler linear precoders for massive MIMO systems will be more practical.

The spatial Matched Filter (MF) precoding has two important properties:

- The radiated beams can be directed to a point and not only to a specific direction.
- Focusing the beams to a specific point can be enhanced if more antennas were used. Focusing beams to specific points will reduce interference between close users.

Fig. 2.7 and 2.8 show the uplink operation with the matched filter decoding, and the downlink operation with conjugate beamforming, respectively. These are the easiest linear precoding and decoding systems.

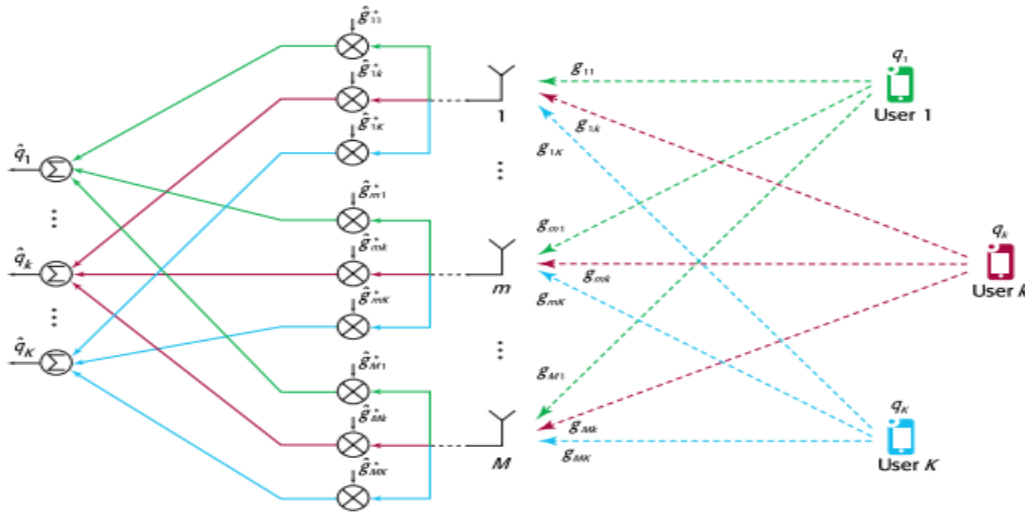


Fig. 2.7. Matched filter decoding for uplink massive MIMO.

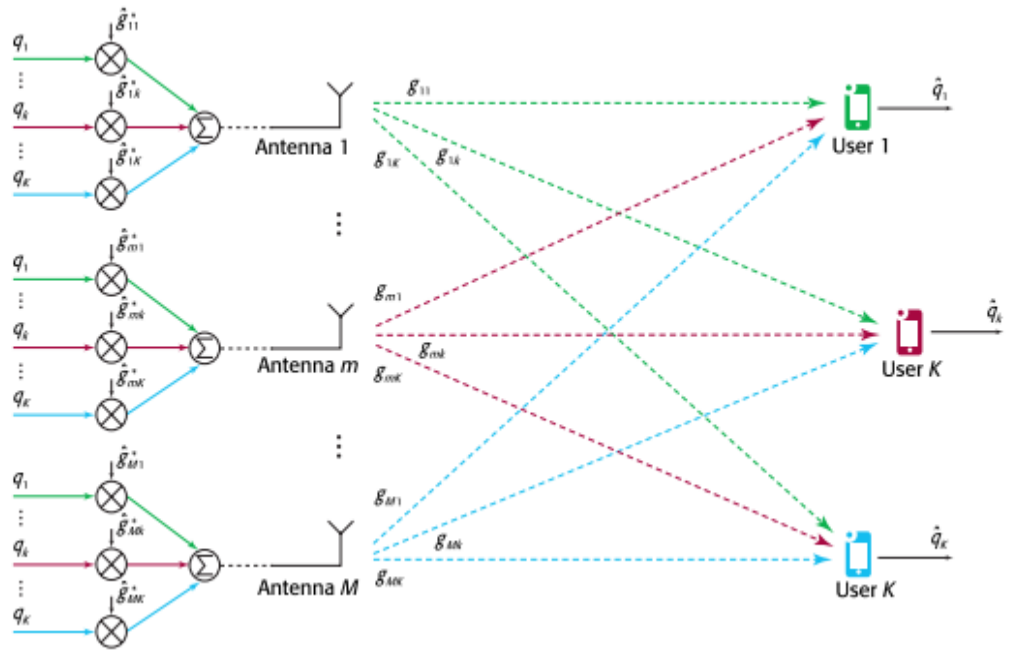


Fig. 2.8. Downlink massive MIMO with Conjugate beamforming.

For the uplink operation, the users send their QAM symbols, which carry data, and all users transmit simultaneously. Now, the QAM symbol transmitted by the  $k$ -th user will be denoted by  $q_k$ , and the frequency response between user  $k$  and the  $m$ -th BS's antenna is known and it is  $g_{mk}$  in Fig. 2.7. In order to find the QAM symbol  $q_k$  again, the inputs from all antennas at the BS will be weighted by the complex conjugate of the corresponding frequency responses of the channel. Then all the weighted inputs are added and hence the symbol  $q_k$  is recovered. If multiple users are transmitting simultaneously, interference will be there. If favorable propagation conditions are satisfied, then the following is correct:

1. If the number of BS's antennas increases, the orthogonality of channels from one user to another will be more.
2. The number of the BS's antennas affect the expected received power of the desired signal, in a way that this expected power will increase faster than the interference power as many times as the number of BS's antennas.

For the downlink operation, the  $k$ -th QAM symbol  $q_k$  is weighted first by the complex conjugate of the estimate for the  $mk$ -th channel coefficients before going to all antennas in BS, and then all other weighted signals are added to the weighted QAM signal before going to each antenna. After that, the signals are transmitted through the channel from all antennas to the  $k$ -th user, and

signals multiplied or modified by the channel matrix will reach the users. User  $k$  will receive the  $k$ -th QAM symbol because of constructive addition for the required signals at this user, and hence  $q_k$  will be recovered and received. In addition, the power for required signals increases faster than the power of the interference as many times as the number of antennas and this is because the channels are orthogonal to each others and they are under favorable propagation environment. The performance of linear precoding and decoding will be affected if the acquired channel estimates were imperfect, and this effect can be summarized as follows: Regardless of the noise added to the channel estimates, the coherent gain increases as the number of BS's antennas increases, this increase is done by a factor which decreases when the estimation error increases. However, other types of linear precoding and decoding can be used. For example, zero forcing filters can provide better performance than the performance of conjugate beamforming and matched filtering if SNR is high.

The signal processing can be done at each antenna of the massive MIMO if conjugate beamforming and matched filtering were used. This is an advantage gained when matched filtering and conjugate beamforming is used.

On the other hand, linear and simple signal detectors are used for massive MIMO systems, such detectors are like the matched filtering, Zero forcing and MMSE detectors. By the use of such detectors, good channel capacity can be achieved if the number of users is much smaller than the number of BS's antennas and if the channel vectors are independent of each others. The same performance of the MF receiver can be achieved if MMSE receiver was used with fewer number of antennas, even if inter-cell interference is available. MMSE receivers are like the optimal MMSE receiver which takes the different power levels coming from many users into account. The suboptimal MMSE receiver assumes equal power levels from all users. In order to have better performance, then nonlinear detection may be used but computations will be much more difficult. An example for non-linear detectors is the block-iterative generalized decision feedback equalizer which has been proposed.

If the number of BS's antennas increases, then the linear precoding and the dirty-paper coding in massive MIMO systems are comparable to each others.

## 2.4.4 Channel Estimation

It is very important to measure the frequency responses of channels for massive MIMO systems to make them operational. The BS or the user transmit known training signals and the receiver for these signals can estimate the channel frequency responses. When the channels are fully estimated, the CSI should be used quickly before the users move and hence a change in channels will take place. Therefore, because of this limitation in time, the available time for training is limited. The time occupied for data transmission and training should be done in a time slot with a duration which is less than the time required for anybody to move more than a fraction of a wavelength. In addition, the users transmit orthogonal pilot sequences in a TDD system. Assume that OFDM symbols are transmitted, then the number of OFDM symbols which can be transmitted through this system is equal to the slot duration divided by the symbol duration. Also, higher mobility can be allowed if shorter slots are used. For example, if the frequency of operation is 1.9 GHz and the speed of the user is 280 km/hr, then this user can move  $\frac{1}{4}$  wavelength in 500 microseconds. Therefore, the slot duration should be 500 microseconds. The equivalent sample duration is 98 and hence 98 users can be trained. However, if this upper limit was used, then there will be no time for transmitting data. However, less than half of the slot should be used for training. Fig. 2.9 shows the TDD slot structure. FDD systems require more time for training than TDD systems. The slot structure for FDD massive MIMO is shown in Fig. 2.10. The time which is required for training in FDD systems is two times the time required for training in TDD systems; the required time will be the downlink training time plus the uplink training time.

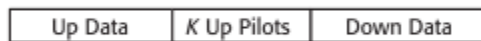


Fig. 2.9. Slot structure for TDD massive MIMO.

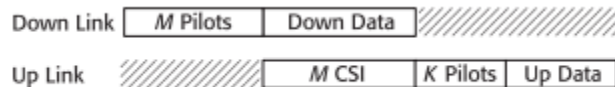


Fig. 2.10. Slot structure for FDD massive MIMO.

The pilot contamination can be mitigated by making the orthogonal pilot sequences seven times longer than what is required.

Massive MIMO systems make use of the channel information which is measured and not assumed, and the increase in number of antennas always help. Because the channel is measured,

the massive MIMO technology is scalable. If the channels information was assumed then massive MIMO will not be scalable anymore. Also, if the channel response is assumed, then finding the user can be done through transmitting beams from BS and transmit downlink pilots in each beam. Each user will choose which beam is best for him during uplink operation, and hence the BS will transmit the downlink data to this user through the preferred beam for him.

### 2.4.5 Power Control

Power control in downlink and uplink operations require the multiplication of the power control coefficients with the K QAM symbols as shown in Eq. (2.25).

$$\begin{aligned}
 \text{downlink: } q_k &\xrightarrow{\text{after multiplication}} q_k \sqrt{\eta_k}, k=1, \dots, K, \sum_{k=1}^K \eta_k \leq 1 \\
 \text{Uplink: } q_k &\xrightarrow{\text{after multiplication}} q_k \sqrt{\eta_k}, k=1, \dots, K, \eta_k \leq 1
 \end{aligned} \tag{2.25}$$

Massive MIMO has a good property that is the beamforming gains are constant over frequency and this is due to the huge number of antennas. However, the beamforming gains depend on the large-scale fading coefficient, and these coefficients are fortunately also independent of frequency. Therefore, the beamforming gains can be frequency independent gains and their impact on the data rates achieved by a user can be found even if the estimates of the channel are not known.

### 2.4.6 Advantages and Benefits of Using Massive MIMO

Some benefits of the massive MIMO systems are:

1. The channel capacity will be enhanced by 10 times and the efficiency of radiated power will be improved by 100 times when massive MIMO systems are used. This increase in the channel capacity is because of the use of the aggressive spatial multiplexing. The radiated energy beams can be directed to specific points with extreme sharpness if the number of used antennas is large, and as a result of that, the energy efficiency will be enhanced more. These phenomena of having focused beams happen physically because of the coherent superposition of wavefronts. If it is required to eliminate the Interference between terminals, then more transmitted power will be required. The number of used antennas affect the spectral efficiency in a direct proportional relation.
2. The used electronic components for massive MIMO systems can be cheap and with low power consumption. Expensive 50 W amplifiers can be replaced with much cheaper



amplifiers which provide output power in the range of milli-watts. Also, it is possible to eliminate large coaxial cables. Also. The constraints on accuracy and linearity of RF chain and amplifiers will be relaxed using massive MIMO. Large number of antennas will be used in massive MIMO systems, and hence fading, noise, and hardware imperfections will be negligible compared with the received signal or signal of interest. The channel of a massive MIMO system has a large null-space, and hence the energy can be focused to required points or directions, and because of that, the energy efficiency of the massive MIMO is better and lower power is consumed. Base stations consuming very low power can be powered by solar or wind energy. Also, the use of massive MIMO will alleviate the problem of electromagnetic exposure.

3. The use of massive MIMO systems reduces the air-interface latency significantly. The problem of latency is due to fading; a signal is transmitted from the BS's antennas, and it goes to the required terminal through many different paths. This can result in destructive interference between the waves coming from different paths and hence a fading dip is generated, and latency took place. However, massive MIMO is built such that it can avoid fading dips by beamforming and hence fading dips are no longer increasing latency.
4. The multiple access layer will be simple when massive MIMO systems are used. Each terminal can be given the whole bandwidth.
5. Robustness against intentional jamming or man-made interference will be more when massive MIMO systems are used.

#### **2.4.7 Limiting Factors of Massive MIMO**

Some limiting factors in the face of massive MIMO systems are:

- **Channel Reciprocity**

Time division duplexing technique depends on having reciprocal channels. If the propagation channel does not include magnetic material with strange magnetic properties, then it is itself a reciprocal channel. But, the hardware chain in the base station and in the terminal may not be reciprocal for uplink and downlink cases. However, Calibration can solve this problem.

- **Pilot Contamination**

An orthogonal uplink pilot sequence will be assigned to each terminal. Unfortunately, the number of available orthogonal pilot sequences is limited. Therefore, some pilot sequences will be reused again, and the negative consequences of this problem is called pilot contamination. This problem causes errors in beamforming and in the estimation of the channel. This problem can be dealt with by some ways, such as:

- a. Optimizing the allocation of pilot waveforms.
- b. Using clever estimation algorithms or by the use of techniques which does not use pilots at all.
- c. The new precoding techniques where network structures are taken into account should be used.

- **Orthogonality and Radio Propagation of Channel Responses**

Favorable propagation property is assumed for massive MIMO systems in most of cases. This assumption defines the radio environment and it assumes that the responses of the propagation channel between the terminals and the base station are very different from each others. It should be mentioned that the sum rate in bits/s/Hz increases as the number of BS's antennas increases, and the variance of the sum rate decreases. In addition, it should be mentioned that when linear complex precoding methods are used, then the propagation channel converges faster to the performance of an i.i.d. channel, and smaller variance of the sum rate will be achieved. Furthermore, the spatial resolution can be enhanced when large arrays are used and when different spatial signatures are used for different users around the corresponding base station. Hence, the capability of separating the users to a large extent is achieved. If the BS's antennas are 10 times more than the number of users, then stable performance close to the theoretical ideal performance can be achieved.

Also, it should be mentioned that massive MIMO depends on favorable propagation. The favorable propagation means that the vector-valued channels to different users grow asymptotically orthogonal with the increase antennas' number.

- **Limited Number of Served Users**

There are a limited number of users who can be served simultaneously, and this is because of the overhead required for CSI acquisition. The number of antennas in BS can be increased, but this

increase will enhance the SINR experienced by each user, and hence some improvements in throughput will be noticed, and this does not solve the problem of limited number of served users.

## **2.4.8 Research Problems for Massive MIMO**

This field of massive MIMO systems has many problems which needs to be improved and solved through research, and here are some research problems:

- **Fast and Distributed Coherent Signal Processing**

The amounts of baseband data is very huge, and it is required to process these baseband data in real time. The processing of these data should be simple and linear.

- **The Challenge of Low-Cost Hardware**

The expensive 40 Watts transceivers are replaced with low power units used in the massive MIMO systems. Each antenna in the massive MIMO system will have its own electronics, low power amplifier, and signal processing units. Therefore, new design ways which are with low cost are required. In addition, massive MIMO systems will require new standards.

- **Internal Power Consumption**

It is required to enhance the energy efficiency of the massive MIMO systems and this can be achieved by reducing the internal power consumption of the massive MIMO systems. For example, the antennas which are not serving can be put into sleep mode, such that the energy efficiency will be enhanced.

- **Energy Efficiency**

Massive MIMO systems enhance the energy efficiencies. In Multi-user MIMO systems and when perfect CSI is used, the power can be reduced by a factor equal to the number of BS's antennas (compared with the consumed power by the SISO system) and the provided performance for a user is like the performance of a user in SISO system which consumes the whole power for serving this single user. If imperfect CSI is used, then the power of multi-user MIMO will be decreased by a factor of square root of the number of BS's antennas such that the same performance of SISO is achieved. Therefore, the energy efficiency increased.

It should be mentioned that the ratio of the spectral efficiency to the transmitted power is the definition of the energy efficiency. If perfect CSI is used, then energy efficiency will be increased if spectral efficiency increases. If the used CSI was imperfect, then energy efficiency increases with the increase in the spectral efficiency in regions where low power is transmitted. On the other hand, the energy efficiency decreases with the increase in spectral efficiency in regions where high power is transmitted and if imperfect CSI is used. In addition, the use of ZF precoder provides better performance in scenarios where the spectral efficiency is high and energy efficiency is low. On the other hand, the use of MF precoders provide better performance in scenarios where the spectral efficiency is low and energy efficiency is high.

Reducing the power consumed by electronics used in massive MIMO systems is very important metric which help in enhancing the energy efficiency. For example, the power consumed by the electronics used to select serving antennas, and other electronics should be minimized in order to enhance the energy efficiency. It was shown also that the energy efficiency can be maximized if all antennas are used when it is possible to ignore the circuit power compared with the transmitted power, or if a subset of the antennas are serving when the transmitted power and the circuit power comparable with each others.

- **Channel Characterization**

The ability to acquire channel information is very important for massive MIMO systems, and the user mobility limits the active users' number. Research is going on to find solutions to mitigate these limitations. Research is going on also on signal processing algorithms and modulation formats. Research is going on also at CSI acquisition issues.

- **Pilot Contamination**

The pilot sequences used by the users available in a cell and available in the surrounding cells should be orthogonal to each others; this is the ideal case. The used time period for a slot and the used bandwidths are limited, hence the number of orthogonal pilot sequences is limited, and as a result of that, the number of served users will be limited also. It can be seen that the pilot sequences are required to be reused in many cells which are close to each others, and hence the number of served users will be more and pilot contamination will take place. Increasing the number of BS's antennas will not solve the problem of limited SINR caused by pilot contamination. In uplink operation, interference in estimating the channel properties will take place because of using same

pilot sequences for users in different cells. In downlink operation, the interference is generated because BSs will transmit based on the received contaminated channel estimates.

Many methods can be used to reduce the problems caused because of the pilot contaminations. Some of these methods are discussed in the subsequent points:

a. *Protocol-based methods:*

This way can be used by a smaller number of active users with same pilot sequences, or through the reuse of frequency. Also, using a scheme which uses a time shifted protocol, the pilot contaminations can be mitigated. The idea here is to divide cell into many groups and a time-shifted protocol is used for each group as shown in Fig. 2.11. It can be shown in Fig. 2.11 that while group 1 uses the first three slots for uplink pilots, the other two groups use the same slots for different jobs and hence the pilot contaminations will be avoided between users in group 1 and in groups 2 and 3.

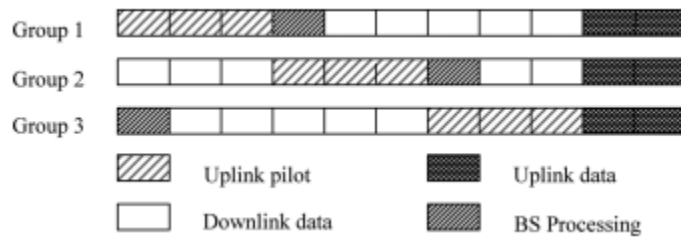


**Fig. 2.11. Time-shifted pilot scheme.**

b. *Precoding methods:*

In this method, the precoding box in a BS will be designed such that the sum of squared errors at its users is minimized, and the interference to the users of other cells is minimized as well. For example, the use of distributed single-cell precoding method provides better performance than the performance acquired if traditional single-cell ZF precoding was used. In addition, using precoding methods with multi-cell cooperation can reduce the pilot contaminations. Also, the information exchange overhead is limited if a pilot contamination precoding is used.

c. *AOA-based methods:*

It was shown that some users with non-orthogonal pilot sequences might have zero interference between them, this was shown under realistic channel models.

d. *Blind methods:*

These methods are based on subspace partitioning and can mitigate the pilot contamination. For example, pilot contamination can be mitigated using iterative least-square with projection estimation of channel vectors and an eigenvalue-decomposition-based channel estimation. Using blind pilot decontamination scheme, the pilot contamination can be eliminated.

- **Non-CSI@TX Operation**
- **New Deployment Scenarios**
- **System Studies and Relation to Heterogeneous Network and Small-Cell Solutions**
- **Prototype Development**
- **Hardware Impairment**
- **Cost of Reciprocity Calibration**

#### **2.4.9 Challenges Facing Massive MIMO Systems**

Many challenges face massive MIMO systems, these challenges are discussed in the subsequent points.

- **Propagation Models**

Many assumptions are presumed for the channel and these assumptions causes errors which should be reduced. For example, it is sometimes assumed that the channels of different users are spatially uncorrelated and the channel vectors are orthogonal to each others under favorable propagation conditions if the number of antennas increases. Another example, it is assumed in theoretical studies that conditions are i.i.d complex Gaussian and this assumption is difficult to be justified. However, the following points were found:

1. Correlation coefficients for real antennas are much larger than what are expected under the assumptions of i.i.d. channels.

2. Assuming orthogonality between the channel vectors when the antennas' number is large is difficult to be achieved.
3. There is a big degradation in performance when the users are located close to each others even if the LOS paths are available; instead of obtaining 80 – 90 % of the bound of the optimum dirty paper coding, 55 % can be achieved.
4. Finally, it was concluded that large fractions of the gains of theoretical performance can be obtained in practice using large antenna arrays, despite of the difference between the measured channel and the i.i.d. assumption.

- **TDD and FDD Modes**

Majority of massive MIMO systems use TDD mode due to feedback issues and channel estimation. However, FDD mode can be used in different cases like when efficient precoding techniques with partial CSI were used. Using FDD mode for massive MIMO systems will be a challenge, and how it is possible to reduce the overhead for CSI feedback is another important challenge. Frequency correction algorithms are required such that it is possible to achieve channel reciprocity in FDD systems. These algorithms are a challenge.

- **Modulation**

It is important to design and build BSs with huge number of antennas, and with power-efficient and low-cost amplifiers, but the problems with high PAPR can stop OFDM from having good performance. The use of single-carrier-transmission will lead us to obtain nearly optimum performance.

- **Pilot Contamination**

Pilot contaminations produces inter-cell interference which increases as the number of BS's antennas increases. Many channel estimations, cooperation and precoding methods were introduced to solve this problem. Also, there are many different methods which give better performance, and they are simple, and they have limited or no cooperation with BS. These methods are required to be studied.

- **Hardware Impairments**

The impact of hardware impairment on massive MIMO systems is important to be studied. Hardware effects can cause an error in channel estimation. An impairment in the user side is more

dangerous compared to that in BS side. Impact of phase noise, mutual coupling, per antenna power constraints, and analog and digital beamforming architectures should be studied from signal processing and transceiver implementation points of view.

- **Antenna Arrays**

Massive MIMO can be implemented on a 2D grid, or 3D distribution. Mutual couplings between the antenna ports and their effect be studied. The increase in computational and in hardware costs happening when large arrays are used should be considered also. The use of electromagnetic lens antenna can enhance the system performance and reduces the complexity and cost of implementation.

Finally, the massive MIMO can also be used in millimeter wave applications, and in heterogeneous networks. In heterogeneous networks, dense coverage and high throughput can be achieved because of the deployment of Pico or femto-cells.

#### **2.4.10 Important Features for mMIMO Systems**

Finally, many features of previous mMIMO systems in the literature were extracted from [144] – [160] such that it is possible to compare the mMIMO design of the thesis work with the previous designs. The subsequent features were extracted:

1. The resonant frequencies of previous mMIMO antennas were 2.6 GHz, 3.6 GHz, 4.8 GHz, 5.8 GHz, 7.25 GHz, 28 GHz, 32.6 GHz or 38 GHz.
2. Bandwidths were ranging from 100 MHz to 200 MHz to 1500 MHz to 10000 MHz.
3. It is possible to have 16 – 121 RF ports per panel at low frequencies.
4. It is possible to have 16 – 256 ports per panel at high frequencies.
5. Single radiating elements are usually patches or dipoles since they provide pure linear polarizations.
6. Maximum gain of a panel was 26.8 dB.
7. Maximum beam tilt was 34 degrees with a gain of 12.5 dB at high frequencies. – 7 dB was lost when going to maximum tilt angle of the beam. This tilt angle is in the azimuthal plane.



8. Maximum beam tilt was 47 degrees with a gain of 18 dB at high frequencies. – 2 dB was lost when going to maximum tilt angle of the beam. This tilt angle is in the azimuthal plane.
9. Isolation between ports were ranging from – 14 to – 35 dB.
10. Two operational modes were used; MIMO mode and Array mode.
11. Electrical separation between single elements is ranging from 0.37 lamda to 2 lamda.
12. Side lobe level is ranging from – 6 dB to – 15 dB.
13. Linear polarization or dual-linear polarizations are used most of times. Therefore, more than one port can be used per a single element of a mMIMO antenna.
14. Cross-polarization level is below the co-polarization level by – 13 dB to – 25 dB.

## 2.5 Direction of Arrival (DOA) Estimation

One well known algorithm used in estimating the DOA is called MUSIC Algorithm [11]. The eigen-structure of the covariance matrix will be subspace in this method. In this method, the covariance matrix will be decomposed into eigenvectors of signal and noise subspaces. By steering the signal vectors which are orthogonal to the noise subspace, the peak of the spatial power spectrum will be found and hence the direction of sources is found. The performance of this method provides good resolution and consistency. Suppose that a narrowband signal  $s(t)$  was impinged on a uniform linear array ULA from a specific elevation angle (theta angle), and  $N$  snapshots were taken, then the output of the array can be written as:

$$\mathbf{x}(t) = \mathbf{a}(\theta)\mathbf{s}(t) + \mathbf{n}(t) \quad (2.26)$$

Where  $\mathbf{n}(t)$  is additive white noise. And  $\mathbf{a}(\theta)$  is the steering vector of ULA defined in Eq. (2.27), where it can be seen that the responses of all array elements are represented in this vector.

$$\mathbf{a}(\theta) = [1 \quad e^{j\frac{2\pi}{\lambda}d\sin\theta} \quad \dots \quad e^{j\frac{2\pi}{\lambda}(M-1)d\sin\theta}] \quad (2.27)$$

The autocovariance matrix of the signal can be written as shown in Eq. (2.28).

$$\mathbf{R} = \frac{1}{N} \sum_{t=1}^N \mathbf{x}(t)\mathbf{x}^H(t) \quad (2.28)$$

It is required now for the MUSIC method that the subspace is estimated from the signal autocovariance matrix, and this subspace estimation will be achieved by eigen-decomposition process. Therefore, the subspace estimation can be given by:

$$\mathbf{R} = \mathbf{Q}_s \mathbf{\Lambda}_s \mathbf{Q}_s^H + \sigma_n \mathbf{Q}_n \mathbf{Q}_n^H \quad (2.29)$$

Where  $\mathbf{Q}_n$  and  $\mathbf{Q}_s$  are the noise and signal subspace eigenvectors, respectively. And,  $\mathbf{\Lambda}_s$  is the signal subspace eigenvalues. Then, the output power in music algorithm can be written as:

$$P_{MUSIC} = \frac{1}{\mathbf{a}^H(\theta) \mathbf{Q}_n \mathbf{Q}_n^H \mathbf{a}(\theta)} \quad (2.30)$$

Eq. (2.30) can be used for Uniform Linear Array (ULA) where its elements are isotropic radiators. For ULA where the used elements are directional radiators, then the steering vector and the power spectrum equations will be corrected as shown in Eq. (2.31) and Eq. (2.32), respectively.

$$\mathbf{a}_d(\theta) = G(\theta) \mathbf{a}(\theta) \quad (2.31)$$

$$P_{MUSIC} = \frac{1}{\mathbf{a}_d^H(\theta) \mathbf{Q}_n \mathbf{Q}_n^H \mathbf{a}_d(\theta)} \quad (2.32)$$

Where  $G(\theta)$  is the gain of the array at the elevation direction theta.

By using MUSIC algorithm, the direction of arrival of incoming signals can be known. After that, beamforming is required in order to receive the required incoming signals and filtered out the unrequired interference signals. It should be mentioned that many other advanced algorithms are available in the literature, one of them for example is the one in [12] where the number of snapshots is 1, and with this number, the direction of arrival of signals can be found. This part here is just to give briefly an idea on how the DOA is done.

This example is taken from [11], if three signals are coming from three elevation angles; one from  $-50$  degrees,  $0$  degrees, and  $60$  degrees, then by using the proposed DOA algorithm proposed in [11], the received signals will be as shown in Fig. 2.12, with isotropic elements used in the linear array. Fig. 2.13 shows the estimated angle of arrival for the received signals when a directional

antenna is used with patterns directed to boresight. Fig. 2.14 shows the pattern of the directional pattern.

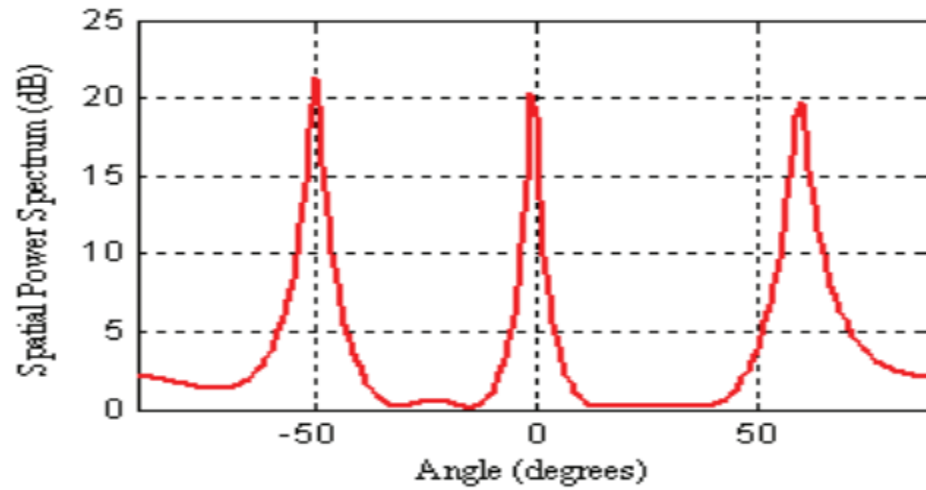


Fig. 2.12. Spatial power spectrum when isotropic antenna array is used.

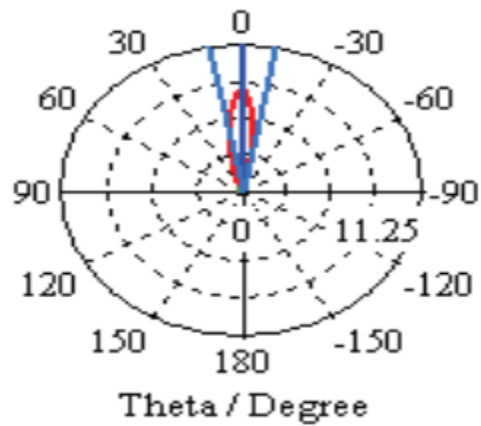


Fig. 2.13. The pattern of the directional element.

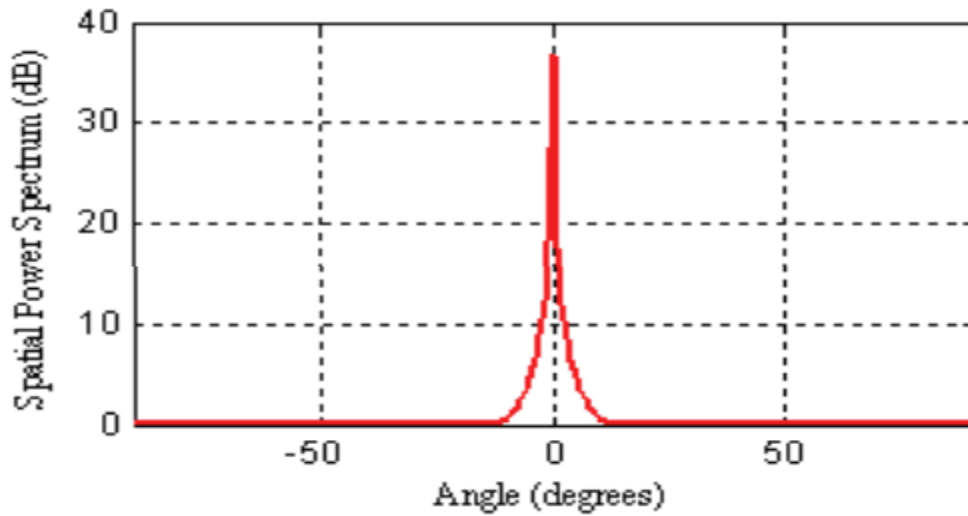


Fig. 2.14. Spatial power spectrum when directional antenna array is used.

## 2.6 FPGA

FPGA is a digital electronic circuit which can be programmed by using Verilog codes. FPGA is very useful in controlling reconfigurable antennas. FPGA is shown in Fig. 2.15.

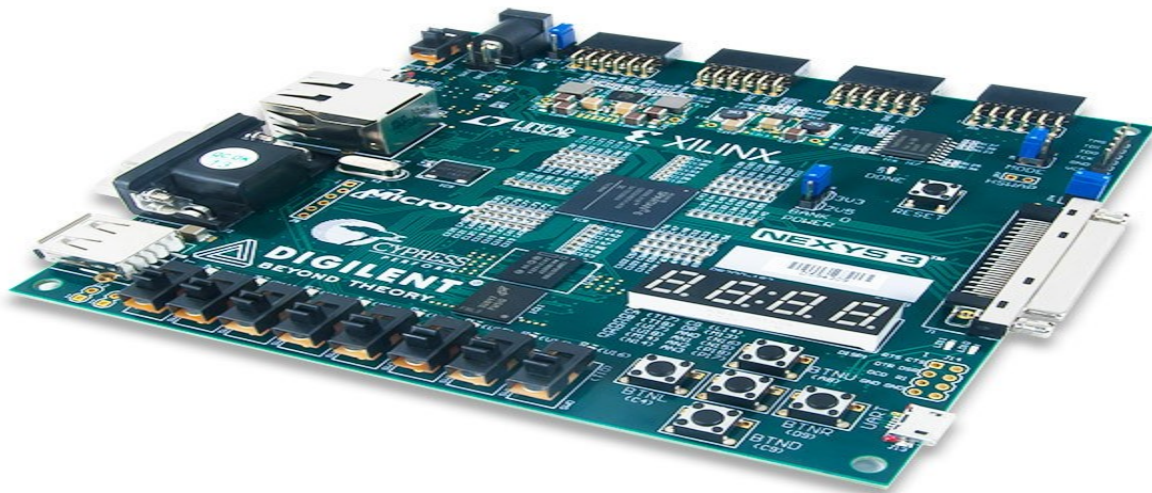


Fig. 2.15. FPGA digital electronic circuit.

## 2.7 Summary

In this chapter, many important topics related to reconfigurable antennas, 5G technology, MIMO systems, mMIMO systems and DOA estimation was presented. The definition of reconfigurability, used methods to achieve different types of reconfigurability, advantages of reconfigurable antennas, applications and future uses of reconfigurable antennas were discussed. After that, 5G technology with the interesting factors of this technology, some engineering requirements, major used techniques in this technology, and the research areas for 5G technology were presented in details. After that, MIMO systems were introduced and the parameters used to measure the performance of MIMO systems were introduced and discussed in details also. After that, the mMIMO systems were introduced and discussed in details. Many important topics related to mMIMO systems were discussed also; such as downlink and uplink operations for mMIMO systems, MIMO types, linear precoding and decoding, channel estimation, power control, advantages of mMIMO systems, challenges facing mMIMO systems, research areas for mMIMO systems, and some important features of mMIMO systems. Finally, this chapter introduces briefly the DOA estimation techniques.

## **CHAPTER 3**

# **LITERATURE REVIEW**

### **3.1 Literature Review Trees**

Fig. 3.1 – 3.7 show the trees of the whole literature review which was done for this research work. The parts which are circled with a red box are the parts of high concern for this research work.

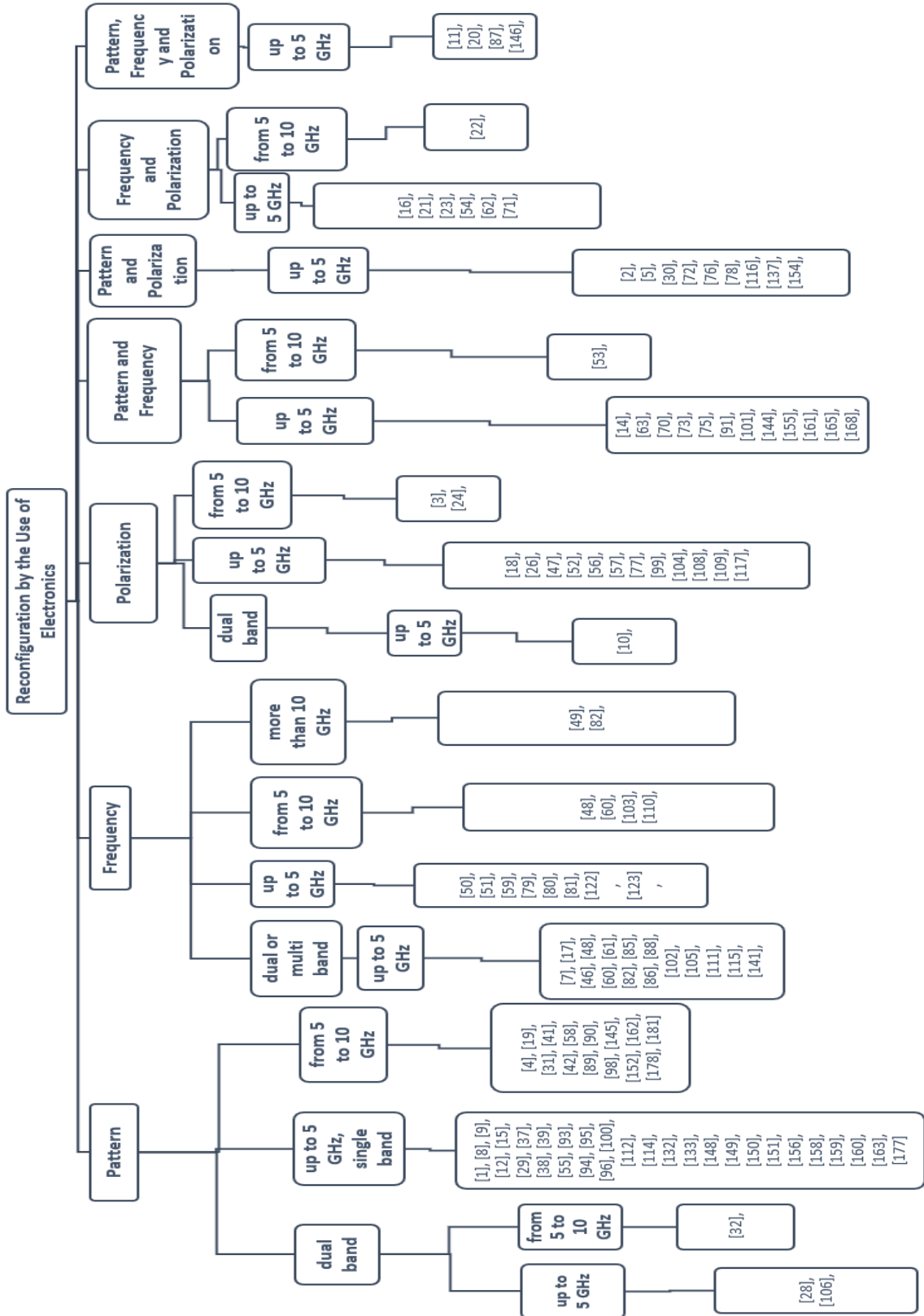


Fig. 3.1. Tree of Literature review about reconfigurable antennas when antennas are reconfigured electronically.

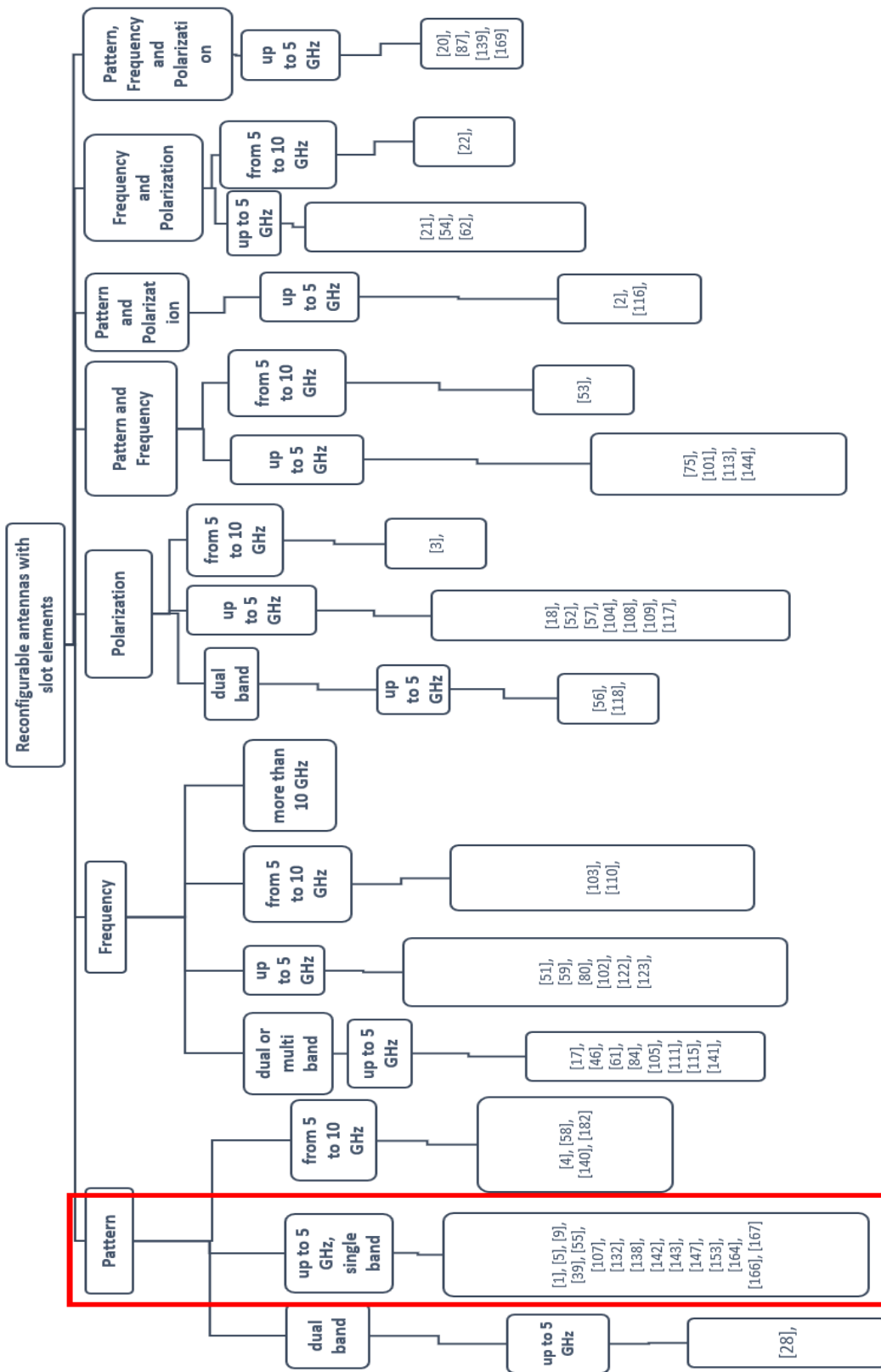
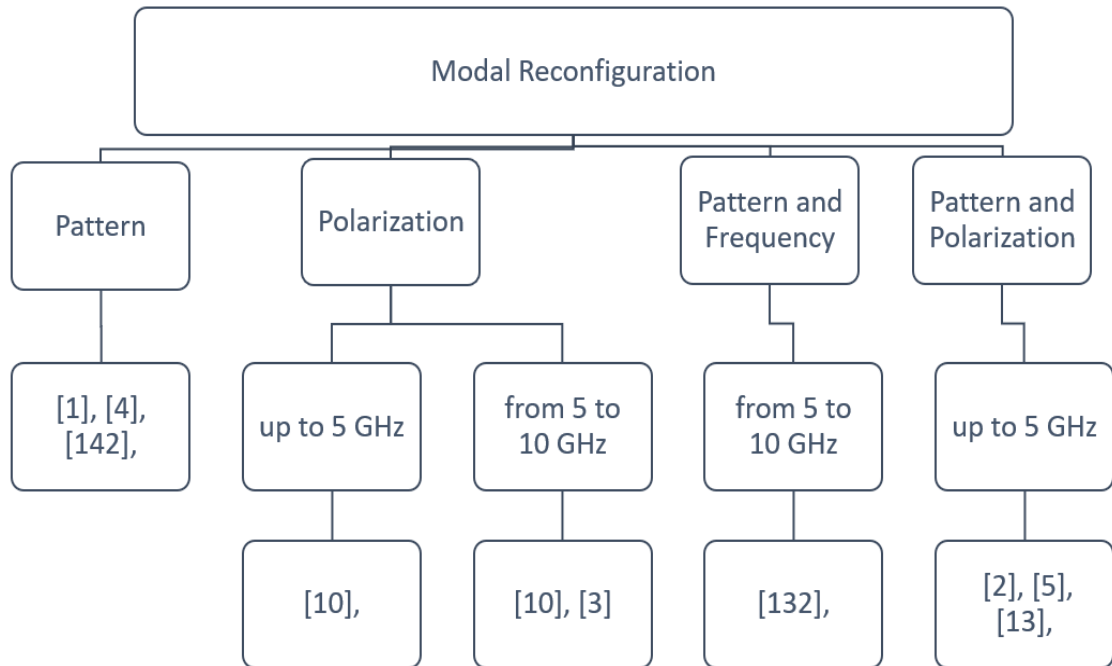
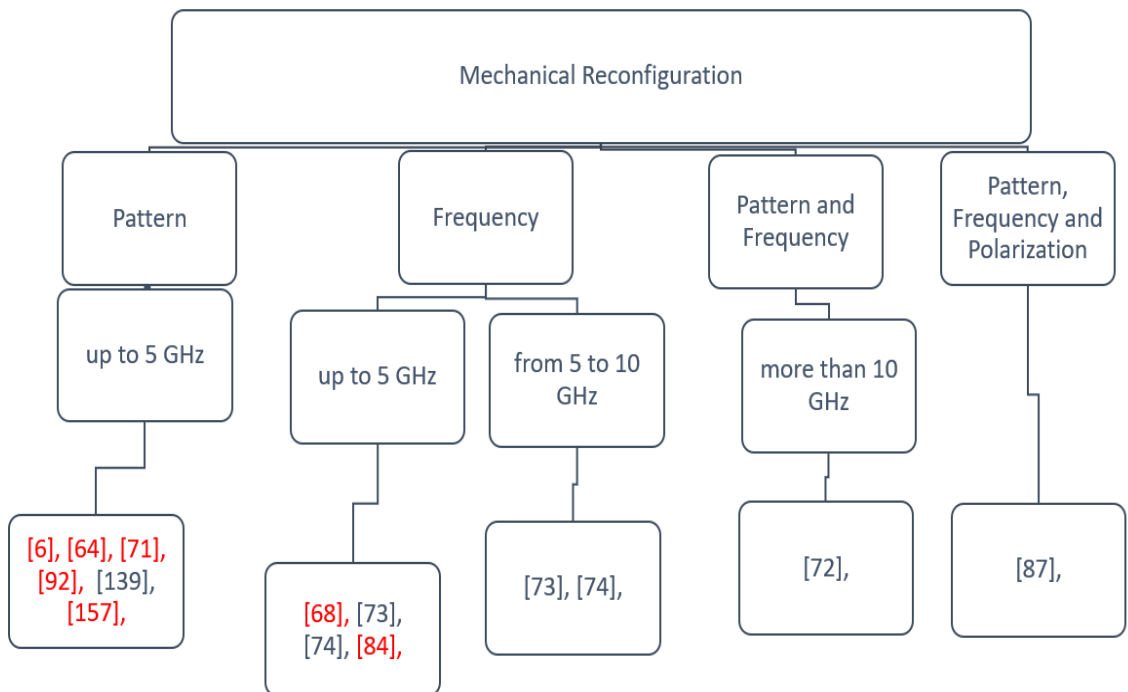


Fig. 3.2. Tree of Literature review about reconfigurable antennas when antennas are slot based antennas.





**Fig. 3.3. Tree of Literature review about reconfigurable antennas when antennas are reconfigured by changing excited modes of antennas.**



**Fig. 3.4. Tree of Literature review about reconfigurable antennas when antennas are reconfigured mechanically.**

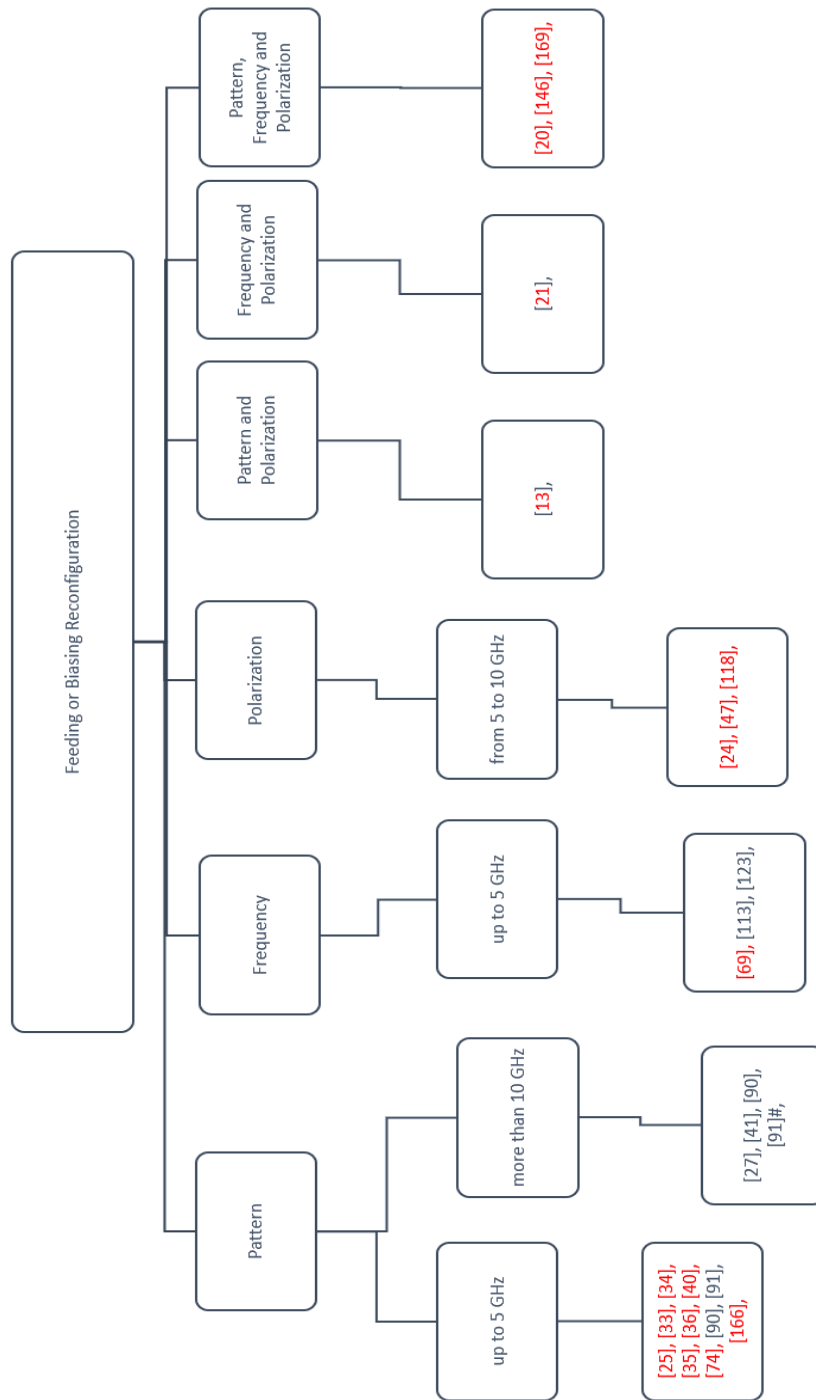


Fig. 3.5. Tree of Literature review about reconfigurable antennas when feeding networks are reconfigured.

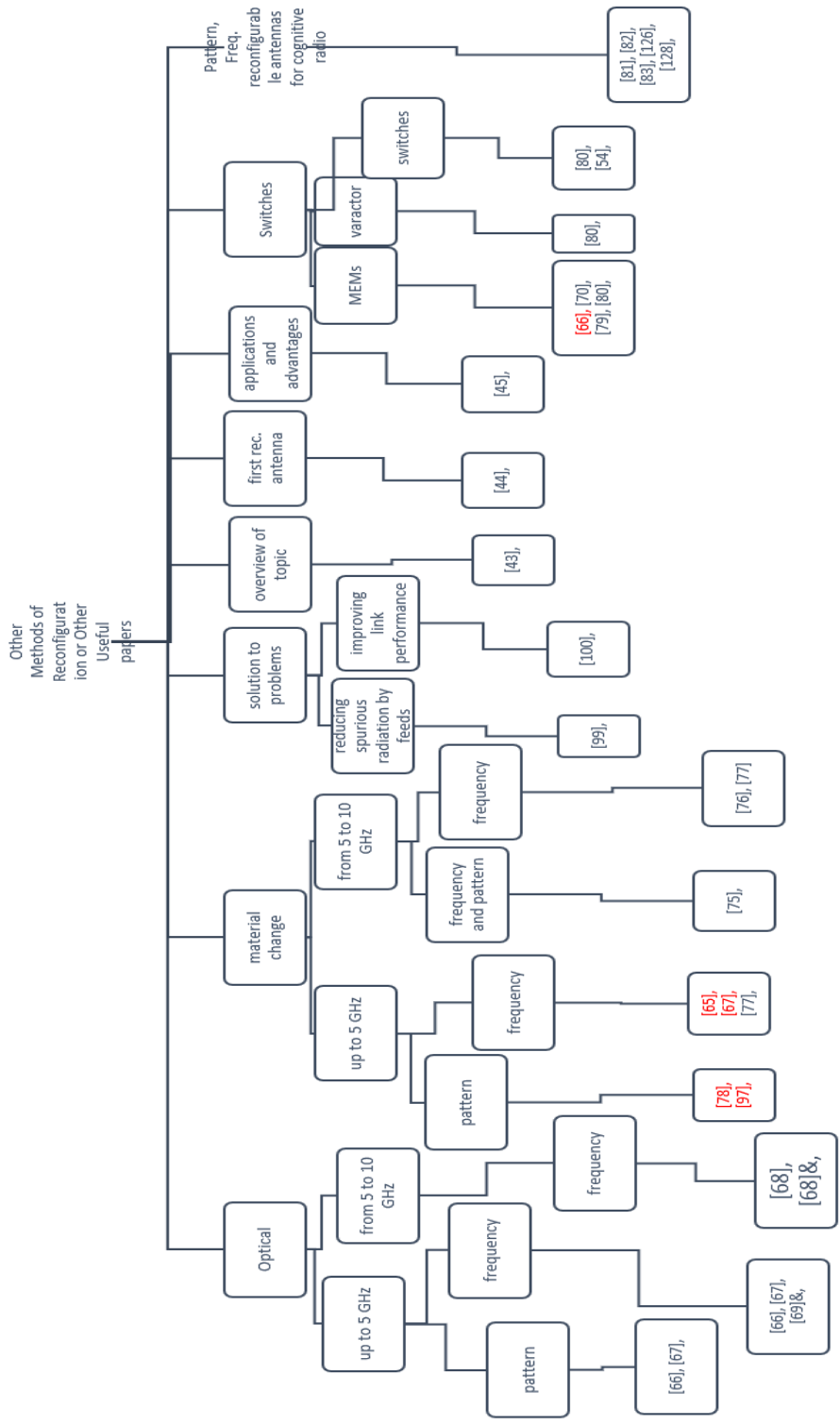


Fig. 3.6. Tree of Literature review about other types of reconfigurable antennas, and about some other useful topics.

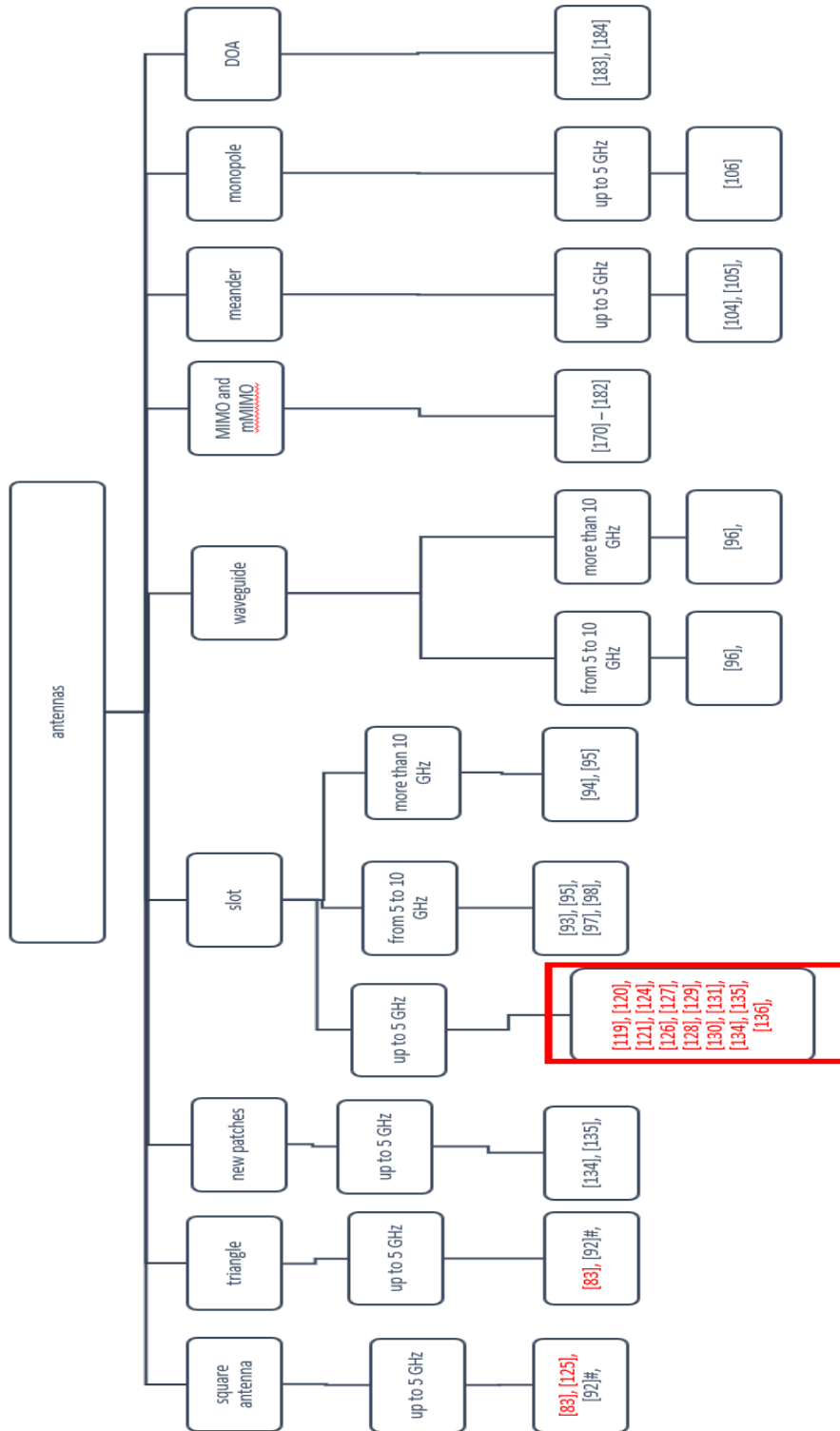


Fig. 3.7. Tree of Literature review about some useful antennas for this research work.

### **3.2 Pattern Reconfigurable Antennas**

Pattern reconfigurable antennas can be achieved by exciting different electromagnetic modes [13] – [15], by changing the radiating edges of an antenna and introducing nulls to some different edges [16] – [17], by reconfiguring the feeding network and changing the excited phases to different radiating elements [18], by mechanically changing the distance between radiating elements and parasitic elements [19] – [20], by exchanging the radiating element and the reflector element [21], by changing locations of directors and reflectors electrically [22] – [37], by using many ports with different input exciting phases [38] – [46], by reconfiguring connections between many parasitic patches electrically [47] – [48], by the use of arrays with different exciting phases [49] – [50], by reconfiguring the shorting vias electronically [51] – [52], by changing the distribution of the standing electric field distribution and changing the length of the radiating element [53] – [54], by controlling the phase constant value using metamaterials; phase constant can be positive in some regions and negative in other regions [55], by changing orientation of radiating elements or having different radiating elements [56] – [63], by changing the substrate curvature [64], by the use of reflectors [65] – [67], by changing magnitudes and phases of many aligned magnetic currents [68], by the use of frequency selective surface [69], or by using different radiating elements with different exciting phases [70].

### **3.3 Frequency Reconfigurable Antennas**

Frequency reconfigurable antennas can be achieved by installing a varactor in the middle of a rectangular slot etched on a patch [71] – [72], bridging slots etched on a patch by the use of diodes [73] – [76], by the use shorting posts connected to a patch [77], by adding metallic parasitics to radiating patch to change current distribution [75], [78] – [79], by loading a patch by a variable capacitance achieved using Coplanar Waveguide stubs with MEMs switches to vary its load [80], by the use of varactors or diodes in a folded dipole [81], by changing the dielectric constant of ferrite material [82] – [83], by changing the radiating structure [84] – [86], by the use of many ports feeding different structures [87], by changing the capacitive load of a PIFA antenna [88], by rotating or bridging rectangular Chebyshev slots etched on the surface of an antenna [89] – [90], by changing length of radiating elements or length of connected parasitics [91], by etching slots on printed monopole antennas to have frequency notches [92], or by adding metallic parasitics around the radiating element [93].

### **3.4 Pattern and Frequency Reconfigurable Antennas**

Pattern and frequency reconfigurable antennas can be achieved by the use of a reconfigurable parasitic pixel layer [94] – [95], by changing ground dimensions to change the used reflector and changing the length of radiating element [96], by the use of arrays and changing the patch dimensions [97], by changing the orientation of the radiating element and changing the length of the radiating element [98], by reconfiguring the antenna structure e.g. from patch to PIFA antenna [99], by reconfiguring the connection of metallic parasitics to the radiating element [100], by changing the phases of exciting fields and changing the substrate's permittivity [101], by changing the current path and by changing the length of the radiating element [102], by exchanging between reflectors and directors and by changing the radiating element size [103], by exciting different modes of the antennas structure and by using varactors [104], by loading the top of patches in an array by varactors [105], by reconfiguring the structure of the radiating element and adding a varactor [106], or by reconfiguring the states of radiating elements and by having different structures of radiating elements [107].

### **3.5 Pattern Reconfigurable Slot Antennas**

Pattern reconfigurable slot-based antennas are not common in literature. Pattern reconfigurable slot-based antennas can be achieved by exciting different electromagnetic modes in the antenna's structure [108] – [109], by the use of slot arrays with installed varactors [110], by the use of slot arrays with reconfiguring between radiating slots [111], by changing the current distribution on the antenna surface by the use of switches to bridge slots [112], by reconfiguring the feeding network [113] – [114], by reconfiguring the orientation or the type of the radiating slot electrically [115] – [120], by reconfiguring the feeding network to choose the radiating slot from available slots and by the use of reflectors [121], by the use of slot-based reflectors and changing the positions of reflectors electrically [122], by the use of Complementary Split-Ring Resonator (CSRR) with a patch to have many radiating elements with same patterns and out-of-phase phases or in-phase phases between the patterns' phases [123].

### **3.6 Frequency Reconfigurable Antennas**

Frequency reconfigurable slot-based antennas are achieved by changing the slot's length electrically [124] – [129], by installing a varactor in the slot [130] – [132], by the use of reconfigurable feeding network [133], or by reconfiguring between many slots with different lengths electrically [134].

### **3.7 Pattern and Frequency Reconfigurable Antennas**

Pattern and frequency slot-based reconfigurable antenna can be achieved by bridging the radiating slot to introduce nulls in the pattern and by reconfigure the feeding network by adding stubs [135], by changing the current path electrically and by adding shunt variable capacitances [136], by changing locations of slot-based reflectors and slot-based directors electrically and by changing the length of the radiating slot [137], or by reconfiguring the orientation of radiating slots electrically and by changing slot's length electrically [138].

### **3.8 MIMO Systems**

In [143], a new MIMO antenna with balanced open slot antennas is proposed for 5G technology. The MIMO antenna is an 8\*8 MIMO built on an FR-4 substrate with a size of 150 mm \* 80 mm \* 0.8 mm. The proposed MIMO antenna is shown in Fig. 3.8. It can be seen from Fig. 3.8(a) that the top face of the substrate includes eight L-shaped 50 ohms transmission lines. The bottom face of the MIMO includes the ground plane etched with 8 balanced open slots as shown in Fig. 3.8(b). The open balanced slot antenna is optimized to work in the frequency band from 3.4 GHz to 3.6 GHz such that LTE band 42 is covered. Therefore, the MIMO antenna operates in the frequency range from 3.4 – 3.6 GHz such that it can be used for future 5G smartphones. The antenna has a value of S11 being below – 10 dB in the frequency bandwidth of the antenna. The efficiency of the antenna is more than 62%, the isolation between the MIMO ports is more than 17.5 dB, and the envelope correlation coefficient is below 0.05. It is good to mention that the branch slot in Fig. 3.8(b) is used in order to make the antenna resonating at the required resonant frequency with less slot length; the branch slot was etched close to E-field null and hence this branch slot will be regarded as inductive loading, and this will help in being able to reduce the slot length more. The

dimensions of the branch slot ( $d$  and  $L_2$  in Fig. 3.8(b)) can change the resonant frequency of the slot antenna. The slot has a length of half wavelength at the required resonant frequency. Isolation between MIMO ports was enhanced by using two intrinsic decoupling techniques; reduced ground effects and orthogonal antenna arrangements. In other words, this high isolation between the MIMO ports was achieved by orienting Ant. 1 and Ant. 5 with respect to other antennas in a way that the polarizations between them are perpendicular to each others. In addition, the open end of the strip lines should be opposite to each others to reduce coupling. In addition, etching the branch slot will cause the electric current to be maximum in the middle of the slot and the current will reduce to minimum values at the open sides of the slot and hence the ground coupling currents between different ports will be reduced much and hence isolation will increase between MIMO ports. The patterns of MIMO antennas have good diversity between them. The ergodic channel capacity of the proposed antenna array is around 40 bps/Hz. This proposed MIMO has a good robustness with the user's hand, battery, frame and LCD.

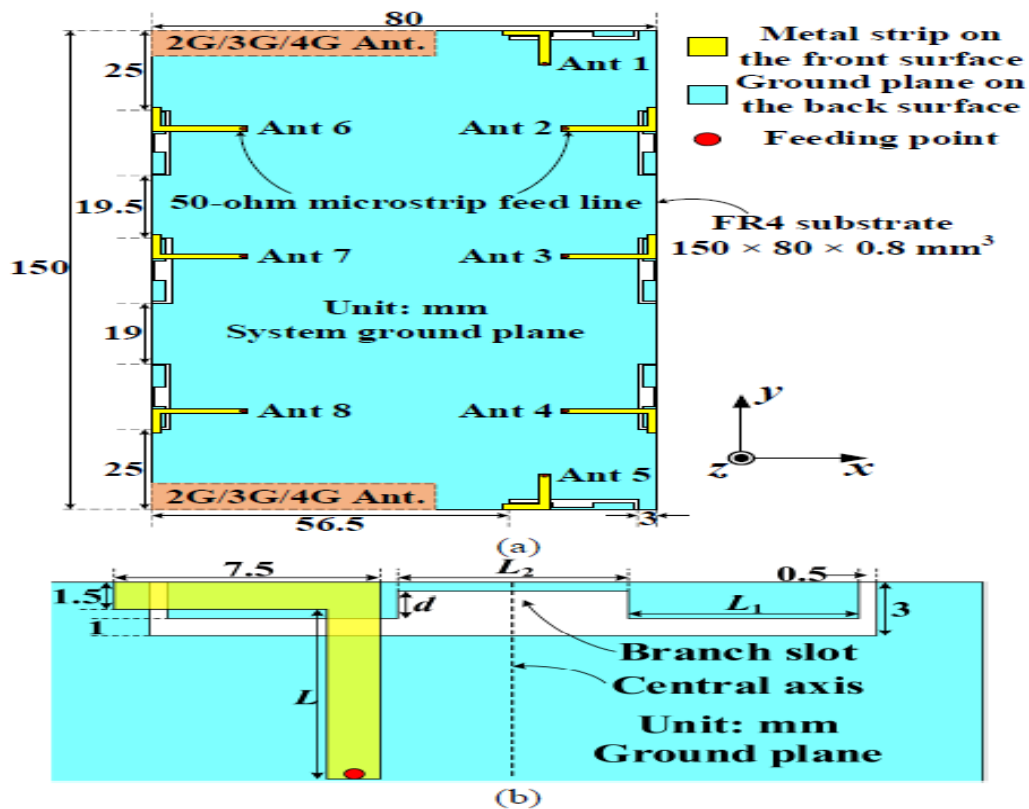


Fig. 3.8. The proposed 8\*8 MIMO antenna in [143].



### 3.9 Massive MIMO Systems

In [144], a massive MIMO system is designed with 24 radiating elements. Each element is an array of four patches, and by changing the phases feeding the patches in an array, different beam tilts are resulted and hence lower correlation coefficient is obtained. The system has 2 Rogers substrates with a dielectric constant of 4.1; the patches are on top layer, feeding lines are in bottom layer, and the middle layer is the ground plane. The massive MIMO is shown in Fig. 3.9. The proposed system is designed to operate at a resonant frequency 3.6 GHz and with a bandwidth of 100 MHz. The separation between patches is 0.89 wavelength to minimize the coupling. Minimum achieved isolation was  $-14.9$  dB. The achieved envelope correlation coefficient was 0.095. The realized gain was 19.5 dB with an efficiency of 64%. The size of the system is 44 cm x 30 cm.

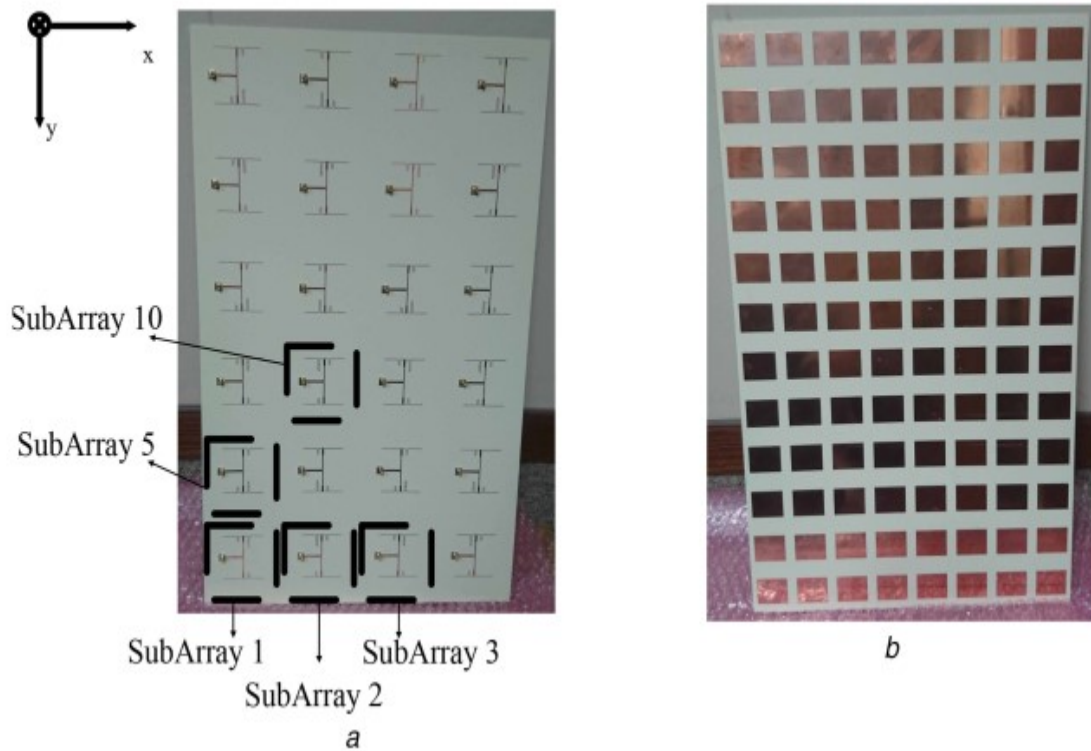


Fig. 3.9. The geometry of the 24 ports massive MIMO system proposed in [144].

The tables of comparison (Tables 3.1 – 3.3) between many massive MMO designs in Literature are shown below.

Table 3.1. Comparison table# 1 for many mMIMO systems in literature.

Reference	Band Coverage (GHz)	BW (MHz)	MIMO Order (RF ports)	Single panel arrangements (rows * columns)	Single-Element Type	Max. Gain (Single Port)	Max. gain (Single Panel)	Geometry	Single sector (panel) Size	Max. Beam Tilt	Elevation coverage	Gain of the beam at maximum tilt	HPBW of the beam at maximum tilt	Min. Isolation bet. ports
[144]	3.6	100	3 * 24	6 * 4	2*2 patches	9.41 dB	19.5 dBi	Triangular (can be hexagonal)	44.4 * 29.6 cm <sup>2</sup>	34 deg.	252 deg.	12.5 dB	23 deg.	-14.9 dB
[145]	5.8	200	64 (single panel)	1 * 64	1*4 patches	13 dBi	18 dBi	Single panel	256*21.5 cm <sup>2</sup>	30	180 deg.	---	--	---
[146]	3.7	185	100 (single panel)	T-shape, 4*25, or 10*10	patch	---	---	Single panel	80*120 cm <sup>2</sup>	---	--	---	--	---
[147]	3.7	160	144	3 * 4	2 * 2 patches	10.5 dB	16.7 dBi	6 panels	64.8 * 64.8 * 25.8 cm <sup>3</sup>	--	--	---	--	-35 dB
[148]	2.6	120	16 (single panel)	4 * 4	Antenna follows a dipole structure with two ports, metallic ring and metallic arms on top face	8.8 dB	12 dBi	---	---	---	---	---	---	-21 dB
[149]	3.6 – 4.8 GHz	1200	64 (single panel)	8 * 8	Two cross dipoles	---	26.8 dB	Single panel	---	---	---	---	---	---
[150]	32.6 GHz	1660	32 (single panel)	4 * 8	patch	---	20 dB	Single panel	2.4 * 4.5 cm	47 deg	282 deg	18 dB	---	-15 dB
[151]	38 GHz	10000	16	4*4	Planar high-gain dielectric-loaded antipodal linearly tapered slot antenna	14.5 dB	25.6 dB	36 * 16; 36 sectors	---	5 deg	360 deg	---	---	---
[152]	28 GHz	--	6*48	12 * 4	Horn	9.47 dB	26.28 dBi	6 sectors	11.66 * 6.81 cm <sup>2</sup>	30 deg	360	25.28 dB	--	---
[153]	28/38 GHz	--	6	2*4	patches	---	12/13.46	6 sector	1.3 * 2 cm <sup>2</sup>	40/30 deg	240/180 deg	--	--	-30 dB
[154]	2.4 GHz	< 254	108	4*1	Patches with slots and square ring patches	6.5 dB	---	Polyhedron ring (9 faces)	---	---	---	---	---	---
[155]	7.25 GHz	2500	121	11 * 11	Multimode antenna element; patch with slots	8 dB	---	Single panel	70 * 70 cm <sup>2</sup>	---	---	---	---	-20 dB
[156]	28 GHz	850	8	8*16	patches	---	25.8 dB	Single panel	15.5 * 14.3 cm <sup>2</sup>	42 deg.	252 deg	22 dB	---	-20 dB
[157]	3.5 GHz	200	16	8*16	Square-ring slot-coupled patch	---	11 dB	Single panel	36.2 * 11.7 * 0.95 cm <sup>3</sup>	12 deg	72 deg.	---	---	-20 dB
[158]	3.5 GHz	200 MHz	8	2 * 2	Monopole loaded into a square slot	---	6 dB	Single panel	12 * 12 * 0.08 cm <sup>3</sup>	---	---	---	---	-14 dB
[159]	28 GHz	9500	4	1*4	Tapered slot antenna	9 dB	15 dB	Single panel	---	35 deg	210 deg	13 dB	---	---
[160]	2.6 GHz	194	32	4*8	patches	10 dB per sub-array	22 dB	Single panel	50* 100 cm <sup>2</sup>	30 deg.	180 deg	---	---	-35 dB

**Table 3.2. Comparison table# 2 for many mMIMO systems in literature.**

Reference	Thickness (mm)	Substrate	Operating modes	# patterns by single element	Max. ECC	Beamforming with same patterns	Single element HPBW	Technique of pattern reconf.	Electrical Separation between elements	Electrical size of single element	Electrical Size of mMIMO	Efficiency of a single element	SLL levels
[144]	1.524 mm	Rogers RO4350b	2 (array operation, and MIMO operation)	4	0.1198	No, because of two modes	70 deg.	Changing phases feeding the patches; different arrays with different phases... Chybecheff method was used also	0.89 lamda * 0.89 lamda	0.89 lamda * 0.89 lamda	5.33 lamda * *3.55 lamda	64%	High
[145]	1 mm	TLX-8	1	1	---	yes	90 deg.	Digital beamforming; weights	0.77 lamda	---	---	---	high
[146]	3.2 mm	Diclad 880	1	1	--	yes	---	AF	0.5 lamda	0.5 lamda * 0.5 lamda	---	--	--
[147]	1.905 mm	Rogers RT5880	1	1	---	yes	53 deg	AF	1.25 lamda	Lamda * lamda	8 lamda* 8 lamda * *3 lamda	---	low
[148]	0.112 lamda	F4B	1	1	---	yes	62 deg	AF	0.37 lamda *	0.86 lamda *	2.8 lamda *	---	high
									0.65 lamda	0.86 lamda	1.7 lamda * 0.112 lamda		
[149]	17 mm	---	1	1	---	yes	---	AF	0.9 lamda	---	---	---	-13.8 dB
[150]	---	---	1	1	---	yes	---	AF with DBF or SDR	0.585 lamda	---	---	---	-6 dB
[151]	1.016 mm	RT6002	1	1	---	yes	38 deg	AF	2.2 lamda* 1.1 lamda	--	--	---	-13.5 dB
[152]	--	--	1	1	---	yes	150 deg in H-plane, 20 deg in the E-plane	AF	0.53 lamda * 2.71 lamda	0.53 lamda * 2.71 lamda	---	--	-15 dB
[153]	0.508 mm	Dielectric constant = 2.2 & 10.2	1	1	---	yes	---	AF	0.466 mm	---	---	---	-12 dB
[154]	14.8mm	FR4	2	2 (patch pattern and monopole pattern)	--	yes	---	AF	0.5* lamda	---	R=150 mm, and height =255 mm	---	---
[155]	0.38 lamda	Rogers RO4003c	2	5	<-20 dB	yes	---	AF	0.58 lamda	0.85 lamda * 0.85 lamda	---	70 %	---

[156]	0.508 mm	Rogers RT Duroid 5880	1	1	---	yes	---	DBF	0.585 lamda	---	---	---	medium
[157]	7.2 mm + 60 mils	AD255C	1	1	---	yes	---	AF	57 mm	---	---	---	Low
[158]	24 mm	---	1	1	---	yes	---	af	---	---	---	60 %	---
[159]	1.1 lamda	Rogers RT/Duroid 5880	1	1	---	yes	---	af	0.5 lamda	---	2.5 lamda * 1.1 lamda	---	-9 dB
[160]	9.5 mm	FR4	1	1	---	yes	For a sub-array; 65 deg in azimuth, and 25 deg in elevation	Amplitude taper or phase taper methods.	0.5 lamda * 2 lamda	0.5 lamda	---	---	low

Lamda is wavelength in free space

**Table 3.3. Comparison table# 3 for many mMIMO systems in literature.**

Reference	Year of publication	Polarizations	Difference between co- & cross-polarizations	# ports per element	Size of single element	Sub-array dimensions	Sub-array size	Electrical sub-array size	Prototype	Application	FTBR	Array HPBW
[144]	2018, IET Microwave antennas prop.	Linear polarization	---	1	74*74 mm <sup>2</sup>	---	--	--	Yes	5G base stations	--	---
[145]	2014, China Communications	Linear Polarization	low	1	320 * 215 mm <sup>2</sup>	---	--	--	yes	5G wireless commun.	--	---
[146]	2014, globecom 2014 workshop	Dual linear polarizations	---	1	---	---	--	--	yes	5G cellular systems, OFDM	--	---
[147]	2016, IEEE transactions on Antennas and propagation	Dual Linear polarization	-25 dB at boresight	2	81 *86 mm <sup>2</sup>	---	32.4 * 8.6 cm <sup>2</sup>	4 lamda * lamda	yes	5G base stations	-15 dB	53 – 13 deg
[148]	2016, IEEE International Conference on Microwave and Millimeter Wave Technology	Dual Linear polarization	---	2	---	1 * 4	---	---	no	---	--	--
[149]	2016, Progress for electromagnetics Research Letters	Dual linear polarizations	---	2	27.2 * 27.2 mm <sup>2</sup>	---	--	--	no	5G mobile communications	--	36 deg

[150]	2017, <del>cited</del> States National Committee of URSI National Radio Science Meeting	Dual linear polarizations	-20 dB	2	---	---	---	---	no	mm-wave BS	---	--
[151]	2014, APS	Linear polarization	---	1	15 * 39 mm2	---	---	---	no	mm-wave BS	--	10.7 deg.
[152]	2011, Proceedings of the Global Communications Conference, GLOBECOM	Linear polarization	---	1	---	---	---	---	no	mm-wave BS	---	---
[153]	2016, 17th International Symposium on Antenna Technology and Applied Electromagnetics (ANTEM)	Linear polarization	---	1	---	---	---	---	no	5G communication systems	---	---
[154]	2016, Progress in Electromagnetics Research	Dual polarization	-22 dB	3	75 * 255 * 14.8 mm3	4 * 1	---	---	no	5G BS	---	---
[155]	2016, IEEE Transactions on Antennas and Propagation	Dual polarization	---	4	30 * 30 mm2	---	---	---	yes	mMIMO	---	---
[156]	2018, IEEE Radio and Wireless Symposium	Linear Polarization	-23.7 dB	1	---	1*16	---	---	yes	mm-wave mMIMO	---	---
[157]	2017, IEEE 28th Annual International Symposium on Personal, Indoor, and Mobile Radio Communications (PIMRC)	+ or - 45 deg. Dual Polarization	-20 dB	2	41 * 41 mm2	1*2	114 * 44 mm2	---	yes	mMIMO	---	75 deg. In hor. And 40 deg. In ver.
[158]	2017, International Workshop on Electromagnetics: Applications and Student Innovation Competition	Dual polarization	-20 dB	2	30 * 30 * 24 mm3	---	---	---	no	5G Applications	---	---
[159]	2017, IEEE transactions on antennas and propagation	Linear polarization	---	1	---	---	---	---	yes	5G mm-wave mMIMO	---	70 deg in H-plane, and 40 deg in E-plane
[160]	2015, International journal of	Dual polarization	-13 dB	1	---	4*1	---	---	no	LTE	---	6.2 deg in elevat
	antennas and propagation											ion, and 12.5 deg in azimuth

### 3.10 DOA Estimation for Massive MIMO Systems

In [161], U-ESPRIT algorithm was used in order to estimate DOA for massive MIMO systems. This algorithm can be used to find the azimuth and elevation information for a massive MIMO. 2D antenna array with  $M * N$  dimension is used in this paper. In addition, the used array is uniform and rectangular. The carrier frequency used in the work of this paper is 3 GHz, with  $16 * 16$  elements used in the massive MIMO and with 0.5 wavelength spacing between the mMIMO (massive MIMO) elements. The system model is shown in Fig. 3.10. One good feature of using this proposed method is that real-valued computations will take place. The unitary wave-way difference along Y and X axes will be used in finding the received signal at an element from a massive MIMO system. After that, unitary matrices will be used such that steering matrix will be changed to real values. After that, the eigenvalues will be found based on estimated signal space and depending on calculations done on x-axis and y-axis steering vectors. By the use these eigenvalues, the direction of arrival will be found by indicating the elevation and azimuthal angles of arrival. The total number of elements used in this massive MIMO is 256 and Monte Carlo simulations were conducted. The used antennas in the massive MIMO were assumed to have omnidirectional patterns. The estimation of DOA is conducted in this work by estimating the elevation angle and azimuthal angle of arrival. Having different array configurations will result in different performance. It was found that largest estimation errors occur when the elevation angle and azimuthal angle of arrival are 90 and  $-45$  degrees, respectively. In addition, it was found that the azimuth estimation is more sensitive to array configurations than elevation estimation. In addition, the array provides better azimuth estimation performance if  $M > N$ , better elevation estimation can be provided if  $M < N$ , and best accuracy of the whole DOA estimation takes place when  $N = M$ .  $N$  and  $M$  are defined in Fig. 3.10.

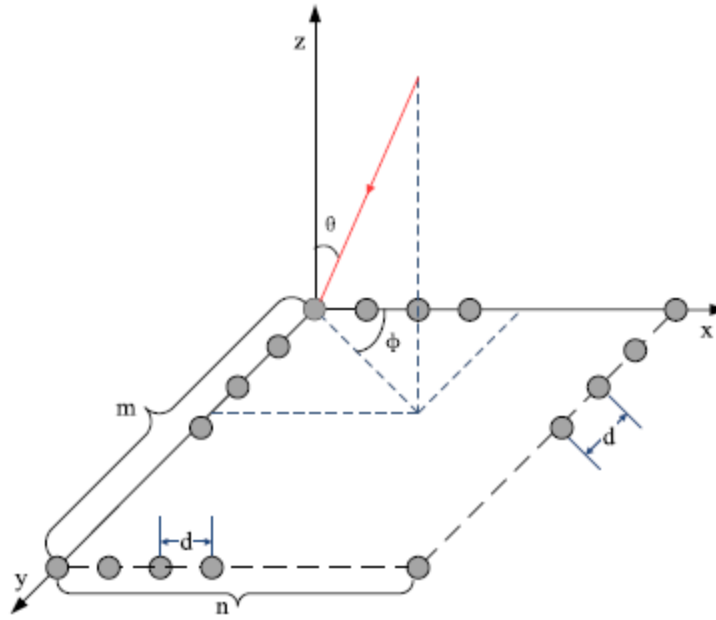


Fig. 3.10. The model of the massive MIMO system used in [161].

In [162], a two-stage MUSIC-based DOA estimation is proposed. In this algorithm, the steering vector matrix is divided in two spaces. The upper side of the matrix depends on the elevation angles, and it is used to perform MUSIC algorithm to estimate the elevation angles of coming signals. The estimated elevation angles then will be substituted in the lower side of the steering matrix, and this lower side of the matrix will be used to estimate the azimuthal angles of the coming signals. In this work, the number of elements along x- and y- dimensions of the mMIMO is 20 elements. Compared to other works where joint search is used, this proposed method has larger MSE and lower BER because the algorithm estimates and then it substitutes. QPSK modulation with zero-forcing equalizer was used. This proposed method is a good candidate for massive MIMO systems, and it has reduced complexity but with slight loss in BER.

## CHAPTER 4

# DESIGNS OF PATTERN RECONFIGURABLE ANTENNAS AND A MASSIVE MIMO ANTENNA

5G technology is capable to support the huge number of the coming required data rates and connected devices to the networks. One of the important systems supporting 5G technology is massive Multiple-Input Multiple-Output (mMIMO) systems. Therefore, designing antennas suitable for mMIMO systems is a very good contribution to 5G technology. In addition, the 5G network performance will be enhanced dramatically if these designed antennas are pattern and frequency reconfigurable antennas, since the system diversity will increase and more bands will be served by one system. Therefore, number of served users/devices will increase sharply, and serving this large numbers of devices is one of the major aims of 5G technology. In other words, designing pattern and frequency reconfigurable mMIMO systems will be a very good contribution to 5G technology. Consequently, it is important to design suitable pattern and frequency reconfigurable antennas which can be used for mMIMO systems.

There are many frequency slots reserved for 5G technology such as 3.4 – 4 GHz, 4 – 5 GHz, 24.25 – 29.5 GHz, 37.37 – 42.5 GHz, and 64 – 71 GHz. These frequency slots differ from country to country. Hence, it is important to design antennas at these frequency slots to make these antennas supporting 5G technology.

Therefore, designing pattern and frequency reconfigurable antennas at the 5G frequency bands can be used for mMIMO systems and support 5G technology. There are a huge number of proposed pattern and frequency reconfigurable antennas in literature. The radiating edges, slots, current distribution or feeding network need to be reconfigured to achieve pattern reconfigurable antenna. On the other hand, the frequency reconfigurable antenna is achieved by changing the surface current distribution or the antenna structure. These reconfigurable techniques can be electrical, mechanical, optical, or material-change techniques. Each one of these techniques has advantages and disadvantages. However, electrical techniques are used most of the times in such reconfigurable antennas.



This chapter presents four antenna designs and one mMIMO antenna. The four antennas, shown in this chapter, are pattern reconfigurable antennas with slot radiating elements. Frequency reconfigurability was added to the first reconfigurable antenna. The fourth pattern reconfigurable antenna was extended to a massive MIMO as will be shown later in this chapter.

#### **4.1 Dual-Band Pattern and Frequency Reconfigurable Slot-Based Antenna**

A new dual-band slot-based pattern and frequency reconfigurable antenna is proposed. This proposed antenna is compact and low-profile antenna working at 3.6 GHz with many pattern configurations, and the frequency at this lower band is reconfigurable also. The patterns at 5.2 GHz are reconfigurable also, while the frequency is not reconfigurable at this higher band. Pattern reconfigurability is achieved using reconfigurable reflectors, and frequency reconfigurability is achieved using varactors. The following sections show the antenna structure, the simulated results, and the measured results of the antenna.

## 4.1.1 Antenna Design

- **Antenna Geometry**

The antenna structure is shown in Fig. 4.1(a). The antenna is built on an FR-4 substrate with a dielectric constant of  $\epsilon_r = 4.4$ , a loss tangent of  $\tan \delta = 0.02$ , and a thickness of 0.72 mm. The size of the antenna is  $40 \times 42 \text{ mm}^2$ . The used radiating elements are 4 U-slots etched on the ground plane (bottom face of the antenna) as shown in Fig. 4.1. The top face of the antenna includes a reconfigurable feeding network including 4 PIN diodes. The pattern configurations at the lower band (3.6 GHz) and at the higher band (5.2 GHz) are achieved by changing the states of these four PIN diodes shown in Fig. 4.1. The frequency reconfiguration at the lower band is achieved by changing the reverse biased junction capacitances of the used diodes. All dimensions of the antenna are mentioned in table 4.1.

Slot 1 was tilted by 5 degrees from the y-axis in order to achieve patterns with lower overlapping between them. The transmission lines on the top face of the antenna with black color in Fig. 4.1 were optimized at 3.6 GHz to achieve very good impedance matching for all required configurations. The dimensions of transmission lines are shown in Fig. 4.2(a). The biasing circuit (with dimensions) for a diode is shown in Fig. 4.2(b); the positive DC polarity will be connected to this shown end, while the negative DC polarity will be connected to the biasing network connected to the central feeding pad as shown in Fig. 4.1(a). Therefore, the biasing network of a diode includes two RF choke inductors with a value of  $1 \mu\text{H}$  and two limiting resistors of  $2.1 \text{ K}\Omega$ . The RF chokes are used to isolate the RF signal from the DC biasing circuit. The limiting resistors are used such that the current flowing in the diode will not be more than the maximum allowed diode's current. The used  $2.1 \text{ K}\Omega$  resistors have the tag (RC0805FR-072K1L) and taken from Digi-Key ELECTRONICS [139]. The used  $1 \mu\text{H}$  RF chokes have the tag (MLF2012A1R0KT000) and taken from Mouser ELECTRONICS [140]. Furthermore, the linewidths of the biasing lines are 0.5 mm to enhance isolation between the RF and DC signals. The inductor has a blue color and the resistor has a yellow color as shown in Fig. 4.2(b).

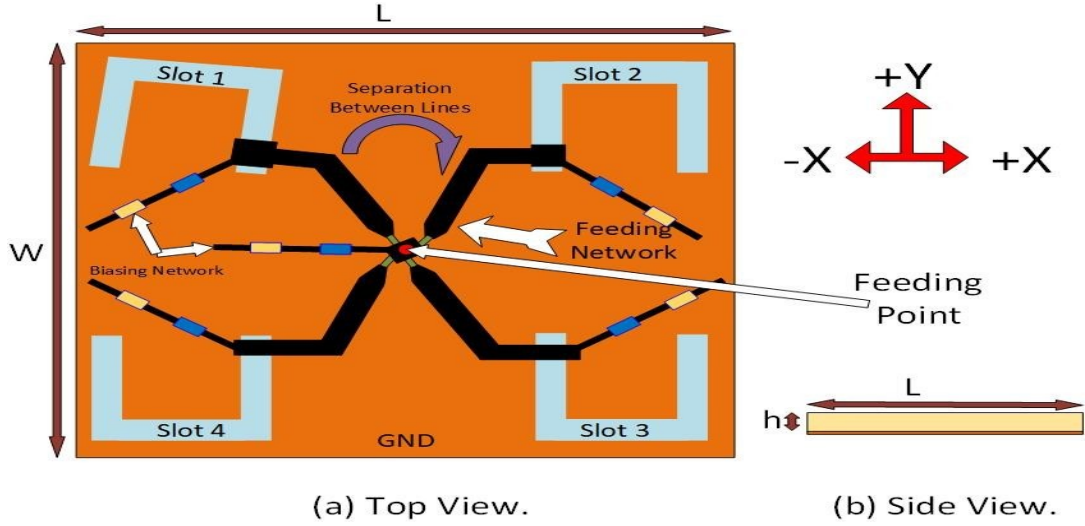


Fig. 4.1. The geometry of the proposed reconfigurable antenna. (a) Top view. (b) Side view.

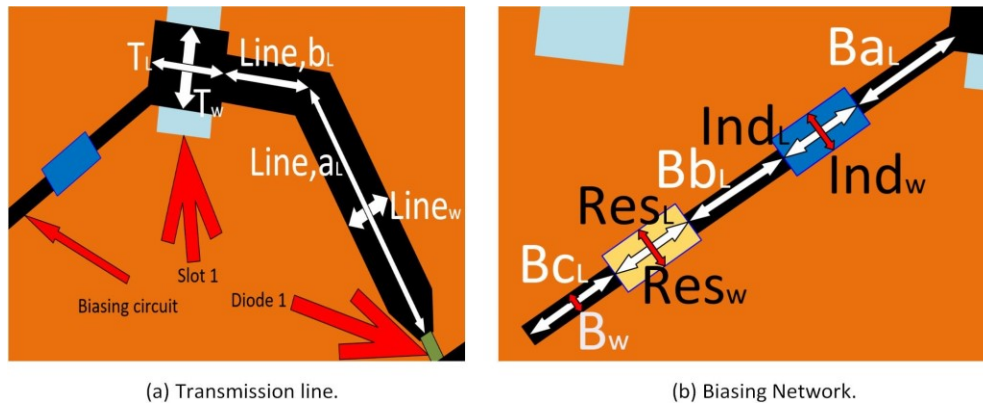


Fig. 4.2. (a) The transmission line details. (b) Biasing network details.

Table 4.1. The parameter of the proposed antenna

Parameters	Value for slot 1 (mm)	Value for slot 2 (mm)	Value for Slot 3 (mm)	Value for Slot 4 (mm)	Other Parameters	Length (mm)
$LS_L$	12	12.5	12.5	12	L	42
$MS_L$	13	13	13	13	W	40
$RS_L$	10	10.5	10.5	10	h	0.72
$L_{da}$	1.51	1.4	1.5	1.5	$Ba_L$	3.3
$L_{db}$	1.32	1.75	1.25	1.5	$Ind_L$	2
$L_{dc}$	2.45	1.75	1.25	1.5	$Ind$	1.25
$L_{g a}$	0.095	0.05	0.935	0.073	w	2
$L_{g b}$	0.408	0.35	0.049	0.427	$Bb_L$	2
$L_t$	0.711	0.386	1.597	0.408	$Res_L$	1.25
$T_L$	2.5	2.5	3	2.5	Res	3.5
$T_W$	2.5	2.4	1.5	1.5	w	0.5
$Line, a_L$	5.46	6.46	6.76	5.78	$Bc_L$	1.55
$Line, b_L$	3.22	2.3	3.05	3.1	$B_w$	-
					$Line_w$	-

Other parameters are fixed for all slots or they are not related to a specific slot.

- **Single U-slot Antenna**

The used radiating elements in this design are U-slot antennas [141] – [142]. The U-slot antenna provides a wide bandwidth around the resonant frequency [141]. The resonant frequency of the U-slot antenna is determined by the length of the slot; i.e. it should be half guided-wavelength at the required resonant frequency, theoretically speaking. The used U-slot radiating element (Slot 1) is shown in details in Fig. 4.3(a). The used U-slots were optimized to provide good input impedance matching at the resonant frequencies. Usually, the radiated patterns for this antenna is bidirectional, and a metallic reflector usually is required to be used behind the antenna to make the patterns unidirectional. However, using this metallic reflector will make the antenna bulky. However, no metallic reflector is used behind this proposed antenna, rather, the ground plane is used as a reflector as will be explained in the coming sections. The patch above the U-slot is used to enhance the input impedance matching for each configuration; it increases the bandwidth of operation also. There are four patches above the slots, and they were optimized well to enhance the input impedance matching at the lower and the higher bands.

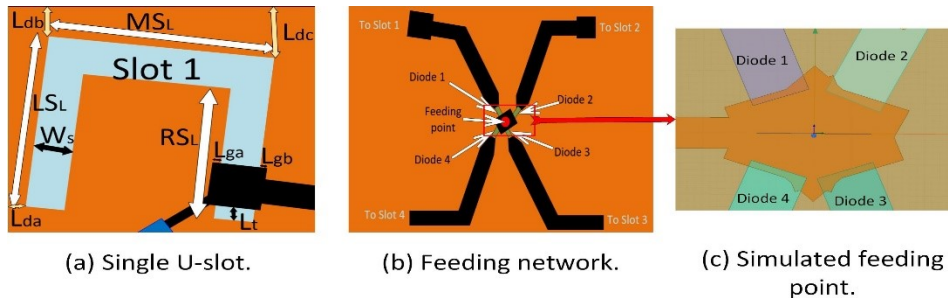


Fig. 4.3. (a) The single U-slot antenna. (b) Reconfigurable feeding network. (c) The simulated feeding point in HFSS.

- **Reconfigurable Feeding Network**

As shown in Fig. 4.3(b) and 4.3(c), this antenna has one port only which is a coaxial cable connected to the center of the design; to the center of the feeding pad. It can be seen also that the feeding network is reconfigurable because four diodes are installed between the feeding pad and the four transmission lines. The separation between the transmission lines shown in Fig. 4.1(a) was optimized such that the coupling between different configurations will be reduced. The feeding pad at the center of the design shown in Fig. 4.3(c) was optimized well such that the input impedance

matching is acceptable for all configurations. This central feeding pad was designed using a rhombus since it has four edges and it is required to feed four slots located at the corners of the antenna. After that, the transmission lines were installed without the diodes' cuts. After that, the diodes' cuts were added around the rhombus. These cuts were optimized to achieve good input impedance matching, and hence the resulted input feeding pad becomes as shown in Fig. 4.3(c).

- **Theory of Operation**

Let us consider the case when diode 1 is ON, then the radiating U-slot will be Slot 1 only; the other diodes are OFF, so, other slots are ideally not radiating. In this case, the dominant electric current at 3.6 GHz around Slot 1 will resemble the electric current flowing in a dipole as shown in Fig. 4.4. Therefore, the patterns tend to be omnidirectional patterns, but the ground plane behind this dominant current operates as a reflector. As a result, the radiated patterns in this case will be directed to Left-up direction. The same scenario will take place when Diode 2, Diode 3, or Diode 4 is ON. Therefore, it can be concluded that there are at least four pattern configurations. However, there are more 4 pattern configurations as will be shown soon.

The achieved pattern configurations at 3.6 GHz are 4 configurations. When Diode 1 only is ON, radiated patterns will be directed to Left-up direction. When Diode 2 is ON only, the radiated patterns will be directed to Right-up direction. When Diode 3 is ON only, the radiated patterns will be directed to Right-bottom direction. Finally, when Diode 4 is ON, the radiated patterns will be directed to Left-bottom direction. The achieved pattern configurations at 5.2 GHz are many configurations as will be shown later. They are achieved by making two diodes or more to be ON at the same time.

Frequency reconfigurability at 3.6 GHz is achieved by varying the reverse biased junction-capacitances of the used diodes; i.e. by the use of varactors. By doing so, the resonant frequency of the previous four pattern configurations will be reconfigured from around 3 GHz to around 3.8 GHz.

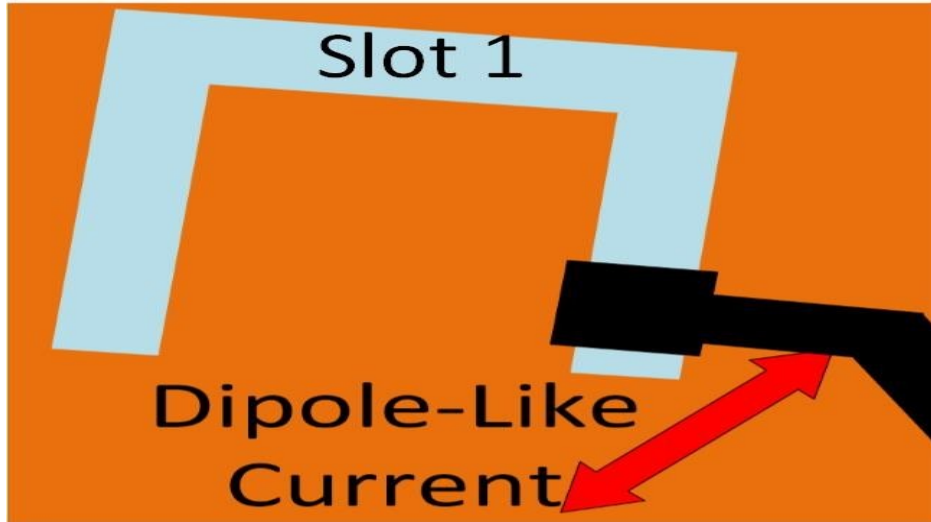


Fig. 4.4. The dominant electric current around the radiating U-slot.

#### 4.1.2 Simulation Results

- **Pattern Reconfigurability**

The proposed antenna was simulated on HFSS with the characteristics mentioned in the previous section. The simulated  $S_{21}$  results for the reconfigurable feeding network shown in Fig. 4.3(b) were found to make sure that the RF power reaches the radiating slot when the diode is ON; these results are shown in Fig. 4.5. It can be seen from Fig. 4.5 that diode's insertion loss is around  $-1.6$  dB at 3.6 GHz when the diode is ON, and the diode's isolation at 3.6 GHz is around  $-14$  dB. On the other hand, the insertion loss of the ON-diode at 5.2 GHz is around  $-3$  dB, and the isolation of the OFF-diode is around  $-11.5$  dB.

The simulated  $S_{11}$  results for the first four pattern-configurations at 3.6 GHz (when one diode only is ON) are shown in Fig. 4.6. It can be seen from Fig. 4.6 that the  $-10$  dB impedance bandwidths are 3.39 – 3.74 GHz (350 MHz), 3.39 – 3.67 GHz (280 MHz), 3.5 – 3.69 GHz (190 MHz), 3.42 – 3.68 (260 MHz) GHz for the left-up configuration, right-up configuration, right-bottom configuration, and left- bottom configuration, respectively. The simulated overlapped

frequency bandwidth between these four configurations is 3.5 – 3.67 GHz which is equal to 170 MHz.

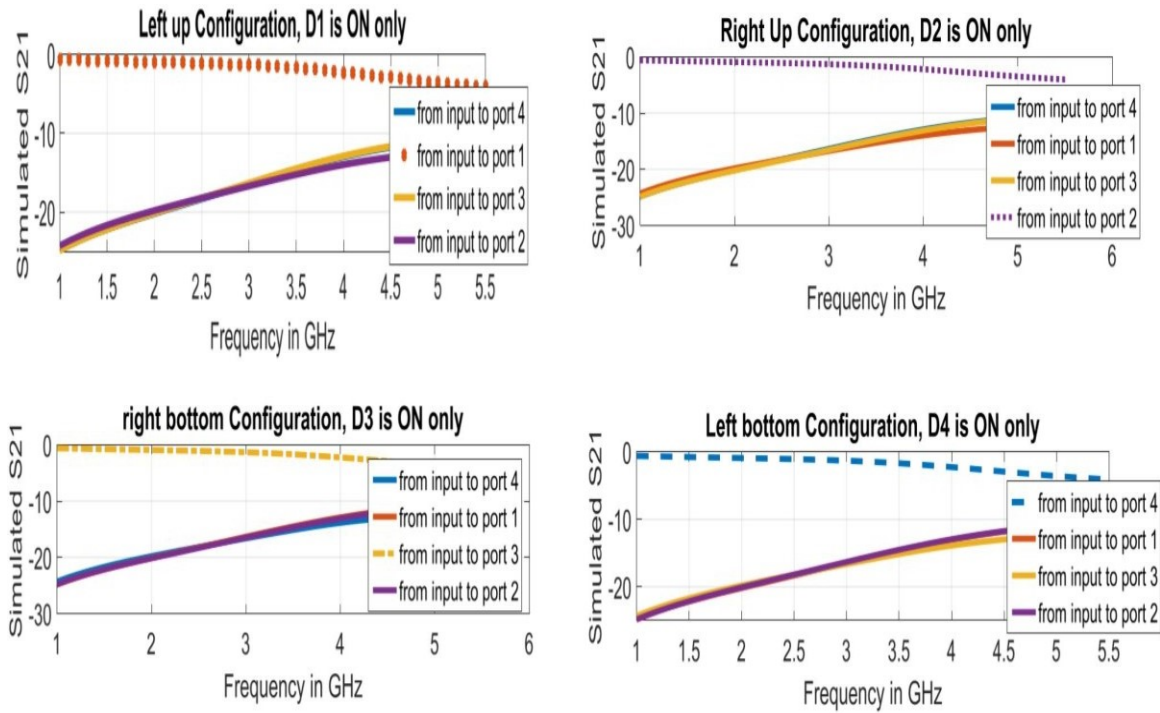


Fig. 4.5. The simulated  $S_{21}$  results of the reconfigurable feeding network in Fig. 4.3(b).

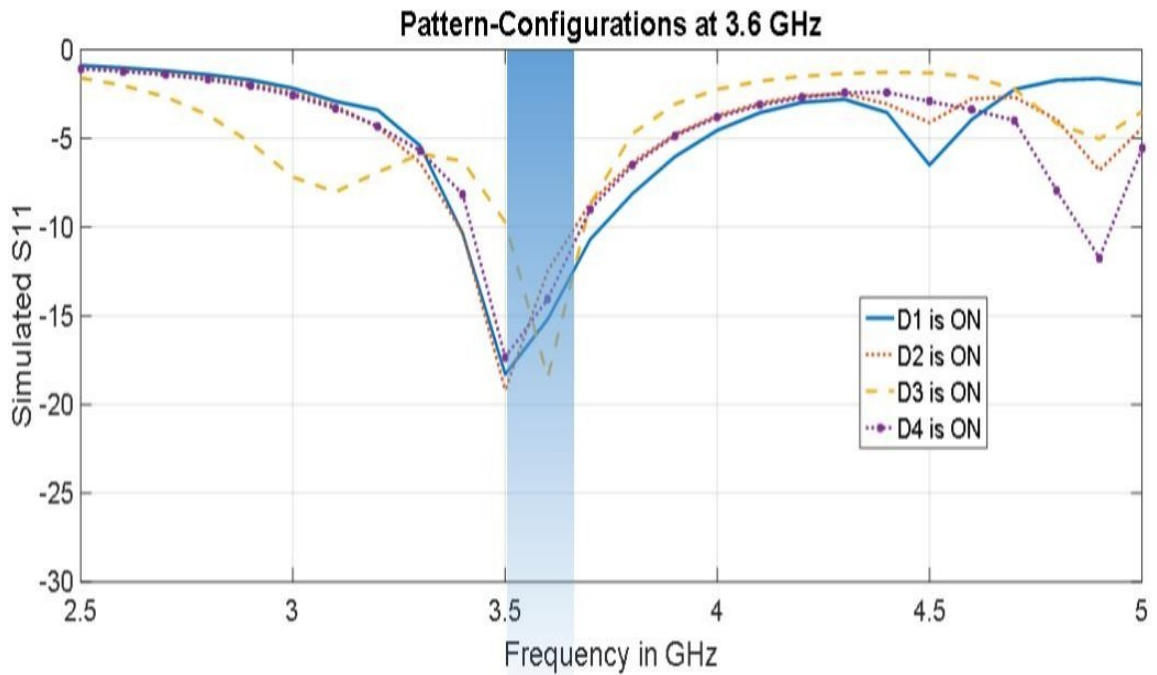
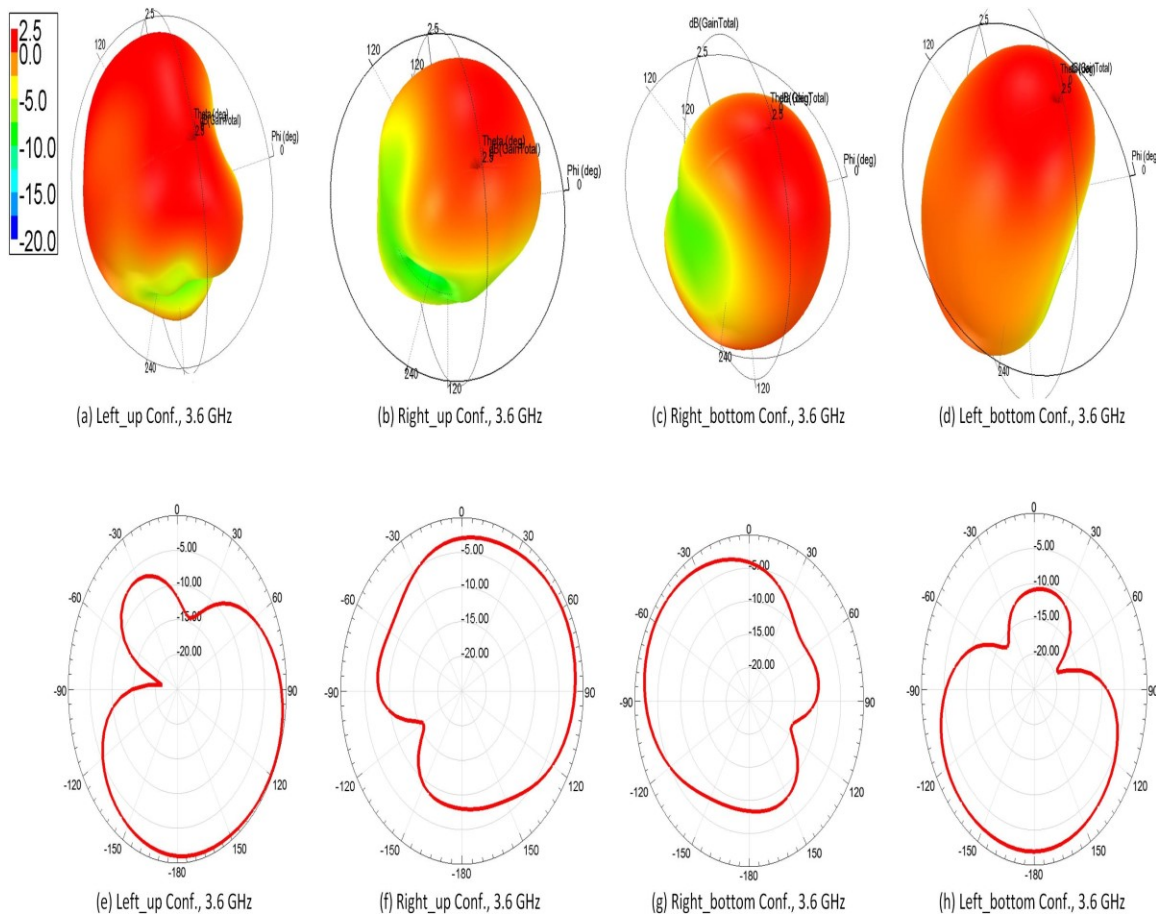


Fig. 4.6. The simulated  $S_{11}$  of the first four pattern configurations of the proposed antenna.

The radiation patterns of the first four pattern-configurations (when one diode is ON) at 3.6 GHz are shown in Fig. 4.7. It can be seen from Fig. 4.7 that the pattern is directed to left-up corner of the antenna when Diode 1 is ON with a maximum gain directed to  $\phi = 120^\circ$  with a value of  $-0.26$  dB. It can be seen also that the pattern is directed to right-up corner when Diode 2 is ON with a maximum gain directed to  $\phi = 60^\circ$  with a value of  $-1.19$  dB. It can be seen also that the pattern is directed to right-bottom direction when Diode 3 is ON with a maximum gain directed to  $\phi = 300^\circ$  with a value of  $-1.38$  dB. It can be seen also that the pattern is directed to left-bottom direction when Diode 4 is ON with a maximum gain directed to  $\phi = 185^\circ$  with a value of  $-1.92$  dB. The HPBWs are  $70^\circ - 223^\circ$  ( $153^\circ$ ),  $343^\circ - 127^\circ$  ( $144^\circ$ ),  $247^\circ - 2^\circ$  ( $115^\circ$ ), and  $115^\circ - 266^\circ$  ( $151^\circ$ ) for the left-up configuration, right-up configuration, right-bottom configuration, and left-bottom configuration, respectively. The simulated radiation efficiencies for these four pattern-configurations at 3.6 GHz are 62.7%, 47.8%, 44.1%, and 45.5% for the left-up configuration, right-up configuration, right-bottom configuration, and left-bottom configuration, respectively.



**Fig. 4.7. The simulated radiation patterns of the first four pattern-configurations (when one diode is ON) of the proposed antenna at 3.6 GHz. (a) – (d) The 3-D radiation patterns. (e) – (h) The xy-plane (2-D) patterns.**



The input impedance matching at 5 GHz will be very good when two diodes or more are ON as shown in Fig. 4.8; this is because a U-slot antenna has many resonances and reducing the number of OFF-diodes will decrease the reverse-biased junction-capacitance, and hence the resonant frequency of the U-slot's resonances will increase.

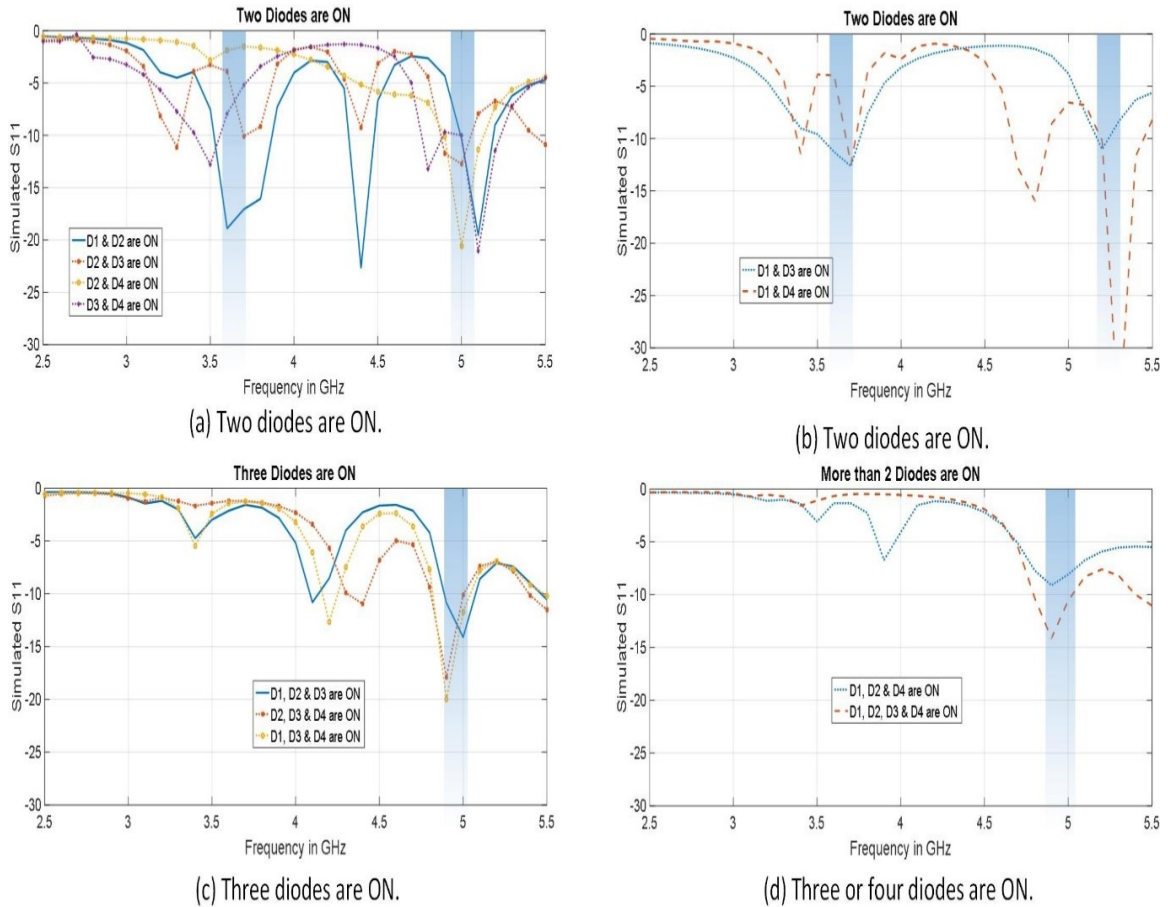


**Fig. 4.8. The simulated  $S_{11}$  results when two diodes or more are ON.**

There are 11 configurations when two diodes or more are ON. Pattern reconfigurability is achieved at 5 GHz and at 3.6 GHz also when two diodes or more are ON, and this can be shown in Fig. 4.9 – Fig. 4.12. Fig. 4.9 and Fig. 4.10 show 3D/2D patterns at 5 GHz, and at 3.6 GHz, respectively, when two diodes only are ON. Fig. 4.11 and Fig. 4.12 show the 3D/2D patterns at 5 GHz, and at 3.6 GHz, respectively, when more than two diodes are ON. The  $-10$  dB impedance bandwidths and the direction of maximum gains for these 11 configurations at 5 GHz are summarized in table 4.2. It should be mentioned that the 2D patterns at 5 GHz are plotted at the plane of  $\theta = 35^\circ$ , while the 2D patterns at 3.6 GHz are plotted at the XY-plane ( $\theta = 90^\circ$ ).

**Table 4.2. Results for configurations when more than 1 diodes are on at 5 GHz**

Config. #	ON Diodes	Direction of Max. Gain at $\theta=35^\circ$ -plane	Max. Gain (dB)	Bandwidth (GHz)
5	3 and 4	$\phi=-10^\circ, \phi=200^\circ$	2.9, 2.2	3.4 – 3.6, 4.76 – 5.24
6	2 and 3	$\phi=0^\circ, \phi=180^\circ$	2.4, 4.8	3.6 – 3.8, 4.85 – 5.1
7	1 and 2	$\phi=10^\circ, \phi=170^\circ$	4, 1.4	3.52 – 3.87, 4.97 – 5.2
8	1 and 4	$\phi=-5^\circ, \phi=190^\circ$	0.8, 5.5	3.6 – 3.75, 5.1 – 5.4
9	2 and 4	$\phi=-30^\circ, \phi=190^\circ$	3.8, 0.7	4.9 – 5.14
10	1 and 3	$\phi=10^\circ, \phi=195^\circ$	4.0, 2.4	3.5 – 3.76, 5.1 – 5.2
11	1, 2 and 3	$\phi=0^\circ, \phi=180^\circ$	2.4, 5.1	4.88 – 5.08
12	2, 3 and 4	$\phi=-15^\circ, \phi=180^\circ$	1.6, 5.5	4.8 – 5.05
13	1, 3 and 4	$\phi=-10^\circ, \phi=185^\circ$	1.7, 5.6	4.82 – 5.05
14	1, 2 and 4	$\phi=0^\circ, \phi=170^\circ$	3.5, 4.9	4.8 – 5.05
15	1, 2, 3 and 4	$\phi=0^\circ, \phi=175^\circ$	1.7, 5.5	4.8 – 5.05

Direction of maximum gain at 5 GHz is found on the  $\theta=35^\circ$ -plane. The two  $\phi$  angles with their maximum gains are mentioned to tell about the direction of maximum gains at the two main radiated beams from the antenna at 5 GHz.

It can be seen from Table 4.2 and from Fig. 4.9 and Fig. 4.11 that patterns are reconfigured to different  $\phi$ -directions by changing the states of the used PIN diodes; under the condition that two diodes or more are switched ON to have good matching at 5 GHz. The simulated efficiencies at 5 GHz of the configurations from 5 to 15 are ranging from 65% to 77%. It can be seen from Fig. 4.10 and Fig. 4.12 that the patterns at 3.6 GHz are also reconfigured to different directions with good matching when two diodes are ON. When three diodes or more are ON, patterns at 3.6 GHz are reconfigurable also but input matching will not be good. The simulated efficiencies at 3.6 GHz when two diodes or more are ON are around 40%.

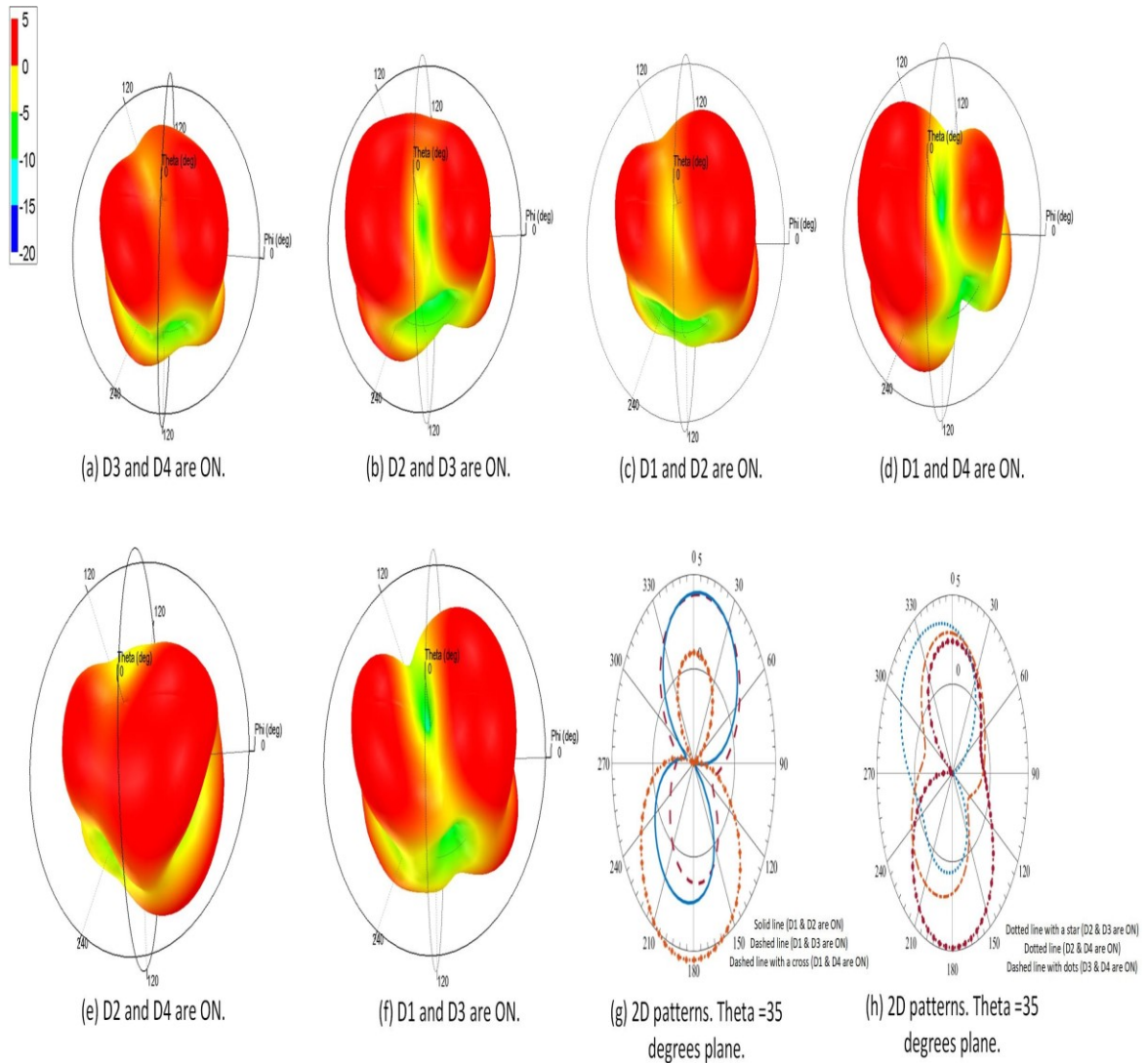


**Fig. 4.9. The simulated radiation patterns at 5 GHz when two diodes are ON. (g) Solid line (D1, D2 are ON), Dashed line (D1, D3 are ON), Dashed line with a cross (D1, D4 are ON). (h) Dotted line with a star (D2, D3 are ON), Dotted line (D2, D4 are ON), Dashed line with dots (D3, D4 are ON).**

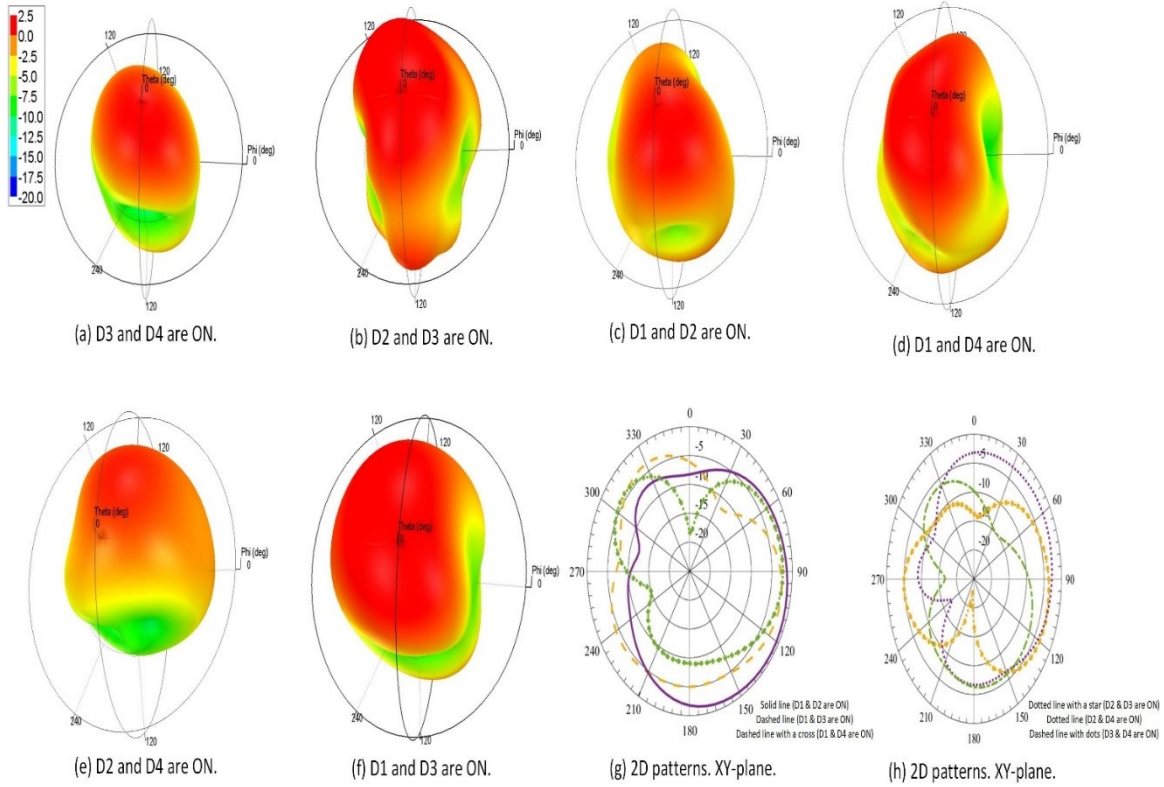


**Fig. 4.10.** The simulated radiation patterns at 3.6 GHz when two diodes are ON. (g) Solid line (D1, D2 are ON), Dashed line (D1, D3 are ON), Dashed line with a cross (D1, D4 are ON). (h) Dotted line with a star (D2, D3 are ON), Dotted line (D2, D4 are ON), Dashed line with dots (D3, D4 are ON).

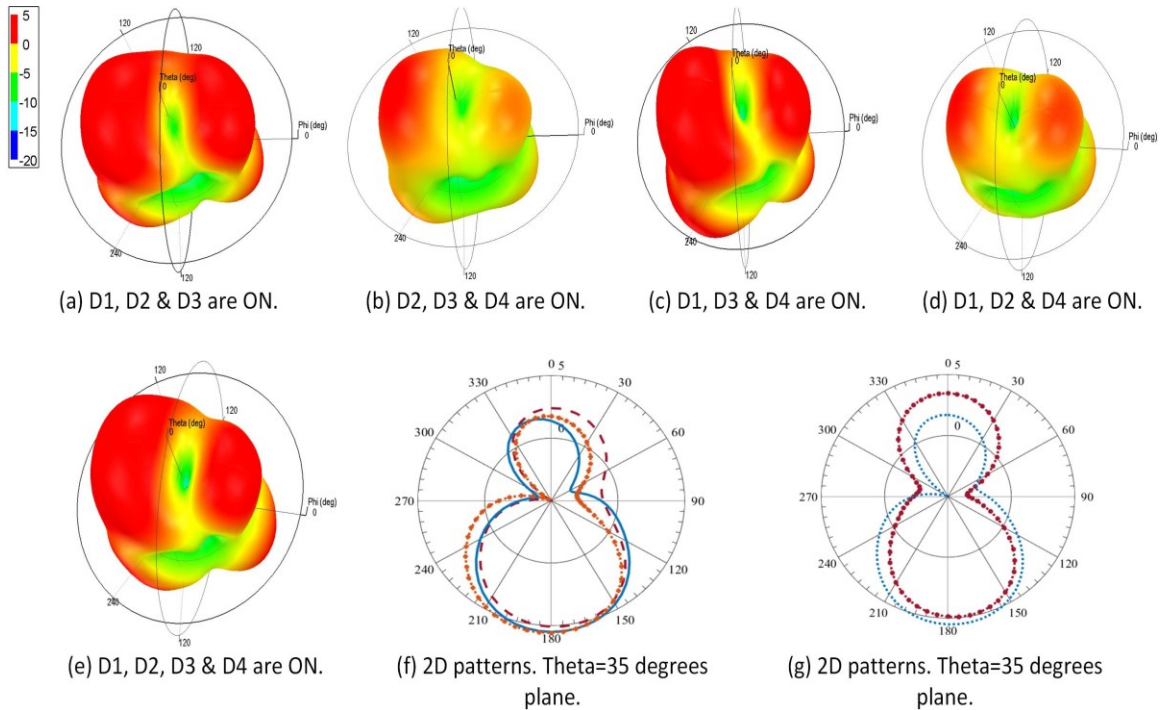


**Fig. 4.11.** The simulated radiation patterns at 5 GHz when more than two diodes are ON. (f) Solid line (D1, D2, D3 are ON), Dashed line (D2, D3, D4 are ON), Dashed line with a cross (D1, D3, D4 are ON). (g) Dotted line with a star (D1, D2, D4 are ON), Dotted line (D1, D2, D3, D4 are ON).

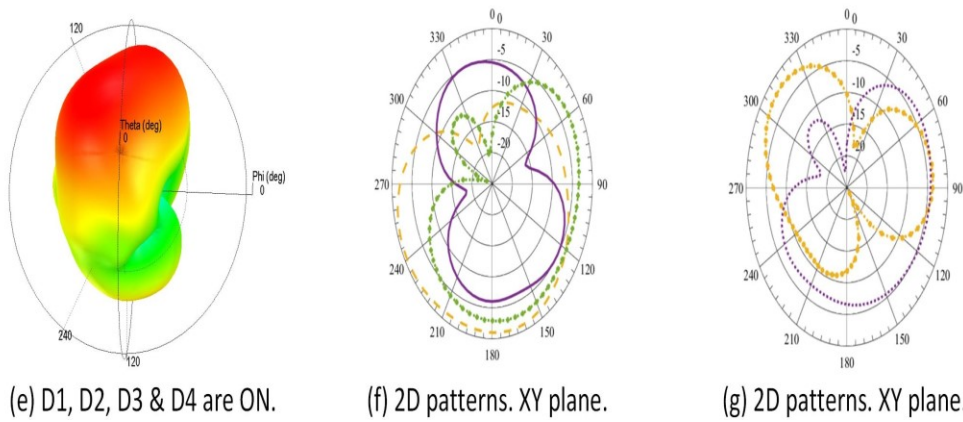
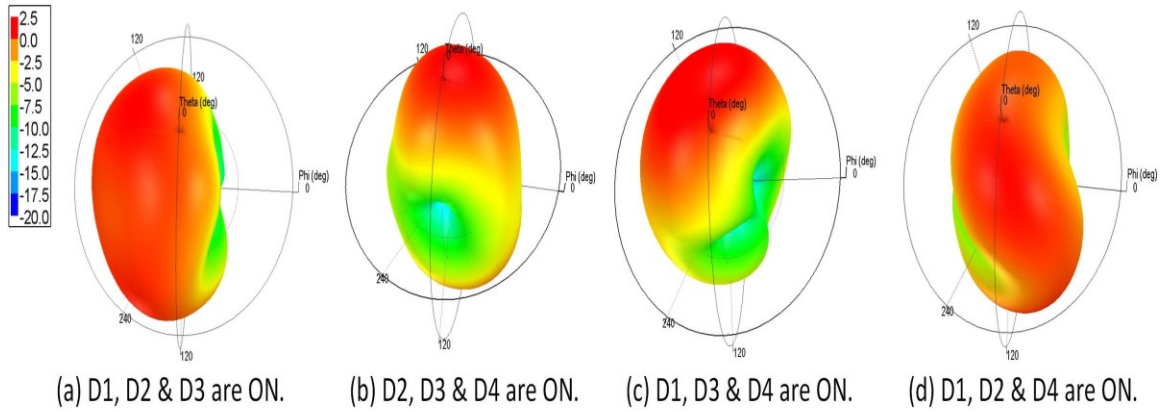


**Fig. 4.12. The simulated radiation patterns at 3.6 GHz when more than two diodes are ON. (f) Solid line (D1, D2 D3 are ON), Dashed line (D2, D3 D4 are ON), Dashed line with a cross (D1, D3 D4 are ON). (g) Dotted line with a star (D1, D2 D4 are ON), Dotted line (D1, D2, D3 D4 are ON).**

- **Frequency Reconfigurability**

If the used PIN diodes in this antenna were replaced by varactors, then it will be possible to achieve frequency reconfigurability at the lower (around 3.6 GHz) and higher (around 5 GHz) operational frequency bands. Fig. 4.13 shows the frequency reconfigurability achieved in the first four pattern configurations of this antenna; when one diode is ON, by changing the values of capacitances of the varactors. In the lower band and as shown in Fig. 4.13, it was possible to reconfigure the resonant frequency of the first four pattern-configurations from 2.9 GHz to 3.8 GHz. On the higher band, it was possible to reconfigure the resonant frequency from 4.8 GHz to 5.2 GHz. Fig. 4.14, Fig. 4.15 and Fig. 4.16 show the patterns of the Left-up, Right-up, Right-bottom, and Left-bottom configurations at 3.7 GHz, 3.4 GHz, and 3.1 GHz, respectively. It can be seen from Fig. 4.14 – Fig. 4.16 that the pattern reconfigurability is achieved and consistent even with this frequency reconfigurability. Table 4.3 shows the values of the varactors' capacitances at different resonant frequencies for the Left-up configuration only; same scenario was followed for the other configurations. It can be seen here that the required resonant frequency in the lower and higher band can be achieved by adjusting the varactors' capacitances to the suitable values.

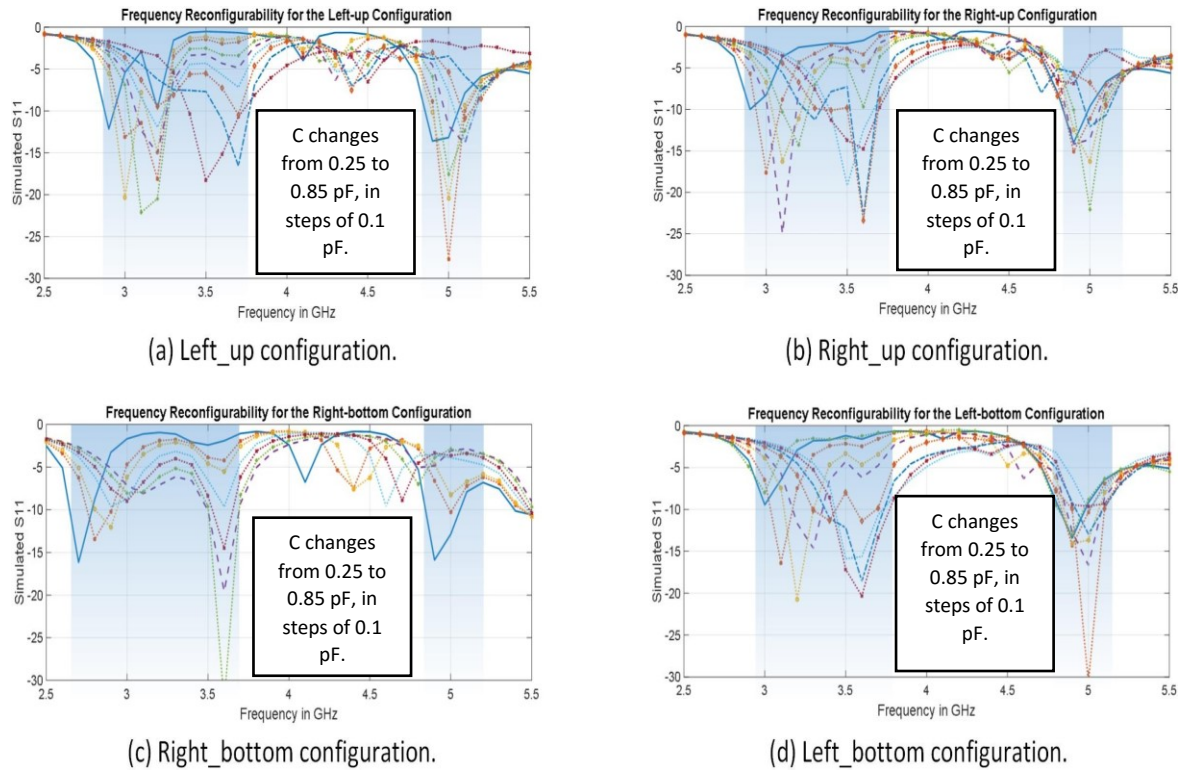


**Fig. 4.13.** The simulated  $S_{11}$  showing the frequency reconfigurability at the lower and higher bands.

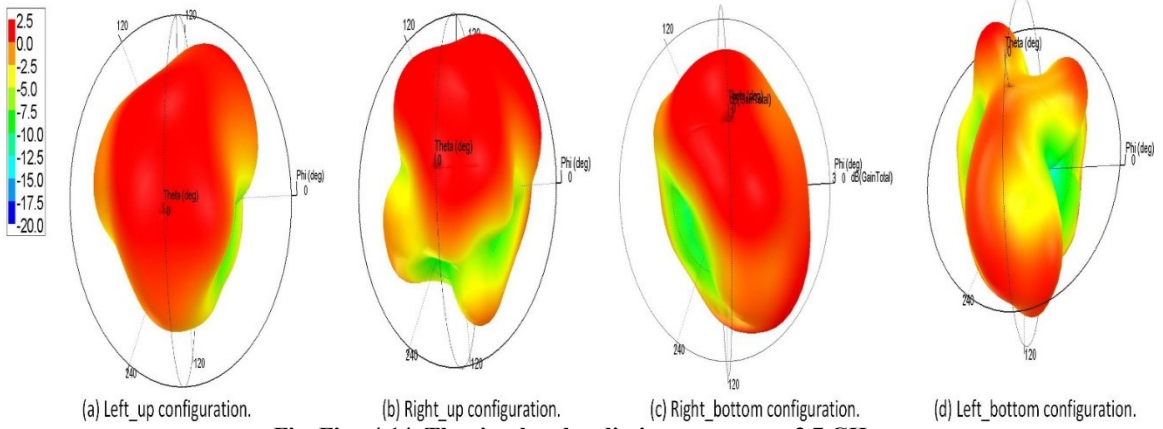


**Fig. Fig. 4.14. The simulated radiation patterns at 3.7 GHz.**

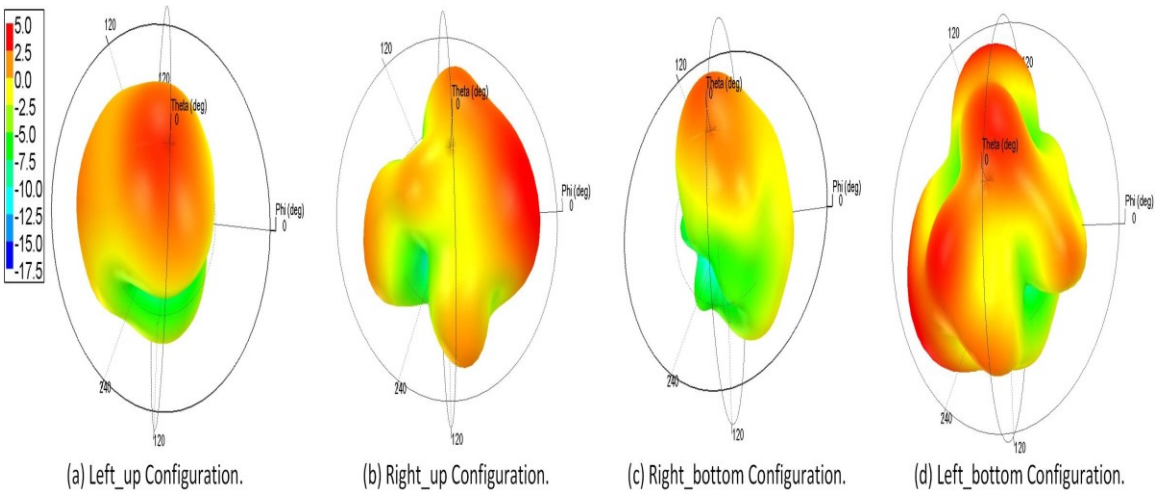


**Fig. 4.15. The simulated radiation patterns at 3.4 GHz.**

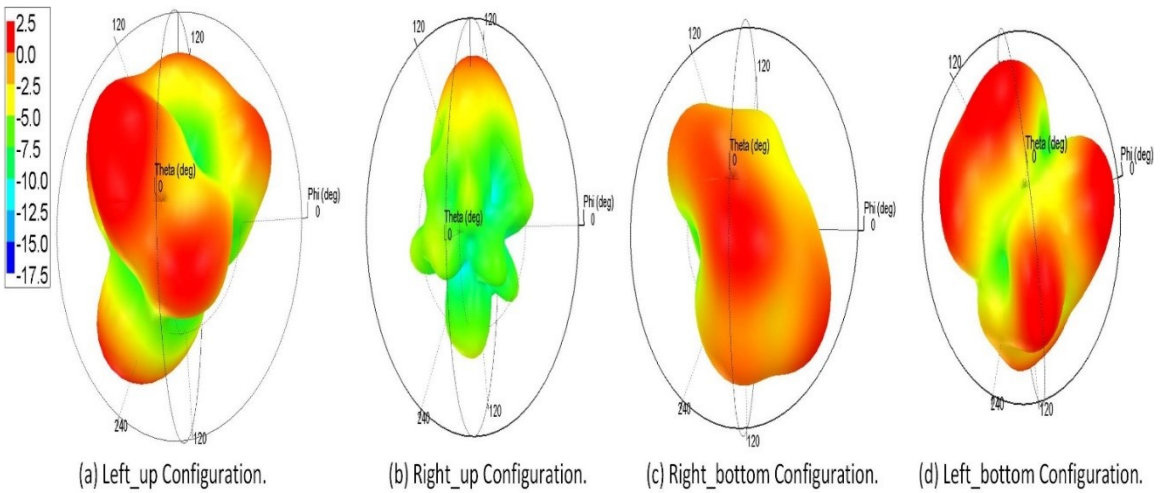


**Fig. 4.16. The simulated radiation patterns at 3.1 GHz.**

**Table 4.3. Varactors' capacitances values at different resonant frequencies in the lower band for the left-up configuration**

Resonant Frequency (GHz)	Diode 1	Varactor 2 capacitance (pF)	Varactor 3 capacitance (pF)	Varactor 4 capacitance (pF)
2.9	ON	0.85	0.85	0.85
3	ON	0.65	0.65	0.65
3.1	ON	0.5	0.5	0.5
3.2	ON	0.4	0.4	0.4
3.3	ON	0.35	0.35	0.35
3.4	ON	0.2	0.2	0.2
3.5	ON	0.17	0.17	0.17
3.6	ON	0.25	0.25	0.25
3.7	ON	0.3	0.3	0.3

Almost same scenario will be used to achieve frequency reconfigurability at the other pattern- configurations of the first four pattern configurations.

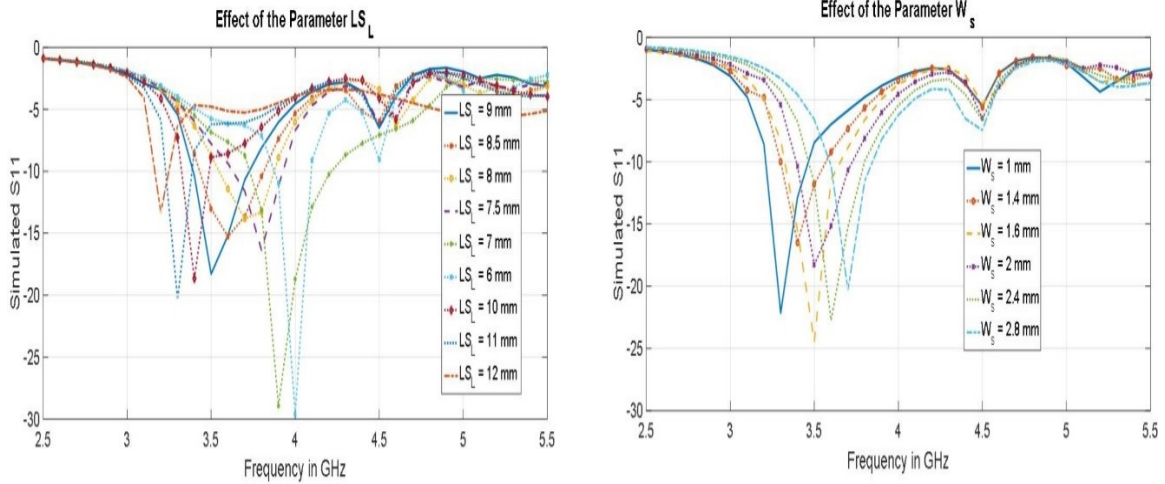
- **Parameters Effects**

Many parameters are going to affect the input impedance matching in a way that it will change the resonant frequency of this antenna. These parameters were optimized well in order to achieve the required resonant frequency and the required pattern reconfigurability. The important parameters affecting the antenna characteristics are  $LS_L, MS_L, RS_L, W_s, L_{db}, L_{dc}, L_{da}, L_t$  and  $L_{gb}$  shown in Fig. 4.3(a). Furthermore, the parameters  $T_L, T_W$  and  $Line_w$  shown in Fig. 4.2(a) are very important, and a change in them affects the resonant frequency of the antenna. Also, as shown in Fig. 4.3(b), location of the diodes in the reconfigurable feeding network and the diodes' cuts, located between the central pads and the tuning pads above the U-slots, were also optimized well to provide the required input impedance matching at the required resonant frequency and to reduce the loss between the feeding point and the tuning pads above the U-slots. In addition, the location of the biasing circuit ends connected to tuning pads were optimized well to enhance the input impedance matching and reduce the effects of these biasing lines on radiation patterns.

- **Effects of the length of the slot ( $LS_L$ )**

In this case, the Left-up configuration (Diode 1 is ON) is activated. Furthermore, the only parameter which will be varied is  $LS_{L1}$ , where number 1 is referred to the slot number as shown in Fig. 4.1(a).  $LS_{L1}$  is shown in Fig. 4.3(a). All other parameters were kept constant. The simulated  $S_{11}$  results for this case is shown in Fig. 4.17(a). In the beginning,  $LS_{L1} = 9$  mm, and as shown in Fig. 4.17(a) that if  $LS_{L1}$  was reduced, the resonant frequency will increase, and vice versa. These are reasonable results, because the resonant frequency of the U-slot antenna is inversely related with the slot's length; i.e. the resonant frequency decreases as the slot's length increases.





(a) The Effect of the Parameter  $LS_L$  (b) The Effect of the Parameter  $W_s$

Fig. 4.17. The Effects on simulated  $S_{11}$  of the Parameters: (a)  $LS_L$ , (b)  $W_s$ .

- **Effects of slot width ( $W_s$ )**

In this case, the Left-up configuration (Diode 1 is ON) is activated also. Furthermore, the only parameter which will be varied is  $W_{s1}$  shown in Fig. 4.3(a). All other parameters were kept constant. The simulated  $S_{11}$  results for this case is shown in Fig. 4.17(b). In the beginning,  $W_{s1} = 2$  mm, and as shown in Fig. 4.17(b) that if  $W_{s1}$  was reduced, the resonant frequency will decrease, and vice versa. It can be seen from these results in Fig. 4.17(b) that the relationship between  $W_s$  and the resonant frequency is a proportional relationship. Moreover, the frequency bandwidth can be enhanced by optimizing this parameter as shown in Fig. 4.17(b).

- **Effects of length and width of a tuning pad ( $T_L$  and  $T_W$ )**

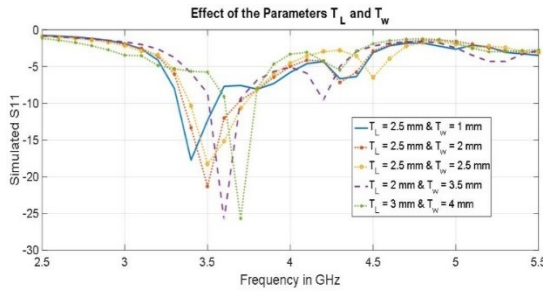
In this case, the Left-up configuration (Diode 1 is ON) is activated also. Furthermore, the only parameters which will be varied are  $T_{L1}$  and  $T_{W1}$  shown in Fig. 4.2(a). All other parameters were kept constant. The simulated  $S_{11}$  results for this case is shown in Fig. 4.18(a). In the beginning,  $T_{L1} = 2.5$  mm and  $T_{W1} = 2.5$  mm. It can be seen from Fig. 4.18(a) that the resonant frequency and the bandwidth of operation can be changed (bandwidth can be enhanced) by varying these two parameters. Also, there are too many choices for the values of these two parameters which will mitigate the optimization process of this proposed antenna.

- **Effects of length of the tuning pad after the slot ( $L_{ga}$ )**

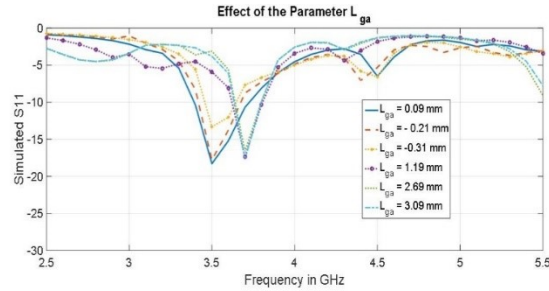
In this case, the Left-up configuration (Diode 1 is ON) is activated also. Furthermore, the only parameter which will be varied is  $L_{ga1}$  shown in Fig. 4.3(a). All other parameters were kept constant. The simulated  $S_{11}$  results for this case is shown in Fig. 4.18(b). In the beginning,  $L_{ga1} = 0.09$  mm. It can be seen from Fig. 4.18(b) that varying this parameter can change the resonant frequency and can enhance the bandwidth of operation. The negative sign for this parameter is with respect to the slot edge; its value will be negative when it is measured from the inner edge side of the slot to the top of the tuning pad.

- **Effects of the length of the slot after the tuning pad ( $L_t$ )**

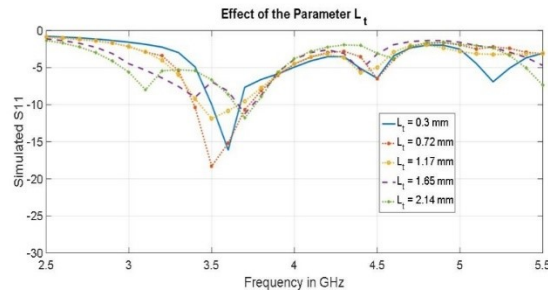
In this case, the Left-up configuration (Diode 1 is ON) is activated also. Furthermore, the only parameter which will be varied is  $L_{t1}$  shown in Fig. 4.3(a). All other parameters were kept constant. The simulated  $S_{11}$  results for this case is shown in Fig. 4.18(c). In the beginning,  $L_{t1} = 0.72$  mm. It can be seen from Fig. 4.18(c) that varying this parameter can change the resonant frequency and can enhance the bandwidth of operation.



(a) Effects of the Parameters  $T_L$  and  $T_W$



(b) Effects of the Parameter  $L_{ga}$



(c) Effects of the Parameter  $L_t$

**Fig. 4.18. The Effects on simulated  $S_{11}$  of the Parameters: (a)  $T_L$  and  $T_W$ ,**

**(b)  $L_{ga}$ , (c)  $L_t$ .**

### 4.1.3 Experimental Results

The design was fabricated and the  $S_{11}$  results were measured using a network analyzer. The fabricated antenna is shown in Fig. 4.19. The measured  $S_{11}$  results is shown in Fig. 4.20 with simulated  $S_{11}$  results shown for comparison. A shift of around 100 MHz took place because taping was used to reconfigure the antenna instead of diodes. When diodes were used, the  $S_{11}$  results are shown in Fig. 4.21. The measured results are in reasonable agreement with the simulated  $S_{11}$  results. The frequency reconfigurability of the antenna was measured also by the use of varactors instead of PIN diodes. It was found that it is possible to reconfigure the resonant frequency in the lower band from around 3.1 GHz to 3.8 GHz. However, when the varactors are used, then it will not be possible to use the antenna in transmitting modes because varactors can't handle large powers.

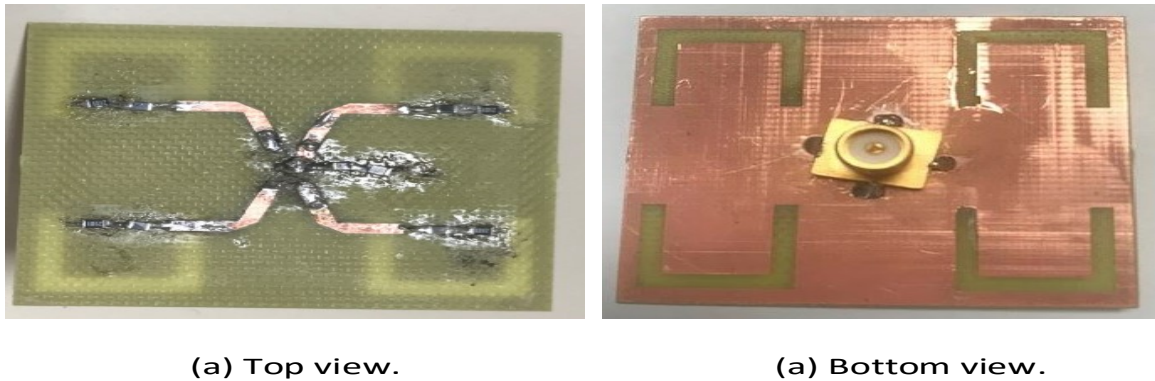
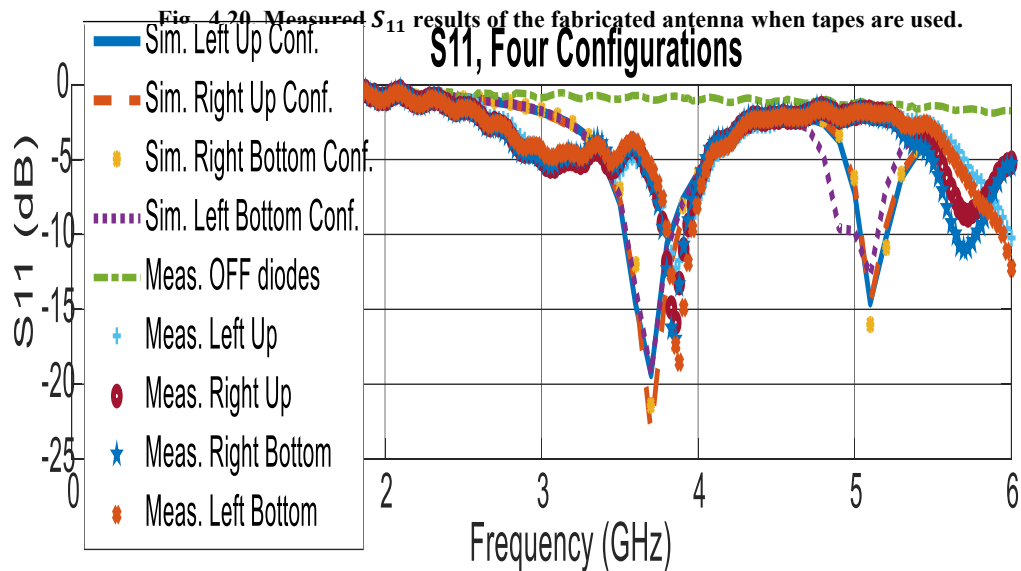


Fig. 4.19. The fabricated design of the first reconfigurable antenna.



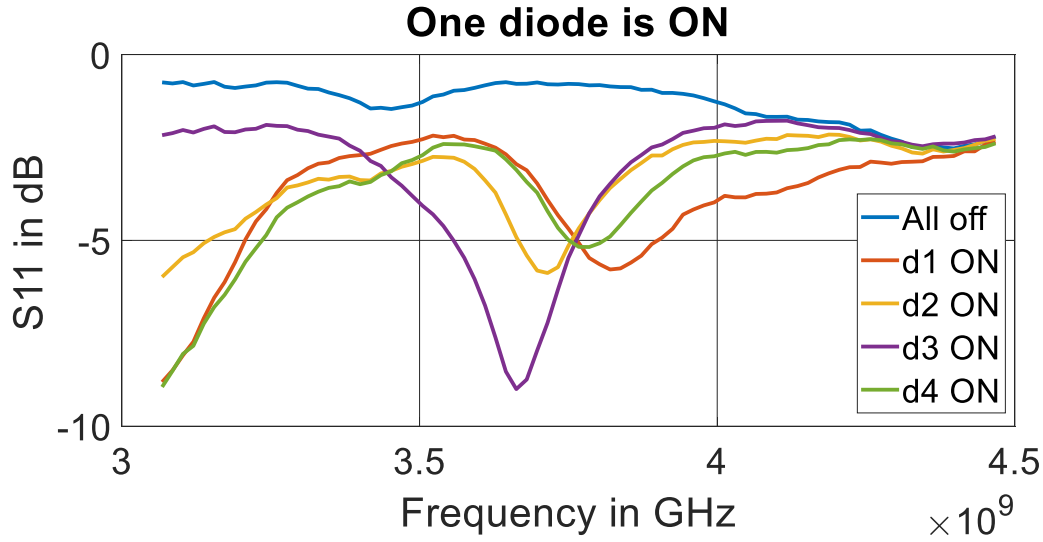


Fig. 4.21. The measured  $S_{11}$  of the antenna when the PIN diodes are used.

#### 4.1.4 Comparison Tables and Discussions

Table 4.4 shows a comparison between the results of this antenna and the competing proposed antenna in [121]. Table 4.5 shows comparisons between this antenna and some of the mentioned reconfigurable antennas in literature review chapter.

Table 4.4. Comparison the simulated results of the antenna under investigation and the results of the proposed antenna in [121].

configuration	The design under investigation				Results in [121]			
	Left_up	Left_bottom	Right_bottom	Right_up	Left_up	Left_bottom	Right_bottom	Right_up
Simulated Resonant frequency in GHz	3.7	3.7	3.7	3.7	2.45	2.45	2.45	2.45
Simulated BW in MHz	318	284	275.6	264.1	170	140	175	130
Simulated $S_{11}$ value at resonant frequency	-19.3919	-19.942	-22.3278	-19.6391	-28	-16	-25	-18.5
Simulated Peak gain in dB	0.95996	0.528	1.01	0.9161	1.9	2.6	2	2.4
Size of antenna	40 mm* 42 mm				52 mm * 52 mm			
Thickness	0.72 mm				0.8 mm			
Availability of Grounding vias	No				yes			

It can be seen from Table 4.4 that the resonant frequency for this antenna is at 3.7 GHz instead of 2.45 GHz used in [121]. The simulated bandwidths of this antenna are much larger than those bandwidths of the antenna in [121]. The size of this antenna is much smaller for this antenna and there are no grounding posts for this antenna compared with the antenna in [121].

**Table 4.5. Comparison between the proposed antenna and available antennas in literature.**

Ref.	Resonant frequency (GHz)	Dielectric constant ( $\tan \delta$ )	Height (mm)	Antenna size	Min. Gain (dB)	BW (MHz)	# pattern modes	Frequency reconfigurability
<b>This work</b>	<b>3.5 &amp; 5.2</b>	<b>4.4 (0.02)</b>	<b>0.72</b>	<b><math>0.5\lambda_o * 0.48\lambda_o</math></b>	<b>0.53</b>	<b>250</b>	<b>8</b>	<b>Yes</b>
[1]	2.02	4.4 (NM)	7	$0.67\lambda_o * 0.67\lambda_o$	2.5	50	2	No
[4]	5.32	2.2 (0.0009)	3.175	$0.89\lambda_o * 0.89\lambda_o$	3	361	3	No
[9]	3	3.55 (NM)	8.5	$0.7\lambda_o * 0.7\lambda_o$	6.1	200	4	No
[39]	2.005	4.3 (0.02)	1.52	$1.17\lambda_o * 1.14\lambda_o$	1.11	52	4	No
[53]	5.2, 5.8, & 6.4	6.15 (0.0025)	0.365	$0.97\lambda_o * 0.97\lambda_o$	-	-	9	Yes
[75]	2.3	4.4 (NM)	0.8	$0.4\lambda_o * 0.4\lambda_o$	0.54	250	2	Yes
[101]	1.79, 1.89 & 2.07	3.54 (0.0018)	46.5	$0.78\lambda_o * 0.95\lambda_o$	3.2	-	9	Yes
[107]	2.45	4.4 (0.02)	0.8	$0.42\lambda_o * 0.42\lambda_o$	1.3	100	10	No
[138]	5	3.48 (0.004)	15	$1.12\lambda_o * 1.12\lambda_o$	6.1	1810	3	No
[139]	2.29, 2.31, 2.33, 2.35 & 2.38	2.33 (NM)	1.575	$0.5\lambda_o * 0.5\lambda_o$	4	-	20	Yes
[140]	6	1.71 (0.02)	1.5	$0.6\lambda_o * 1.2\lambda_o$	6.11	280	3	No

[142]	2	2.65 (NM)	1.5	-	6.4	1740	4	No
[143]	6.5	4.4 (NM)	1	$0.95\lambda_0 * 0.87\lambda_0$	-	4000	3	No

Table 4.5 shows that among the designs in the literature review, this design has smaller size with only one feeding port and large number of pattern and frequency reconfigurable configurations. The antenna has good gains. The bandwidths of this antenna are very good compared to other designs. The efficiency of the antenna with the used cheap FR-4 substrate shows that the design is really good compared to other designs in literature.

#### 4.1.5 Summary of the first pattern reconfigurable slot-based antenna

A low-profile and compact dual-band slot-based pattern and frequency reconfigurable antenna was proposed. The antenna resonates at 3.6 GHz and 5.2 GHz. 4 different patterns with gains greater than 0.5 dB were achieved at 3.6 GHz by electrically controlling the used pin diodes. 4 different patterns with gains greater 4 dB were achieved at 5 GHz by electrically controlling the used pin diodes under the condition that two diodes are ON at a time. The radiation efficiencies were above 50 %. This antenna can be modified more to be useful for mMIMO systems. However, it is a good candidate for future drones.

## 4.2 A Slot Based Pattern Reconfigurable Antenna

Data rates in communication systems increases very rapidly with time, and 5G technology is a great opportunity which will enhance data rates dramatically. Massive Multiple-Input Multiple-Output (mMIMO) antennas will be used in 5G technology since they enhance the diversity in the channel. Hence, mMIMO enhances data rates also. The patterns of antennas used for mMIMO should be reconfigurable for better diversity and better beamforming capabilities.

Pattern reconfigurability in an antenna design can be achieved by many methods such as using the idea of Yagi-Uda to direct the patterns to specific directions. However, slot antennas with pattern reconfigurability are not common in literature. In the literature, it can be found that the patterns of slot antennas can be reconfigured by changing the path of current around the slot, by having radiating elements with same amplitude and different phases, or by using the ground plane as a reflector.

In [130], a dual-band L-shaped slot was used with a varactor loaded at its end in order to get a dual-band frequency reconfigurable antenna. Four L-shaped slots like the one used in [130] were used in this proposed design in order to achieve a pattern reconfigurable antenna by changing the phases of the exciting fields which feed the different slots. Varactors were not included in this design, but they can be included later to make this antenna frequency and pattern reconfigurable antenna. In this stage, this design is capable to direct the patterns to many different directions at the frequency bands 2.3 GHz and 3.7 GHz.

### 4.2.1 Antenna Design

This antenna is composed of one FR-4 substrate with a dielectric constant of 4.4, a loss tangent of 0.02, a thickness of 0.72 mm, and a size of  $61.4 \times 61.4 \times 0.72 \text{ mm}^3$ . The top side has the feeding network, and the bottom side is the ground plane. Fig. 4.22 shows the proposed antenna. The feeding network includes three Wilkinson power dividers such that it is possible to feed the four slots. These Wilkinson power dividers and the 50 ohms transmission lines are designed at 3.7 GHz. The exciting fields which feed the slots can feed with same phase or with different phases.

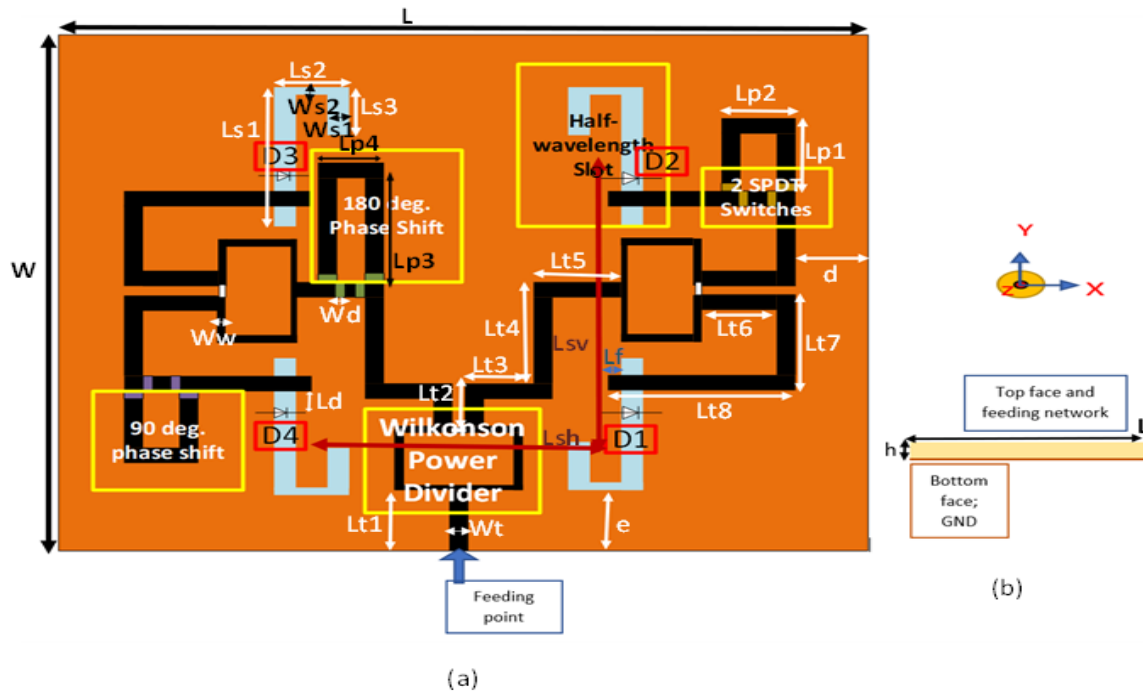


Fig. 4.22. The antenna design (a) Top view. (b) Side view.

Feeding the slots with different phases is achieved by making the lengths of the transmission lines feeding the slots different. In this way, the second slot can be fed with  $90^\circ$  or  $0^\circ$  phase shifts, the third slot can be fed with  $0^\circ$  or  $180^\circ$  phase shifts, and the fourth slot can be fed with  $0^\circ$ ,  $90^\circ$ ,  $180^\circ$  or  $270^\circ$ . So, the feeding network is reconfigurable, and this is achieved by using electrical switches. Therefore, the antenna has many pattern configurations at 2.3 GHz and 3.7 GHz. Four L-shaped slot antennas were etched on the ground plane as shown in Fig. 4.22, and four diodes are used to bridge these slots such that more pattern reconfigurability can be achieved at first and second frequency bands. The biasing circuits are not connected because tapes were used to connect the required phase shifters and to bridge the required slots, and this is done for the time being just to show that the antenna works as expected. However, switches with their biasing circuits will be



connected to the design in future in order to show that the antenna is working as required. Also, phase shifter components can be added to the antenna in future.

The distance between the slots is half-wavelength. The antenna dimensions shown in Fig. 4.22(a) are  $L=61.4\text{mm}$ ,  $W=61.4\text{ mm}$ ,  $h=0.72\text{ mm}$ ,  $Ls1=15.59\text{ mm}$ ,  $Ls2=7\text{ mm}$ ,  $Ls3=6\text{ mm}$ ,  $Ws1=2\text{ mm}$ ,  $Ws2=0.5\text{ mm}$ ,  $Lt1=8\text{ mm}$ ,  $Lt2= 4.68\text{ mm}$ ,  $Lt3= 5\text{ mm}$ ,  $Lt4= 13\text{ mm}$ ,  $Lt5= 8\text{ mm}$ ,  $Lt6=5.72\text{ mm}$ ,  $Lt7= 9.38\text{ mm}$ ,  $Lt8= 14\text{ mm}$ ,  $Wt= 1.38\text{ mm}$ ,  $Ww= 0.73\text{ mm}$ ,  $Lp1= 8.96\text{ mm}$ ,  $Lp2= 6.38\text{ mm}$ ,  $Lp3= 11.7\text{ mm}$ ,  $Lp4=5.82\text{ mm}$ ,  $Wd= 1.32\text{ mm}$ ,  $Ld= 1.08\text{ mm}$ ,  $Lf= 1\text{ mm}$ ,  $Lsh = 24\text{ mm}$ ,  $Lsv= 28\text{ mm}$ ,  $e= 9.1\text{ mm}$  and  $d= 4.32\text{ mm}$ .  $Lf$  was optimized such that the input impedance matching is enhanced.  $Ld$  was chosen in a way that when the diode is on, the bridged slot will not radiate. Also,  $Lp1$ ,  $Lp2$ ,  $Lp3$  and  $Lp4$  were optimized such that the attained patterns are with good performance and pattern reconfigurability will be enhanced. It should be mentioned also that the length of the antenna could be reduced also. Also, the white rectangles on top of Wilkinson power dividers are 100 ohms resistors.

#### **4.2.2 Theory of Operation**

The phase shifters shown in Fig. 4.23 are used to reconfigure the feeding phases to the different slots. The diodes  $D1 - D4$  shown in Fig. 4.23 are used to increase the possible number of configurations of the antenna.

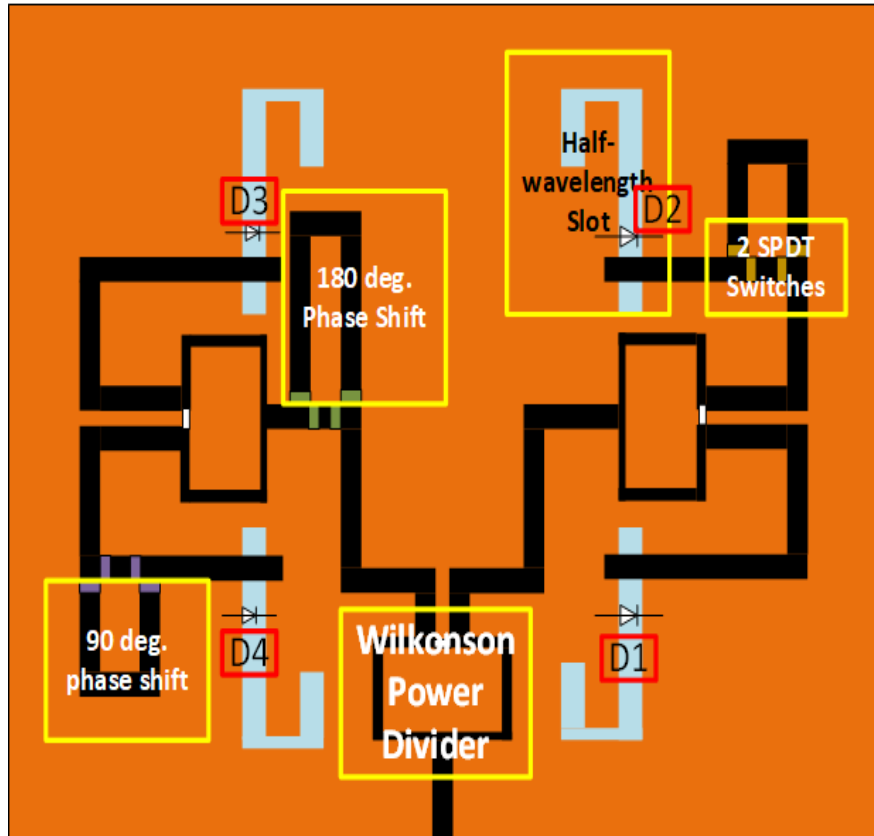


**Fig. 4.23. The Geometry of the proposed pattern reconfigurable antenna.**

The distance between the slots as shown in Fig. 4.24 is half guided-wavelength at 3.7 GHz. There are two 90 degrees phase shifters and one 180 degrees phase shifter as shown in Fig. 4.25. Therefore, the possible phase configurations are shown in table 4.6, and Fig. 4.26 shows the slot numbers. In addition, more configurations are achieved by bridging different slots using diodes. These configurations achieved by bridging the slots are shown in table 4.7, and Fig. 4.27 shows the used diodes and their numbers in the antenna.

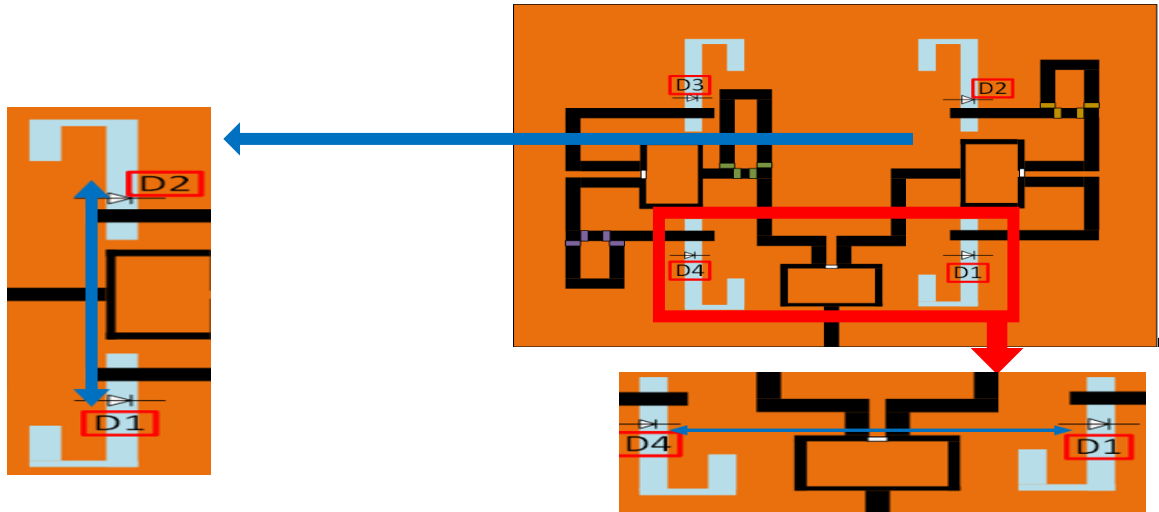


Fig. 4.24. The antenna geometry showing the distances between the L-slots.

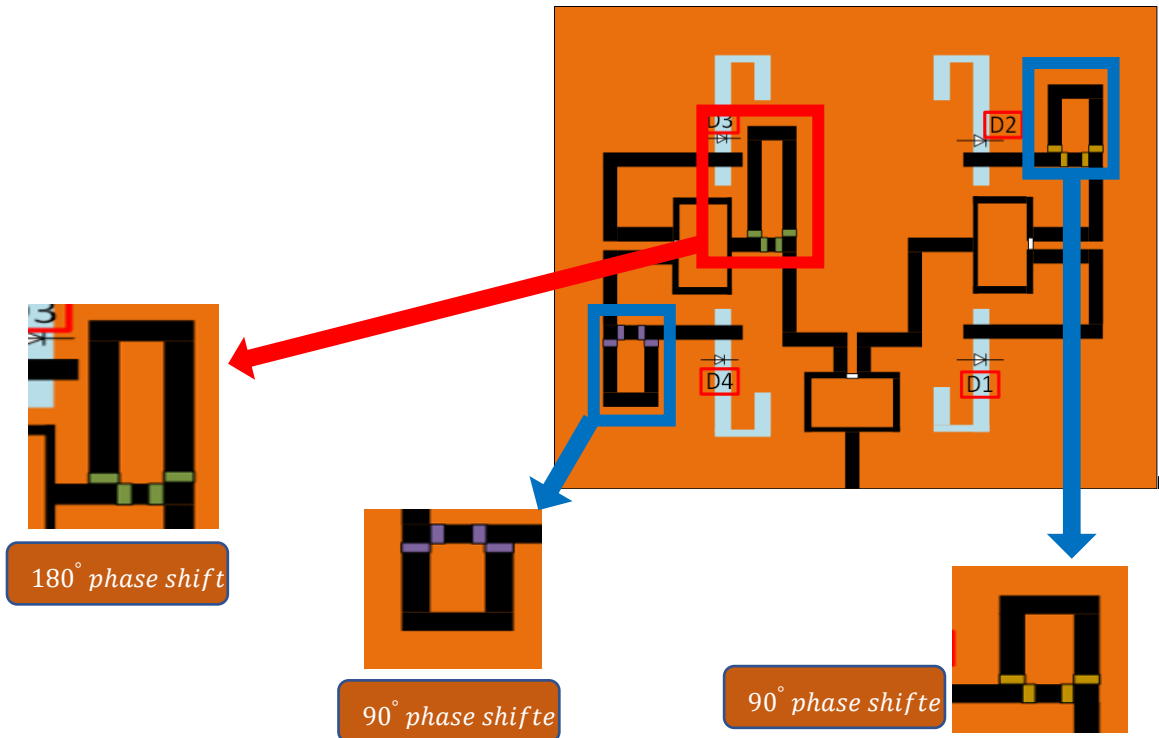


Fig. 4.25. The antenna geometry showing the used phase shifters.

Table 4.6. The possible phases feeding the used slots.

Config. Number	Phase at slot 1	Phase at slot 2	Phase at slot 3	Phase at slot 4
1	0	0	0	0
2	0	90	0	0
3	0	90	180	180
4	0	90	180	270
5	0	0	180	180
6	0	0	180	270
7	0	0	0	90
8	0	90	0	90

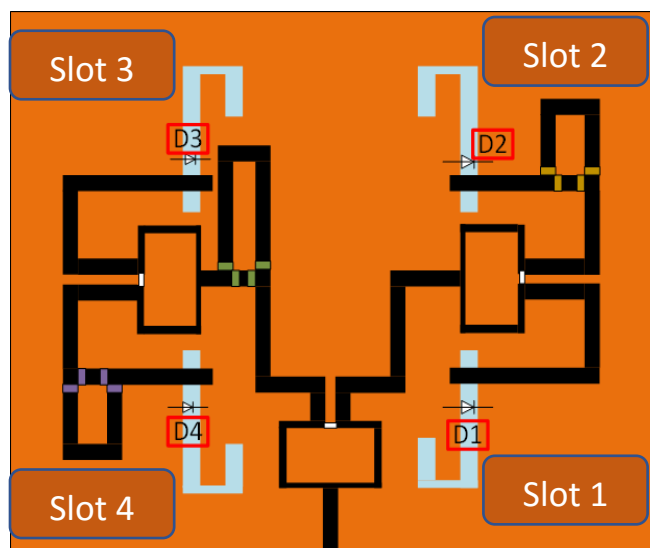


Fig. 4.26. The number of slots in the antenna.

**Table 4.7. The attained configurations by switching the diodes bridging the slots.**

<b>Config. Number</b>	<b>Diode 1</b>	<b>Diode 2</b>	<b>Diode 3</b>	<b>Diode 4</b>
0	OFF	OFF	OFF	OFF
1	ON	OFF	OFF	OFF
2	OFF	ON	OFF	OFF
3	OFF	OFF	ON	OFF
4	OFF	OFF	OFF	ON
5	ON	ON	OFF	OFF
6	ON	OFF	ON	OFF
7	ON	OFF	OFF	ON
8	OFF	ON	ON	OFF
9	OFF	ON	OFF	ON
10	OFF	OFF	ON	ON
11	ON	ON	ON	OFF
12	OFF	ON	ON	ON
13	ON	OFF	ON	ON
14	ON	ON	OFF	ON

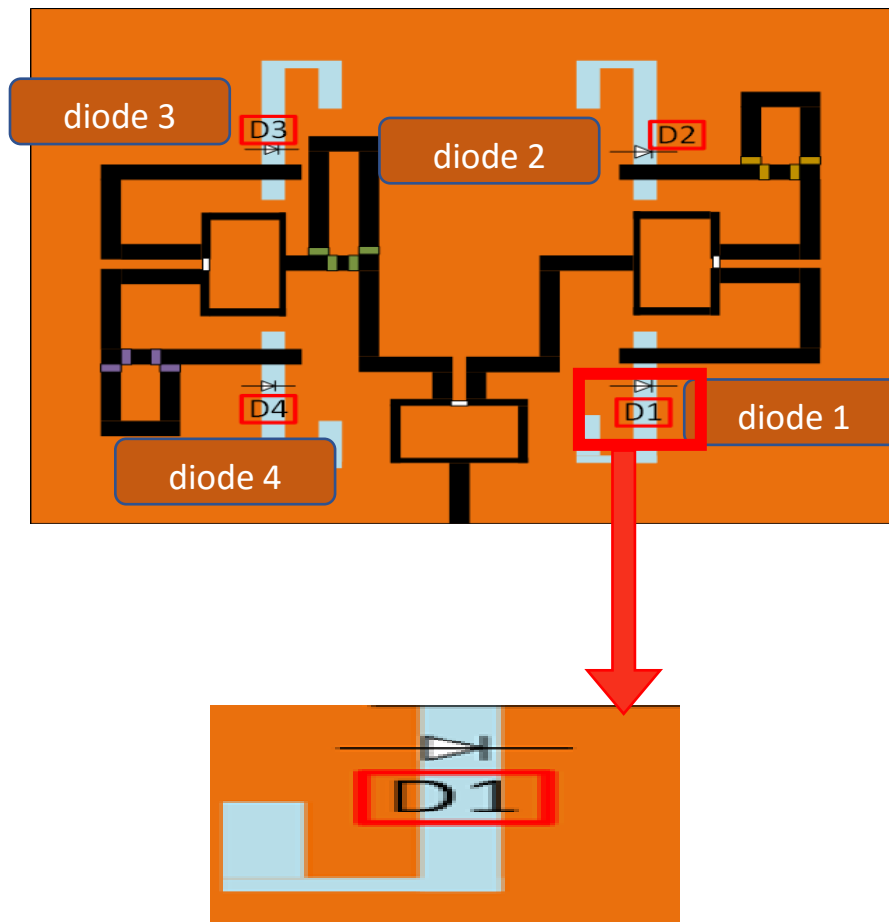


Fig. 4.27. The diodes used to bridge the slots for more configurations.

Therefore, it can be seen that many configurations are achieved by this antenna. These configurations are achieved because of the use of different phase shifters and by bridging different L-slots. Therefore, pattern and frequency reconfigurabilities are achieved for this design. The biasing circuits for the diodes are shown in Fig. 4.28. The biasing network includes limiting resistors with  $2.1\text{Kohms}$ , and RF-chokes with  $1\ \mu\text{H}$ . Linewidths of biasing lines is  $0.5\ \text{mm}$  to enhance isolation of RF signals from biasing network. Diode and the capacitors are in the ground

plane (Bottom face of the substrate). RF chokes and limiting resistors are on the top face. The capacitors are used to provide paths for the RF current.

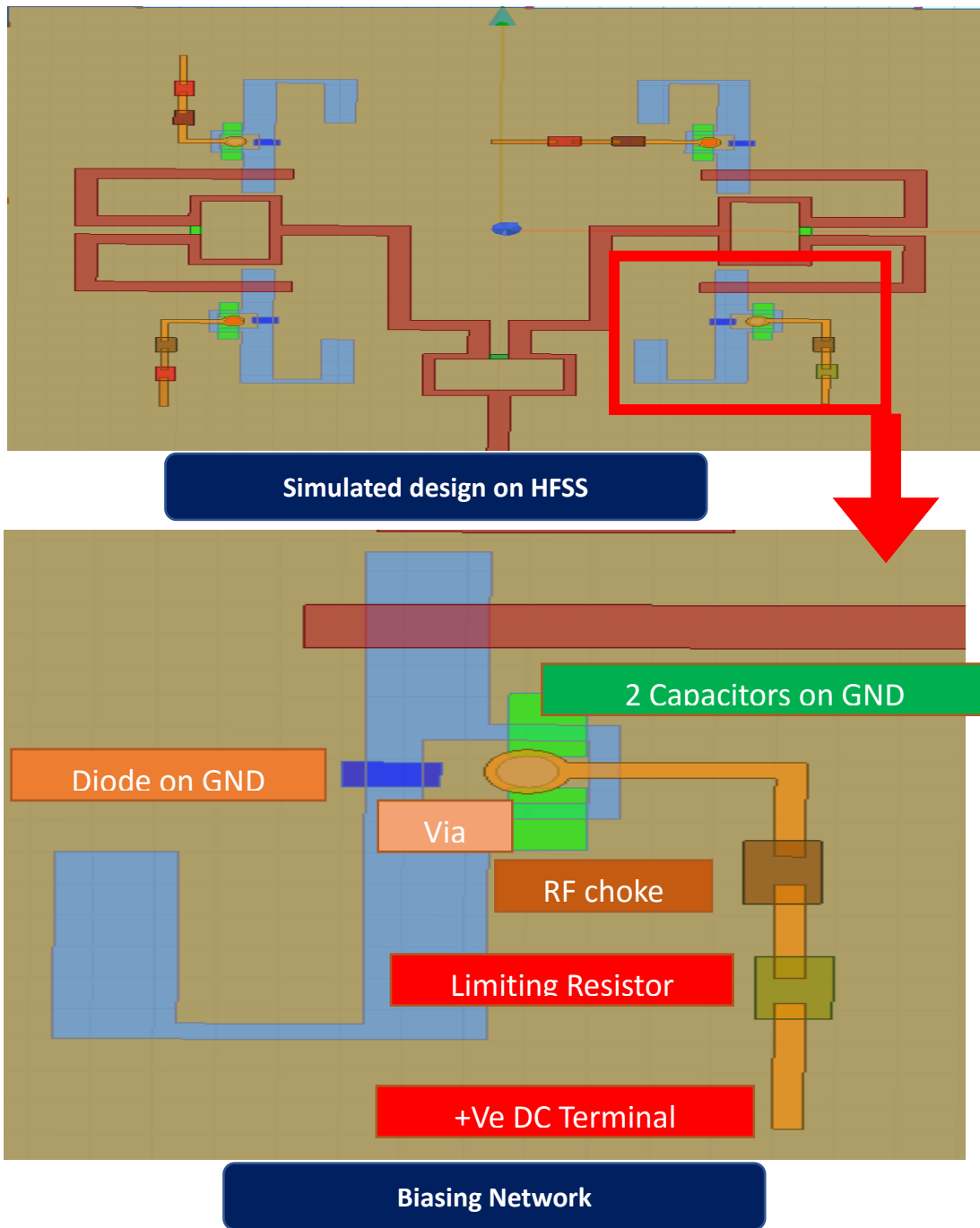


Fig. 4.28. The biasing circuits for the diodes.

### 4.2.3 Simulation Results

The antenna was modeled and simulated on HFSS. The patterns of the antenna can be reconfigured depending on the phase shifters' states and depending on which ones of the slots are bridged. The simulated  $S_{11}$  results for many configurations at the first and second bands are shown in Fig. 4.29 and Fig. 4.30, respectively.

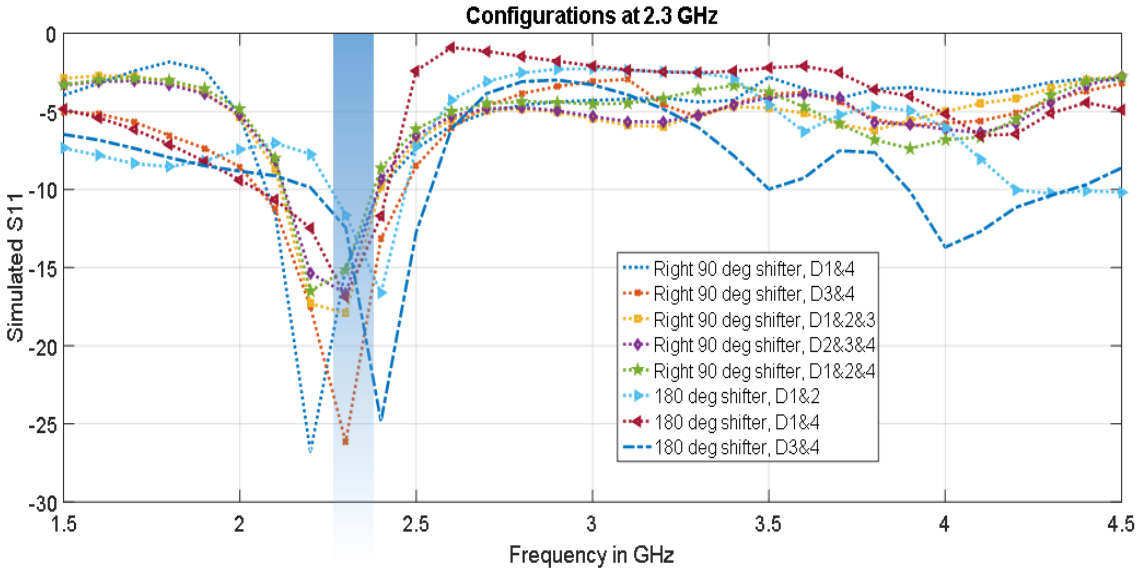


Fig. 4.29. Simulated  $S_{11}$  results at the lower band of the proposed antenna. The used diodes and phase shifters are mentioned.

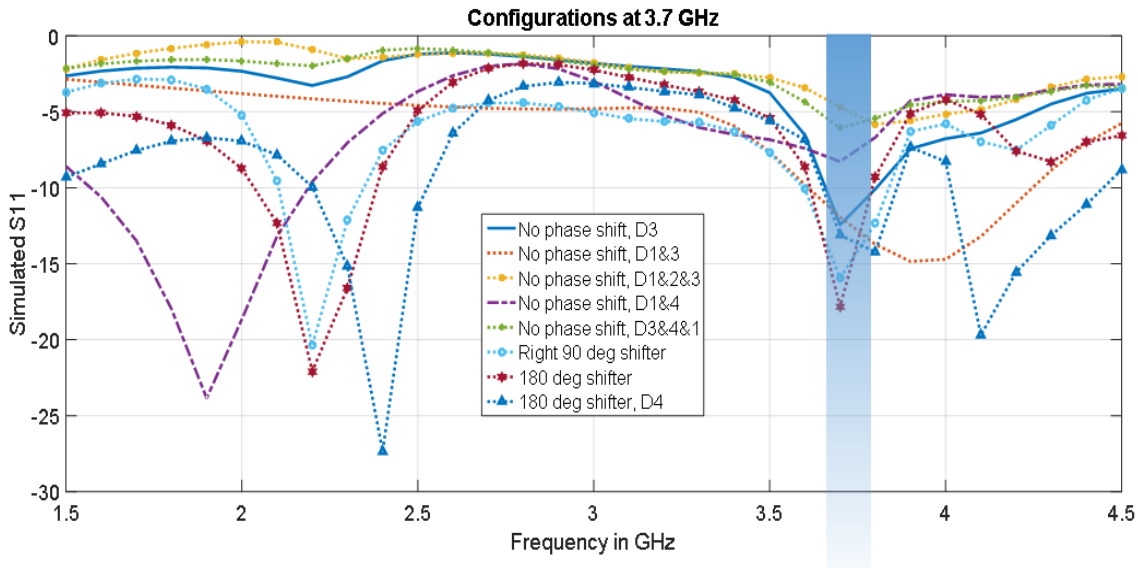
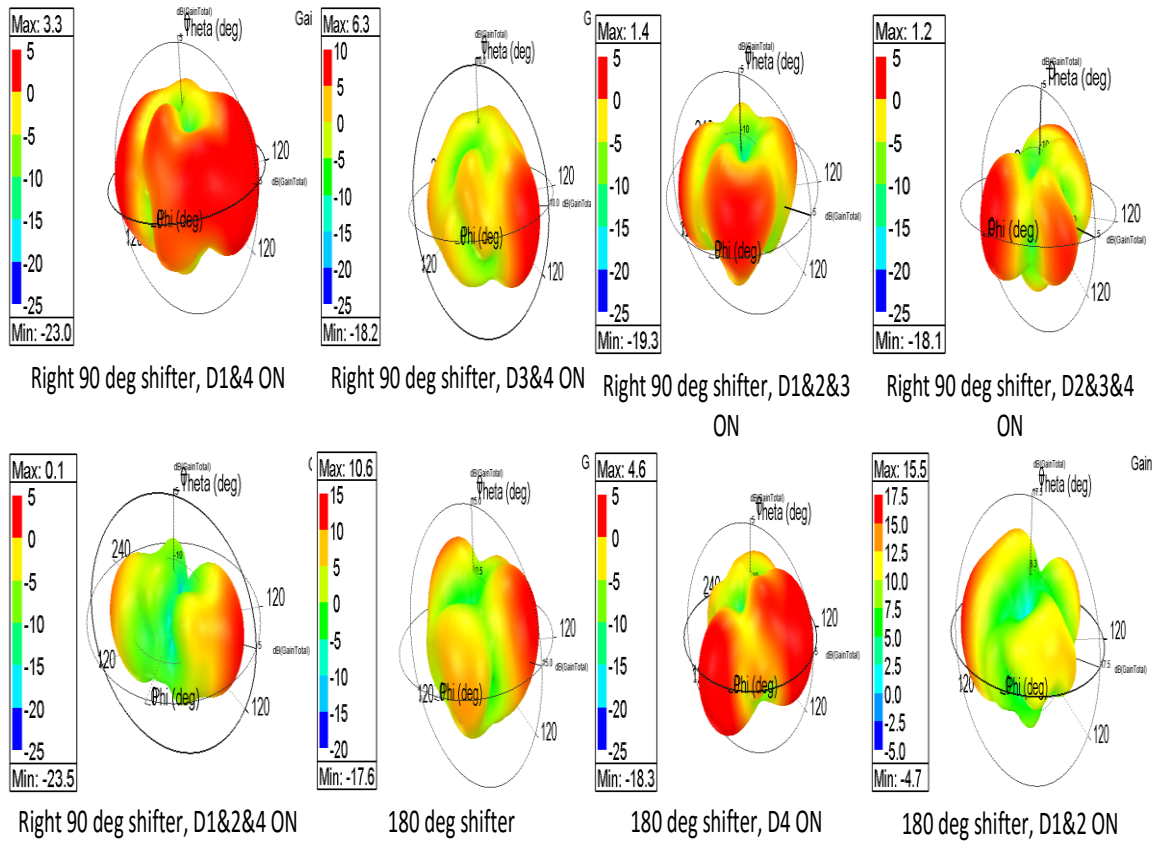


Fig. 4.30. Simulated  $S_{11}$  results at the higher band of the proposed antenna. The used diodes and phase shifters are mentioned.



It can be seen from Fig. 4.29 and Fig. 4.30 that many pattern configurations have a resonant frequency of 2.3 GHz, and many other pattern configurations have a resonant frequency of 3.7 GHz. The simulated – 10 dB overlapped bandwidth for configurations at 2.3 GHz and 3.7 GHz is 100 MHz.

The simulated 3-D pattern configurations at 2.3 GHz and 3.7 GHz are shown in Fig. 4.31 and Fig. 4.32, respectively, and their corresponding simulated  $S_{11}$  results are shown in Fig. 4.29 and Fig. 4.30.



**Fig. 4.31. 3-D radiation patterns at 2.3 GHz, scales might change.**

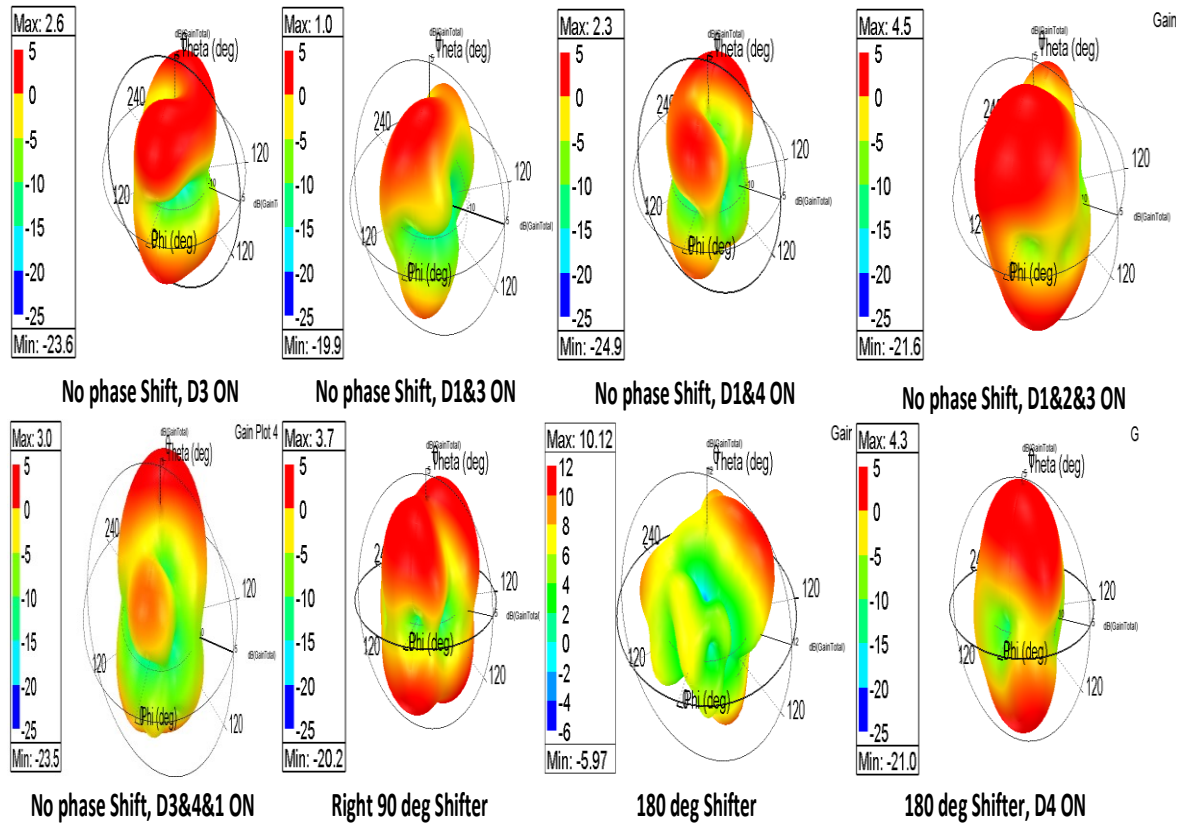
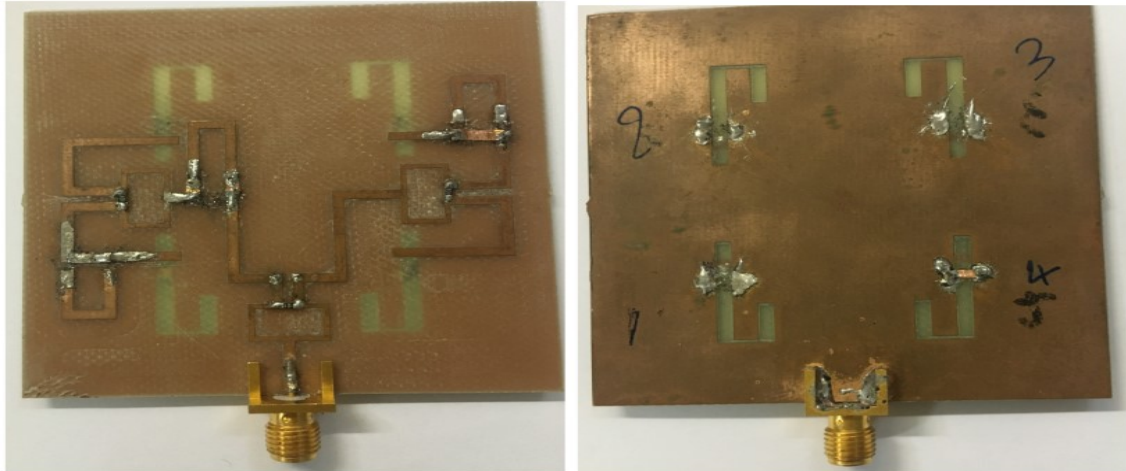


Fig. 4.32. 3-D radiation patterns at 3.7 GHz.

It can be seen from Fig. 4.31 and Fig. 4.32 that the radiation patterns of the antenna can be reconfigured by bridging some of the slots and by reconfiguring the phase shifters used in the transmission lines. The simulated peak gains at 2.3 GHz are ranging from 1 dB to 6.3 dB for different configurations. The simulated peak gains at 3.7 GHz are ranging from 1 dB to 4.5 dB for different configurations. The simulated radiation efficiencies are more than 30 % at 2.3 GHz and more than 40% at 3.7 GHz.

#### 4.2.4 Experimental Results

The  $S_{11}$  results of the antenna were measured using the network analyzer. The fabricated design is shown in Fig. 4.33 where it can be seen that tapes are used in order to bridge slots or to choose between the phase shifters.



(a) Top View

(b) Bottom View

Fig. 4.33. The fabricated design of the proposed pattern reconfigurable L-slot antenna.

The measured  $S_{11}$  results when no phase shifter is used are shown in Fig. 4.34; all slots are fed with same amplitude and same phase. It can be seen that the antenna is resonating around 3.7 GHz, and there is a reasonable shift due to the use of tapes instead of diodes.

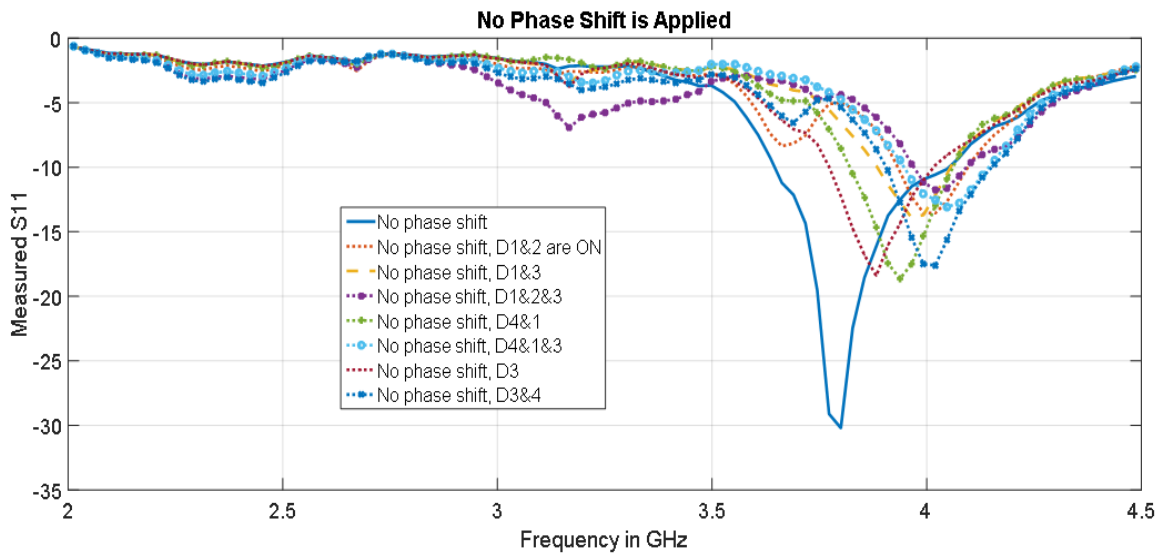


Fig. 4.34. The measured  $S_{11}$  results of the antenna when no phase shifter is used.

The measured  $S_{11}$  results when the right 90 degrees phase shifter is used are shown in Fig. 4.35 and Fig. 4.36. It can be seen that the antenna is resonating at two bands with a shift between simulated and measured results because tapes are used instead of diodes. Fig. 4.37 shows the measured  $S_{11}$  when the 180 degrees phase shifter is used.

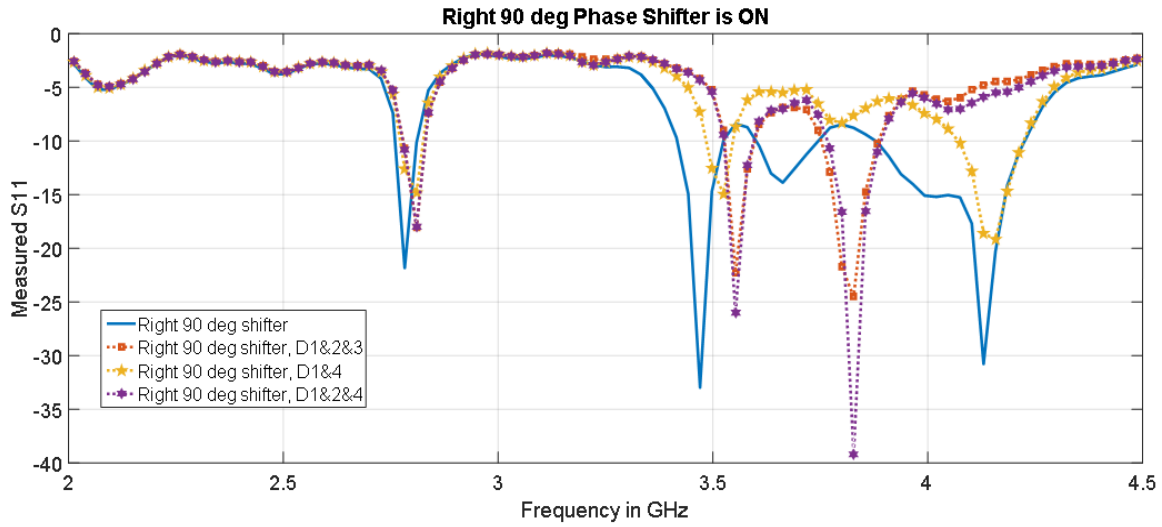


Fig. 4.35. The measured S11 results of the antenna when the right 90 degrees phase shifter is used.

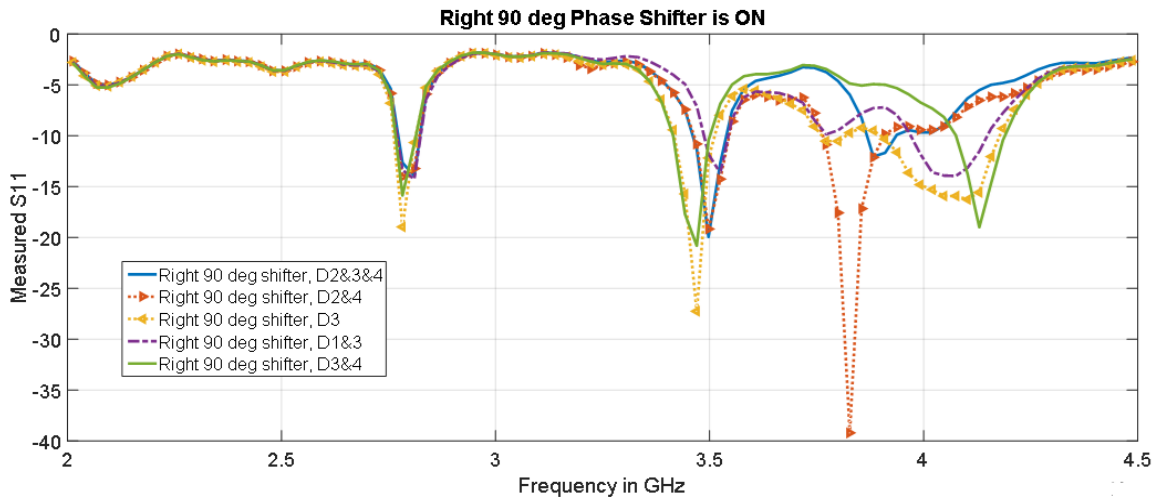


Fig. 4.36. The measured S11 results of the antenna when the right 90 degrees phase shifter is used.

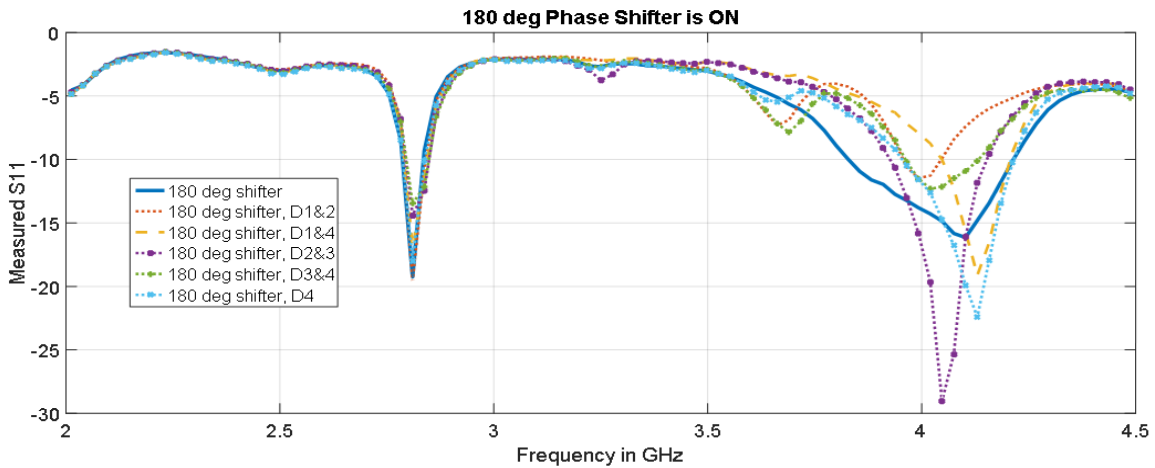


Fig. 4.37. The measured S11 results of the antenna when the right 90 degrees phase shifter is used.

## 4.2.5 Comparison Table and Discussions

Table 4.8 shows a comparison table between this proposed antenna and other slot-based pattern reconfigurable antennas in the literature.

**Table 4.8. Comparison table between the proposed slot-based pattern reconfigurable antenna and other slot-based pattern reconfigurable antennas in literature.**

Ref.	Resonant frequency (GHz)	Dielectric constant ( $\tan \delta$ )	Height (mm)	Antenna size	Min. Gain (dB)	BW (MHz)	# pattern modes	Frequency - reconfigurability
<b>This work</b>	<b>2.3, 3.7</b>	<b>4.4 (0.02)</b>	<b>0.72</b>	<b><math>0.75\lambda_o * 0.75\lambda_o</math></b>	<b>1</b>	<b>100</b>	<b>16</b>	<b>Yes</b>
[1]	2.02	4.4 (NM)	7	$0.67\lambda_o * 0.67\lambda_o$	2.5	50	2	No
[4]	5.32	2.2 (0.0009)	3.175	$0.89\lambda_o * 0.89\lambda_o$	3	361	3	No
[9]	3	3.55 (NM)	8.5	$0.7\lambda_o * 0.7\lambda_o$	6.1	200	4	No
[39]	2.005	4.3 (0.02)	1.52	$1.17\lambda_o * 1.14\lambda_o$	1.11	52	4	No
[53]	5.2, 5.8, & 6.4	6.15 (0.0025)	0.365	$0.97\lambda_o * 0.97\lambda_o$	-	-	9	Yes
[75]	2.3	4.4 (NM)	0.8	$0.4\lambda_o * 0.4\lambda_o$	0.54	250	2	Yes
[101]	1.79, 1.89 & 2.07	3.54 (0.0018)	46.5	$0.78\lambda_o * 0.95\lambda_o$	3.2	-	9	Yes
[107]	2.45	4.4 (0.02)	0.8	$0.42\lambda_o * 0.42\lambda_o$	1.3	100	10	No
[138]	5	3.48 (0.004)	15	$1.12\lambda_o * 1.12\lambda_o$	6.1	1810	3	No
[139]	2.29, 2.31, 2.33, 2.35 & 2.38	2.33 (NM)	1.575	$0.5\lambda_o * 0.5\lambda_o$	4	-	20	Yes
[140]	6	1.71 (0.02)	1.5	$0.6\lambda_o * 1.2\lambda_o$	6.11	280	3	No

[142]	2	2.65 (NM)	1.5	-	6.4	1740	4	No
[143]	6.5	4.4 (NM)	1	$0.95\lambda_o * 0.87\lambda_o$	-	4000	3	No

It can be seen from table 4.8 that the proposed antenna has a competing size, a good overlapped bandwidth, a competing number of pattern configurations, and the antenna is a dual-band antenna.

#### 4.2.6 Summary of the second slot-based pattern reconfigurable antenna

A low-profile and compact slot-based pattern and frequency reconfigurable antenna was proposed and presented. Table 4.9 summarizes the pattern configurations achieved for this antenna at the two bands.

**Table 4.9. The summary of the pattern configurations of the proposed pattern reconfigurable L-slot antenna.**

Pattern Config. Number	$S_{11}$ at 2.3 GHz	$S_{11}$ at 3.7 GHz	Used Phase Shifter	ON Diodes
1	Good matching	No matching	Right 90° phase shifter only	D1 & D4
2	Good matching	No matching	Right 90° phase shifter only	D3 & D4
3	Good matching	No matching	Right 90° phase shifter only	D1 & D2 & D3
4	Good matching	No matching	Right 90° phase shifter only	D2 & D3 & D4
5	Good matching	No matching	Right 90° phase shifter only	D1 & D2 & D4
6	Good matching	Good matching	180° phase shifter only	All diodes are OFF
7	Good matching	Good matching	180° phase shifter only	D4

8	<b>Good matching</b>	<b>No matching</b>	180° phase shifter only	D1 & D2
9	<b>No matching</b>	<b>Good matching</b>	No Phase Shifter	D3
10	<b>No matching</b>	<b>Good matching</b>	No Phase Shifter	D1 & D3
11	<b>No matching</b>	<b>Good matching</b>	No Phase Shifter	D1 & D4
12	<b>No matching</b>	<b>Good matching</b>	No Phase Shifter	D1 & D2 & D3
13	<b>No matching</b>	<b>Good matching</b>	No Phase Shifter	D1 & D3 & D4
14	<b>Good matching</b>	<b>Good Matching</b>	Right 90° phase shifter only	All Diodes are OFF

It can be seen from Table 4.8 that 8 different pattern configurations were achieved at 2.3 GHz with an overlapped bandwidth of 100 MHz and via the control of the phase shifters and the states of the used diodes. In addition, 8 different pattern configurations were achieved at 3.7 GHz with an overlapped bandwidth of 100 MHz and via the control of the used phase shifters and the states of the used diodes. This antenna is a good candidate for projects where it is require to locate the oil wells in large areas.

## 4.3 A Compact Pattern Reconfigurable Antenna for UHF Internet of

### Things Applications

The number of connected devices to the internet is increasing sharply with time. These devices will be controlled or monitored wirelessly using Internet of Things (IoT) technology. Hence, it is important to design antennas working for IoT applications to serve this huge number of connected devices. Enhancing the antennas by pattern or polarization reconfigurability will improve the reliability of the IoT wireless systems. UHF frequency are preferred because of higher penetration in buildings and long distance coverage. Comparing IoT with mobile phone technology, the wireless link robustness must be enforced in IoT applications, as it may not be possible for the object to move to improve its network level connection. Thus, additional mechanisms should be integrated to compensate for channel multi-path and blockage effects. Diversity schemes can be used to improve average Signal to Noise ratio (SNR). Many solutions have been proposed in literature to achieve diversity with compact antenna.

Pattern reconfigurable antennas with uncorrelated patterns provide different received signals by the antenna, and the best received signal can be used to provide better results and better control for the IoT systems. The use of slot antennas in reconfigurable antennas is not common in literature and it will help in providing compact antennas. Slot-based pattern reconfigurable systems can be achieved by exciting different electromagnetic modes, by changing the feeding phases, by reconfiguring the feeding network, by reconfiguring the slot orientations or slot types, by bridging slots to change current paths, or by the use of directors and reflectors. Monopole antennas can be used to achieve pattern reconfigurability by changing the monopole orientation.

The objective of this work is to design a compact terminal with reconfigurable pattern capabilities at 868MHz. In order to maximize diversity, the Envelope Correlation Coefficient (ECC) between different modes must be minimized.

#### 4.3.1 Antenna Geometry

- **Design Procedure**

Many IoT applications require compactness to ease device integration in existing objects. A credit card form factor ( $80 \times 50$  mm<sup>2</sup>) has been targeted for several use cases. In this study, 3



different antennas are integrated in the terminal, and a switching feeding circuit is used to select one of the three radiating elements. Different antenna configurations are studied in order to determine the best configuration. It is well-known that magnetic and electric dipoles provide orthogonal radiation patterns. In a compact surface, electric dipole can be generated with a meandered line. Magnetic dipole can be usually created with meandered slots.

As shown in Fig. 4.38(a), the first antenna prototype includes four slots at the antenna corners. Hence, there are four pattern configurations for this prototype. The patterns are omnidirectional along the xy-plane but directed to different corners for different configurations because of the ground plane behind the slots. The problem with this design was the high correlation coefficients between Slots 1 and 2, and between Slots 3 and 4; i.e. the correlation coefficients between them were above 0.8. Many techniques were employed to reduce the correlation coefficients, such as making the phase shift between Slots 1 and 2 to be  $180^\circ$ , and changing the orientation of Slot 2 by  $90^\circ$ . However, the ECC results were still high between Slots 1 and 2, and between Slots 3 and 4.

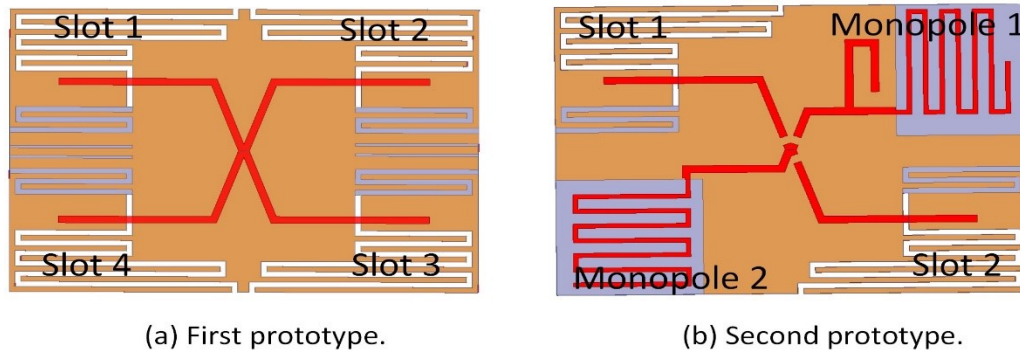


Fig. 4.38. The antenna prototypes in designing the proposed antenna.

The electric monopoles were used to replace Slot 2 and Slot 4 as shown in Fig. 4.38(b) to reduce the Envelope Correlation Coefficient (ECC) between the patterns. It can be seen from Fig. 4.38(b) that the used two monopoles have different orientations in order to get a low ECC. Unfortunately, ECC between the patterns of the two monopoles was more than 0.8. Therefore, and after this study, it was concluded that the antenna, with two slots and one monopole, shown in Fig. 3.40 is the best solution since the correlation coefficients between the three patterns are well below 0.5. Hence, the proposed antenna in this design has three pattern configurations with low correlation coefficients.

The correlation coefficient between Slots 1 and 2 is low because the polarizations of the dominant electric fields (red arrows in Fig. 4.39) of the two configurations are different than each

others as it can be seen from Fig. 4.39. In addition, the two slots are not close to each others which helps in reducing the correlation coefficients between the two configurations.

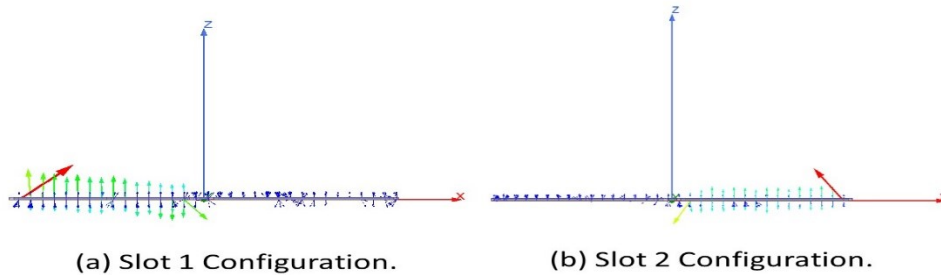


Fig. 4.39. The electric field distribution around the slots at 868 MHz for Slot 1 and Slot 2 configurations.

- **Design Description**

The proposed pattern reconfigurable antenna working for IoT applications is designed on an FR-4 substrate with a dielectric constant of 4.4, a loss tangent of  $\tan\delta = 0.02$ , and a thickness of  $h = 0.72$  mm. The antenna geometry is shown in Fig. 4.40. The size of the antenna is  $80 \times 55$  mm<sup>2</sup>; i.e. the electrical size of the antenna is  $0.23\lambda_0 \times 0.16\lambda_0$ . It can be seen from Fig. 4.40 that the antenna is composed of one substrate with a top and bottom faces. The top face includes the reconfigurable feeding network, the monopole and the biasing lines, and they are shown in Fig. 4.40 with black color. This reconfigurable feeding network includes  $50 \Omega$  transmission lines with four PIN diodes used to control the feeding network. The bottom face of the antenna includes the ground plane with a brown color in Fig. 4.40 etched by two meandered slots and a cut in the ground plane for the monopole to radiate. The biasing network shown on the top face includes RF chokes with  $1 \mu\text{H}$  and limiting resistors of  $2.1 \text{ K}\Omega$  to protect the diodes from overloading currents. As shown in Fig. 4.40, the inductors are shown with blue color, resistors are shown with dark brown color, and the diodes are shown with yellow color. The dimensions and the equivalent circuits of the used PIN diodes (Infineon BAR64-02 V PIN diodes), the used inductors and resistors are inserted in simulations as per their data sheets. One Coaxial feeding port is used in this antenna and it is located at the center of the antenna as shown in Fig. 4.40 with a red point at the center. The left-bottom corner of the terminal is available for electronic components used to control this reconfigurable antenna and to receive/transmit RF signals (i.e. microcontroller, transceiver, and a small battery to operate these electronics).

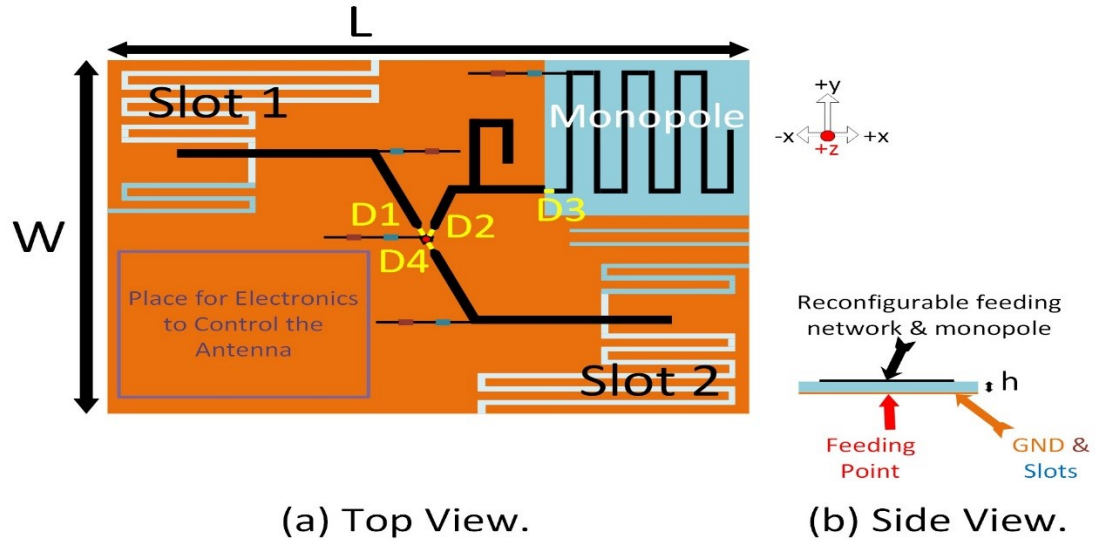


Fig. 4.40. The geometry of the proposed antenna.

This antenna is designed to operate at a resonant frequency of 868 MHz such that it can be used for IoT applications. It can be seen from Fig. 4.40 that Slot 1 and Slot 2 are meandered and etching the ground plane at both ends of the slots; this is done in order to make the resonant frequencies of these slots centered at 868 MHz. The total length of the used slots is 246 mm. On the other hand, it can be seen also that the monopole is meandered with a length of 142.87 mm such that its resonant frequency becomes at 868 MHz. The dimensions for this antenna are shown in Fig. 4.41 and in Table 4.10. The stub shown in Fig. 4.41 before the monopole is an open circuited stub used to enhance the input impedance matching at 868 MHz when the monopole is activated to radiate. It can be seen also from Fig. 4.41 that there are two slits in the ground plane with a width of 0.5 mm used to reduce the current coupling between the monopole cut and Slot 2 in the ground plane. It is good to mention here also that the width of the biasing lines is 0.5 mm in order to help in isolating the RF signals from the DC circuit.

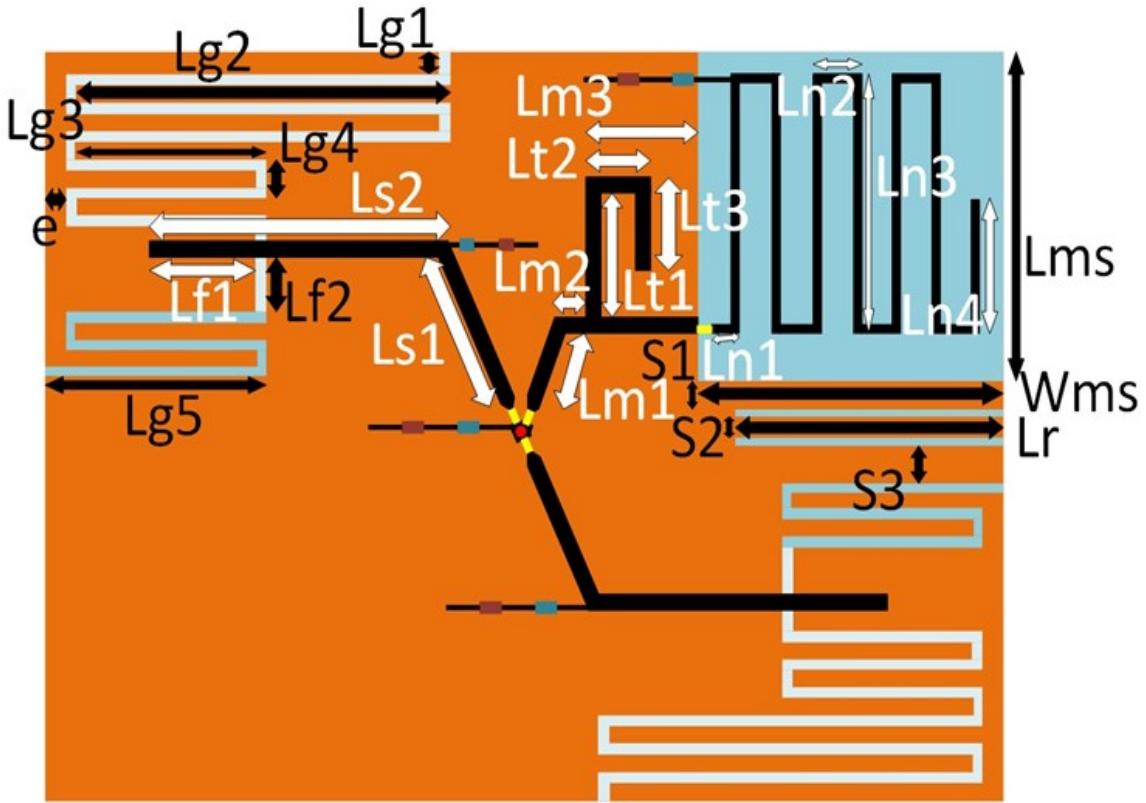


Fig. 4.41. The proposed antenna with important dimensions.

Table 4.10. Dimensions of the proposed antenna

Parameter	Length (mm)	Parameter	Length (mm)
L	80	W	55
Slot width	1	Monopole width	0.8
$Lg\ 1$	1	$Lg\ 2$	37
$Lg\ 3$	19	$Lg\ 4$	3
$Lg\ 5$	21	E	1
$Ls1$	11.14	$Ls2$	27
$Lf\ 1$	11.66	$Lf\ 2$	4.2
$Lm1$	4.49	$Lm2$	6.9
$Lm3$	8.42	$Lt1$	11.62
$Lt2$	5.76	$Lt3$	10
$Ln1$	1.67	$Ln2$	3.6
$Ln3$	19.2	$Ln4$	10
$Lms$	25	$Wms$	22
$Lr$	21	$S_1$	1
$S_2$	1.5	$S_3$	2.5
$h$	0.72	Transmission line width	1.3

In addition, the reconfigurable feeding network was analyzed (without the antennas) in simulations to check the isolation of the diodes when they are OFF and their insertion loss when they are ON. The simulated results when the diode D1 is ON is shown in Fig. 4.42 where it can be seen that antenna is well matched over the bandwidth of interest. It can be seen also that the isolation of the OFF-diodes is around  $-25$  dB through the bandwidth of interest, and the insertion loss of the ON-diode is around  $-0.8$  dB.

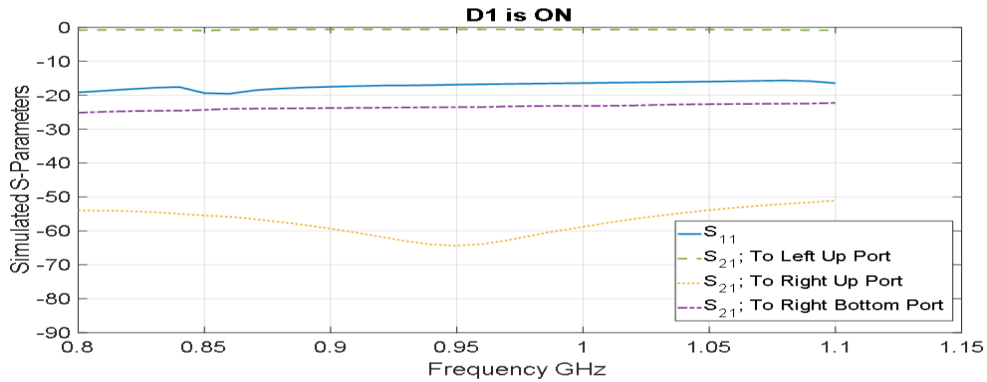


Fig. 4.42. The simulated S-parameters to different ports in the antenna.

- **Reconfiguration Mechanism**

This antenna is a pattern reconfigurable antenna with three configurations. The first configuration, called Slot 1 configuration, is achieved when diode D1 only in Fig. 4.40 is ON. In this configuration, Slot 1 is radiating and the pattern is an omnidirectional pattern of a magnetic dipole along the azimuthal plane which is directed more towards left-up corner because of the ground plane behind Slot 1. The ground plane in this case is working as a reflector. The second configuration, called the monopole configuration, is achieved when both diodes D2 and D3 in Fig. 4.40 are ON while other diodes are OFF. In this configuration, the monopole is radiating and the radiated pattern is an omnidirectional pattern of an electrical monopole and the pattern is along an elevation plane. The third configuration, called Slot 2 configuration, is achieved when the diode D4 in Fig. 4.40 is ON only. In this configuration, Slot 2 is radiating and the pattern is an omnidirectional pattern along the azimuthal plane, and the pattern is directed more to the right bottom corner of the antenna because of the ground plane behind Slot 2.

When Slot 2 configuration or the monopole configuration is activated, current coupling between the monopole cut in the ground plane and Slot 2 is realized. The use of the two slits, shown in Fig. 4.40, etched between the monopole cut and slot 2 reduces this coupling by a good amount. In addition, it can be seen from Fig. 4.40 that the monopole configuration requires two diodes (D2

and D3), where D2 is used to maintain the impedance matching for Slot 1 configuration and Slot 2 configuration, while D3 is used to avoid radiation from the monopole when Slot 1 configuration or Slot 2 configuration is activated. Also, the use of diode D3 reduces the ECC between the patterns of the three configurations dramatically. The ECC between the three patterns are acceptable since they are well below 0.5.

### 4.3.2 Simulation Results

The simulated  $S_{11}$  results for the three configurations are shown in Fig. 4.43, where it can be seen that the resonant frequency is at 0.87 GHz for the three configurations. It is shown also that the  $-10$  dB impedance bandwidths are 9.1 MHz, 9 MHz, and 27.4 MHz for Slot 1 configuration, Slot 2 configuration, and Monopole configuration, respectively. Therefore, the overlapped  $-10$  dB impedance bandwidth is 9 MHz, which is enough for IoT applications. The simulated peak gains for the three configurations are shown in Fig. 4.44, where it can be seen that the peak gains in the required bandwidth of operation are around  $-1.67$  dB,  $-1.98$  dB, and  $-1.3$  dB for Slot 1 configuration, Slot 2 configuration, and Monopole configuration, respectively. The simulated radiation efficiencies for the three configurations are shown in Fig. 4.45, where it can be seen that the efficiencies in the required bandwidth of operation are around 35.1%, 33.2%, and 44% for Slot 1 configuration, Slot 2 configuration, and Monopole configuration, respectively. These results are reasonable because the antenna is electrically small, and the used substrate is a lossy substrate. Hence, a degradation in the efficiencies and in the peak gains has to be accepted. It can be seen from Fig. 4.40 that some part of the FR-4 material is etched below Slot 1 and Slot 2 in order to enhance the radiation efficiency. This removal of the FR-4 material below the slots was done after observing the concentration of the currents around the slot, and the FR-4 material around the places with high current concentrations was removed. This removal of the FR-4 material enhanced the efficiency and the peak gains sharply for Slot 1 and Slot 2 configurations. Also, it can be seen from Fig. 4.43, Fig. 4.44, and Fig. 4.45 that the results of Slot 1 and Slot 2 configurations are close to each other and this is because of the symmetry between them.

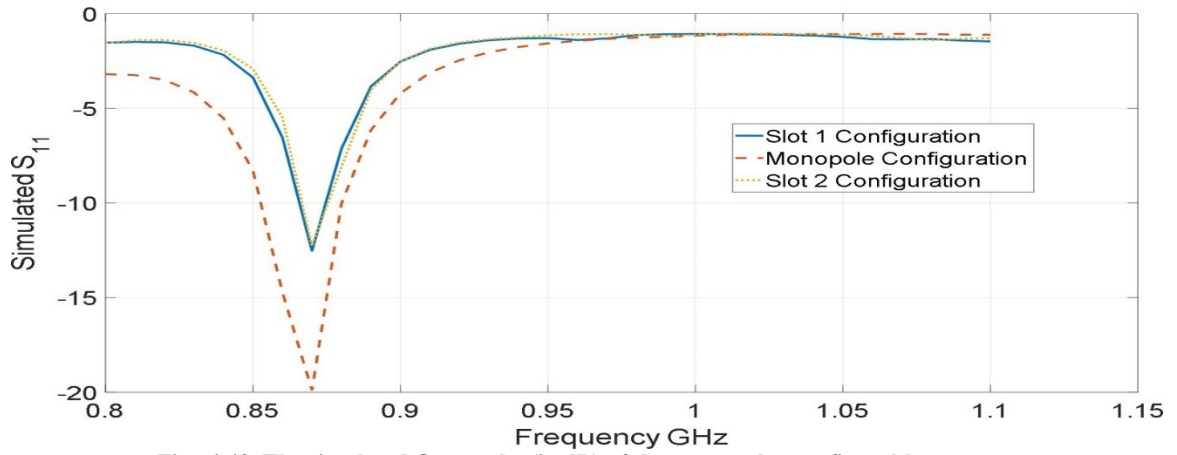


Fig. 4.43. The simulated  $S_{11}$  results (in dB) of the proposed reconfigurable antenna.

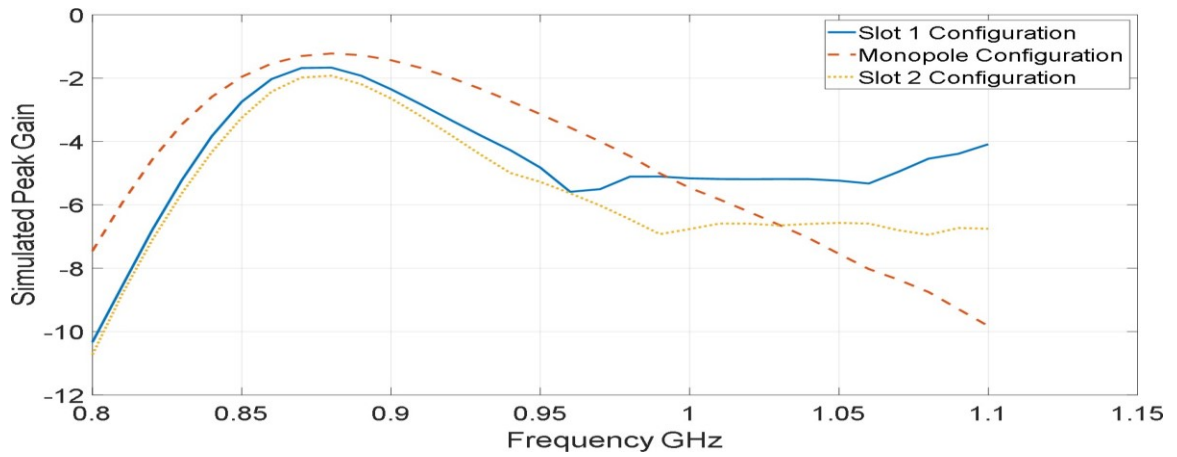


Fig. 4.44. The simulated Peak Gain Results (in dB) of the proposed reconfigurable antenna.

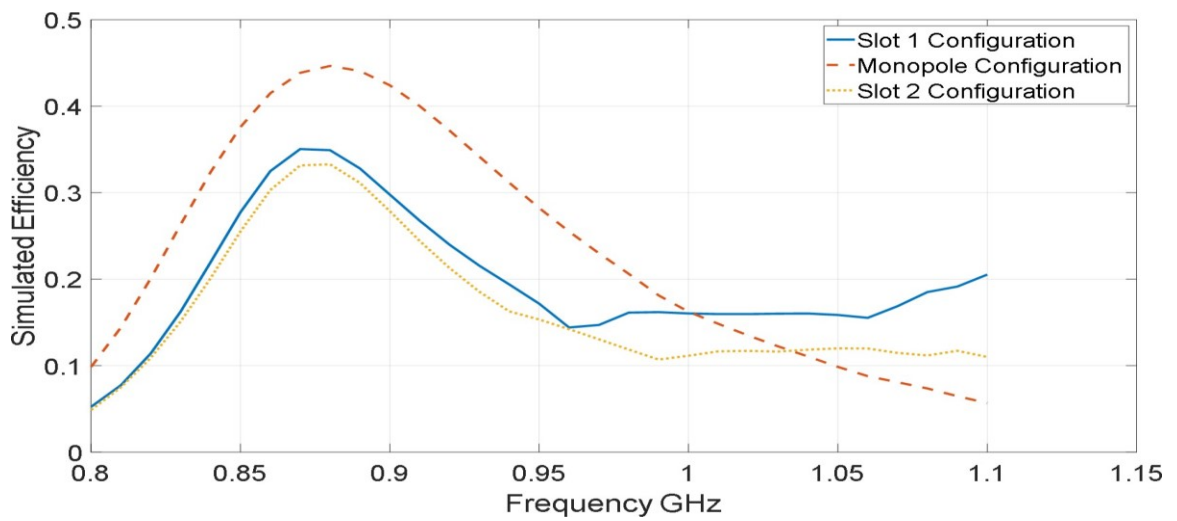
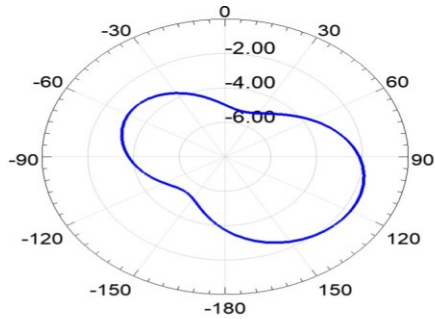


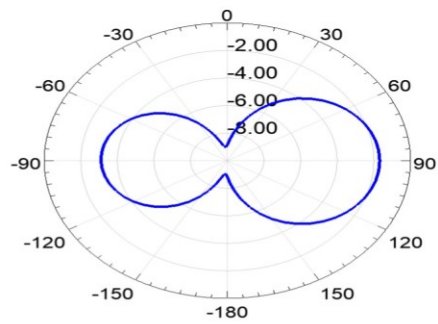
Fig. 4.45. The simulated Efficiency results (in linear scale) of the proposed reconfigurable antenna.

The 2D radiation patterns of the three configurations are shown in Fig. 4.46. The 2D patterns for Slot 1 configuration are shown in Fig. 4.46((a) and (b)). The 2D patterns for Monopole configuration are shown in Fig. 4.46((c) and (d)). The 2D patterns for Slot 2 configuration are shown in Fig. 4.46((e) and (f)). The first pattern of each configuration shows the xy-plane pattern, while the second one is showing the pattern in the elevation plane at which the maximum peak gain is achieved. It can be seen from Fig. 4.46((a) and (b)) that the patterns of Slot 1 configuration is omnidirectional pattern along the xy-plane since it follows the patterns of a magnetic dipole, and the HPBW is  $110^\circ$  in the elevation plane. However, it can be seen from Fig. 4.46(a) that the pattern is directed more to  $\phi = 120^\circ$  because of the ground plane behind Slot 1. On the other hand, it can be seen from Fig. 4.46((e) and (f)) that the patterns of Slot 2 configuration is omnidirectional pattern along the xy-plane since it follows the patterns of a magnetic dipole, and the HPBW is  $120^\circ$  in the elevation plane. However, it can be seen from Fig. 4.46(e) that the pattern is directed more to  $\phi = -70^\circ$  because of the ground plane behind Slot 2. It can be seen from Fig. 4.46((c) and (d)) that the patterns of the Monopole configuration is omnidirectional pattern along the elevation plane  $\phi = 120^\circ$  since it is the pattern of an electrical monopole, and the HPBW is  $80^\circ$  in the azimuthal plane. The ECC between the three patterns of this antenna at 0.87 GHz were found using the radiated electric fields, and they are shown in Table 4.11 where it can be seen that the obtained correlation coefficients between the simulated patterns were below 0.5. Hence, the patterns are uncorrelated. This low ECC between the patterns is achieved because of different polarizations between the patterns and different directions of radiated power as were stated in the previous paragraph.

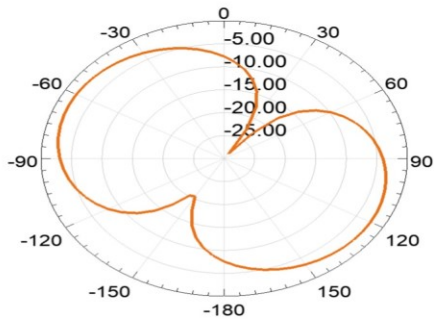




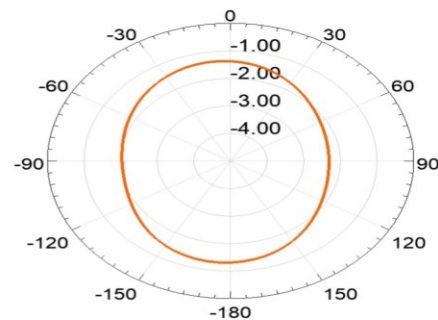
(a) xy plane, Slot 1 Configuration.



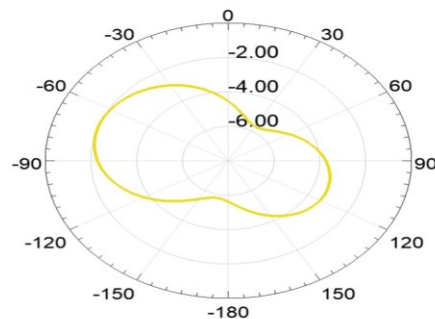
(b)  $\phi=120$  degrees plane, Slot 1 Configuration.



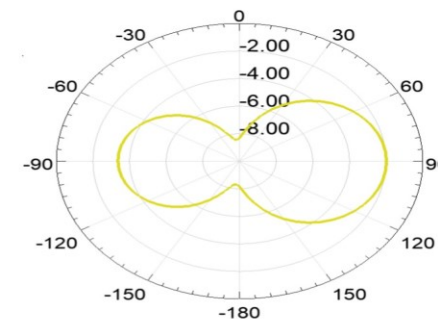
(c) xy plane, Monopole Configuration.



(d)  $\phi=120$  degrees plane, Monopole Configuration.



(e) xy plane, Slot 2 Configuration.



(f)  $\phi=290$  degrees plane, Monopole Configuration.

Fig. 4.46. The simulated 2D-patterns (in dB) of the proposed reconfigurable antenna for three configurations.

Scales are different to show details.

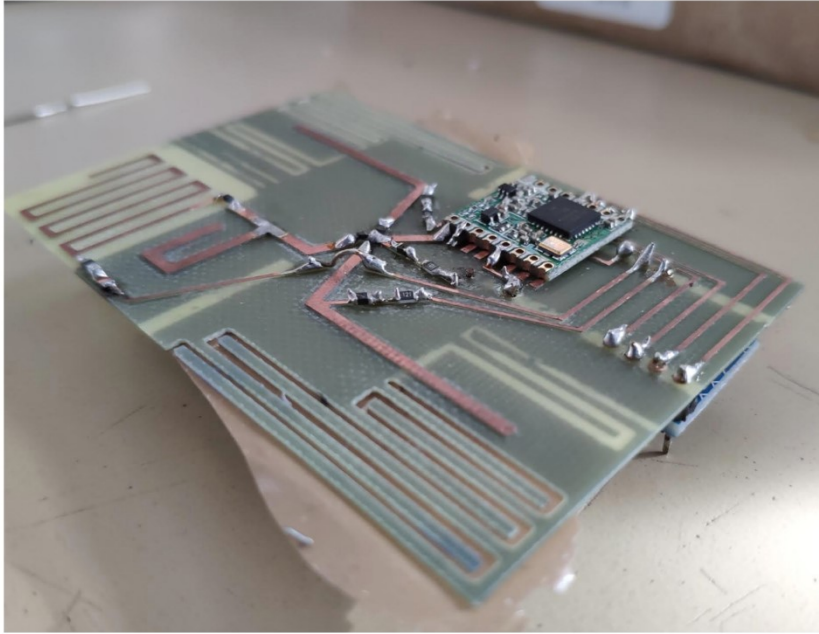
Table 4.11. Correlation coefficients between the patterns of the antenna at 870 MHz

Configuration	Slot 1	Monopole	Slot 2
Slot 1	1	0.2713	0.0367
Monopole	0.2713	1	0.45
Slot 2	0.0367	0.45	1

### 4.3.3 Experimental Results

The antenna was fabricated at Université Côte d'Azur in France, and the fabricated antenna is shown in Fig. 4.47(a). It can be seen from Fig. 4.47(a) that RF transceiver providing an RF signal at 865 MHz was added to the top face of the antenna. An Arduino was added to the bottom face of the antenna in order to control the different antenna modes and to trigger ON the RF transceiver. The patterns of the antenna were measured in a Satimo LAB as shown in Fig. 4.47(b). The measured patterns for Slot 1 configuration, slot 2 configuration, and the monopole configuration are shown in Fig. 4.48, Fig. 4.49, and Fig. 4.50, respectively. These measured patterns were measured at 865 MHz. It was found that the measured results agree well with the simulation results. The measured gains for Slot 1 & 2 configurations are around  $-2$  dB, and it is around  $0$  dB for the monopole configuration. It can be seen also from Fig. 4.48, Fig. 4.49 and Fig. 4.50 that the pattern reconfigurability is achieved by switching the pin diodes states. It was observed also from measurement results that two polarizations were achieved by reconfiguring the antenna patterns from slot mode to monopole mode.

Fig. 4.51 shows many important results achieved by this antenna and observed from the measured results. The radiation patterns of the slot mode and the monopole mode when the antenna is inside a plastic casing and on top of an artificial hand mimicking the physical properties of a real hand are shown in Fig. 4.51(a) and Fig. 4.51(b), respectively. It was found that the slot mode lost around  $6$  dB in gain because of hand and plastic casing effects, while the monopole mode lost more than  $10$  dB in gain. Therefore, slot radiating elements are less sensitive to hand and plastic casing effects at IoT bands compared with monopole radiating elements. Fig. 4.51(c) shows the radiation pattern when slot 1 & 2 configurations are activated at the same time. It can be seen from Fig. 4.51 that a pure pattern of a magnetic dipole was achieved since the difference between co-polarization to cross-polarization is more than  $-20$  dB. The gain of this magnetic dipole pattern is around  $-6$  dB, and it can be enhanced much more by enhancing the input impedance matching when the two configurations are operated at the same time.



(a) The fabricated antenna with RF transceiver and Arduino.



(b) The fabricated antenna in the chamber for measurements.

**Fig. 4.47. The fabricated pattern reconfigurable IoT antenna.**

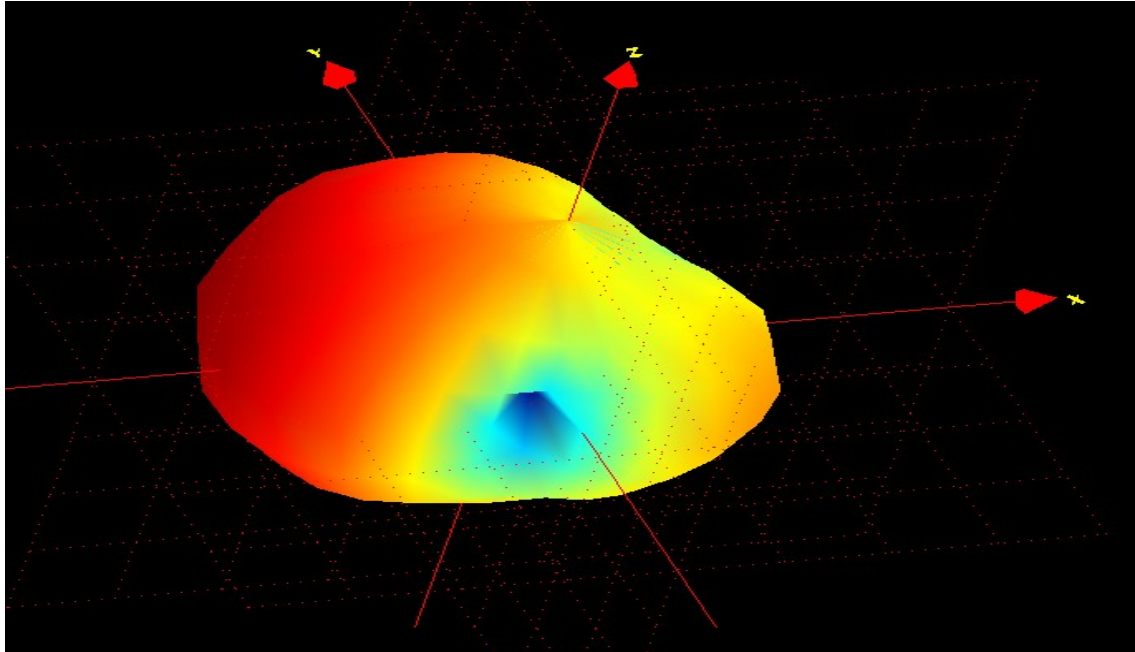


**Fig. 4.48. Radiation pattern of Slot 1 Configuration.**

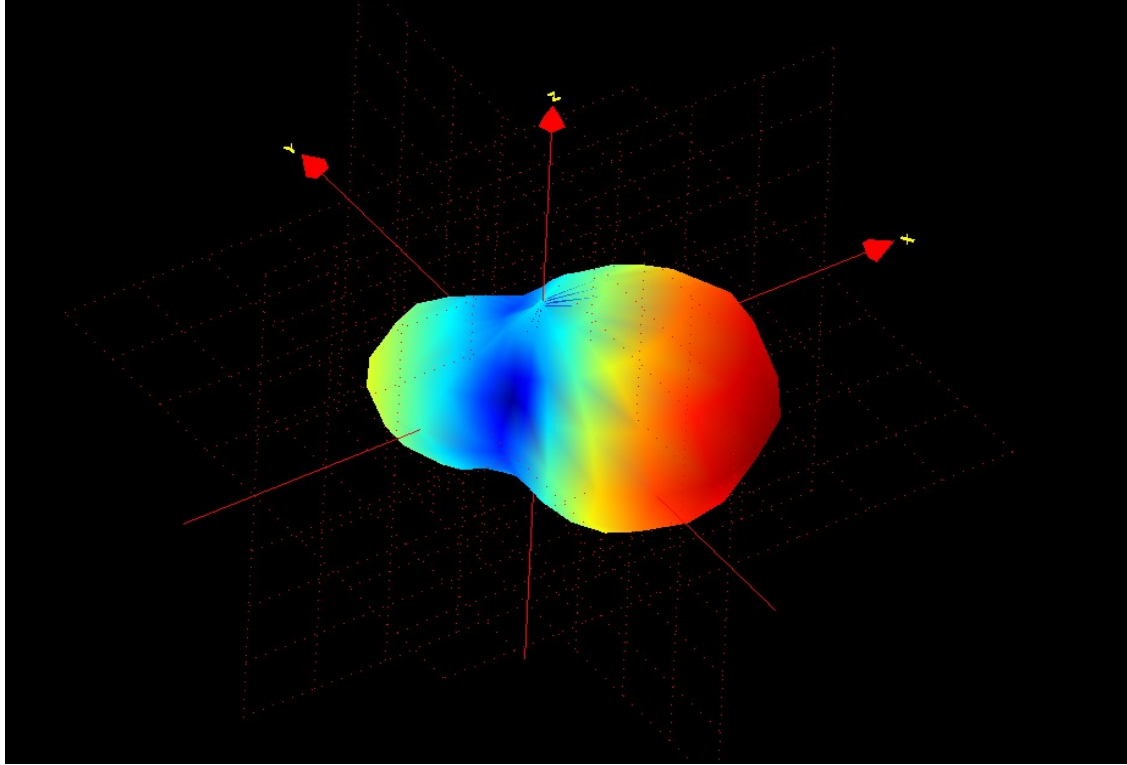


**Fig. 4.49. Radiation pattern of Slot 2 Configuration.**

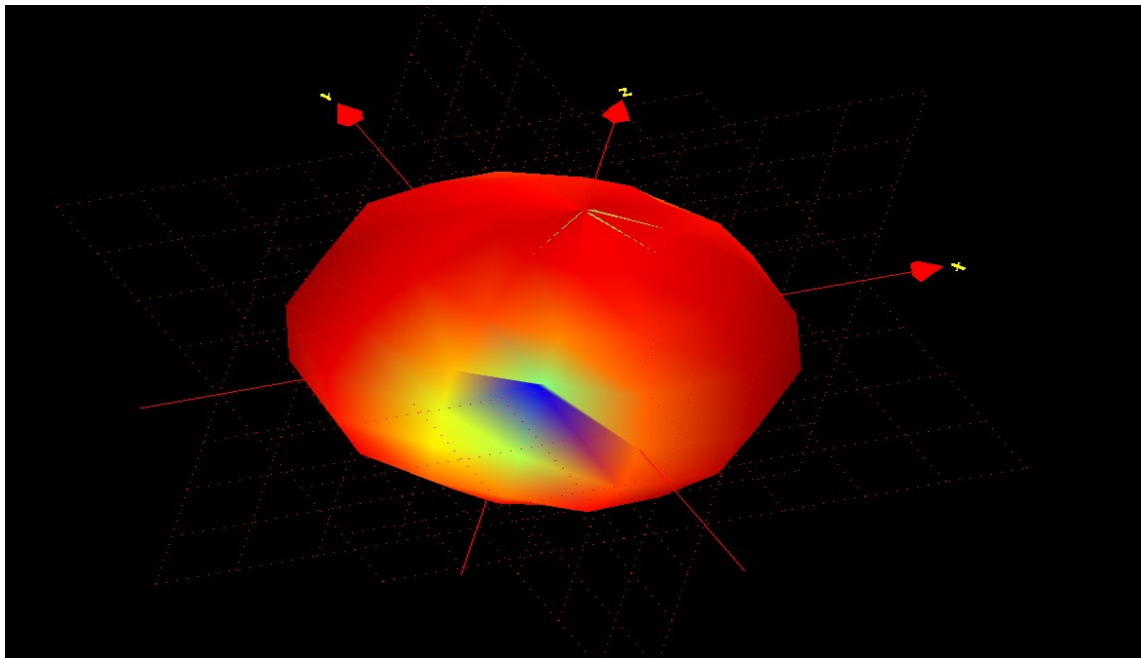
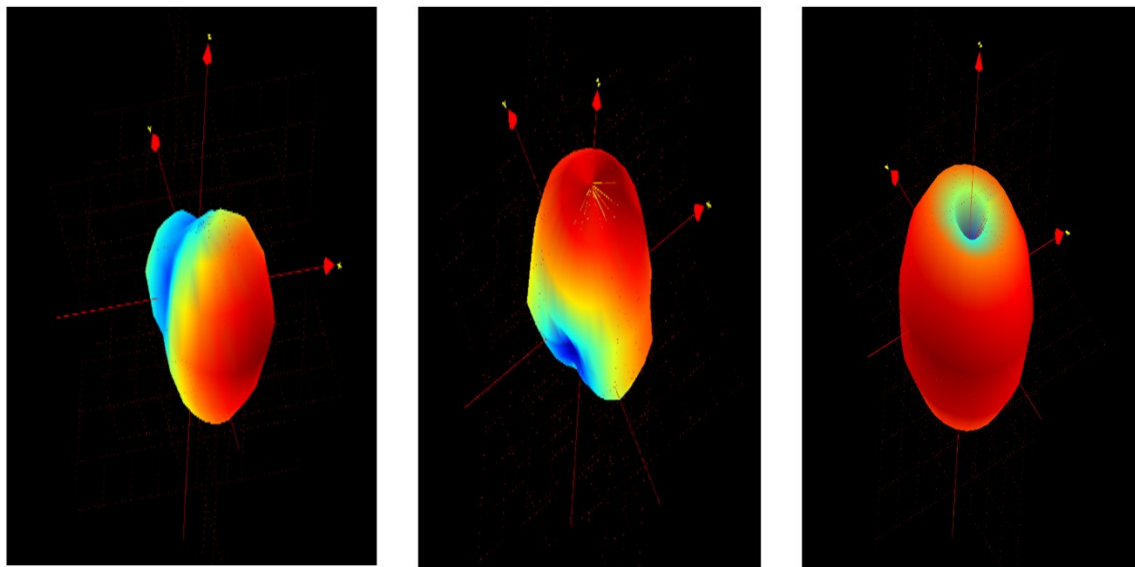


**Fig. 4.50. Radiation pattern of Monopole Configuration.**



(a) Pattern of Slot configuration with hand and plastic casing effects.

(b) Pattern of Monopole configuration with hand and plastic casing effects.

(c) Pattern when both Slot 1 & 2 configurations are switched ON.

**Fig. 4.51. Radiation patterns of the antenna for different important cases.**

#### 4.3.4 Summary of the IoT antenna

A new compact and low-profile pattern reconfigurable antenna for IoT applications was proposed and presented. The antenna size is like the size of a credit card. The antenna includes two meandered slots and one meandered monopole. Three pattern configurations are achieved from this antenna with ECC well below 0.5 and electrically controlled. The antenna resonates at 868 MHz with an overlapped bandwidth of 10 MHz which is enough for IoT applications. The peak gains are above  $-2$  dB, and radiation efficiencies are above 30% for all pattern configurations. It was found that measured results are in good agreement with simulated results. It was concluded also that the slot radiating elements are less sensitive to hand and plastic casing effects at IoT bands compared with monopole radiating elements.

## **4.4 A New Pattern Reconfigurable Slot Antenna for 5G Technology**

A new pattern reconfigurable slot-based antenna is proposed in this section such that it can be extended to a massive MIMO system with pattern reconfigurability capabilities. This work contributes to 5G technology which will open the doors for huge data rates to be transferred from a point to another, and it will allow the huge number of devices and mobile phones to be connected to the network.

### **4.4.1 Design Geometry**

- **Design Procedure**

In the beginning, a reflector was used such that the radiated patterns from the slot becomes directional, since this antenna is designed to make it possible to be used for a massive MIMO where it is required to produce directional patterns. The reflector was positioned below the slot antenna by quarter of a wavelength. Then, a simple U-slot antenna was etched on the ground plane and fed by a 50 ohms transmission line on top of the U-slot around one of its ends. The length of the slot was optimized such that it has a good resonance at 3.6 GHz. After that, the second slot was added to the antenna with a 90 degrees change in the slot orientation to have different polarization such that it is possible to obtain different patterns with low ECC. The two slots provided two different patterns at 3.6 GHz with low ECC between them. Hence, the third slot was added with a 90 degrees change in orientation. Three patterns were achieved at 3.6 GHz with low ECC between them. Finally, the fourth slot was added with 90 degrees change in orientation. The results were four different directional patterns directed to different directions and with low ECC between them as will be shown in the coming sections. The resulted antenna is the one shown in Fig. 4.52. The antenna with the reflector is shown in Fig. 4.53.

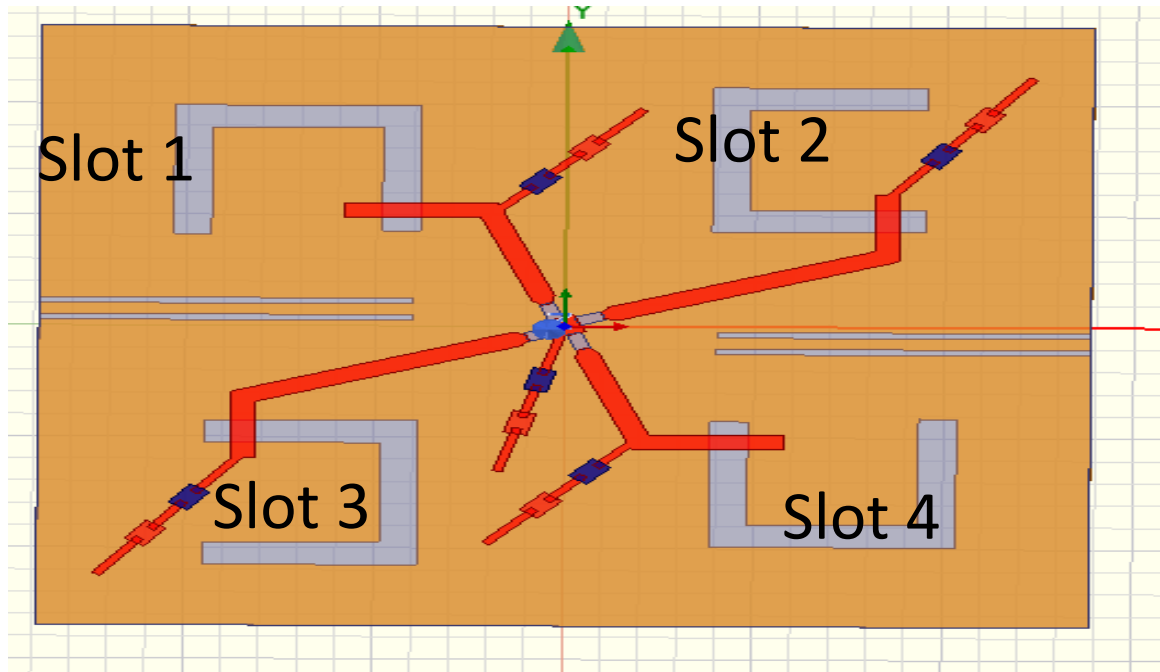


Fig. 4.52. The resulted pattern reconfigurable antenna with the four U-slots.

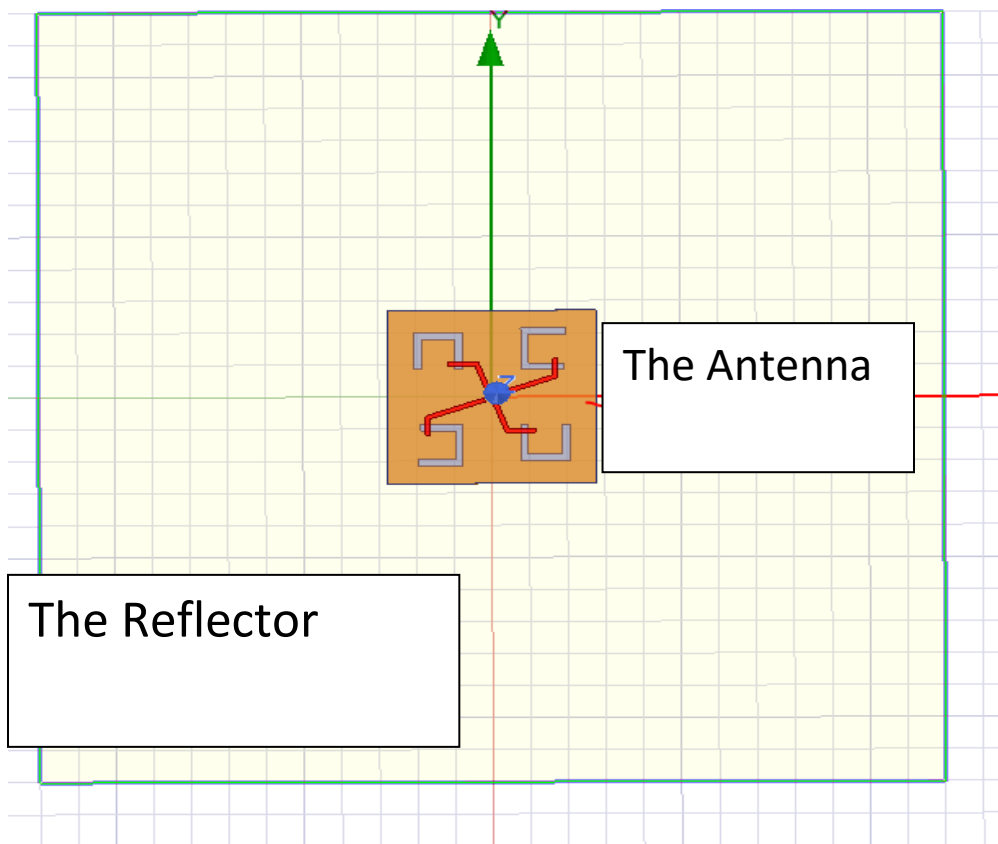


Fig. 4.53. The proposed antenna with the reflector behind it.

After that, four pin diodes were added to the antenna to be able to reconfigure the feeding network as shown in Fig. 4.54. After that, it was found that there are coupling currents between the different four configurations. Hence, four slits with a width of 0.5 mm were etched in the ground plane as shown in Fig. 4.54 in order to reduce the coupling currents between the different configurations. After that, biasing circuits were added to the antenna as shown in Fig. 4.55.

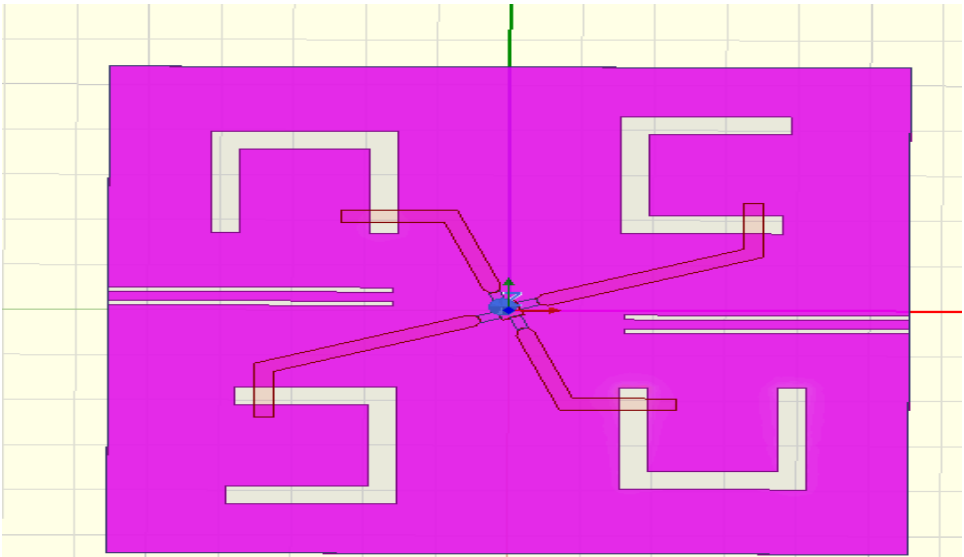


Fig. 4.54. The resulted antenna with four pin diodes and four slits to reduce coupling currents.

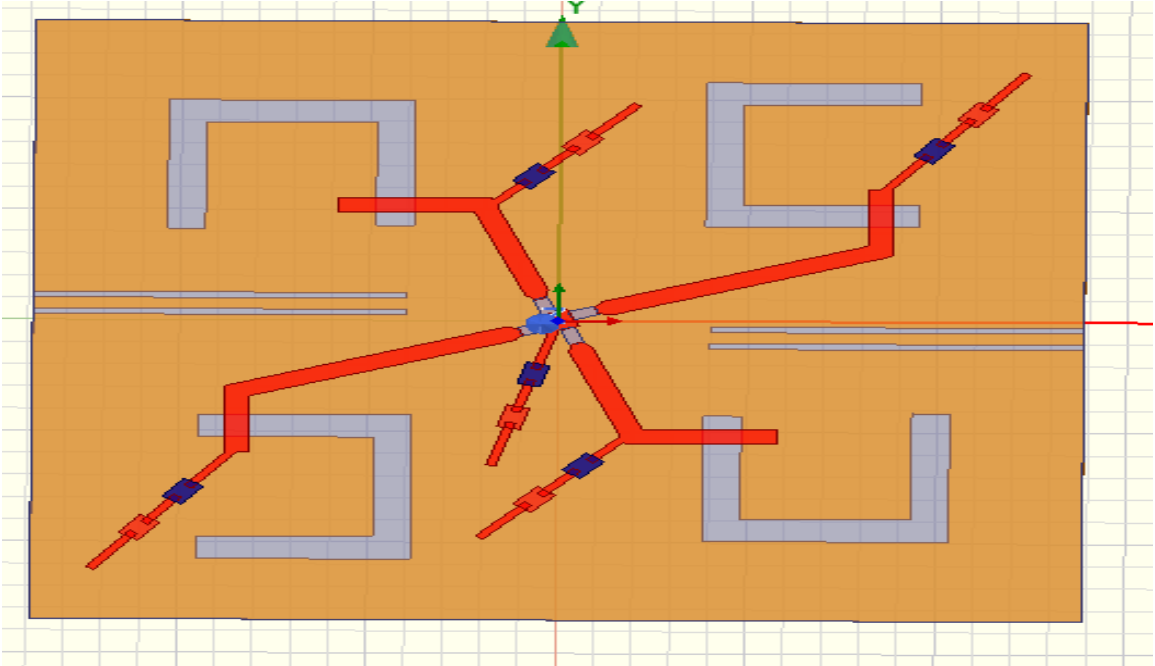


Fig. 4.55. The proposed pattern reconfigurable U-slot antenna with the biasing circuits.



- **Design Description**

The antenna is built on an FR-4 substrate with a dielectric constant of 4.4, a loss tangent of 0.02 and a thickness of 0.72 mm. A reflector was positioned behind the antenna in order to make the radiated patterns directional. One coaxial cable is used where the reflector will be considered as the ground plane for the antenna, and the active conductor will be connected to the center pad of the antenna on the top face of the FR-4 substrate. The top face of the FR-4 substrate includes the 50 ohms transmission lines, the biasing circuits and the 4 pin diodes. The diodes are used to switch between the different pattern configurations of the antenna. The bottom face of the antenna includes four U-slots optimize to resonate at 3.6 GHz. The size of the reflector is  $240 \times 240 \text{ mm}^2$ , while the size of the antenna element is  $54 \times 55 \text{ mm}^2$ . The height between the reflector and the FR-4 substrate is 21 mm. It can be seen that the lengths of the transmission lines to slots are not the same along the x- or the y- directions. Hence, the slots are fed with different phases.

- **Reconfiguration Mechanism**

When Slot 1 is activated; Diode 1 is ON, the first pattern is achieved. When Slot 2 is activated; Diode 2 is ON, the second pattern is achieved. When Slot 3 is activated; Diode 3 is ON, the third pattern is achieved. When Slot 4 is activated; Diode 4 is ON, the fourth pattern is achieved. These four different patterns are directional. It can be seen also that four more patterns can be achieved by beamforming along the x-axis or along the y-axis. It can be seen from Fig. 4.55 that slot 1 and slot 2 are two slots along the x-axis; they form a linear array along the x-axis with different phases fed between them since the lengths of the two transmission lines to the two slots are different. The fifth pattern is achieved from this first x-axis array. The second x-axis array is formed by Slot 3 and slot 4, hence sixth pattern will be attained from this second x-axis array. There are also two y-axis arrays which will provide two more patterns. Therefore, this antenna has 8 different patterns at 3.6 GHz. Therefore, 8 directional pattern configurations are achieved electrically from this antenna.

#### **4.4.2 Simulation Results**

This antenna was simulated on HFSS. The simulated  $S_{11}$ , peak gains and efficiency results of the antenna when one slot is activated; one diode is ON, are shown in Fig. 4.56, Fig. 4.57 and Fig. 4.58, respectively. It can be seen from Fig. 4.56 that the overlapped – 10 dB bandwidth is from 3.58 GHz to 3.68 GHz which is around 100 MHz. The minimum achieved peak gains for the first four pattern configurations (when one diode is ON) is 6.8 dB at 3.6 GHz as shown in Fig.

4.57. The minimum radiation efficiency among the first four pattern configurations (when one diode is ON) is 53% as shown in Fig. 4.58.

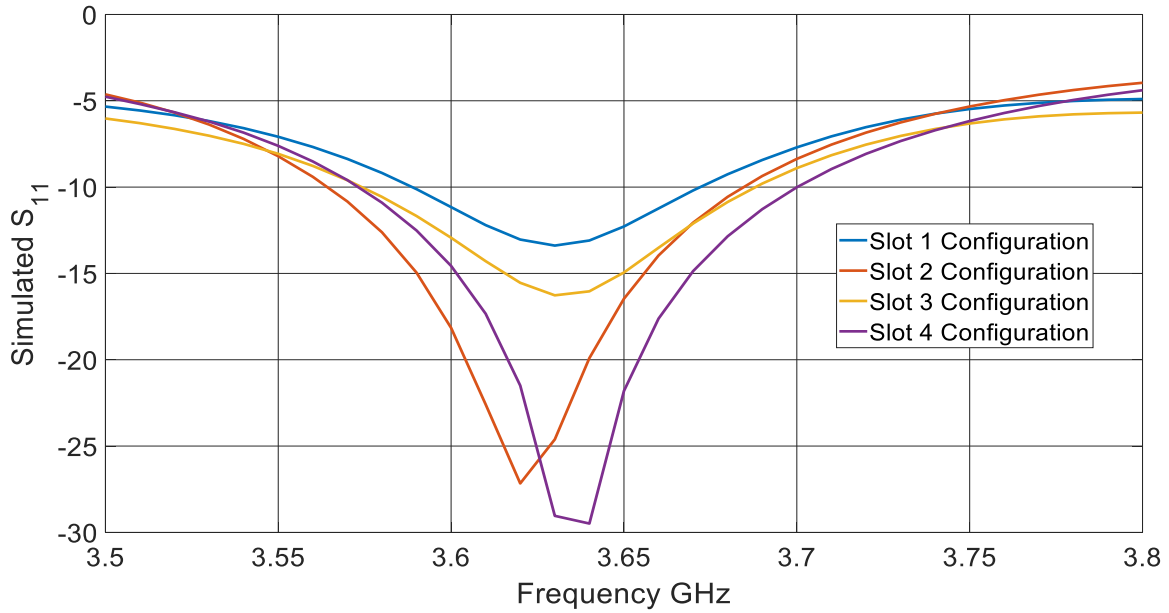


Fig. 4.56. The simulated  $S_{11}$  results of the antenna when one slot is activated.

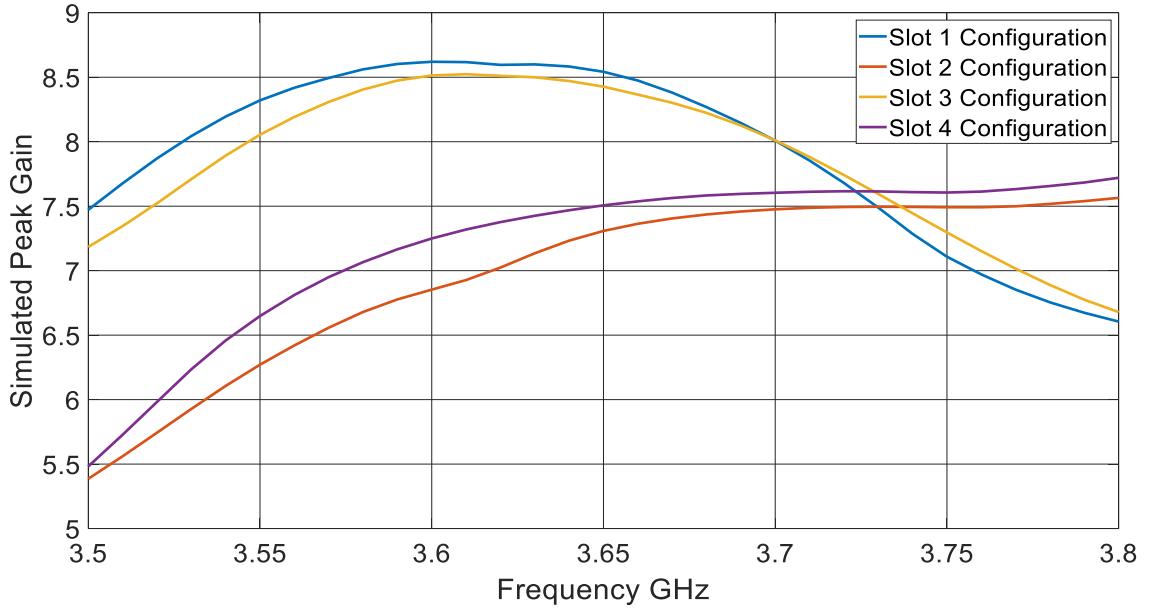


Fig. 4.57. The simulated Peak Gains of the antenna when one slot is activated.

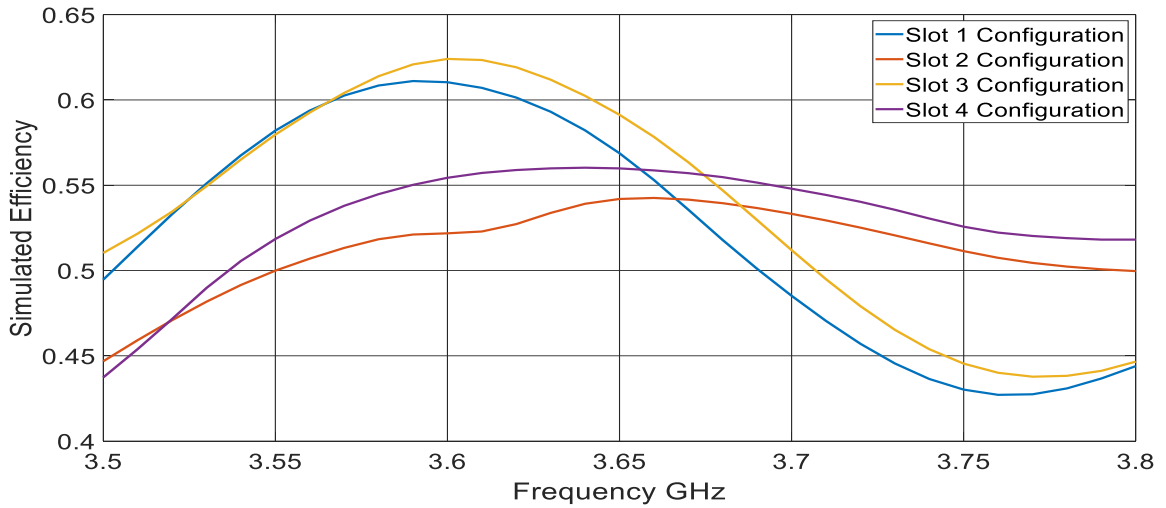


Fig. 4.58. The simulated radiation efficiency of the antenna when one slot is activated.

The radiation patterns of the four configurations of the antenna when one slot is activated are shown in Fig. 4.59. It can be seen from Fig. 4.59 that four different patterns were achieved when one slot is activated. It can be seen the patterns go to bottom direction, left direction, up direction, and right direction for slot 1 configuration, slot 2 configuration, slot 3 configuration, and slot 4 configuration, respectively.

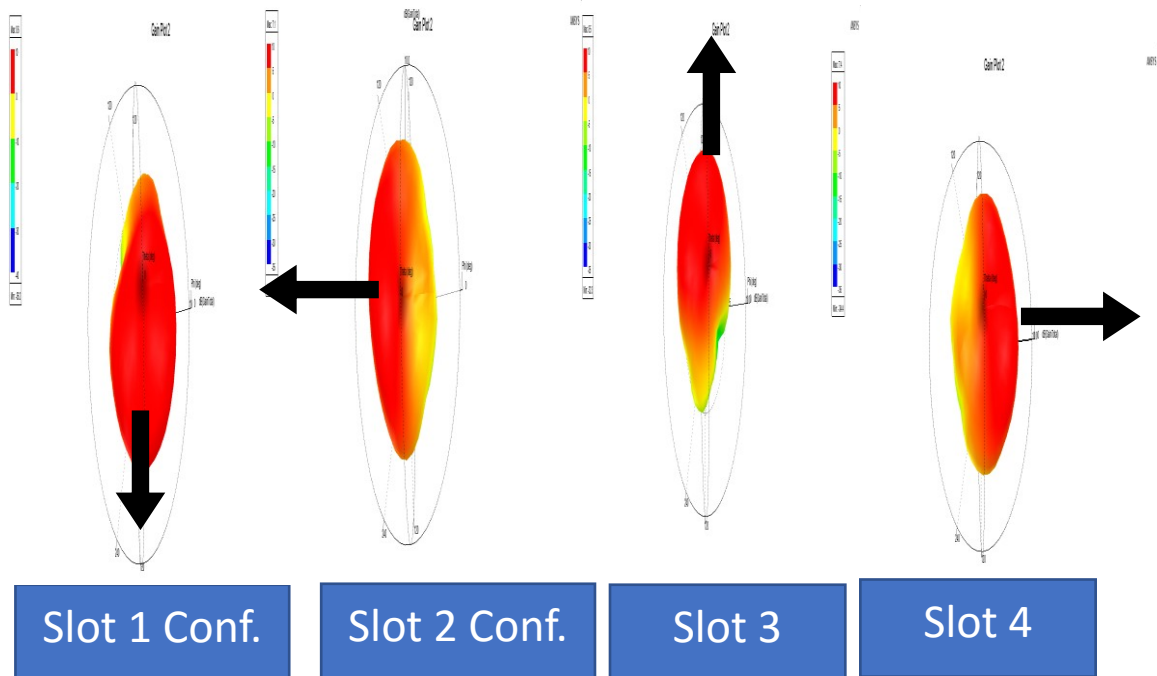


Fig. 4.59. The radiation patterns of the antenna when one slot is activated.

The simulated  $S_{11}$ , the peak gains and the efficiencies of the antenna when two slots are activated are shown in Fig. 4.60, Fig. 4.61, and Fig. 4.62, respectively. It can be seen from Fig. 4.60 that the four 2-slot pattern configurations resonate around 3.6 GHz. The minimum achieved peak gain among the four 2-slot pattern configurations is 6.6 dB at 3.6 GHz as shown in Fig. 4.61. The minimum achieved radiation efficiency among the four 2-slot configurations is 60% at 3.6 GHz as shown in Fig. 4.62.

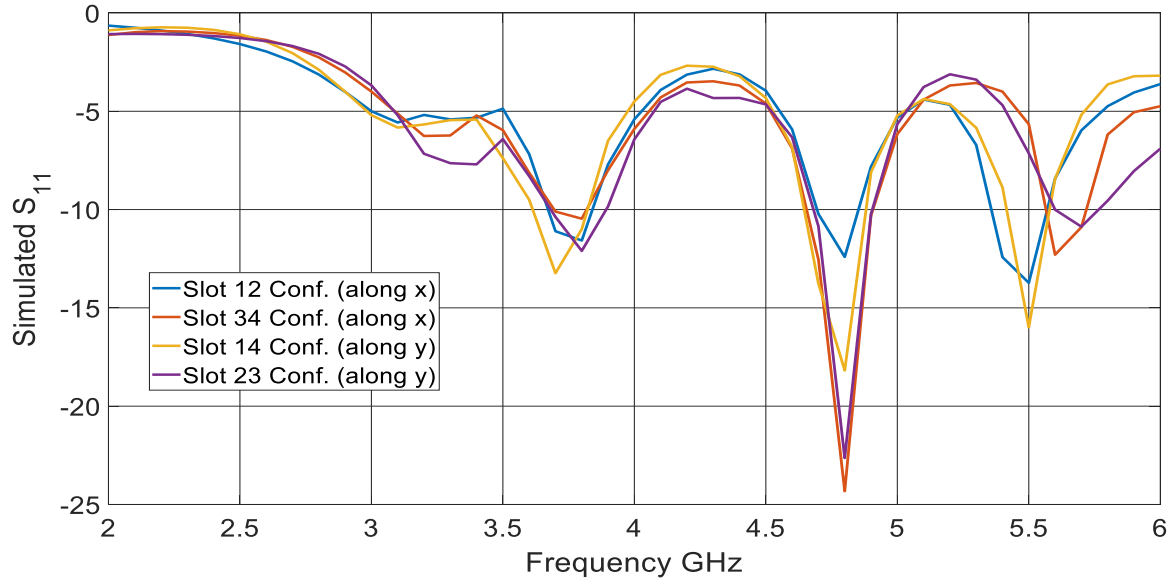


Fig. 4.60. The simulated  $S_{11}$  when two slots are activated.

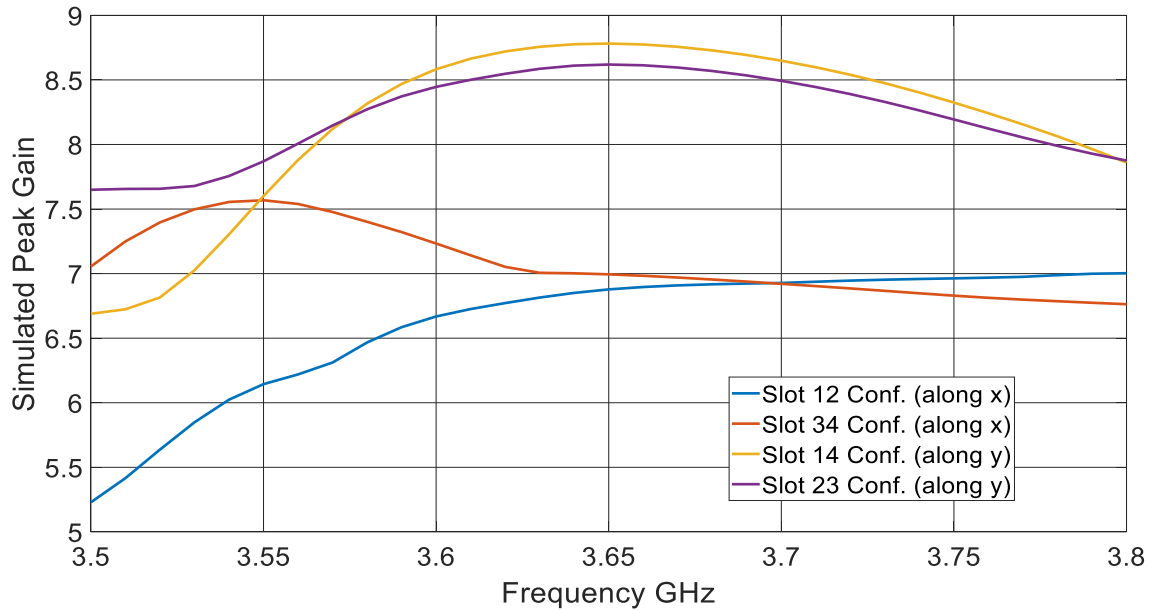
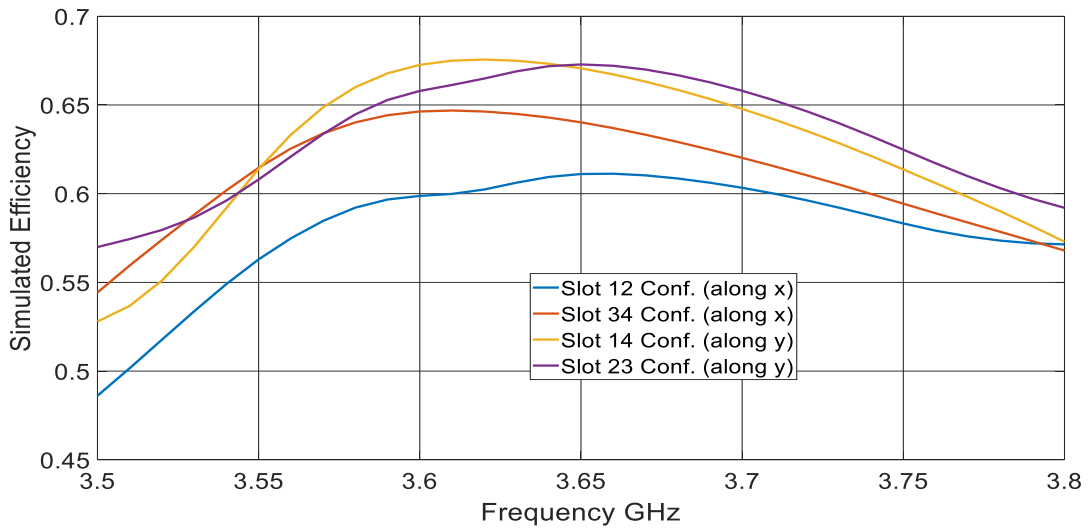
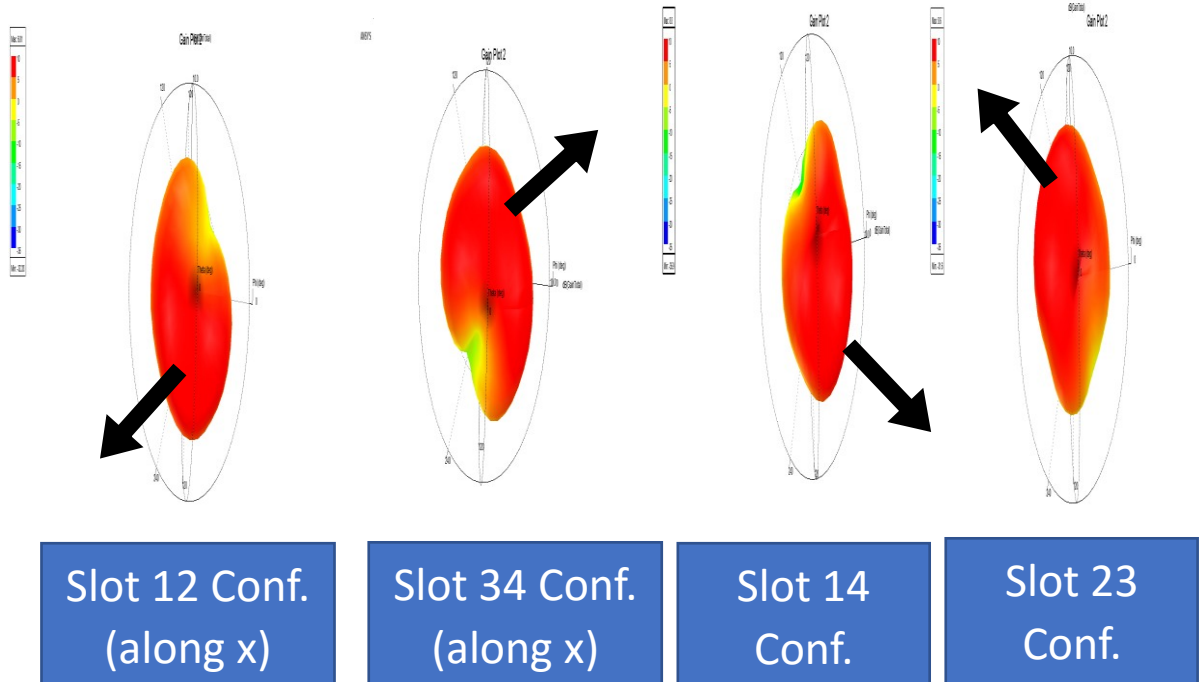


Fig. 4.61. The simulated Peak Gains when two slots are activated.



**Fig. 4.62.** The simulated radiation efficiencies when two slots are activated.

The patterns of the 2-slot configurations are shown in Fig. 4.63 where it can be seen that the patterns are directed to left-bottom direction, right-up direction, right-bottom direction and left-up direction for slot 12 configuration, slot 34 configuration, slot 14 configuration, and slot 23 configuration, respectively.



**Fig. 4.63.** The radiation patterns of the antenna when 2 slots are activated.

The maximum ECC between the 8 patterns of the antenna in the band from 3.5 GHz to 3.8 GHz are shown in table 4.12. It can be seen from table 4.11 that most of the ECC between the patterns are below 0.5.

**Table 4.12. The maximum ECC between the 8 patterns of the antenna in the band from 3.5 GHz to 3.8 GHz.**

Conf.	Slot 1	Slot 2	Slot 3	Slot 4	Slot 1&2	Slot 3&4	Slot 1&4	Slot 2&3
Slot 1	1	0.0335	0.0766	0.1831	0.45	0.1815	0.6781	0.0214
Slot 2	0.0335	1	0.1372	0.0189	0.7249	0.0813	0.0236	0.7973
Slot 3	0.0766	0.1372	1	0.0211	0.0218	0.4026	0.0513	0.5633
Slot 4	0.1831	0.0189	0.0211	1	0.0914	0.7081	0.7171	0.0323
Slot 1&2	0.45	0.7249	0.0218	0.0914	1	0.0915	0.3439	0.4965
Slot 3&4	0.1815	0.0813	0.4026	0.7081	0.0915	1	0.387	0.2911
Slot 1&4	0.6781	0.0236	0.0513	0.7171	0.3439	0.387	1	0.0132
Slot 2&3	0.0214	0.7973	0.5633	0.0323	0.4965	0.2911	0.0132	1

### 4.4.3 Table of Comparison and Discussions

Table 4.13 shows a comparison between the proposed slot-based pattern reconfigurable antenna and other slot-based pattern reconfigurable antennas in the literature. It can be seen from table 4.13 that the proposed antenna has a competing size, a good bandwidth, and a competing number of different pattern configurations. The proposed antenna shows that it provided best radiation gain among the other antennas in the literature. In addition, the patterns of the proposed antenna is directional.

**Table 4.13. A comparison table between the third slot-based pattern reconfigurable antenna and other slot-based pattern reconfigurable antennas in literature**

Ref.	Resonant frequency (GHz)	Dielectric constant ( $\tan \delta$ )	Height (mm)	Antenna size	Min. Gain (dB)	BW (MHz)	# pattern modes	Frequency - reconfigurability
<b>This work</b>	<b>3.6</b>	<b>4.4 (0.02)</b>	<b>0.72</b>	<b><math>0.66\lambda_o * 0.66\lambda_o</math></b>	<b>6.5</b>	<b>100</b>	<b>8</b>	<b>NO</b>
[1]	2.02	4.4 (NM)	7	$0.67\lambda_o * 0.67\lambda_o$	2.5	50	2	No
[4]	5.32	2.2 (0.0009)	3.175	$0.89\lambda_o * 0.89\lambda_o$	3	361	3	No
[9]	3	3.55 (NM)	8.5	$0.7\lambda_o * 0.7\lambda_o$	6.1	200	4	No
[39]	2.005	4.3 (0.02)	1.52	$1.17\lambda_o * 1.14\lambda_o$	1.11	52	4	No
[53]	5.2, 5.8, & 6.4	6.15 (0.0025)	0.365	$0.97\lambda_o * 0.97\lambda_o$	-	-	9	Yes
[75]	2.3	4.4 (NM)	0.8	$0.4\lambda_o * 0.4\lambda_o$	0.54	250	2	Yes
[101]	1.79, 1.89 & 2.07	3.54 (0.0018)	46.5	$0.78\lambda_o * 0.95\lambda_o$	3.2	-	9	Yes
[107]	2.45	4.4 (0.02)	0.8	$0.42\lambda_o * 0.42\lambda_o$	1.3	100	10	No
[138]	5	3.48 (0.004)	15	$1.12\lambda_o * 1.12\lambda_o$	6.1	1810	3	No
[139]	2.29, 2.31, 2.33, 2.35 & 2.38	2.33 (NM)	1.575	$0.5\lambda_o * 0.5\lambda_o$	4	-	20	Yes
[140]	6	1.71 (0.02)	1.5	$0.6\lambda_o * 1.2\lambda_o$	6.11	280	3	No
[142]	2	2.65 (NM)	1.5	-	6.4	1740	4	No
[143]	6.5	4.4 (NM)	1	$0.95\lambda_o * 0.87\lambda_o$	-	4000	3	No

#### **4.4.4 Summary of the third slot-based pattern reconfigurable antenna**

A new compact slot-based pattern reconfigurable antenna for 5G technology was proposed and presented. The antenna resonates at 3.6 GHz with 8 different pattern configurations and an overlapped bandwidth of 100 MHz. Four different pattern configurations with ECC well below 0.3 were achieved when one diode is ON. Four different pattern configurations were achieved with low ECC when two slots along x-axis or two slots along y-axis are activated. Among the 8 different radiation patterns, the peak gains are above 6.5 dB and the radiation efficiencies are above 52%. This antenna is a good candidate for mMIMO antennas working at 3.6 GHz. This antenna is the one used as the building element for the pattern mMIMO antenna designed for this thesis and shown in the next section.



## 4.5 A New Pattern Reconfigurable Massive MIMO Antenna for 5G Technology

### 4.5.1 Design Description

The pattern reconfigurable antenna shown in Fig. 4.55 was extended to a 4X4 massive MIMO working at 3.6 GHz since it is required to make it operating for 5G technology. The massive MIMO antenna is shown in Fig. 4.64. This massive MIMO antenna is a pattern reconfigurable massive MIMO because the used single element is a pattern reconfigurable antenna with 8 pattern configurations as it was shown in the previous section. It can be seen from Fig. 4.64 that the massive MIMO antenna includes 16 pattern reconfigurable antennas. The reflector is the ground plane in order to enhance the peak gain of the antenna and the peak gain of the massive MIMO antenna. The size of the massive MIMO is  $240 \times 240 \times 21.02 \text{ mm}^3$ . In the beginning, a 2X1 MIMO was built and it was working as expected. Then, it was extended to 2X2 massive MIMO, the simulated  $S_{11}$ ,  $S_{12}$ , peak gains, efficiencies and simulated radiation patterns show that the antenna is working as expected and reasonable as per the theoretical equations of beamforming. After that, the mMIMO antenna was extended to 3X3 massive MIMO, and the simulated results were also reasonable. Finally, the antenna was extended to a 4 X 4 massive MIMO antenna and with good simulated results as will be shown in the next subsections. The phase progresses in x-direction and in y-direction need to be changed in order to steer the pattern to different directions. The pattern of the massive MIMO antenna is directional and can be steered to many different directions by reconfiguring the antenna pattern, by changing the phase progress in x- and y- directions, and by changing the amplitudes of currents feeding different antenna elements. When an antenna element is not required to be working, then all of its diodes will be OFF in order to reduce the coupling between the RF ports. It can be seen that there are 16 ports to 16 antenna elements. Each element has 4 diodes, and the total number of diodes will be 64 diodes for this massive MIMO antenna.

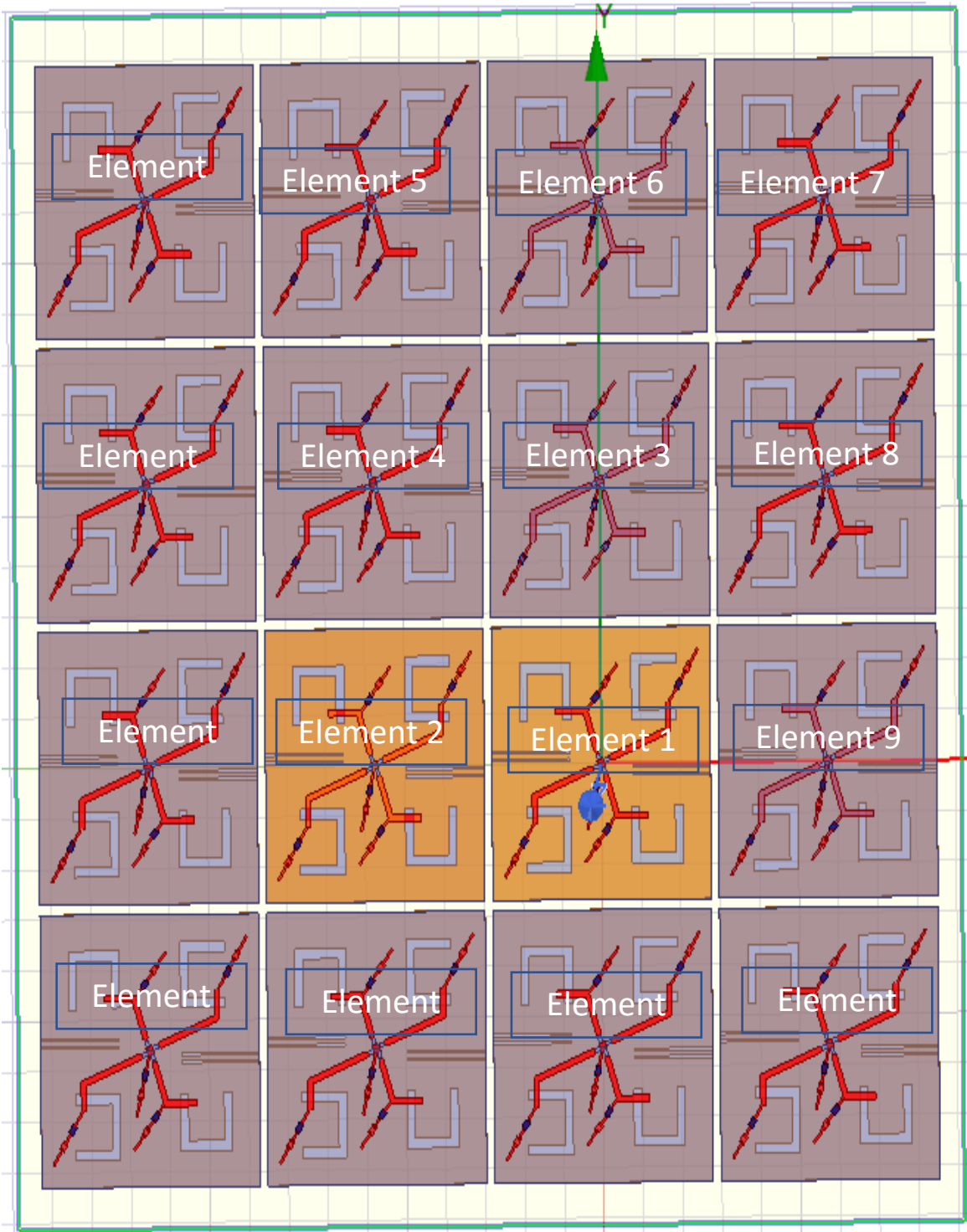


Fig. 4.64. The pattern reconfigurable 4x4 massive MIMO for 5G technology.

## 4.5.2 Simulated Results

- **Elements 3, 6, 7 and 8 are Active (2X2 MIMO) & Slot 3 Configuration is Chosen**

The simulated  $S_{11}$ , and the simulated  $S_{21}$ , when the elements 3, 6, 7 and 8 shown in Fig. 4.64 are activated and slot 3 is activated, are shown in Fig. 4.65 and Fig. 4.66, respectively. It can be seen from Fig. 4.65 that the  $S_{11}$  results of the elements 3, 6, 7 and 8 are well below  $-10$  dB around 3.6 GHz, and this is as expected. On the other hand, it can be seen from Fig. 4.66 that the  $S_{21}$  results between the 16 ports are well below  $-18$  dB which shows a very good isolation between the mMIMO's ports.

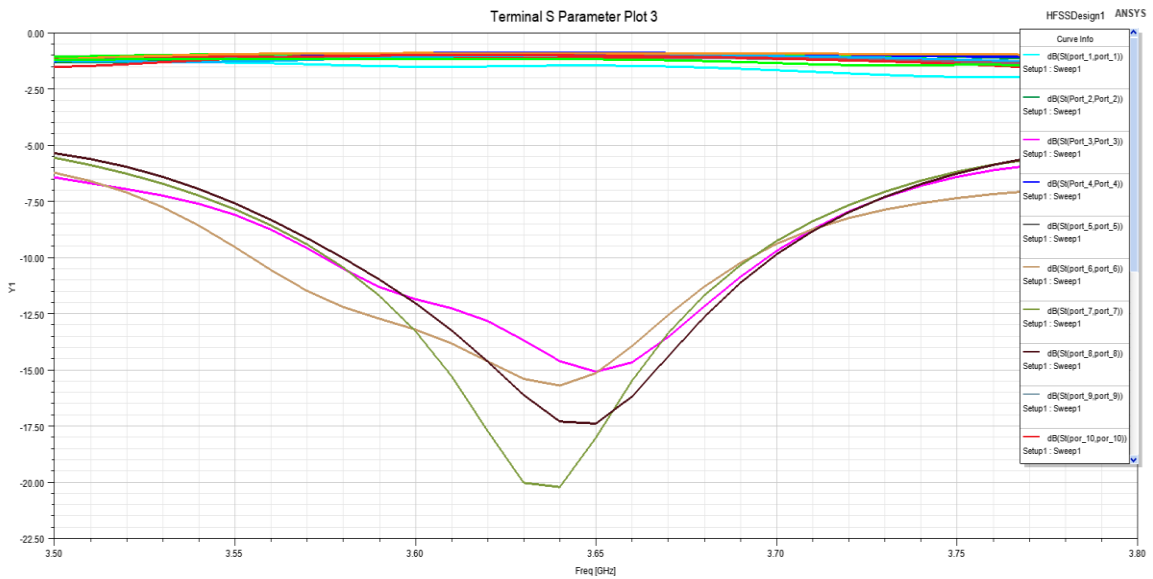


Fig. 4.65. The simulated  $S_{11}$  of the mMIMO when elements 3, 6, 7 and 8 are activated.

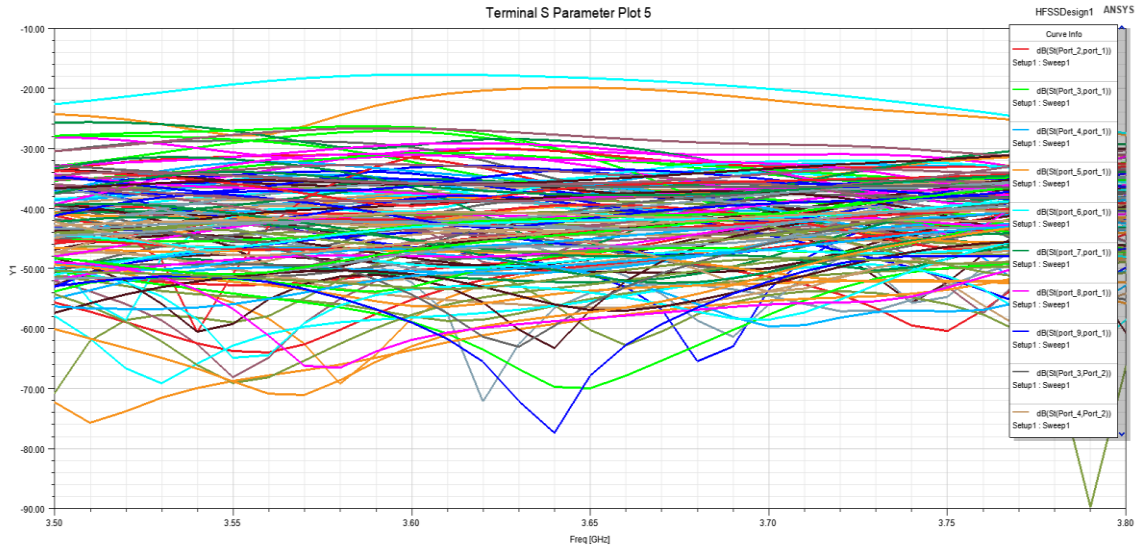


Fig. 4.66. The simulated  $S_{21}$  of the mMIMO when elements 3, 6, 7 and 8 are activated.

The simulated patterns of the mMIMO antenna, when the progressive phase in the x-direction is 0 degrees and in the y-direction is 0 degrees, is shown in Fig. 4.67 where it can be seen that the maximum gain is 10.8 dB at 3.63 GHz.

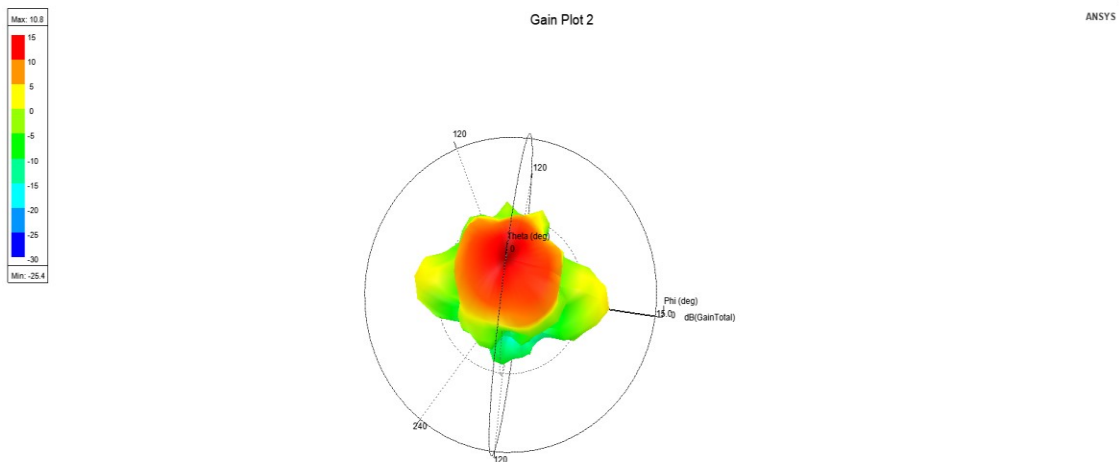
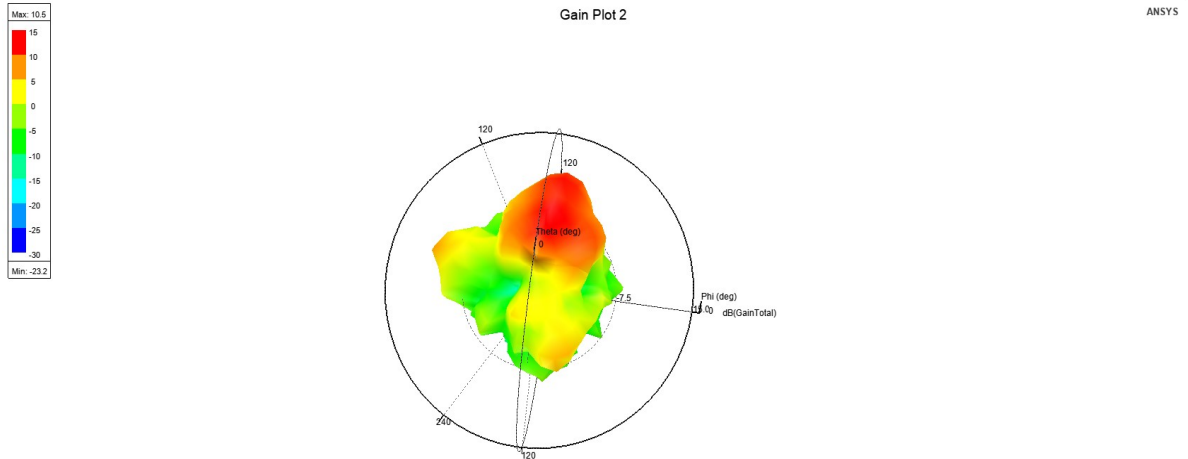


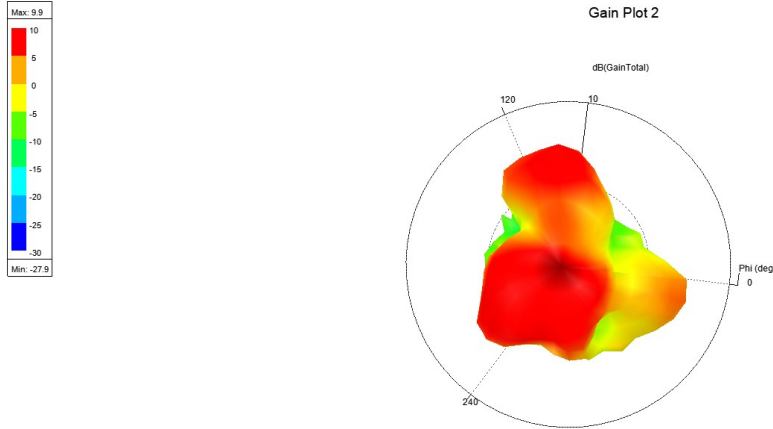
Fig. 4.67. The patterns at 3.63 GHz when elements 3, 6, 7 and 8 are activated and  $B_x=0$  degrees and  $B_y=0$  degrees.

The simulated patterns of the mMIMO antenna, when the progressive phase in the x-direction is  $-50$  degrees and in the y-direction is  $-100$  degrees, is shown in Fig. 4.68 where it can be seen that the maximum gain is 10.5 dB at 3.63 GHz.



**Fig. 4.68.** The patterns at 3.63 GHz when elements 3, 6, 7 and 8 are activated and  $B_x = -50$  degrees and  $B_y = -100$  degrees.

The simulated patterns of the mMIMO antenna, when the progressive phase in the x-direction is  $+50$  degrees and in the y-direction is  $+100$  degrees, is shown in Fig. 4.69 where it can be seen that the maximum gain is 9.9 dB at 3.63 GHz. It can be seen from Fig. 4.69 that there are large grating lobes, this is expected because slot 3 configuration is activated, and the patterns of this slot will go to up direction, and beamforming is taking place to the bottom side of the mMIMO antenna. Therefore, this mMIMO antenna with these active elements and with choosing slot 3 configuration to be working, good results will be achieved if beamforming takes place in the up side ( $+y$  direction) of the mMIMO antenna. This is also clear from Fig. 4.68 where it can be seen that there is almost no grating lobe because beamforming is taking place in the  $+y$  direction and slot 3 configuration is operating.



ANSYS

**Fig. 4.69.** The patterns at 3.63 GHz when elements 3, 6, 7 and 8 are activated and  $B_x = +50$  degrees and  $B_y = +100$  degrees.

- **Elements 2, 12, 13 and 14 are Active (2X2 MIMO) & Slot 1 Configuration is Chosen**

The simulated  $S_{11}$ , and the simulated  $S_{21}$ , when the elements 2, 12, 13 and 14 shown in Fig. 4.64 are activated and slot 1 is activated, are shown in Fig. 4.70 and Fig. 4.71, respectively. It can be seen from Fig. 4.70 that the  $S_{11}$  results of the elements 2, 12, 13 and 14 are well below  $-10$  dB around 3.6 GHz, and this is as expected. On the other hand, it can be seen from Fig. 4.71 that the  $S_{21}$  results between the 16 ports are well below  $-18$  dB which shows a very good isolation between the mMIMO's ports.

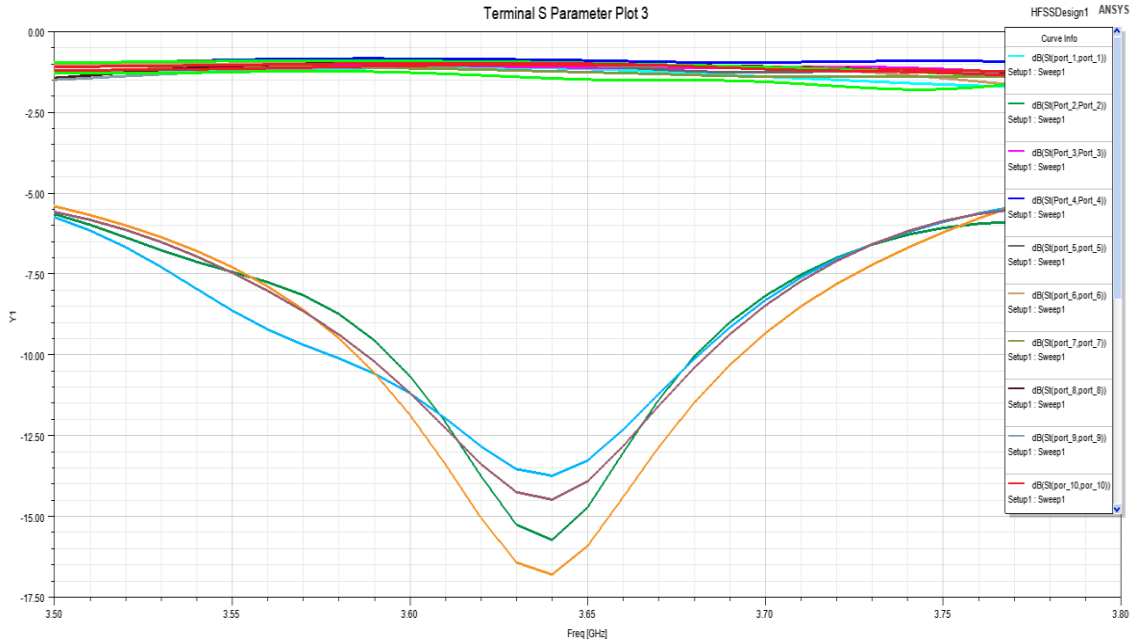


**Fig. 4.70.** The simulated  $S_{11}$  of the mMIMO when elements 2, 12, 13 and 14 are activated.

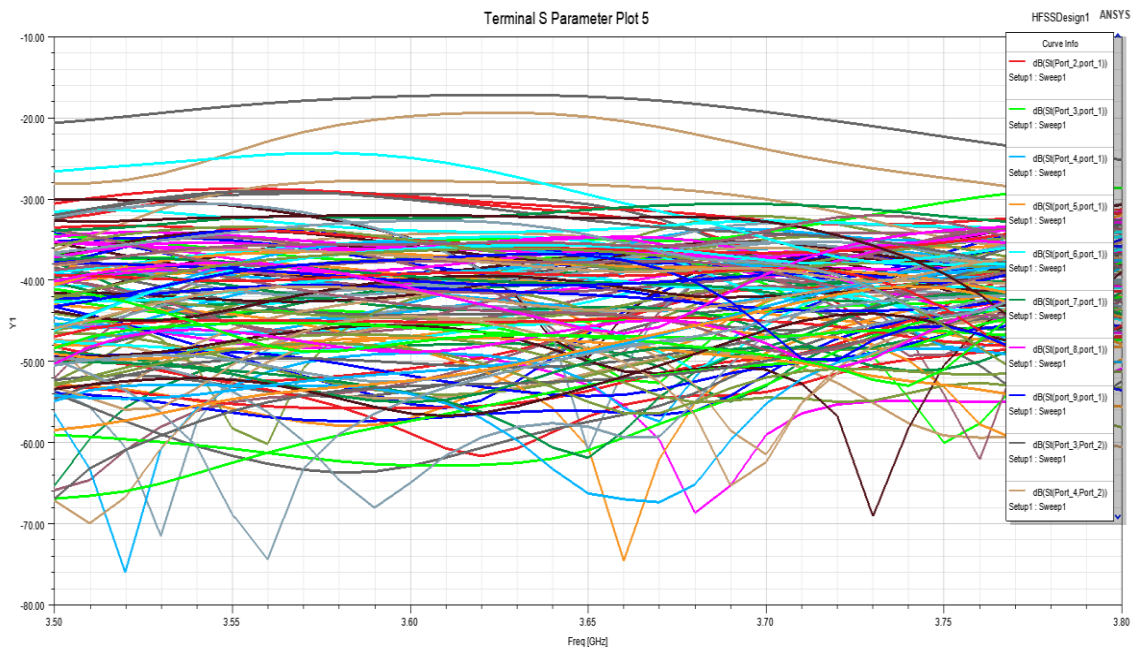
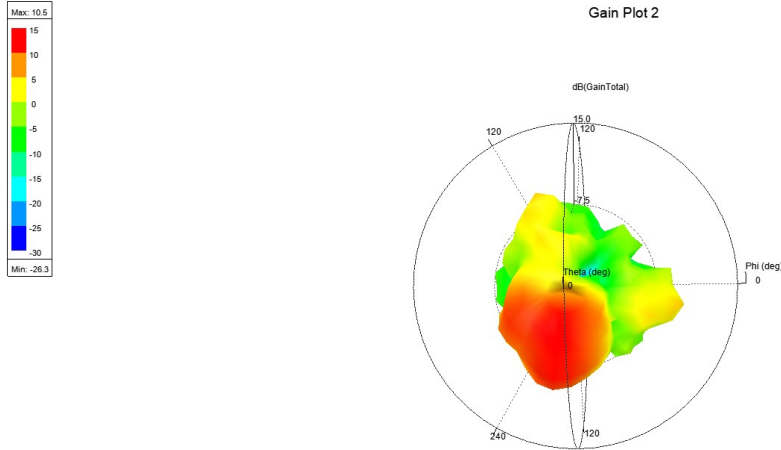


**Fig. 4.71.** The simulated  $S_{21}$  of the mMIMO when elements 2, 12, 13 and 14 are activated.

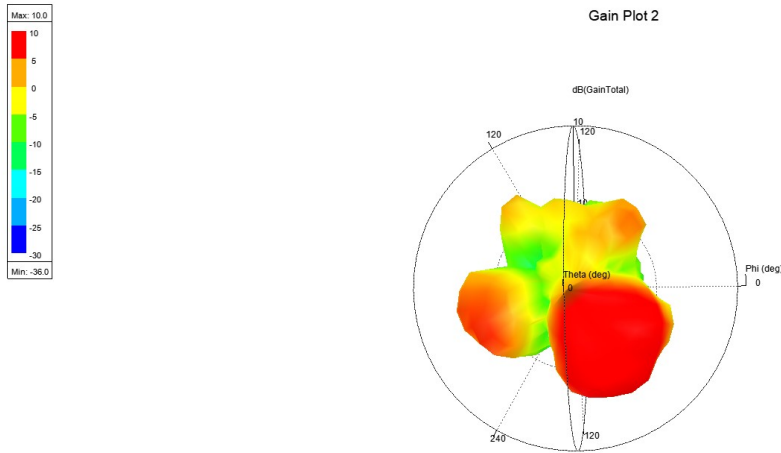
The simulated patterns of the mMIMO, when the progressive phase in the x-direction is + 50 degrees and in the y-direction is + 100 degrees, is shown in Fig. 4.72 where it can be seen that the maximum gain is 10.5 dB at 3.63 GHz.



ANSYS

**Fig. 4.72.** The patterns at 3.63 GHz when elements 2, 12, 13 and 14 are activated and  $B_x = + 50$  degrees and  $B_y = + 100$  degrees.

The simulated patterns of the mMIMO, when the progressive phase in the x-direction is  $- 250$  degrees and in the y-direction is  $+ 100$  degrees, is shown in Fig. 4.73 where it can be seen that the maximum gain is 10.5 dB at 3.63 GHz. The progressive phase in x-direction is large because there are two elements in the x-direction and it is required to steer the beam to a new direction other than the one shown in Fig. 4.72.



ANSYS

**Fig. 4.73.** The patterns at 3.63 GHz when elements 2, 12, 13 and 14 are activated and  $B_x = - 250$  degrees and  $B_y = + 100$  degrees.



- **Elements 1, 2, 3, 4, 5, 6, 14, 15 and 16 are Active (3X3 MIMO) & Slot 2 Configuration is Chosen**

The patterns in this case will be more directive. The simulated  $S_{11}$ , and the simulated  $S_{21}$ , when the elements 1, 2, 3, 4, 5, 6, 14, 15 and 16 shown in Fig. 4.64 are activated and slot 2 is activated, are shown in Fig. 4.74 and Fig. 4.75, respectively. It can be seen from Fig. 4.74 that the  $S_{11}$  results of the elements 1, 2, 3, 4, 5, 6, 14, 15 and 16 are well below  $-10$  dB around 3.6 GHz, and this is as expected. On the other hand, it can be seen from Fig. 4.75 that the  $S_{21}$  results between the 16 ports are well below  $-15.5$  dB which shows a good isolation between the mMIMO's ports.

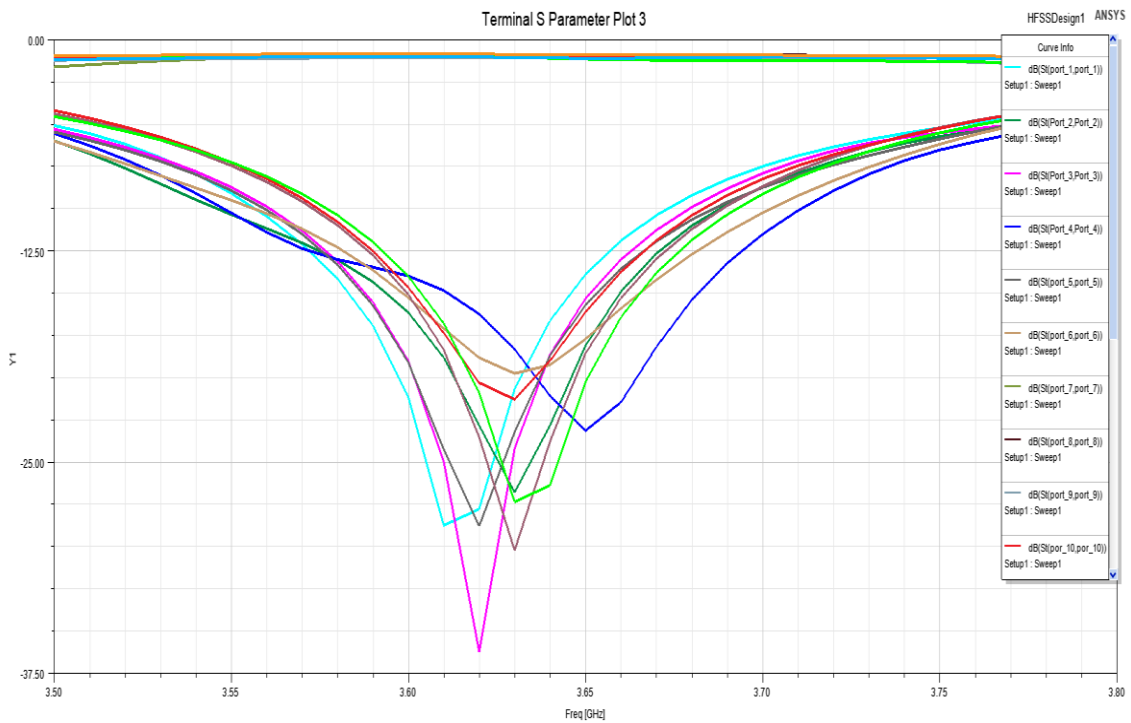


**Fig. 4.74.** The simulated  $S_{11}$  of the mMIMO when elements 1, 2, 3, 4, 5, 6, 14, 15 and 16 are activated.

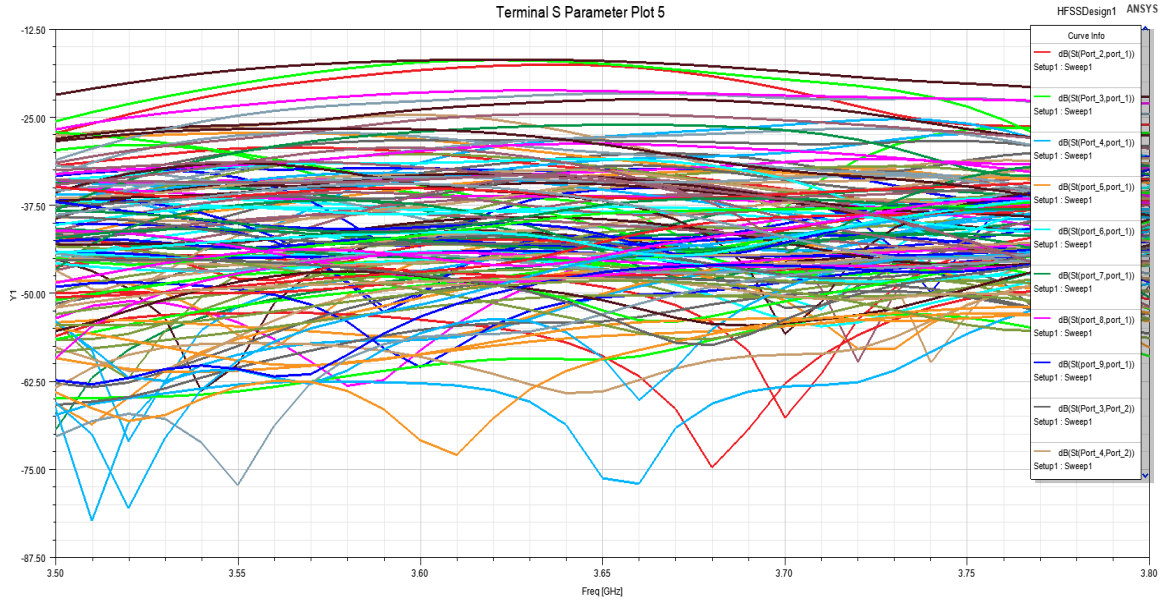


**Fig. 4.75.** The simulated  $S_{21}$  of the mMIMO when elements 1, 2, 3, 4, 5, 6, 14, 15 and 16 are activated.

The simulated patterns of the mMIMO, when the progressive phase in the x-direction is + 50 degrees and in the y-direction is + 100 degrees, is shown in Fig. 4.76 where it can be seen that the maximum gain is 11.2 dB at 3.63 GHz.

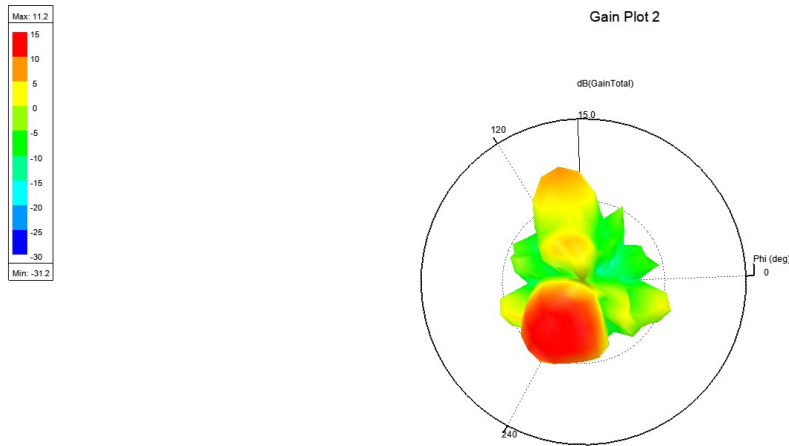
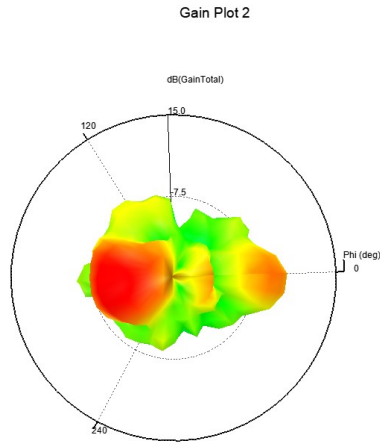
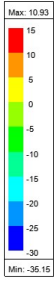


**Fig. 4.76.** The patterns at 3.63 GHz when elements 1, 2, 3, 4, 5, 6, 14, 15 and 16 are activated and  $B_x = + 50$  degrees and  $B_y = + 100$  degrees.

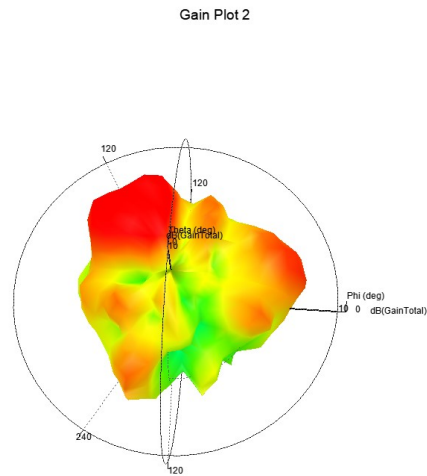
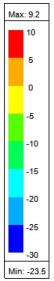
The simulated patterns of the mMIMO, when the progressive phase in the x-direction is + 100 degrees and in the y-direction is + 0 degrees, is shown in Fig. 4.77 where it can be seen that the maximum gain is 10.93 dB at 3.63 GHz.



ANSYS

**Fig. 4.77.** The patterns at 3.63 GHz when elements 1, 2, 3, 4, 5, 6, 14, 15 and 16 are activated and  $B_x = +100$  degrees and  $B_y = 0$  degrees.

The simulated patterns of the mMIMO, when the progressive phase in the x-direction is + 100 degrees and in the y-direction is - 100 degrees, is shown in Fig. 4.78 where it can be seen that the maximum gain is 9.2 dB at 3.63 GHz.



ANSYS

**Fig. 4.78.** The patterns at 3.63 GHz when elements 1, 2, 3, 4, 5, 6, 14, 15 and 16 are activated and  $B_x = +100$  degrees and  $B_y = -100$  degrees.

- **Elements 1, 2, 3, 4, 5, 6, 7, 8, 9, 10, 11 and 12 are Active (4X3 MIMO) & Slot 4 Configuration is Chosen**

The patterns in this case will be more directive than the previous cases. The simulated  $S_{11}$ , and the simulated  $S_{21}$ , when the elements 1, 2, 3, 4, 5, 6, 7, 8, 9, 10, 11 and 12 shown in Fig. 4.64 are activated and slot 4 is activated, are shown in Fig. 4.79 and Fig. 4.80, respectively. It can be seen from Fig. 4.79 that the  $S_{11}$  results of the elements 1, 2, 3, 4, 5, 6, 7, 8, 9, 10, 11 and 12 are well below  $-10$  dB around 3.6 GHz, and this is as expected. On the other hand, it can be seen from Fig. 4.80 that the  $S_{21}$  results between the 16 ports are well below  $-15.5$  dB which shows a good isolation between the mMIMO's ports.

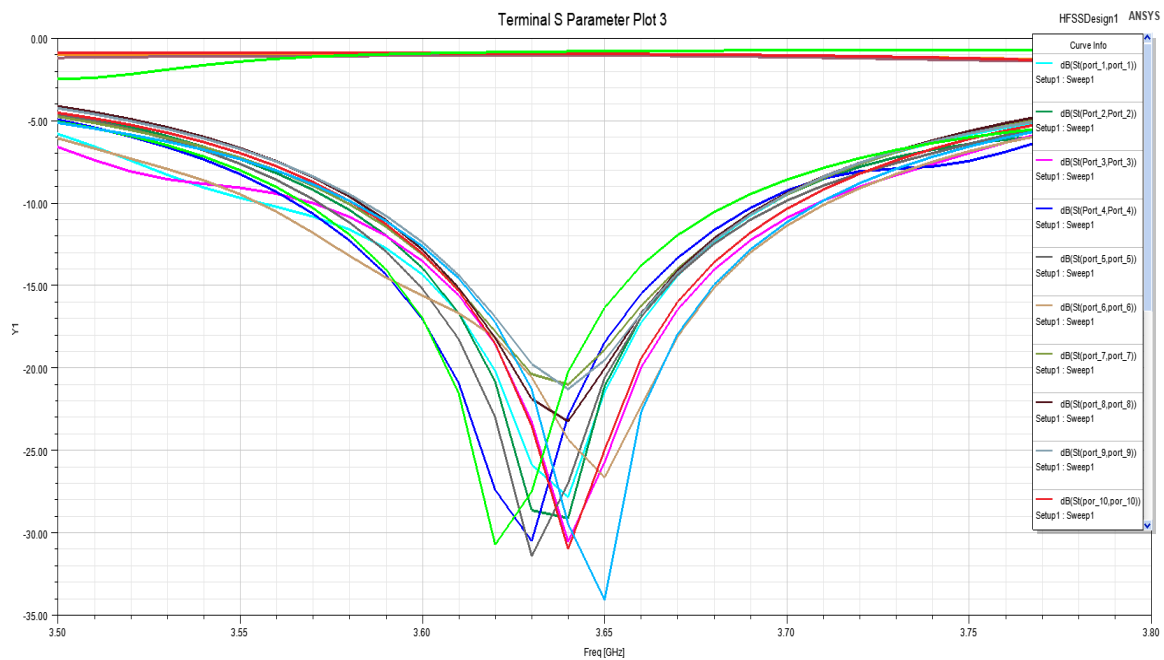


**Fig. 4.79. The simulated S11 of the mMIMO when elements 1, 2, 3, 4, 5, 6, 7, 8, 9, 10, 11 and 12 are activated.**

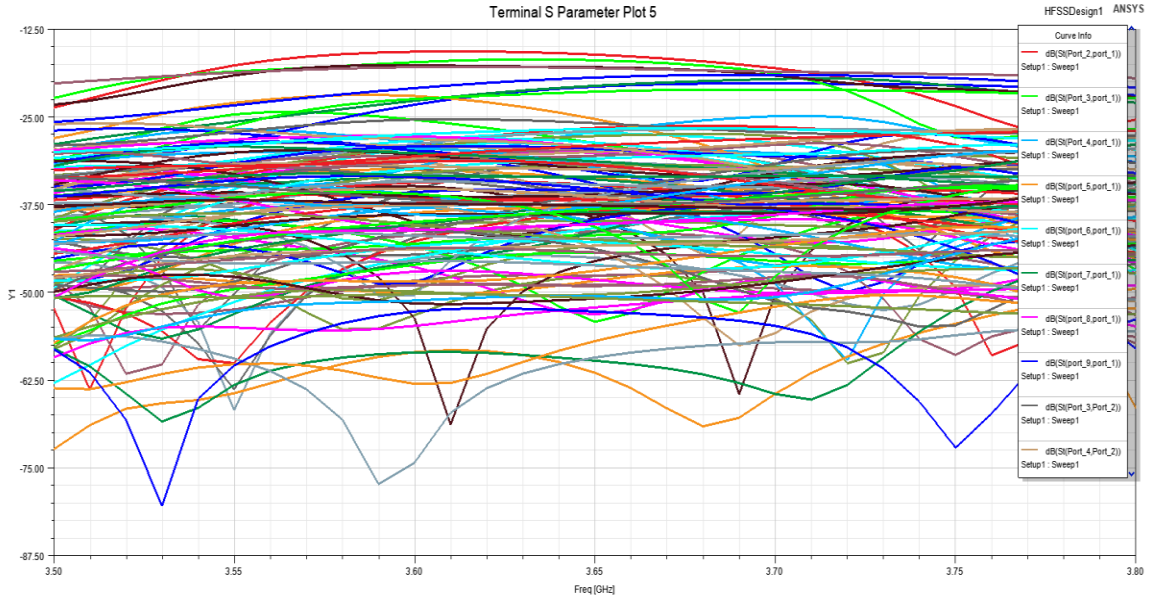


Fig. 4.80. The simulated S21 of the mMIMO when elements 1, 2, 3, 4, 5, 6, 7, 8, 9, 10, 11 and 12 are activated.

The simulated patterns of the mMIMO, when the progressive phase in the x-direction is  $-50$  degrees and in the y-direction is  $+100$  degrees, is shown in Fig. 4.81 where it can be seen that the maximum gain is 11.9 dB at 3.63 GHz.

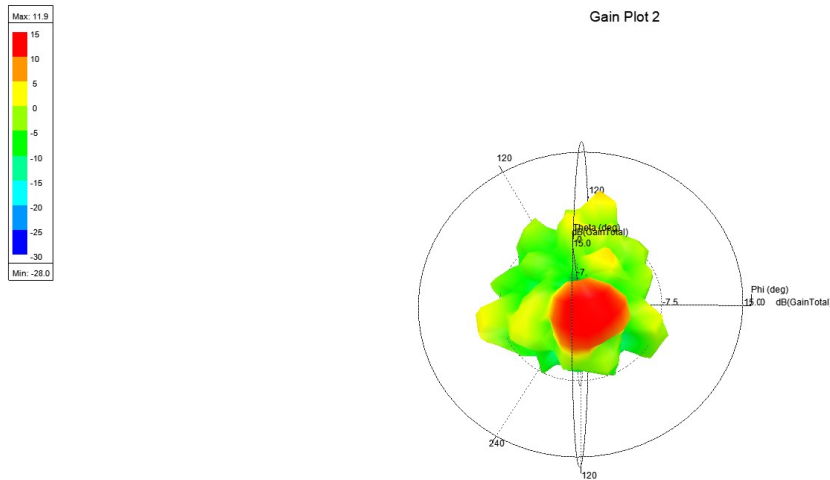
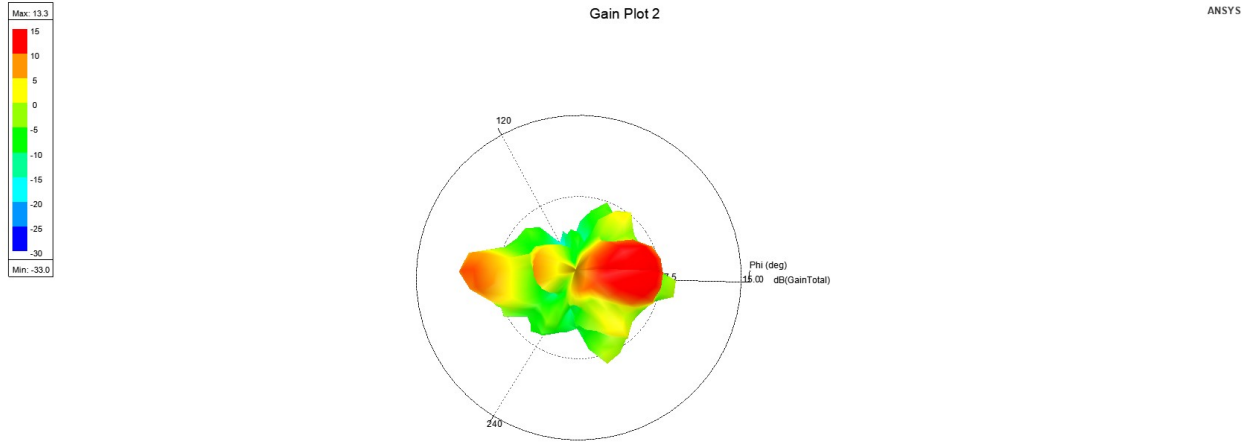


Fig. 4.81. The patterns at 3.63 GHz when elements 1, 2, 3, 4, 5, 6, 7, 8, 9, 10, 11 and 12 are activated and  $B_x = -50$  degrees and  $B_y = +100$  degrees.

The simulated patterns of the mMIMO, when the progressive phase in the x-direction is  $-100$  degrees and in the y-direction is  $+0$  degrees, is shown in Fig. 4.82 where it can be seen that the maximum gain is 13.3 dB at 3.63 GHz.



**Fig. 4.82.** The patterns at 3.63 GHz when elements 1, 2, 3, 4, 5, 6, 7, 8, 9, 10, 11 and 12 are activated and  $B_x = -100$  degrees and  $B_y = +0$  degrees.

The simulated patterns of the mMIMO, when the progressive phase in the x-direction is  $-100$  degrees and in the y-direction is  $-100$  degrees, is shown in Fig. 4.83 where it can be seen that the maximum gain is 13.6 dB at 3.63 GHz.

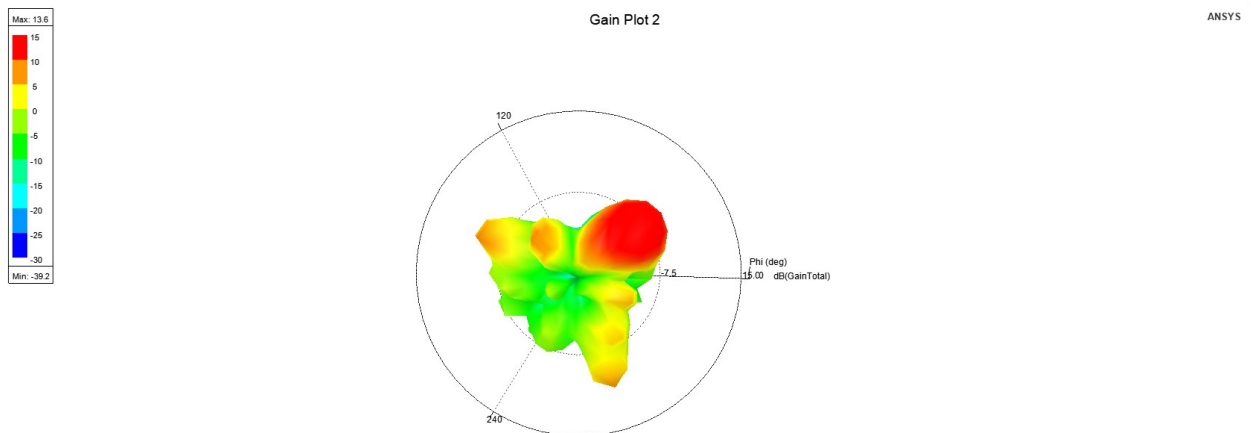


**Fig. 4.83.** The patterns at 3.63 GHz when elements 1, 2, 3, 4, 5, 6, 7, 8, 9, 10, 11 and 12 are activated and  $B_x = -100$  degrees and  $B_y = -100$  degrees.

- **All Elements are Active (4X4 mMIMO) & Slot 1 is Chosen**

The patterns in this case will be more directive than the previous cases. The simulated  $S_{11}$ , and the simulated  $S_{21}$ , when all elements shown in Fig. 4.64 are activated and slot 1 is activated, are shown in Fig. 4.84 and Fig. 4.85, respectively. It can be seen from Fig. 4.84 that the  $S_{11}$  results of all elements are well below  $-10$  dB around 3.6 GHz, and this is as expected. On the other hand, it can be seen from Fig. 4.85 that the  $S_{21}$  results between the 16 ports are well below  $-15.5$  dB which shows a good isolation between the mMIMO's ports.

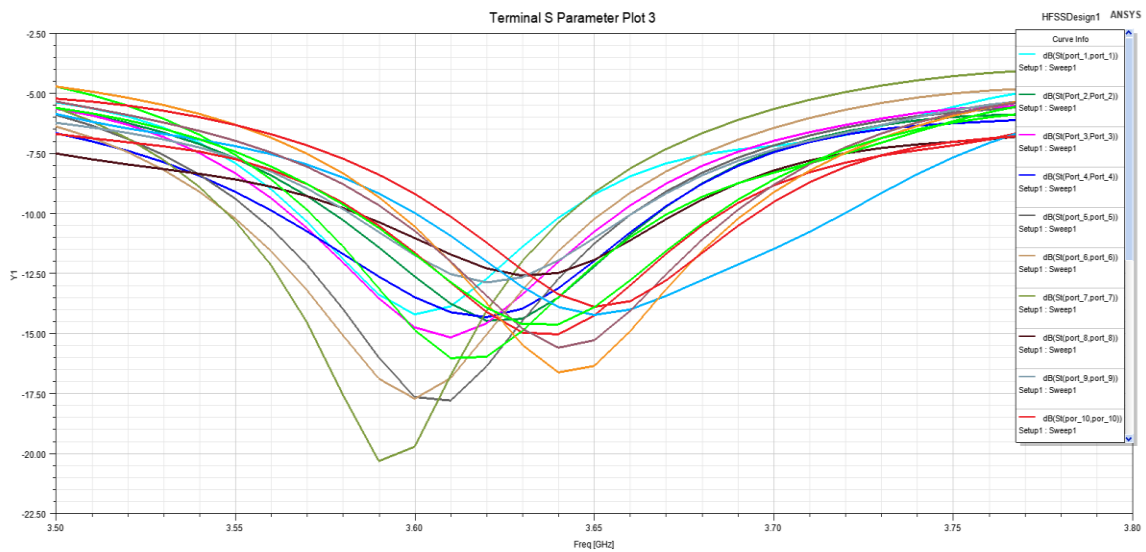


**Fig. 4.84.** The simulated  $S_{11}$  of the mMIMO when all elements are activated.

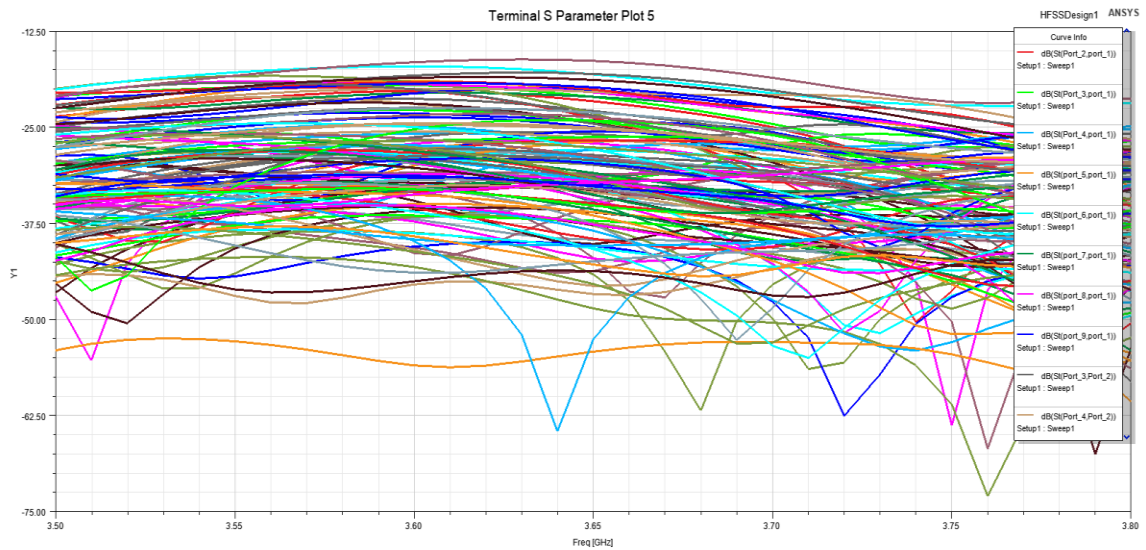


**Fig. 4.85.** The simulated  $S_{21}$  of the mMIMO when all elements are activated.

The simulated patterns of the mMIMO, when the progressive phase in the x-direction is  $-50$  degrees and in the y-direction is  $+100$  degrees, is shown in Fig. 4.86 where it can be seen that the maximum gain is 15.4 dB at 3.63 GHz.

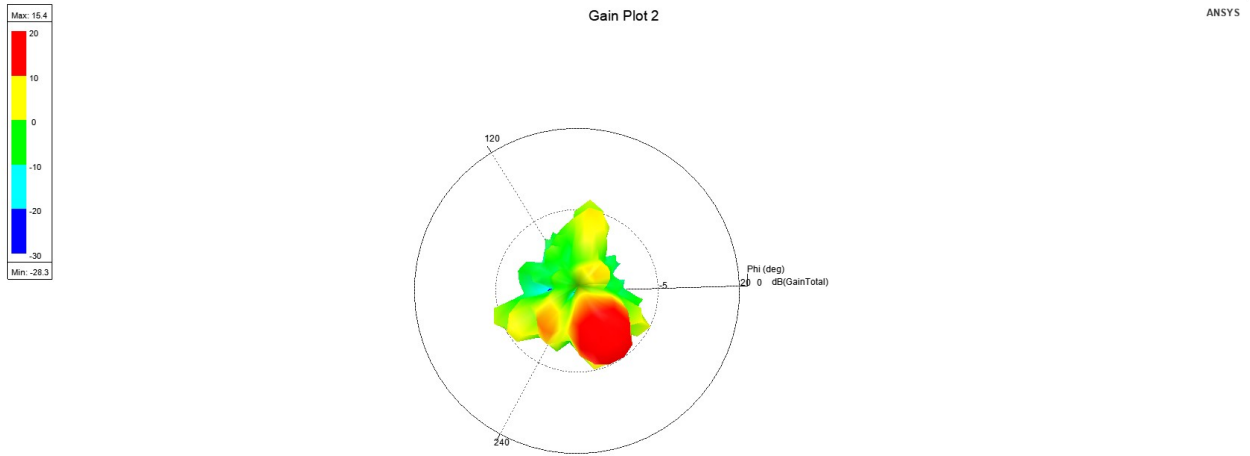


**Fig. 4.86.** The patterns at 3.63 GHz when all elements are activated and  $B_x = -50$  degrees and  $B_y = +100$  degrees.

The simulated patterns of the mMIMO, when the progressive phase in the x-direction is  $0$  degrees and in the y-direction is  $+100$  degrees, is shown in Fig. 4.87 where it can be seen that the maximum gain is 15.3 dB at 3.63 GHz.

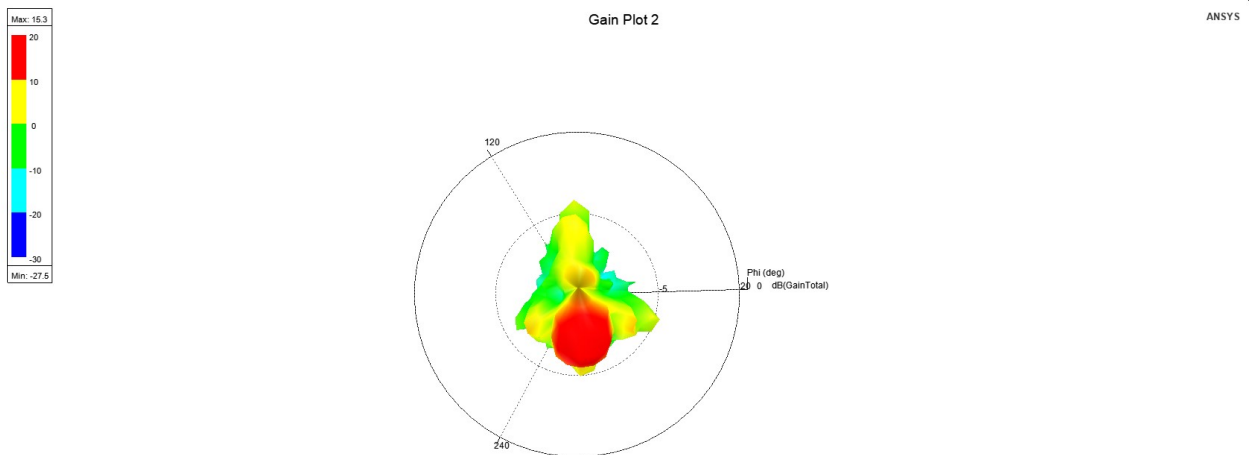


**Fig. 4.87.** The patterns at 3.63 GHz when all elements are activated and  $B_x = 0$  degrees and  $B_y = +100$  degrees.



The simulated patterns of the mMIMO, when the progressive phase in the x-direction is + 50 degrees and in the y-direction is +100 degrees, is shown in Fig. 4.88 where it can be seen that the maximum gain is 13.6 dB at 3.63 GHz.

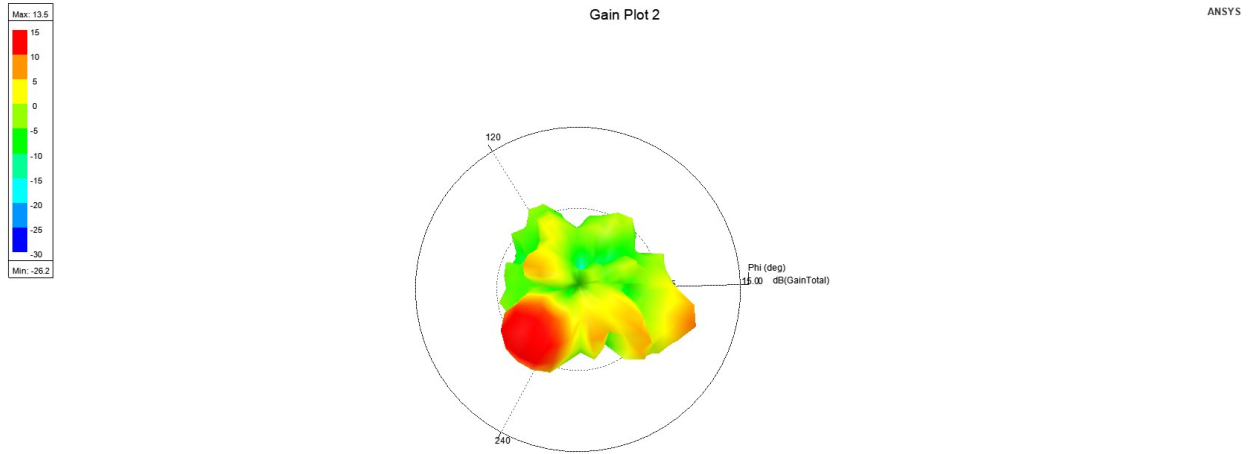


Fig. 4.88. The patterns at 3.63 GHz when all elements are activated and  $B_x = 100$  degrees and  $B_y = +100$  degrees.

### 4.5.3 Comparison Table and discussions

Table 4.14 shows a comparison table between the proposed pattern reconfigurable slot-based mMIMO antenna and other mMIMO antenna available in literature. It can be seen that the proposed mMIMO antenna has a competing size if compared with mMIMO antennas working at sub-6 GHz band. In addition, the bandwidth of the proposed mMIMO antenna is also competing if compared with mMIMO antennas working at sub-6 GHz band. The maximum beam tilt angle of the proposed mMIMO antenna was the maximum among the mMIMO antennas working at the sub-6 GHz band. In addition, the proposed mMIMO antenna uses a pattern reconfigurable slot-based antenna as the single radiating element, and this is the first time of having such a single element as per the best of our knowledge. The separation between the single elements of the proposed mMIMO antenna is really competing if compared with separation between elements in other mMIMO antennas in the literature.

**Table 4.14. A comparison table between the proposed mMIMO antenna and other mMIMO antennas in the literature**

Ref.	Resonant frequency (GHz)	# ports	separation	Antenna size	Max. Panel Gain (dB)	BW (MHz)	Max. Tilt Angle (degrees)	Radiating Elements
<b>This work</b>	<b>3.6</b>	<b>16 (4*4)</b>	$0.66 \lambda_o$	<b>24 * 24 cm2</b>	<b>15.4</b>	<b>100</b>	<b>45</b>	<b>Pattern reconfigurable U-slot</b>
[14]	2.4	9 * 12	$0.5 \lambda_o$	7.5 * 25.5 cm2	-	<254	-	Multimode patch
[6]	2.6	6 * 32	$0.5 \lambda_o * 2 \lambda_o$	-	-	198	30	1 * 4 patches
[8]	2.6	6 * 4	$0.37 \lambda_o * 0.65 \lambda_o$	-	12.4	120	-	1 * 4 patches
[16]	3.6	3 * 24	$0.89 \lambda_o$	44.4 * 29.6 cm2	19.5	100	34	2*2 patches
[5]	3.7	100	$0.5 \lambda_o$	60 * 120 cm2	-	138	-	Dual-polarized patches
[7]	3.7	3 * 6 * 8	$1.25 \lambda_o$	32.4 * 8.6 cm2	16.7	160	-	2*2 patches
[9]	3.6 – 4.8	64	$0.9 \lambda_o$	-	26.8	1200	-	Crossed-polarized dipoles
[4]	5.8	64	$0.77 \lambda_o$	256 * 21.5 cm2	18	200	30	1 * 4 patches
[15]	6 – 8.5	121	$0.58 \lambda_o$	70 * 70 cm2	-	2500	-	Four-mode modified sheet
[12]	28	6 * 48	$0.53 \lambda_o * 2.71 \lambda_o$	11.66 * 6.81 cm2	26.28	-	30	Horn
[13]	28, 38	12 * 8	0.466 mm	20 * 13 mm2	-	-	-	Elliptical patch

[10]	32	32	$0.585 \lambda_o$	23.22 * 44.58 mm <sup>2</sup>	-	1660	47	Dual-polarized patch
[11]	38	36 * 16	$2.2 \lambda_o * 1.1$ $\lambda_o$	-	25.6	10000	-	Antipodal linearly tapered slot

#### 4.5.4 Summary about the pattern reconfigurable mMIMO Antenna

A new slot-based pattern reconfigurable 4X4 massive MIMO antenna at 3.6 GHz with a bandwidth of 100 MHz was proposed and presented. It was found that using pattern reconfigurable antennas in mMIMO antennas help in reducing grating lobes if the right configuration is selected for the required beamforming. The maximum peak gain per a panel reached 15.4 dB for a panel. The isolations between the ports were above – 15 dB, and the maximum tilt of the beam reached around 42 degrees. It is expected that the use of this pattern reconfigurable mMIMO antenna can enhance performance of the Direction of Arrival estimation.

## 4.6 Summary of Contributions

- A new compact, and low-profile pattern reconfigurable Slot-based antenna for 5G technology was presented. The antenna is a dual-band antenna with four different patterns achieved at 3.6 GHz, and four different patterns achieved at 5.2 GHz. Electrical switching was used.
- A new compact, and low profile pattern reconfigurable slot-based antenna for 5G technology was presented. The antenna is a dual-band antenna with 8 patterns at each frequency. Electrical switching was used.
- A pattern reconfigurable IOT antenna with 3 different pattern configurations and 2 different polarizations was presented. The slot modes lost 6 dB gain because of hand and plastic effects. Electrical switching was used. ECC is well below 0.5.
- A new compact and low profile slot-based pattern reconfigurable antenna for 5G technology was presented. The antenna has 8 different patterns at 3.6 GHz with low ECC between the patterns.
- A new compact and low profile slot-based pattern reconfigurable mMIMO for 5G technology was presented. The patterns were dedicated with relatively high gains, and good tilt angle.

## CHAPTER 5

# CONCLUSIONS AND FUTURE WORK

### 5.1 Conclusions

- Using pattern reconfigurable antennas enhances the performance of mMIMO systems, and enhances the reliability of the IoT antennas.
- 4 different patterns at 3.7 GHz and 4 different patterns at 5.2 GHz were achieved by the first 5G slot-based pattern reconfigurable antenna. The antenna was controlled electrically. The antenna can be used for future drones.
- 8 different patterns at 2.3 GHz and 8 different patterns at 3.7 GHz were achieved by the first 5G antenna. The antenna was controlled electrically. This antenna is a good candidate for projects where it is require to locate the oil wells in large areas.
- It was found that radiation patterns of slots for IoT antennas are less sensitive to hand and plastic casing effects comparing to the radiation patterns of monopoles.
- 8 different patterns at 3.6 GHz were achieved electrically by the third 5G slot-based pattern reconfigurable antenna. The patterns are directional and this antenna is a good candidate for mMIMO applications for 5G technology.

## 5.2 Future Work

- RF-front end processing circuits can be built to control the mMIMO antenna. These circuits should have power amplifier, Low-noise amplifier, microcontrollers, RF transceivers, band-pass filters and phase shifters. Hence, the mMIMO can be used for transmitting and receiving modes.
- The DOA Algorithms can be assessed using this mMIMO system to check how much improvements will take place because of the used pattern reconfigurability in the proposed mMIMO antenna. It is expected that the accuracy and the performance of DOA algorithms will be enhanced because of the used pattern reconfigurability in the mMIMO antenna. MUSIC algorithm for example can be used to check if its performance was enhanced by the use of pattern reconfigurability. Also, machine learning can be used to detect the direction from which the signal of interest is coming.
- The difference between co-polarization to cross-polarization levels can be enhanced more for the single element used for the mMIMO antenna. Usually, patches or dipoles are used in mMIMO since they provide pure linear polarizations in the 3 dB beamwidth. Therefore, the difference between the co-polarization and cross-polarization levels can be enhanced using some techniques in the literature.
- The maximum tilt angle can be increased more to 60 degrees with good gains such that it is possible to cover one full sector of 120 degrees by one panel. The gain drop when the beam steered from boresight to maximum tilt angle should not be large.

## REFERENCES

- [1] "Cisco Visual Networking Index: Global Mobile Data Traffic Forecast Update, 2017–2022 White Paper." *Cisco*, 19 Feb. 2019, [www.cisco.com/c/en/us/solutions/collateral/service-provider/visual-networking-index-vni/white-paper-c11-738429.html](http://www.cisco.com/c/en/us/solutions/collateral/service-provider/visual-networking-index-vni/white-paper-c11-738429.html).
- [2] Hu, Fei. *Opportunities in 5G Networks: a Research and Development Perspective*. CRC Press, 2016.
- [3] M. Agiwal, A. Roy, and N. Saxena, "Next Generation 5G Wireless Networks: A Comprehensive Survey," *IEEE Communications Surveys and Tutorials*, vol. 18, no. 3, pp. 1617-1655, 2016, DOI: 10.1109/comst.2016.2532458.
- [4] C. G. Christodoulou, Y. Tawk, S. A. Lane, and S. R. Erwin, "Reconfigurable Antennas for Wireless and Space Applications," *Proceedings of the IEEE*, vol. 100, no. 7, pp. 2250-2261, Jul 2012, DOI: 10.1109/jproc.2012.2188249.
- [5] J. G. Andrews et al., "What will 5G be?" *IEEE J. Sel. Areas Commun.*, vol. 32, no. 6, pp. 1065–1082, Jun. 2014.
- [6] Sharawi, Mohammad S. "Printed Multi-Band MIMO Antenna Systems and Their Performance Metrics [Wireless Corner]." *IEEE Antennas and Propagation Magazine*, vol. 55, no. 5, 2013, pp. 218–232., DOI:10.1109/map.2013.6735522.
- [7] E. G. Larsson, F. Tufvesson, O. Edfors, and T. L. Marzetta, "Massive MIMO for next generation wireless systems," *IEEE Commun. Mag.*, vol. 52, no. 2, pp. 186–195, Feb. 2014.
- [8] T. L. Marzetta, "Massive MIMO: An Introduction," *Bell Labs Technical Journal*, Vol. 20, no. , pp. 11-22, 2015.
- [9] Lu, L., Geoffrey, Y. L., Swindlehurst, A. L., Alexei, A., & Rui, Z. (15 april 2014). An Overview of Massive MIMO: Benefits and Challenges. *IEEE JOURNAL OF SELECTED TOPICS IN SIGNAL PROCESSING*, 8(5), 742-758. DOI:10.1109/JSTSP.2014.2317671
- [10] Rusek, F., Persson, D., Lau, B. K., Larsson, E. G., Marzetta, T. L., Edfors, O., & Tufvesson, F. (2013). Scaling Up MIMO: Opportunities and Challenges with Very Large Arrays. *IEEE Signal Processing Magazine*, 30(1), 40-60. DOI:10.1109/MSP.2011.2178495
- [11] Sanudin, R., Noordin, N. H., El-Rayis, A. O., Haridas, N., Erdogan, A. T., & Arslan, T. (2011). Analysis of DOA estimation for directional and isotropic antenna arrays. *2011 Loughborough Antennas & Propagation Conference*. DOI:10.1109/lapc.2011.6114043
- [12] Rocca, P., Hannan, M. A., Salucci, M., & Massa, A. (2017). Single-Snapshot DoA Estimation in Array Antennas With Mutual Coupling Through a Multiscaling BCS Strategy. *IEEE Transactions on Antennas and Propagation*, 65(6), 3203-3213. DOI:10.1109/tap.2017.2684137

- [13] Piazza, D., Mookiah, P., Damico, M., Dandekar, K. R. (2010). Ex- perimental Analysis of Pattern and Polarization Reconfigurable Circular Patch Antennas for MIMO Systems. *IEEE Transactions on Vehicular Technology*, 59(5), 2352-2362. DOI:10.1109/tvt.2010.2043275
- [14] Yang, Y., Simorangkir, R. B., Zhu, X., Esselle, K., Xue, Q. (2017). A Novel Boresight and Conical Pattern Reconfigurable Antenna With the Diversity of 360° Polarization Scanning. *IEEE Transactions on Antennas and Propagation*, 65(11), 5747-5756. DOI:10.1109/tap.2017.2754412
- [15] Yan, S., Vandenbosch, G. A. (2016). Radiation Pattern-Reconfigurable Wearable Antenna Based on Metamaterial Structure. *IEEE Antennas and Wireless Propagation Letters*, 15, 1715-1718. DOI:10.1109/lawp.2016.2528299
- [16] Qin, P., Guo, Y. J., Wely, A. R., Liang, C. (2012). A Pattern Reconfigurable U-Slot Antenna and Its Applications in MIMO Sys- tems. *IEEE Transactions on Antennas and Propagation*, 60(2), 516-528. DOI:10.1109/tap.2011.2173439
- [17] Alam, M. S., Abbosh, A. M. (2016). Beam-Steerable Planar Antenna Using Circular Disc and Four PIN-Controlled Tapered Stubs for WiMAX and WLAN Applications. *IEEE Antennas and Wireless Propagation Letters*, 15, 980-983. DOI:10.1109/lawp.2015.2489684
- [18] W. Q. Cao, B. N. Zhang, A. J. Liu, T. B. Yu, D. S. Guo, and K. G. Pan, "A Reconfigurable Microstrip Antenna With Radiation Pattern Selectiv- ity and Polarization Diversity," *IEEE Antennas and Wireless Propagation Letters*, vol. 11, pp. 453-456, 2012, DOI: 10.1109/lawp.2012.2193549.
- [19] Mazlouman, S. J., Mahanfar, A., Menon, C., Vaughan, R. G. (2012). Square Ring Antenna With Reconfigurable Patch Using Shape Memory Alloy Actuation. *IEEE Transactions on Antennas and Propagation*, 60(12), 5627-5634. DOI:10.1109/tap.2012.2213053
- [20] Mazlouman, S. J., Soleimani, M., Mahanfar, A., Menon, C., Vaughan, R. (2011). Pattern reconfigurable square ring patch antenna actuated by hemispherical dielectric elastomer. *Electronics Letters*, 47(3), 164. DOI:10.1049/el.2010.3585
- [21] Zhang, G., Song, G., Hong, J., Wang, B. (2012). Design and analysis of a compact wideband pattern-reconfigurable antenna with alternate reflector and radiator. *IET Microwaves, Antennas Propagation*, 6(15), 1629-1635. DOI:10.1049/iet-map.2012.0005
- [22] M. Jusoh, T. Aboufoul, T. Sabapathy, A. Alomainy, and M. R. Kamarudin, "Pattern-Reconfigurable Microstrip Patch Antenna With Multidirectional Beam for WiMAX Application," *Ieee Antennas and Wireless Propagation Letters*, vol. 13, pp. 860-863, 2014, DOI: 10.1109/lawp.2014.2320818.
- [23] Shi, S., Ding, W. (2015). Radiation pattern reconfigurable microstrip antenna for WiMAX application. *Electronics Letters*, 51(9), 662-664. DOI:10.1049/el.2015.0568
- [24] Yang, X., Wang, B., Zhang, Y. (2004). Pattern-reconfigurable quasi-yagi microstrip antenna using a photonic band gap structure. *Microwave and Optical Technology Letters*, 42(4), 296-297. DOI:10.1002/mop.20283
- [25] Yang, X., Wang, B., Wu, W. (n.d.). Pattern Reconfigurable Patch Antenna with Two Orthogonal Quasi-Yagi Arrays. 2005 *IEEE Antennas and Propagation Society International Symposium*. DOI:10.1109/aps.2005.1552087
- [26] Alam, M. S., Abbosh, A. M. (2017). Wideband Pattern-Reconfigurable Antenna Using Pair of Radial Radiators on Truncated Ground With Switchable Director and Reflector. *IEEE Antennas and Wireless Propa- gation Letters*, 16, 24-28. DOI:10.1109/lawp.2016.2552492
- [27] Katare, K. K., Biswas, A., Esselle, K. P. (2017). Directive array based pattern reconfigurable antenna. 2017 11th European Conference on An- tennas and Propagation (EUCAP). DOI:10.23919/eucap.2017.7928038
- [28] Saurav, K., Sarkar, D., Srivastava, K. V. (2017). A dual-band recon- figurable Yagi-Uda antenna with diverse radiation patterns. *Applied Physics A*, 123(7). DOI:10.1007/s00339-017-1087-y
- [29] M. F. Ismail, M. K. A. Rahim, H. A. Majid, M. R. Hamid, M. F. M. Yusoff, and R. Dewan, "Pattern reconfigurable antenna using elec- tromagnetic band gap structure," *Applied Physics a-Materials Science Processing*, vol. 123, no. 1, Jan 2017, Art no. 17, DOI: 10.1007/s00339- 016-0657-8.



- [30] S. Zhang, G. H. Huff, J. Feng, and J. T. Bernhard, "A pattern reconfigurable microstrip parasitic array," *IEEE Transactions on Antennas and Propagation*, vol. 52, no. 10, pp. 2773-2776, Oct 2004, DOI: 10.1109/tap.2004.834372.
- [31] Sheel, S., Coetzee, J. (2018). Electronically Steerable Circularly Polarized Planar Antenna. 12th European Conference on Antennas and Propagation (EuCAP 2018). DOI:10.1049/cp.2018.0403
- [32] Lee, C. M., Jung, C. W. (2015). Radiation-Pattern-Reconfigurable Antenna Using Monopole-Loop for Fitbit Flex Wristband. *IEEE Antennas and Wireless Propagation Letters*, 14, 269-272. DOI:10.1109/lawp.2014.2361895
- [33] J. Ren, X. Yang, J. Y. Yin, and Y. Z. Yin, "A Novel Antenna with Reconfigurable Patterns Using H-Shaped Structures," *IEEE Antennas and Wireless Propagation Letters*, vol. 14, pp. 915-918, 2015, DOI: 10.1109/lawp.2014.2387292.
- [34] Kittiyapunya, C., Krairiksh, M. (2013). A Four-Beam Pattern Reconfigurable Yagi-Uda Antenna. *IEEE Transactions on Antennas and Propagation*, 61(12), 6210-6214. DOI:10.1109/tap.2013.2282914
- [35] T. Aboufoul, C. Parini, X. D. Chen, and A. Alomainy, "Pattern-Reconfigurable Planar Circular Ultra-Wideband Monopole Antenna," *IEEE Transactions on Antennas and Propagation*, vol. 61, no. 10, pp. 4973-4980, Oct 2013, DOI: 10.1109/tap.2013.2274262.
- [36] Marantis, L., Rongas, D., Paraskevopoulos, A., Oikonomopoulos-Zachos, C., Kanatas, A. (2018). Pattern reconfigurable ESPAR antenna for vehicle-to-vehicle communications. *IET Microwaves, Antennas Propagation*, 12(3), 280-286. DOI:10.1049/iet-map.2017.0209
- [37] X. Ding and B. Z. Wang, "A Novel Wideband Antenna With Reconfigurable Broadside and Endfire Patterns," *IEEE Antennas and Wireless Propagation Letters*, vol. 12, pp. 995-998, 2013, DOI: 10.1109/lawp.2013.2278139.
- [38] Narbudowicz, A., Bao, X., Ammann, M. J. (2014). Omnidirectional microstrip patch antenna with reconfigurable pattern and polarisation. *IET Microwaves, Antennas Propagation*, 8(11), 872-877. DOI:10.1049/iet-map.2013.0665
- [39] Pal, A., Mehta, A., Mirshekar-Syahkal, D., Nakano, H. (2017). A Twelve-Beam Steering Low-Profile Patch Antenna With Shorting Vias for Vehicular Applications. *IEEE Transactions on Antennas and Propagation*, 65(8), 3905-3912. DOI:10.1109/tap.2017.2715367
- [40] Pal, A., Mehta, A., Mirshekar-Syahkal, D., Massey, P. (2009). Doughnut and Tilted Beam Generation Using a Single Printed Star Antenna. *IEEE Transactions on Antennas and Propagation*, 57(10), 3413-3418. DOI:10.1109/tap.2009.2030523
- [41] Pal, A., Mehta, A., Mirshekar-Syahkal, D., Massey, P. (2008). Short-circuited feed terminations on beam steering square loop antennas. *Electronics Letters*, 44(24), 1389. DOI:10.1049/el:20082350
- [42] Deo, P., Mehta, A., Mirshekar-Syahkal, D., Massey, P. J., Nakano, H. (2010). Thickness Reduction and Performance Enhancement of Steerable Square Loop Antenna Using Hybrid High Impedance Surface. *IEEE Transactions on Antennas and Propagation*, 58(5), 1477-1485. DOI:10.1109/tap.2010.2044339
- [43] A. Pal, A. Mehta, D. Mirshekar-Syahkal, P. Deo, and H. Nakano, "Dual-Band Low-Profile Capacitively Coupled Beam-Steerable Square-Loop Antenna," *IEEE Transactions on Antennas and Propagation*, vol. 62, no. 3, pp. 1204-1211, Mar 2014, DOI: 10.1109/tap.2013.2294866.
- [44] Narbudowicz, A., Bao, X., Ammann, M., Shakhmouradian, H., Heberling, D. (2014). Circularly Polarized Antenna With Steerable Dipole-Like Radiation Pattern. *IEEE Transactions on Antennas and Propagation*, 62(2), 519-526. DOI:10.1109/tap.2013.2289323
- [45] Pal, A., Mehta, A., Mirshekar-Syahkal, D., Nakano, H. (2011). A Square-Loop Antenna With 4-Port Feeding Network Generating Semi-Doughnut Pattern for Vehicular and Wireless Applications. *IEEE Antennas and Wireless Propagation Letters*, 10, 338-341. DOI:10.1109/lawp.2011.2144559

- [46] Honma, N., Seki, T., Nishikawa, K., Tsunekawa, K., Sawaya, K. (2006). Compact Six-Sector Antenna Employing Three Intersecting Dual-Beam Microstrip Yagi-Uda Arrays With Common Director. *IEEE Transactions on Antennas and Propagation*, 54(11), 3055-3062. DOI:10.1109/tap.2006.883980
- [47] Z. Y. Li, E. Ahmed, A. M. Eltawil, and B. A. Cetiner, "A Beam-Steering Reconfigurable Antenna for WLAN Applications," *IEEE Transactions on Antennas and Propagation*, vol. 63, no. 1, pp. 24-32, Jan 2015, DOI: 10.1109/tap.2014.2367500.
- [48] Lotfi, P., Soltani, S., Murch, R. D. (2016). Broadside Beam-Steerable Planar Parasitic Pixel Patch Antenna. *IEEE Transactions on Antennas and Propagation*, 64(10), 4519-4524. DOI:10.1109/tap.2016.2588525
- [49] Nieh, C., Wei, C., Lin, J. (2015). Concurrent Detection of Vibration and Distance Using Unmodulated CW Doppler Vibration Radar With An Adaptive Beam-Steering Antenna. *IEEE Transactions on Microwave Theory and Techniques*, 63(6), 2069-2078. DOI:10.1109/tmtt.2015.2422692
- [50] Poussot, B., Laheurte, J., Cirio, L., Picon, O., Delcroix, D., Dussopt, (2008). Diversity Measurements of a Reconfigurable Antenna With Switched Polarizations and Patterns. *IEEE Transactions on Antennas and Propagation*, 56(1), 31-38. DOI:10.1109/tap.2007.913032
- [51] Mehta, A., Mirshekar-Syahkal, D. (2004). Spiral antenna with adaptive radiation pattern under electronic control. *IEEE Antennas and Propagation Society Symposium*, 2004. DOI:10.1109/aps.2004.1329802
- [52] Mehta, A., Mirshekar-Syahkal, D., Nakano, H. (2006). Beam adaptive single arm rectangular spiral antenna with switches. *IEEE Proceedings- Microwaves, Antennas and Propagation*, 153(1), 13. DOI:10.1049/ip-map:20050045
- [53] Huff, G., Bernhard, J. (2006). Integration of Packaged RF MEMS Switches With Radiation Pattern Reconfigurable Square Spiral Microstrip Antennas. *IEEE Transactions on Antennas and Propagation*, 54(2), 464-469. DOI:10.1109/tap.2005.863409
- [54] Jung, C., Lee, M., Li, G., Deflaviis, F. (2006). Reconfigurable Scan-Beam Single-Arm Spiral Antenna Integrated With RF-MEMS Switches. *IEEE Transactions on Antennas and Propagation*, 54(2), 455-463. DOI:10.1109/tap.2005.863407
- [55] Suntives, A., Hum, S. V. (2012). A Fixed-Frequency Beam-Steerable Half-Mode Substrate Integrated Waveguide Leaky-Wave Antenna. *IEEE Transactions on Antennas and Propagation*, 60(5), 2540-2544. DOI:10.1109/tap.2012.2189726
- [56] Z. Y. Li, Z. W. Du, and K. Gong, "Compact Reconfigurable Antenna Array for Adaptive MIMO Systems," *IEEE Antennas and Wireless Propagation Letters*, vol. 8, pp. 1317-1320, 2009, DOI: 10.1109/lawp.2009.2038182.
- [57] Chuang, H., Kuo, L. (2003). 3-D FDTD design analysis of a 2.4-GHz polarization-diversity printed dipole antenna with integrated balun and polarization-switching circuit for WLAN and wireless communication applications. *IEEE Transactions on Microwave Theory and Techniques*, 51(2), 374-381. DOI:10.1109/tmtt.2002.807838
- [58] Ji, J. (2017). Compact dual-band pattern reconfigurable antenna using switched parasitic array. *Electronics Letters*, 53(4), 211-212. DOI:10.1049/el.2016.3486
- [59] Ullah, M. H., Islam, M. T., Mandeep, J. S., Misran, N. (2012). A new double L-shaped multiband patch antenna on a polymer resin material substrate. *Applied Physics A*, 110(1), 199-205. DOI:10.1007/s00339-012-7114-0
- [60] Syrytsin, I., Vesterager, H., Nørgaard, S., Thomsen, L., Barrio, S. C., Pedersen, G. (2018). Pattern-Reconfigurable Mobile Terminal Antenna System for MIMO and Link Stabilization in LTE. *12th European Conference on Antennas and Propagation (EuCAP 2018)*. DOI:10.1049/cp.2018.0892

- [61] C. Rhee et al., "Pattern-Reconfigurable MIMO Antenna for High Isolation and Low Correlation," *IEEE Antennas and Wireless Propagation Letters*, vol. 13, pp. 1373-1376, 2014, DOI: 10.1109/lawp.2014.2339012.
- [62] Raman, S., Mohanan, P., Timmons, N., Morrison, J. (2013). Microstrip- Fed Pattern- and Polarization- Reconfigurable Compact Truncated Monopole Antenna. *IEEE Antennas and Wireless Propagation Letters*, 12, 710-713. DOI:10.1109/lawp.2013.2263983
- [63] M. C. Tang, B. Y. Zhou, Y. L. Duan, X. M. Chen, and R. W. Zi-olkowski, "Pattern-Reconfigurable, Flexible, Wideband, Directive, Electrically Small Near-Field Resonant Parasitic Antenna," *IEEE Transactions on Antennas and Propagation*, vol. 66, no. 5, pp. 2271-2280, May 2018, DOI: 10.1109/tap.2018.2814220.
- [64] J. Q. Hu, S. Lin, and F. H. Dai, "Pattern Reconfigurable Antenna Based on Morphing Bistable Composite Laminates," *IEEE Transactions on Antennas and Propagation*, vol. 65, no. 5, pp. 2196-2207, May 2017, DOI: 10.1109/tap.2017.2677258.
- [65] Kang, W., Park, J., Yoon, Y. (2008). Simple reconfigurable antenna with radiation pattern. *Electronics Letters*, 44(3), 182. DOI:10.1049/el:20082994
- [66] Zhu, H. L., Yuk, T. I., Cheung, S. W. (2015). Mechanically pattern reconfigurable antenna using metasurface. *IET Microwaves, Antennas Propagation*, 9(12), 1331-1336. DOI:10.1049/iet-map.2014.0676
- [67] D. Patron, A. S. Daryoush, and K. R. Dandekar, "Optical Control of Reconfigurable Antennas and Application to a Novel Pattern- Reconfigurable Planar Design," *Journal of Lightwave Technology*, vol. 32, no. 20, pp. 3394-3402, Oct 2014, DOI: 10.1109/jlt.2014.2321406.
- [68] R. Wang, B. Z. Wang, G. F. Gao, X. Ding, and Z. P. Wang, "Low-Profile Pattern-Reconfigurable Vertically Polarized Endfire Antenna With Magnetic-Current Radiators," *IEEE Antennas and Wireless Propagation Letters*, vol. 17, no. 5, pp. 829-832, May 2018, DOI: 10.1109/lawp.2018.2817682.
- [69] Mahmood, S. M., Denidni, T. A. (2016). Pattern-Reconfigurable Antenna Using a Switchable Frequency Selective Surface With Improved Bandwidth. *IEEE Antennas and Wireless Propagation Letters*, 15, 1148- 1151. DOI:10.1109/lawp.2015.2496501
- [70] Jiang, X., Zhang, Z., Li, Y., Feng, Z. (2014). A Novel Null Scanning Antenna Using Even and Odd Modes of a Shorted Patch. *IEEE Transactions on Antennas and Propagation*, 62(4), 1903-1909. DOI:10.1109/tap.2014.2298884
- [71] A. Khidre, F. Yang, and A. Z. Elsherbeni, "A Patch Antenna With a Varactor-Loaded Slot for Reconfigurable Dual-Band Operation," *IEEE Transactions on Antennas and Propagation*, vol. 63, no. 2, pp. 755-760, Feb 2015, DOI: 10.1109/tap.2014.2376524.
- [72] E. Erfani, J. Nourinia, C. Ghobadi, M. Niroom-Jazi, and T. A. Denidni, "Design and Implementation of an Integrated UWB/Reconfigurable- Slot Antenna for Cognitive Radio Applications," *IEEE Antennas and Wireless Propagation Letters*, vol. 11, pp. 77-80, 2012, DOI: 10.1109/lawp.2011.2182631.
- [73] Zhang, P., Huang, X., Chen, R., Liu, S. (2016). A Reconfigurable Microstrip Patch Antenna with Frequency and Circular Polarization Diversities. *Chinese Journal of Electronics*, 25(2), 379-383. DOI:10.1049/cje.2016.03.027
- [74] Anantha, B., Merugu, L., Rao, P. S. (2017). A novel single feed frequency and polarization reconfigurable microstrip patch antenna. *AEU - International Journal of Electronics and Communications*, 72, 8-16. DOI:10.1016/j.aeue.2016.11.012
- [75] S. Nikolaou, N. D. Kingsley, G. E. Ponchak, J. Papapolymerou, and M. Tentzeris, "UWB Elliptical Monopoles With a Reconfigurable Band Notch Using MEMS Switches Actuated Without Bias Lines," *IEEE Transactions on Antennas and Propagation*, vol. 57, no. 8, pp. 2242- 2251, Aug 2009, DOI: 10.1109/tap.2009.2024450.

- [76] Yang, F., Rahmat-Samii, Y. (2001). Switchable dual-band circularly polarised patch antenna with single feed. *Electronics Letters*, 37(16), 1002. DOI:10.1049/el:20010695
- [77] D. H. Schaubert, F. G. Farrar, A. Sindoris, and S. T. Hayes, "MICROSTRIP ANTENNAS WITH FREQUENCY AGILITY AND POLARIZATION DIVERSITY," *IEEE Transactions on Antennas and Propagation*, vol. 29, no. 1, pp. 118-123, 1981, DOI: 10.1109/tap.1981.1142546.
- [78] Shelley, S., Costantine, J., Christodoulou, C. G., Anagnostou, D. E., Lyke, J. C. (2010). FPGA-Controlled Switch-Reconfigured Antenna. *IEEE Antennas and Wireless Propagation Letters*, 9, 355-358. DOI:10.1109/lawp.2010.2048550
- [79] Costantine, J., Christodoulou, C. G., Barbin, S. E. (2007). A new reconfigurable multi band patch antenna. 2007 SBMO/IEEE MTT-S International Microwave and Optoelectronics Conference. DOI:10.1109/imoc.2007.4404216
- [80] Erdil, E., Topalli, K., Unlu, M., Civi, O., Akin, T. (2007). Frequency Tunable Microstrip Patch Antenna Using RF MEMS Technology. *IEEE Transactions on Antennas and Propagation*, 55(4), 1193-1196. DOI:10.1109/tap.2007.893426
- [81] P. Y. Qin, A. R. Weily, Y. J. Guo, T. S. Bird, and C. H. Liang, "Frequency Reconfigurable Quasi-Yagi Folded Dipole Antenna," *IEEE Transactions on Antennas and Propagation*, vol. 58, no. 8, pp. 2742-2747, Aug 2010, DOI: 10.1109/tap.2010.2050455.
- [82] Liu, L., Langley, R. (2008). Liquid crystal tunable microstrip patch antenna. *Electronics Letters*, 44(20), 1179. DOI:10.1049/el:20081995
- [83] Pozar, D., Sanchez, V. (1988). Magnetic tuning of a microstrip antenna on a ferrite substrate. *Electronics Letters*, 24(12), 729. DOI:10.1049/el:19880491
- [84] Tawk, Y., Bkassiny, M., El-Howayek, G., Jayaweera, S., Avery, K., Christodoulou, C. (2011). Reconfigurable front-end antennas for cognitive radio applications. *IET Microwaves, Antennas Propagation*, 5(8), 985. DOI:10.1049/iet-map.2010.0358
- [85] Patnaik, A., Anagnostou, D., Christodoulou, C., Lyke, J. (2005). Neurocomputational analysis of a multiband reconfigurable planar antenna. *IEEE Transactions on Antennas and Propagation*, 53(11), 3453-3458. DOI:10.1109/tap.2005.858617
- [86] Kingsley, N., Anagnostou, D., Tentzeris, M., Papapolymerou, J. (2007). RF MEMS Sequentially Reconfigurable Sierpinski Antenna on a Flexible Organic Substrate With Novel DC-Biasing Technique. *Journal of Microelectromechanical Systems*, 16(5), 1185-1192. DOI:10.1109/jmems.2007.902462
- [87] Wu, T., Li, R. L., Eom, S. Y., Myoung, S. S., Lim, K., Laskar, J., . . . Tentzeris, M. M. (2010). Switchable Quad-Band Antennas for Cognitive Radio Base Station Applications. *IEEE Transactions on Antennas and Propagation*, 58(5), 1468-1476. DOI:10.1109/tap.2010.2044472
- [88] Feldner, L. M., Rodenbeck, C. T., Christodoulou, C. G., Kinzie, (2007). Electrically Small Frequency-Agile PIFA-as-a-Package for Portable Wireless Devices. *IEEE Transactions on Antennas and Propagation*, 55(11), 3310-3319. DOI:10.1109/tap.2007.908815
- [89] Costantine, J., Al-Saffar, S., Christodoulou, C., Kabalan, K., El-Hajj, (2009). The Analysis of a Reconfigurable Antenna With a Rotating Feed Using Graph Models. *IEEE Antennas and Wireless Propagation Letters*, 8, 943-946. DOI:10.1109/lawp.2009.2029137
- [90] Christodoulou, C. G., Kim, J., Costantine, J., Barbin, S. E. (2007). Reconfigurable RF and antenna systems. 2007 SBMO/IEEE MTT-S International Microwave and Optoelectronics Conference. DOI:10.1109/imoc.2007.4404203
- [91] Zachou, V., Christodoulou, C. G., Chryssomallis, M. T., Anagnostou, D., Barbin, S. (2006). Planar Monopole Antenna With Attached Sleeves. *IEEE Antennas and Wireless Propagation Letters*, 5, 286-289. DOI:10.1109/lawp.2006.876970
- [92] Lee, W., Kim, D., Kim, K., Yu, J. (2006). Wideband planar monopole antennas with dual band-notched characteristics. *IEEE Transactions on Microwave Theory and Techniques*, 54(6), 2800-2806. DOI:10.1109/tmmt.2006.874895

- [93] Zaker, R., Ghobadi, C., Nourinia, J. (2009). Bandwidth Enhancement of Novel Compact Single and Dual Band-Notched Printed Monopole Antenna With a Pair of L-Shaped Slots. *IEEE Transactions on Antennas and Propagation*, 57(12), 3978-3983. DOI:10.1109/tap.2009.2023475
- [94] Rodrigo, D., Cetiner, B. A., Jofre, L. (2014). Frequency, Radiation Pattern and Polarization Reconfigurable Antenna Using a Parasitic Pixel Layer. *IEEE Transactions on Antennas and Propagation*, 62(6), 3422- 3427. DOI:10.1109/tap.2014.2314464
- [95] Pringle, L., Harms, P., Blalock, S., Kiesel, G., Kuster, E., Friederich, P., . . . Smith, G. (2004). A Reconfigurable Aperture Antenna Based on Switched Links Between Electrically Small Metallic Patches. *IEEE Transactions on Antennas and Propagation*, 52(6), 1434-1445. DOI:10.1109/tap.2004.825648
- [96] Li, P. K., Shao, Z. H., Wang, Q., Cheng, Y. J. (2015). Frequency- and Pattern-Reconfigurable Antenna for Multistandard Wireless Applications. *IEEE Antennas and Wireless Propagation Letters*, 14, 333-336. DOI:10.1109/lawp.2014.2359196
- [97] B. Babakhani, S. K. Sharma, and N. R. Labadie, "A Frequency Agile Microstrip Patch Phased Array Antenna With Polarization Reconfiguration," *IEEE Transactions on Antennas and Propagation*, vol. 64, no. 10, pp. 4316-4327, Oct 2016, DOI: 10.1109/tap.2016.2598156.
- [98] D. Piazza, N. J. Kirsch, A. Forenza, R. W. Heath, and K. R. Dandekar, "Design and evaluation of a reconfigurable antenna array for MIMO systems," *IEEE Transactions on Antennas and Propagation*, vol. 56, no. 3, pp. 869-881, Mar 2008, DOI: 10.1109/tap.2008.916908.
- [99] Ali, M., Sayem, A. T., Kunda, V. K. (2007). A Reconfigurable Stacked Microstrip Patch Antenna for Satellite and Terrestrial Links. *IEEE Transactions on Vehicular Technology*, 56(2), 426-435. DOI:10.1109/tvt.2007.891412
- [100] D. Ressiguier, J. Costantine, Y. Tawk, C. G. Christodoulou, and IEEE, "A Reconfigurable Multi-Band Microstrip Antenna based on open ended microstrip lines," 2009 3rd European Conference on Antennas and Propagation, Vols 1-6, pp. 745-+, 2009.
- [101] Y. Z. Zhao, C. Huang, A. Y. Qing, and X. G. Luo, "A Frequency and Pattern Reconfigurable Antenna Array Based on Liquid Crystal Technology," *Ieee Photonics Journal*, vol. 9, no. 3, Jun 2017, Art no. 4600307, DOI: 10.1109/jphot.2017.2700042.
- [102] Y. P. Selvam et al., "A Low-Profile Frequency- and Pattern-Reconfigurable Antenna," *IEEE Antennas and Wireless Propagation Letters*, vol. 16, pp. 3047-3050, 2017, DOI: 10.1109/lawp.2017.2759960.
- [103] Selvam, Y. P., Elumalai, L., Alsath, M. G., Kanagasabai, M., Subbaraj, S., Kingsly, S. (2017). Novel Frequency- and Pattern-Reconfigurable Rhombic Patch Antenna With Switchable Polarization. *IEEE Antennas and Wireless Propagation Letters*, 16, 1639-1642. DOI:10.1109/lawp.2017.2660069
- [104] Nguyen-Trong, N., Hall, L., Fumeaux, C. (2016). A Frequency-and Pattern-Reconfigurable Center-Shorted Microstrip Antenna. *IEEE Antennas and Wireless Propagation Letters*, 15, 1955-1958. DOI:10.1109/lawp.2016.2544943
- [105] S. N. M. Zainarry, N. T. Nghia, and C. Fumeaux, "A Frequency- and Pattern-Reconfigurable Two-Element Array Antenna," *IEEE Antennas and Wireless Propagation Letters*, vol. 17, no. 4, pp. 617-620, Apr 2018, DOI: 10.1109/lawp.2018.2806355.
- [106] Wu, C., Ma, T. (2014). Pattern-Reconfigurable Self-Oscillating Active Integrated Antenna With Frequency Agility. *IEEE Transactions on Antennas and Propagation*, 62(12), 5992-5999. DOI:10.1109/tap.2014.2361897
- [107] Ye, M., Gao, P. (2015). Back-to-back F semicircular antenna with frequency and pattern reconfigurability. *Electronics Letters*, 51(25), 2073-2074. DOI:10.1049/el.2015.3029
- [108] Chen, S., Row, J., Wong, K. (2007). Reconfigurable Square-Ring Patch Antenna With Pattern Diversity. *IEEE Transactions on Antennas and Propagation*, 55(2), 472-475. DOI:10.1109/tap.2006.889950

- [109] Liu, W., Chen, T., Chen, S., Row, J. (2007). Reconfigurable microstrip antenna with pattern and polarisation diversities. *Electronics Letters*, 43(2), 77. DOI:10.1049/el:20073373
- [110] Bai, Y., Xiao, S., Liu, C., Shuai, X., Wang, B. (2013). Design of Pattern Reconfigurable Antennas Based on a Two—Element Dipole Array Model. *IEEE Transactions on Antennas and Propagation*, 61(9), 4867-4871. DOI:10.1109/tap.2013.2270175
- [111] M. Z. M. Nor, S. K. A. Rahim, M. I. Sabran, P. J. Soh, and G. A. E. Vandenbosch, "Dual-Band, Switched-Beam, Reconfigurable Antenna for WLAN Applications," *IEEE Antennas and Wireless Propagation Letters*, vol. 12, pp. 1500-1503, 2013, DOI: 10.1109/lawp.2013.2289919.
- [112] S. V. S. Nair and M. J. Ammann, "Reconfigurable Antenna With Elevation and Azimuth Beam Switching," *IEEE Antennas and Wireless Propagation Letters*, vol. 9, pp. 367-370, 2010, DOI:10.1109/lawp.2010.2049332.
- [113] Wu, S., Ma, T. (2008). A Wideband Slotted Bow-Tie Antenna With Reconfigurable CPW-to-Slotline Transition for Pattern Diversity. *IEEE Transactions on Antennas and Propagation*, 56(2), 327-334. DOI:10.1109/tap.2007.915454
- [114] Ha, S., Jung, C. W. (2011). Reconfigurable Beam Steering Using a Microstrip Patch Antenna With a U-Slot for Wearable Fabric Applications. *IEEE Antennas and Wireless Propagation Letters*, 10, 1228-1231. DOI:10.1109/lawp.2011.2174022
- [115] J. Sarrazin, Y. Mahe, S. Avrillon, and S. Toutain, "Pattern Reconfigurable Cubic Antenna," *IEEE Transactions on Antennas and Propagation*, vol. 57, no. 2, pp. 310-317, Feb 2009, DOI:10.1109/tap.2008.2011221.
- [116] Z. L. Lu, X. X. Yang, and G. N. Tan, "A Wideband Printed Tapered- Slot Antenna With Pattern Reconfigurability," *IEEE Antennas and Wireless Propagation Letters*, vol. 13, pp. 1613-1616, 2014, DOI:10.1109/lawp.2014.2342737.
- [117] Zhang, G., Hong, J., Wang, B., Song, G., Li, P. (2011). Design and Time-Domain Analysis for a Novel Pattern Reconfigurable Antenna. *IEEE Antennas and Wireless Propagation Letters*, 10, 365-368. DOI:10.1109/lawp.2011.2146225
- [118] Lim, I., Yun, T., Lim, S. (2014). Low-Profile Pattern-Reconfigurable Antenna with Vertical and Horizontal Shorting Lines in Grounded CPW Technology. *IEEE Antennas and Wireless Propagation Letters*, 13, 1589-1592. DOI:10.1109/lawp.2014.2346254
- [119] Lim, I., Lim, S. (2013). Monopole-Like and Bore-sight Pattern Reconfigurable Antenna. *IEEE Transactions on Antennas and Propagation*, 61(12), 5854-5859. DOI:10.1109/tap.2013.2283926
- [120] Jeong, J. G., Ahn, J., Yoon, Y. J. (2015). Ultra-wideband reconfigurable radiation pattern antenna for diversity applications. *Electronics Letters*, 51(25), 2086-2087. DOI:10.1049/el.2015.2324
- [121] Lai, M., Wu, T., Hsieh, J., Wang, C., Jeng, S. (2008). Compact Switched-Beam Antenna Employing a Four-Element Slot Antenna Array for Digital Home Applications. *IEEE Transactions on Antennas and Propagation*, 56(9), 2929-2936. DOI:10.1109/tap.2008.928775
- [122] Cao, Y. F., Zhang, X. Y. (2018). A Wideband Beam-Steerable Slot Antenna Using Artificial Magnetic Conductors With Simple Structure. *IEEE Transactions on Antennas and Propagation*, 66(4), 1685-1694. DOI:10.1109/tap.2018.2804480
- [123] Lu, Z., Yang, X., Tan, G. (2017). A Multidirectional Pattern-Reconfigurable Patch Antenna With CSRR on the Ground. *IEEE Antennas and Wireless Propagation Letters*, 16, 416-419. DOI:10.1109/lawp.2016.2581834
- [124] Cetiner, B., Crusats, G., Jofre, L., Biyikli, N. (2010). RF MEMS Integrated Frequency Reconfigurable Annular Slot Antenna. *IEEE Transactions on Antennas and Propagation*, 58(3), 626-632. DOI:10.1109/tap.2009.2039300
- [125] D. Peroulis, K. Sarabandi, and L. P. B. Katehi, "Design of reconfigurable slot antennas," *IEEE Transactions on Antennas and Propagation*, vol. 53, no. 2, pp. 645-654, Feb 2005, DOI: 10.1109/tap.2004.841339.

- [126] Perruisseau-Carrier, J., Pardo-Carrera, P., Miskovsky, P. (2010). Modeling, Design and Characterization of a Very Wideband Slot Antenna With Reconfigurable Band Rejection. *IEEE Transactions on Antennas and Propagation*, 58(7), 2218-2226. DOI:10.1109/tap.2010.2048872
- [127] Majid, H. A., Rahim, M. K., Hamid, M. R., Ismail, M. F. (2012). A Compact Frequency-Reconfigurable Narrowband Microstrip Slot Antenna. *IEEE Antennas and Wireless Propagation Letters*, 11, 616-619. DOI:10.1109/lawp.2012.2202869
- [128] Anagnostou, D., Gheethan, A. (2009). A Coplanar Reconfigurable Folded Slot Antenna Without Bias Network for WLAN Applications. *IEEE Antennas and Wireless Propagation Letters*, 8, 1057-1060. DOI:10.1109/lawp.2009.2031989
- [129] H. A. Majid, M. K. A. Rahim, M. R. Hamid, N. A. Murad, and M. F. Ismail, "Frequency-Reconfigurable Microstrip Patch-Slot Antenna," *IEEE Antennas and Wireless Propagation Letters*, vol. 12, pp. 218-220, 2013, DOI: 10.1109/lawp.2013.2245293.
- [130] Behdad, N., Sarabandi, K. (2006). A Varactor-Tuned Dual-Band Slot Antenna. *IEEE Transactions on Antennas and Propagation*, 54(2), 401-408. DOI:10.1109/tap.2005.863373
- [131] White, C. R., Rebeiz, G. M. (2009). Single- and Dual-Polarized Tunable Slot-Ring Antennas. *IEEE Transactions on Antennas and Propagation*, 57(1), 19-26. DOI:10.1109/tap.2008.2009664
- [132] Mahlaoui, Z., Antonino-Daviu, E., Ferrando-Bataller, M., Benchakroun, H., Latif, A. (2017). Frequency reconfigurable patch antenna with defected ground structure using varactor diodes. 2017 11th European Conference on Antennas and Propagation (EUCAP). DOI:10.23919/eucap.2017.7928358
- [133] Mak, A. C., Rowell, C. R., Murch, R. D., Mak, C. (2007). Reconfigurable Multiband Antenna Designs for Wireless Communication Devices. *IEEE Transactions on Antennas and Propagation*, 55(7), 1919-1928. DOI:10.1109/tap.2007.895634
- [134] Saghati, A. P., Azarmanesh, M., Zaker, R. (2010). A Novel Switchable Single- and Multifrequency Triple-Slot Antenna for 2.4-GHz Bluetooth, 3.5-GHz WiMax, and 5.8-GHz WLAN. *IEEE Antennas and Wireless Propagation Letters*, 9, 534-537. DOI:10.1109/lawp.2010.2051401
- [135] S. Nikolaou et al., "Pattern and frequency reconfigurable annular slot antenna using PIN diodes," *IEEE Transactions on Antennas and Propagation*, vol. 54, no. 2, pp. 439-448, Feb 2006, DOI:10.1109/tap.2005.863398.
- [136] Lai, M., Wu, T., Hsieh, J., Wang, C., Jeng, S. (2009). Design of reconfigurable antennas based on an L-shaped slot and PIN diodes for compact wireless devices. *IET Microwaves, Antennas Propagation*, 3(1), 47. DOI:10.1049/iet-map:20080049
- [137] H. A. Majid, M. K. A. Rahim, M. R. Hamid, and M. F. Ismail, "Frequency and Pattern Reconfigurable Slot Antenna," *IEEE Transactions on Antennas and Propagation*, vol. 62, no. 10, pp. 5339-5343, Oct 2014, DOI: 10.1109/tap.2014.2342237.
- [138] Ge, L., Li, Y., Wang, J., Sim, C. (2017). A Low-Profile Reconfigurable Cavity-Backed Slot Antenna With Frequency, Polarization, and Radiation Pattern Agility. *IEEE Transactions on Antennas and Propagation*, 65(5), 2182-2189. DOI:10.1109/tap.2017.2681432
- [139] RC0805FR-072K1L TDK: Digi-Key. (n.d.). Retrieved from <https://www.digikey.com/product-detail/en/yageo/RC0805FR-072K1L/311-2.10KCRCT-ND/730617>
- [140] MLF2012A1R0KT000 TDK: Mouser. (n.d.). Retrieved from <https://eu.mouser.com/ProductDetail/TDK/MLF2012A1R0KT000?qs=/PzWLGNeQ+gHs6g4HdBaeW==>
- [141] Liu, W., Yin, Y., Xu, W., Zuo, S. (2011). Compact Open-Slot Antenna With Bandwidth Enhancement. *IEEE Antennas and Wireless Propagation Letters*, 10, 850-853. doi:10.1109/lawp.2011.2165197
- [142] Li, C., Tong, C., Qi, L. (2015). Compact slot Yagi-Uda like antenna design with directional pattern. 2015 IEEE International Conference on Communication Software and Networks (ICCSN). DOI:10.1109/iccsn.2015.7296143

- [143] Li, Yixin, et al. "High-Isolation 3.5-GHz 8-Antenna MIMO Array Using Balanced Open Slot Antenna Element for 5G Smartphones." *IEEE Transactions on Antennas and Propagation*, 2019, pp. 1–1., DOI:10.1109/tap.2019.2902751.
- [144] Al-Tarifi, M., Sharawi, M. and Shamim, A. (2018). Massive MIMO antenna system for 5G base stations with directive ports and switched beamsteering capabilities. *IET Microwaves, Antennas & Propagation*, 12(10), pp.1709-1718.
- [145] Xingdong, P., Wei, H., Tianyang, Y. and Linsheng, L. (2014). Design and implementation of an active multibeam antenna system with 64 RF channels and 256 antenna elements for massive MIMO application in 5G wireless communications. *China Communications*, 11(11), pp.16-23.
- [146] Vieira, Joao, et al. "A Flexible 100-Antenna Testbed for Massive MIMO." *2014 IEEE Globecom Workshops (GC Wkshps)*, 2014, doi:10.1109/glocomw.2014.7063446.
- [147] Gao, Y., Ma, R., Wang, Y., Zhang, Q. and Parini, C. (2016). Stacked Patch Antenna With Dual-Polarization and Low Mutual Coupling for Massive MIMO. *IEEE Transactions on Antennas and Propagation*, 64(10), pp.4544-4549.
- [148] Zhou, Hao, et al. "A New Low-Profile and Closely Spaced Dual-Polarized Antenna for Massive-MIMO Applications." *2016 IEEE International Conference on Microwave and Millimeter Wave Technology (ICMMT)*, 2016, doi:10.1109/icmmt.2016.7762400.
- [149] Yuan, H., Cui, G. and Fan, J. (2017). A METHOD FOR ANALYZING BROADCAST BEAMFORMING OF MASSIVE MIMO ANTENNA ARRAY. *Progress In Electromagnetics Research Letters*, 65, pp.15-21.
- [150] Krishna, Sandhya, and Satish K. Sharma. "A Dual Polarization Massive MIMO Panel Array Antenna at Ka-Band with Beamforming Capability." *2017 United States National Committee of URSI National Radio Science Meeting (USNC-URSI NRSM)*, 2017, doi:10.1109/usnc-ursi-nrsm.2017.7878300.
- [151] Ma, Runbo, et al. "Antipodal Linearly Tapered Slot Antenna Array for Millimeter-Wave Base Station in Massive MIMO Systems." *2014 IEEE Antennas and Propagation Society International Symposium (APSURSI)*, 2014, doi:10.1109/aps.2014.6904887.
- [152] Rajagopal, S., et al. "Antenna Array Design for Multi-Gbps MmWave Mobile Broadband Communication." *2011 IEEE Global Telecommunications Conference - GLOBECOM 2011*, 2011, doi:10.1109/glocom.2011.6133699.
- [153] Ali, Mohamed Mamdouh M., and Abdel-Razik Sebak. "Design of Compact Millimeter Wave Massive MIMO Dual-Band (28/38 GHz) Antenna Array for Future 5G Communication Systems." *2016 17th International Symposium on Antenna Technology and Applied Electromagnetics (ANTEM)*, 2016, doi:10.1109/antem.2016.7550213.
- [154] Jain, A. and Yadav, S. (2016). DESIGN AND ANALYSIS OF COMPACT 108 ELEMENT MULTIMODE ANTENNA ARRAY FOR MASSIVE MIMO BASE STATION. *Progress In Electromagnetics Research C*, 61, pp.179-184.
- [155] Manteuffel, D. and Martens, R. (2016). Compact Multimode Multielement Antenna for Indoor UWB Massive MIMO. *IEEE Transactions on Antennas and Propagation*, 64(7), pp.2689-2697.



- [156] Krishna, Sandhya, et al. "A Series Fed Planar Microstrip Patch Array Antenna with 1D Beam Steering for 5G Spectrum Massive MIMO Applications." *2018 IEEE Radio and Wireless Symposium (RWS)*, 2018, doi:10.1109/rws.2018.8304989.
- [157] Du, Mingde, and Dong Han. "Dual-Polarized Square-Ring Slot-Coupled Patch Antenna for Massive MIMO Application." *2017 IEEE 28th Annual International Symposium on Personal, Indoor, and Mobile Radio Communications (PIMRC)*, 2017, doi:10.1109/pimrc.2017.8292723.
- [158] Liao, Kuan-Chieh, et al. "Massive MIMO 5G Small Cell Antenna with High Isolation." *2017 International Workshop on Electromagnetics: Applications and Student Innovation Competition*, 2017, doi:10.1109/iwem.2017.7968759.
- [159] Yang, B., Yu, Z., Dong, Y., Zhou, J. and Hong, W. (2017). Compact Tapered Slot Antenna Array for 5G Millimeter-Wave Massive MIMO Systems. *IEEE Transactions on Antennas and Propagation*, 65(12), pp.6721-6727.
- [160] Tzanidis, I., Li, Y., Xu, G., Seol, J. and Zhang, J. (2015). 2D Active Antenna Array Design for FD-MIMO System and Antenna Virtualization Techniques. *International Journal of Antennas and Propagation*, 2015, pp.1-9.
- [161] T. Wang, B. Ai, R. He, and Z. D. Zhong, "Two-Dimension Direction-of-Arrival Estimation for Massive MIMO Systems," *IEEE Access*, vol. 3, pp. 2122-2128, 2015, DOI: 10.1109/access.2015.2496944.
- [162] K. Y. Yang, J. Y. Wu, W. H. Li, and IEEE, *A Low-Complexity Direction-of-Arrival Estimation Algorithm for Full-Dimension Massive MIMO Systems* (2014 IEEE International Conference on Communication Systems). 2014, pp. 472-476.
- [163] S. S. Jehangir and M. S. Sharawi, "A Single Layer Semi-Ring Slot Yagi-Like MIMO Antenna System With High Front-to-Back Ratio," *IEEE Transactions on Antennas and Propagation*, vol. 65, no. 2, pp. 937-942, Feb 2017, DOI: 10.1109/tap.2016.2633938.
- [164] M. I. Lai, T. Y. Wu, J. C. Hsieh, C. H. Wang, and S. K. Jeng, "Design of reconfigurable antennas based on an L-shaped slot and PIN diodes for compact wireless devices," *IET Microwaves Antennas & Propagation*, vol. 3, no. 1, pp. 47-54, Feb 2009.
- [165] C. Z. Li, C. M. Tong, L. H. Qi, and IEEE, "Compact Slot Yagi-Uda like Antenna Design with Directional Pattern," in *Proceedings of 2015 IEEE International Conference on Communication Software and Networks*, (International Conference on Communication Software and Networks, 2015, pp. 147-150.

# VITAE

Name : Saeed Ahmad Haydhah

Nationality : Saudi

Date of Birth : 03/08(August)/1991

Email : saeedhaydhah@gmail.com

Address : Saudi Arabia, Dhahran, KFUPM

Academic Background : Electrical Engineering

- Master of Science (M.Sc.) in Electrical Engineering, King Fahd University of Petroleum and Minerals, December 2019.
- Bachelor of Science (B.Sc.) in Electrical Engineering, King Fahd University of Petroleum and Minerals, August 2014.

## LIST OF PUBLICATIONS

[J1] **Haydhah, Saeed A.**, Ferrero, Fabien, Lizzi, Leonardo, Zerguine, Azzedine, & Sharawi, Mohammad S. (2020). A New Compact Pattern Reconfigurable IOT Antenna. IEEE AWPL Antennas and Wireless Propagation Letters. Ready to Submit.

[C3] **Haydhah, Saeed A.**, Ferrero, Fabien, Lizzi, Leonardo, Zerguine, Azzedine, & Sharawi, Mohammad S. (2020). A Compact Pattern Reconfigurable Antenna for UHF Internet of Things Applications. (EUCAP 2020). Accepted.

[C2] **Haydhah, Saeed A.**, Hussain, R., Muqaibel, A., and Sharawi, Mohammad S. (2019). A Slot Based Pattern Reconfigurable Antenna. Asia-Pacific Conference on Antennas and Propagation (APCAP 2019). Accepted.

[C1] **Haydhah, Saeed A.**, Hussain, R., and Sharawi, Mohammad S. (2019). NEW PATTERN RECONFIGURABLE ANTENNA WITH 4 U-SLOTS FOR MIMO APPLICATIONS. IEEE International Symposium on Antennas and Propagation and USNC-URSI Radio Science (APS/URSI 2019). Published.